January 2015

ON THE INTERACTION OF SUBLIMATING GAS WITH COMETARY BODIES

Jordan Kenneth Steckloff
Purdue University

Graduate School Form 30
Updated 1/15/2015

PURDUE UNIVERSITY
GRADUATE SCHOOL
Thesis/Dissertation Acceptance

This is to certify that the thesis/dissertation prepared

By Jordan Kenneth Steckloff

Entitled
ON THE INTERACTION OF SUBLIMATING FAS WITH COMETARY BODIES

For the degree of Doctor of Philosophy

Is approved by the final examining committee:

H. Jay Melosh
Chair

David Minton

Rafael Lang

Marc Caffee

To the best of my knowledge and as understood by the student in the Thesis/Dissertation Agreement, Publication Delay, and Certification Disclaimer (Graduate School Form 32), this thesis/dissertation adheres to the provisions of Purdue University's "Policy of Integrity in Research" and the use of copyright material.

Approved by Major Professor(s): H. Jay Melosh

Approved by: John Finley 8 December 2015

Head of the Departmental Graduate Program Date

ON THE INTERACTION OF SUBLIMATING GAS WITH COMETARY BODIES

A Dissertation

Submitted to the Faculty

of

Purdue University

by

Jordan K. Steckloff

In Partial Fulfillment of the

Requirements for the Degree

of

Doctor of Philosophy

December 2015

Purdue University

West Lafayette, Indiana

For my wife, Holly Hopkins, who supported me and who moved with me to Indiana to allow me to continue my education. Also for my parents and sister, who have cultivated my curiosity throughout my life.

ACKNOWLEDGEMENTS

I would like to acknowledge my advisor, H. Jay Melosh, who guided me through my graduate research and encouraged my pursuit of independent research, which comprises the entirety of this dissertation. I would also like to acknowledge all of the co-authors of these research projects, without whom this work could not have been completed: Karl Battams, Timothy Bowling, Kevin Graves, Masatoshi Hirabayashi, Seth Jacobson, Brandon Johnson, Carey Lisse, H. Jay Melosh, David Minton, and James Richardson. Lastly, I would like to acknowledge the members of my PhD committee, whose commitment and comments led to significant improvements in my research, H. Jay Melosh, David Minton, Rafael Lang, and Marc Caffee.

TABLE OF CONTENTS

Page
LIST OF TABLES v
LIST OF FIGURES vi
ABSTRACT vii
CHAPTER 1. INTRODUCTION 1
References 4
CHAPTER 2. A BRIEF HISTORY OF COMET SCIENCE 5
References 37
CHAPTER 3. SUBLIMATION PRESSURE 40
3.1 Introduction 41
3.2 Theory/calculation 42
3.2.1 Computing Mass Flux, Force, Temperature, and Sublimation Pressure 47
3.2.2 Differential Stress 51
3.3 Results 55
3.4 Discussion 57
3.4.1 Supervolatiles and Amorphous Ice 59
3.4.2 Hydrostatic Pressure and Fragmentation Timescale 63
3.4.3 Strengths of Other Comets 65
3.5 Conclusions 67
References 68
CHAPTER 4. A SUBLIMATIVE ANALOGUE TO THE YORP EFFECT 73
4.1 Introduction 74
4.2 Radiation Pressure 76
4.3. Sublimation-Driven Stria Formation Model 79
4.3.1 Step 1: Parent chunks leave comet 81
4.3.2 Step 2: Sublimation Pressure instead of Radiation Pressure 83
4.3.3 Step 2 continued: Rotational acceleration due to SYORP 87
4.3.3.1 The YORP Effect 88
4.3.3.2 The SYORP Effect 88
4.3.4 Step 3: Critical failure of the body 90
4.3.5 Step 4: Runaway Fragmentation Cascade 93
4.3.6 Step 5: Onset of Stria Formation 97
4.3.7 Modeling and Constraints on Stria Formation 98
4.4. Striae of Comet West 102

Page
4.5. Discussion 109
4.6. Summary & Conclusions 113
References 116
CHAPTER 5. ROTATIONALLY INDUCED AVALANCHES
AND THE ACTIVATION OF COMET HARLTLEY 2 124
5.1 Introduction 125
5.2 Methods 129
5.3 Results 132
5.4 Discussion 137
5.5 Conclusions 146
References 148
VITA 151
PUBLICATIONS 152
Dynamic sublimation pressure and the catastrophic breakup of Comet ISON 152
The formation of striae within cometary dust tails
by a sublimation-driven YORP-like effect 160

LIST OF TABLES

Table Page
4.1 Heliocentric and Cometocentric locations of stria formation for Comet West and their best-fit parent chunks..... 104

LIST OF FIGURES

Figure Page
1.1 Comet Halley in the Bayeux Tapestry 3
2.1 Orbit of the Great Comet of 1680 14
2.2 Edmund Halley's Table of Cometary Orbital Elements 20
2.3 Drawing of the Head of Comet Donati by George Bond 31
3.1 Schematic of Dynamic Sublimation Pressure Disruption Mechanism and Comparison to Atmospheric Impact 45
3.2 Azimuthal Dependence of Dynamic Sublimation Pressure 50
3.3 Schematic of how Sublimation Pressure Induces Differential Stresses 52
3.4 Dynamic Gas Sublimation Pressures for Major Volatile Species 56
4.1 Illustrating Stria and Synchrones 75
4.2 A Cartoon of SYORP-induced Stria Formation 80
4.3 Peak Sublimation Pressure as a Function of Heliocentric Distance 86
4.4 A plot of the gamma factor for various species 91
4.5: Comet West stria formation heliocentric distance versus parent chunk ejection heliocentric distance 100
4.6: Cumulative Size-frequency distribution of the best-fit parent chunks of Comet West's striae. Here we plot the number of chunks 108
5.1 Overview of relevant regions of comet 103P/Hartley 2 126
5.2: Surface slopes of 103P/Hartley 2 under different rotation rates 133
5.3: Finite Element Model (FEM) Analysis of Plastic Stresses in the body of Hartley 2 at Critical Rotation Period. 136
5.4 Size-Frequency Distribution of Mounds on Nucleus of Hartley 2 141
5.5: Specific Potential Map of Hartley 2 at Various Spin Period 143

ABSTRACT

Steckloff, Jordan K. Ph.D., Purdue University, December 2015. On the Interaction of Sublimating Gas with Cometary Bodies. Major Professor: H. Jay Melosh

Sublimation of volatiles is a defining process of comet nuclei, and profoundly affects their dynamics, structure, and appearance. Central to understanding the processes by which comets formed and subsequently evolved is a careful computation of this sublimation pressure as a function of heliocentric distance. Unlike previous efforts, I develop a thermodynamic method to numerically compute the sublimation pressure of any species from limited knowledge of its physical properties. I then describe a novel cometary disruption mechanism in which this sublimation pressure induces differential stresses within the body of the nucleus that exceed its material strength, resulting in structural failure and breakup of the nucleus. I show that this mechanism is consistent with the behavior of Comet ISON (C/2012 S1), and use it to estimate the cohesive strength of ISON's nucleus, a first for a Long-Period Comet.

Sublimating volatiles can also generate sublimative torques that alter the rotation state of the nucleus. However, computing these torques requires high-resolution information on the shape and activity of the nucleus, which is available only for the few nuclei visited by spacecraft. To remedy this, I develop a novel framework based on the

YORP Effect (the torques asteroids experience by emitting thermal photons from their asymmetric shapes) to study the effects of sublimative torques on populations of cometary bodies. I take advantage of the similar manner in which surfaces emit both thermal photons and sublimating molecules to derive numerical relationships that describe sublimative torques by appropriately scaling the YORP torque equations. I then use this framework to explain the formation of dust striae (long linear features in the tails of Long-Period Comets that align with the Sun), which has remained an enigma for more than a century. I show that the observed ~10-100 m chunks ejected from comet nuclei experience sublimative torques that spin them up to the point of disruption, forming the observed striae.

Sublimative torques can also significantly affect nuclei themselves, and cause large avalanches that excavate buried supervolatile ices. The activity of Comet 103P/Hartley 2 is dominated by CO_2 driven sublimation at the tip of its bilobate nucleus. This CO_2 ice responds to the nucleus's diurnal cycle, and must therefore be very near the surface. However, CO_2 ices were expected to have receded deep below Hartley 2's surface during its ~10 million year migration from the Kuiper Belt to the Jupiter Family, suggesting that these ices were somehow brought to the surface. I map the gravitational slopes of Hartley 2's surface as a function of rotation period, and show that large avalanches capable of excavating these CO_2 ices set in at a rotation period of ~11 hours, and are entirely confined to the regions of the nucleus exhibiting CO_2 driven activity. This suggests that a period of fast rotation activated this CO_2 activity. At the rate of spin-down observed by EPOXI, this avalanche likely occurred between 1984 and 1991, and would have significantly brightened the comet, consistent with its discovery in 1986.

Furthermore, this mechanism allows me to date nearly all terrains imaged by EPOXI, a first for a comet.

"When beggars die there are no comets seen;
The heavens themselves blaze forth the death of princes."
-William Shakespeare

CHAPTER 1. INTRODUCTION

For as long as there have been humans, those humans have observed the night sky, which acted as a calendar, and regulated the yearly cycle. So intimate was the cosmos' perceived control of events on earth, that the appearance of a comet, which was seen as an unfavorable star (disastrum in Latin, the origin of the word disaster (Oxford English Dictionary, 2015) that upset the predictable cosmic order of the stars and planets impending calamity. Flavius Josephus, a Romano-Jewish historian recalled how the Jews, prior to their revolt against the Romans in 66 C.E., gave no "credit to the signs that were so evident, and did so plainly foretell their future desolation...a star resembling a sword, which stood over the city, and a comet, that continued a whole year" (Josephus, 75 C.E.). That comet was the 66 C.E. apparition of Comet Halley, which has been unambiguously observed at every apparition since 2406 B.C.E. (Tsu, 1934). The "star resembling a sword" is likely either the pre-perihelion or post-perihelion leg of Comet Halley's orbit, as the two motions of the comet were viewed as two separate objects at that time.

Comets were sometimes omens of good fortune. The Ancient Romans practiced apotheosis, whereby a deceased ruler was deified by his successor. Shortly after the assassination of Julius Caesar in 44 B.C.E., one of the brightest comets ever recorded appeared in the sky, on the day of his apotheosis. This Great Comet of 44 B.C. (formally C/-43 K1) was visible in the daytime sky for 7 days "and was believed to be the soul of Caesar, who had been taken to heaven" (Suetonius, 121 C.E.). The 1066 apparition of Comet Halley was recorded in the Bayeux Tapestry as an omen of success for Duke William II of Normandy's conquest of England (See Figure 1.1). Later that year at the Battle of Hastings, William II defeated and killed King Harold of England, and conquered England.

Although comets have been associated with significant events throughout human history, the following work is concerned not with the historical, sociological, or archaeoastronomical aspects of cometary apparitions, but rather with the development of physical theories of their origins, structure, and behavior. While all ancient civilizations may have observed comets and wondered as to their purpose and origin, the oldest surviving theories on the physical nature of comets as part of a wider and comprehensive cosmology can be traced to the ancient Greeks, particularly Aristotle. I therefore begin my discussion of scientific cometology in ancient Greece.

Figure 1.1 Comet Halley in the Bayeux Tapestry.

The Bayeux Tapestry, which tells the story of the Norman conquest of England, notes the apparition of Comet Halley in 1066, visible as a star with a large tail. The tapestry includes the caption "ISTI MIRANT STELLA" (the men watch the star), referring to the Normans (left side of tapestry) seeing this new "star" (Comet Halley) as an omen of success in their invasion of England that same year. King Harold himself may have also seen the comet as an omen doom, foretelling of his disastrous defeat and death at the Battle of Hastings. (Photo Credit: Myrabella, 2015)

References

Oxford English Dictionary. online.www.oed.com. accessed 8 oct, 2015

Josephus. *De Bello Ivdaico* **Book VI**. Translated 1737 by Whiston, W; (75 C.E.)

Myrabella, Bayeux Tapestry - scene 32. *commons.wikimedia.org*. Image retrieved 7 October, 2015

Suetonius, "Divus Julius". *De Vita Caesarum*. Translated 1914 by Rolfe, J.C. (121 C.E.)

Tsu, W.S.; The Observations of Halley's Comet in Chinese History. *Popular Astronomy* **42**, 191-201 (1934)

"It's a warm summer evening, circa 600 B.C., you've finished your shopping at the local market, or agora, and you look up at the night sky. There you notice some of the stars seem to move, so you name them planētēs, or wanderer."

-Dr. Sheldon Cooper, PhD
The Big Bang Theory (2009)

CHAPTER 2. A BRIEF HISTORY OF COMET SCIENCE

Aristotle was not the first natural philosopher to ponder the nature of comets. Before Aristotle, Anaxagoras and Democritus (who first pondered the existence of molecules) believed comets to be a conjunction of at least two of the five (known) planets (Mercury, Venus, Mars, Jupiter, Saturn) (Aristotle, 350a B.C.E.), which would produce an elongated, illuminated object (Heidarzadeh, 2008 p. 10). Earlier, the Pythagorean school of philosophy had taught that comets are apparitions of a 6th planet, whose orbit rises only a little above the horizon (like Mercury) and which has a very long orbital period such that it only appears after long intervals (Aristotle, 350a B.C.E.). These thinkers placed comets squarely in the celestial realm of the planets, and the Pythagoreans were remarkably accurate in describing the orbits of some known comets. However, Aristotle had reasonable and well thought out objections to such ideas placing comets in the realm of the planets.

The ancient Greeks observed that the Sun, Moon, and planets move along the zodiacal path (Aristotle, 350a B.C.E.), which traces the projection of the Solar System's ecliptic plane on the sky, against the firmament of the fixed stars. Aristotle noted that sometimes all five planets are visible at the same time as a comet, and reasoned that a conjunction of the planets cannot therefore produce a comet. Furthermore, many comets follow paths outside the zodiac, suggesting that comets are distinct from the planets. Finally, Aristotle noted that sometimes multiple comets are simultaneously visible in the night sky. Thus, the addition of a cometary planet to the Solar System, regardless of its path in the sky, could not explain simultaneous cometary apparitions. Aristotle therefore did not believe that cometary phenomena were a part of the heavens. (Aristotle, 350a B.C.E.)

Aristotle's cosmology divided the universe into two realms, the celestial and the terrestrial: the celestial realm is one of perpetual circular motion and clockwork predictability (Aristotle, 350b B.C.E.), while the terrestrial realm is imperfect, unpredictable, and where the natural position of an object is to come to rest in its element (Aristotle, 350a B.C.E.). The terrestrial realm was stratified into four layers representing the natural state of the four elements (bottom to top: earth, water, air, fire). Thus, a fire reaches skyward and hot air rises because the fire element is at the top of the terrestrial realm (in contact with the celestial realm), while rain falls to the ground and continues to flow across its surface until it reaches a lake, stream, or ocean and comes to rest. This division seemed to explain why the planets move in predictable, perpetual motion along a common path in the sky, while moving objects on the earth eventually slow down and come to rest. Although Aristotle did not consider that friction is responsible for this

difference in motion, he did consider that the planets move through a resistanceless æther, which permeates the celestial realm (Heidarzadeh, 2008 p. 4-16). Thus the heavens, which begin at the Moon, are subject to a different set of physical principles than the terrestrial realm.

For Aristotle, any satisfactory physical explanation of comets had to explain their non-zodiacal motion and unpredictable apparitions, and provide a mechanism for generating a tail (Heidarzadeh, 2008 p. 12). Aristotle believed meteors, comets, and the Milky Way to be related phenomena. Heidarzadeh (2008) summarized Aristotle's theory on the nature of comets:

> "When the hot and dry exhalation [of the earth] rises to the so-called fire layer, it participates in the circular motion of the fire caused by the revolution of the celestial sphere… Under special conditions, shooting stars appear in the sky. Shooting stars, however, consume their fuel quickly and burn out in a matter of seconds… By contrast, it is expected that if a mass of condensed (and therefore less inflammable) exhalation encounters an adequate amount of the element fire (not so strong as to burn the material instantly and not so weak as to extinguish it quickly) it will create a longer lasting fire. In fact, in such a case, the flame cannot spread rapidly through the fuel, but stops in the densest part of it. Then, this semi-steady burning fuel, which is moving with the motion of the so-called fire layer, will create a relatively durable fire, seen as a comet." (Heidarzadeh, 2008 p. 12)

Thus, comets are the result of flammable materials that rise to the top of the fire layer of the terrestrial realm and slowly smolder, forming a long-lived, smoky apparition. Additionally, because the fire layer touches the perpetually-revolving celestial realm, the

top of the fire layer gets dragged toward the west, blowing on the smoky comet and forming a tail.

Aristotle also postulated a second type of comet that forms when a star or planet generates an exhalation that moves (naturally) toward the fire layer, forming a luminous fringe that follows the motion of its source. While this form of comet does not appear to replicate the perceived motion of comets in the sky, which move relative to the fixed stars, it illustrates the relationship of comets to the Milky Way. Aristotle described the Milky Way as a region where the exhalations tend to gather, forming a long-lived luminous phenomenon. Furthermore, because few exhalations remain, and because the necessary conditions to form comets are rare, comet apparitions are very infrequent. Aristotle's comet theory therefore explains the random paths and rare apparitions of comets, their fuzzy, smoky appearance, and provides a mechanism to form comet tails.

Thus, Aristotle incorrectly believed comets to be merely a phenomenon located in the upper layer of the terrestrial realm, and placed the location of comets between the Earth and the Moon, which fit with the wider Aristotelian cosmology. That this view persisted for nearly 2 millennia, is a testament to how advanced and comprehensive Aristotle's empirical philosophy was at the time, and how rarely naked eye comets appear in the sky, the observations of which could facilitate a revision of the Aristotelian comet theory. That is becuase the Aristotelian theory of comets made testable predictions on the behavior and orientation of comets. First, because the theory places comets in the sublunar realm, they should exhibit a diurnal parallax greater than the ~1 degree parallax angle of the moon. This means that the apparent location of the comet in relation to the fixed stars should appear to move over the course of a night on account of the motion of

the observer as the Earth rotates. Additionally, if a comet in fact comes to conjunction with a planet, the planet's appearance and color should change as the planet's light passes through the comet. Finally, because the comet tail is formed by the effect of the celestial realm's east-west rotation, the Aristotelian theory predicts that all comet tails are oriented in an east-west direction (Heidarzadeh, 2008 p. 17-18).

Abū Ma'shar, a preeminent Islamic astrologer, recorded his observations of a comet in *Albumasar in Sadan*:

> The philosophers say, and Aristotle himself, that comets are in the sky in the sphere of fire, and that nothing of them is formed in the heavens, and that the heavens undergo no alteration. But they have all erred in this opinion. For I saw with my own eyes a comet beyond Venus. And I know that the comet was above Venus, because its color was not affected. And many have told me that they have seen a comet beyond Jupiter and sometimes beyond Saturn." (Thorndike, 1954 p. 23)

Thus Abū Ma'shar recorded clear evidence that comets are a celestial, rather than atmospheric, phenomenon. Abū Ma'shar's observations inspired subsequent observers to measure cometary parallaxes and determine whether comets are a terrestrial or celestial phenomenon (Heidarzadeh, 2008 p. 29-31).

Abu Ma'shar's observations were, like most contemporary surviving records of comets, purely qualitative. Improvements in astronomical tools and techniques over the subsequent centuries allowed for better, more quantitative measurements. Georg von Peurbach recorded his observations on the parallax of the comet of 1456 (another apparition of Comet Halley). From his measurements, he concluded that the comet was

at an altitude of 1,000 German miles (7,500 km) (Heidarzadeh, 2008 p. 35). 16 years later, Regiomontanus measured the altitude of the comet of 1472 to be 8,200 German miles (62,000 km) (Heidarzadeh, 2008 p. 36-37). Interestingly, these flawed measurements, likely the result of the crude instruments available at the time, were too low even for the Aristotelian comet theory, placing comets in the air layer, rather than the fire layer. However, these measurements revolutionized the study of comets by introducing mathematical methods to their study.

In 1531-1533, three bright naked eye comets allowed Peter Apian and Girolamo Fracastoro to independently discover that comet tails always point away from the Sun, rather than in an East-West direction as predicted by Aristotle (Heidarzadeh, 2008 p.37). Gemma Frisius explained this phenomenon with his optical theory of Comets, in which he proposed that comet tails are the result of refracted sunlight (Heidarzadeh, 2008 p. 37-38). Jean Pena elaborated on this theory by proposing that comets were denser that their surrounding air, allowing them to act as a spherical lens (Heidarzadeh, 2008 p. 38). This theory is incomplete, as it is never specified what material intercepts the rays of the Sun and reflects them toward the observer.

Finally, in 1577, Tycho Brahe (whom Edmund Halley called "that great Restorer of Astronomy" [Halley, 1705]) measured the diurnal (daily) parallax of a comet (Halley, 1705). Only five years prior, Tycho had attempted to measure the diurnal parallax of the nova (literally "new [star]") of 1572 using a sextant (Gingerich, 2005). Although primitive when compared to modern instrumentation, the astronomical instruments available to Tycho were an order of magnitude more accurate than the instruments available to the preceding generation (Heidarzadeh, 2008 p. 50). Having failed to detect

any parallax despite extensive observations, Tycho had convincingly shown that novae were celestial, shattering the Aristotelian notion that the heavens were perpetual and unchanging (Gingerich, 2005). Tycho's observations were so careful and precise, that his recorded position of the nova was off by only three arcminutes (remarkable given the technology at the time), which we learned when its remnant was finally discovered in the 1950's (Gingerich, 2005). This discovery was so sensational, that the Danish king literally gave Tycho more than a ton of gold to build an observatory (Gingerich, 2005).

From his new observatory, Tycho Brahe observed the comet of 1577 on each clear night (~30 total), measuring its position relative to the fixed stars multiple times each night (Heidarzadeh, 2008 p. 41), but failing to measure any observable parallax angle (Halley, 1705). From the precision of this measurement, he determined that the comet must be at least 197,800 German Miles (~1.5 million km) from the Earth and be at least 465 German Miles (3,490 km) across (Heidarzadeh, 2008 p. 41-45). Tycho therefore determined that comets travel beyond the celestial orb of the Moon, and are planet-sized.

Johannes Kepler, who worked for Tycho, succeeded him as imperial mathematician after Tycho's unexpected death. Kepler observed the comets of 1607 and 1618 and detected their annual parallax, which conclusively placed them nearer to the Earth than Jupiter (Halley, 1705). This discovery placed the location of comets clearly in the realm of the planets. From the measurements of Tycho as well as his own, Kepler concluded that comets travel in approximately rectilinear paths. However, Hevelius found that his own observations did not agree with rectilinear motion (Halley, 1705).

Thus, the theory of Aristotle had been conclusively disproven through quantitative measurements, and was supplanted by a theory that explained the great distance of the comets as well as the orientations of their tails. However, their path through the heavens was poorly understood.

The early 17th century was a period of rapid development in our understanding of the cosmos. The heliocentric model of the Solar System proposed by Copernicus in the mid-sixteenth century was becoming widely used. The invention of the telescope allowed Galileo Galilee to first view the large moons of Jupiter that now bear his name, and to observe that the Jovian system resembled a miniature Solar System. Later, Johannes Kepler developed his laws of planetary motion. Observers were treated to rare appearance of three bright naked-eye comets in five months of 1618, with the last of the three being the brightest. Galileo observed that the brightest comet of 1618 traveled more than 90 degrees of arc in ~40 days. However, if it were the same comet at the great comet of 1577, then it shouldn't have traveled even a single degree in that span of time. Thus, Galileo deduced that either comets do not follow circular paths, or that there must be more than one comet (Heidarzadeh, 2008 p. 61-64). Kepler further considered that comets travel in straight lines, but the motion of the Earth around the Sun made comet trajectories appear curved (Heidarzadeh, 2008 p.64-65). For reasons unknown, Kepler never applied his laws of planetary motion to comets.

The Great Comet of 1680 was one of the brightest comets observed in recorded history (Yeomans, 2007), and the first known sungrazing comet, having a perihelion distance only ~⅓ of a Solar Radius above the photosphere of the Sun (Halley, 1705; JPL Solar System Dynamics). Georg Samuel Dörffel and Isaac Newton independently

determined that this comet followed a parabolic path (Heidarzadeh, 2008 p. 88-93). John Flamsteed and Robert Hooke proposed that a central force acted in the Solar System to generate these paths (Heidarzadeh, 2008 p. 88-93), however neither could explain how it worked.

Isaac Newton stated, in his magnum opus *Philosophiæ Naturalis Principia Mathematica,* that a gravitational force governs the motion of all bodies in the universe whose strength varies by the inverse-square of the heliocentric distance. This causes comets to "move in some of the conic sections, having their foci in the center of the sun; and by radii drawn to the sun describe areas proportional to the times." (Newton, 1726, p. 332) Thus, Isaac Newton used his law of gravitation to derive Kepler's second law of planetary motion, and showed that it applies to comets as well as planets. Newton also noted that cometary "orbits will be so near to parabolas, that parabolas may be us'd [used] for them without sensible error" (Newton, 1726 p. 332). While this approximation worked well for the Great Comet of 1680 and most other long-period comets, it would eventually break down with the discovery of Jupiter Family Comets (JFCs), which have significantly less eccentric, elliptical orbits, with a Tisserand parameter with respect to Jupiter (T_J) of $2 < T_J < 3$, and typically have an aphelion of 5-6 AU (Lowry et al. p. 397-410).

Newton realized that comets and other celestial objects follow their observed paths because "the celestial spaces [are] free and without resistance" (Newton, 1726 p. 369). He therefore concluded that the æther did not impede the motion of objects in the same manner as air (Newton, 1726 p.230-232). Because the Great Comet of 1680

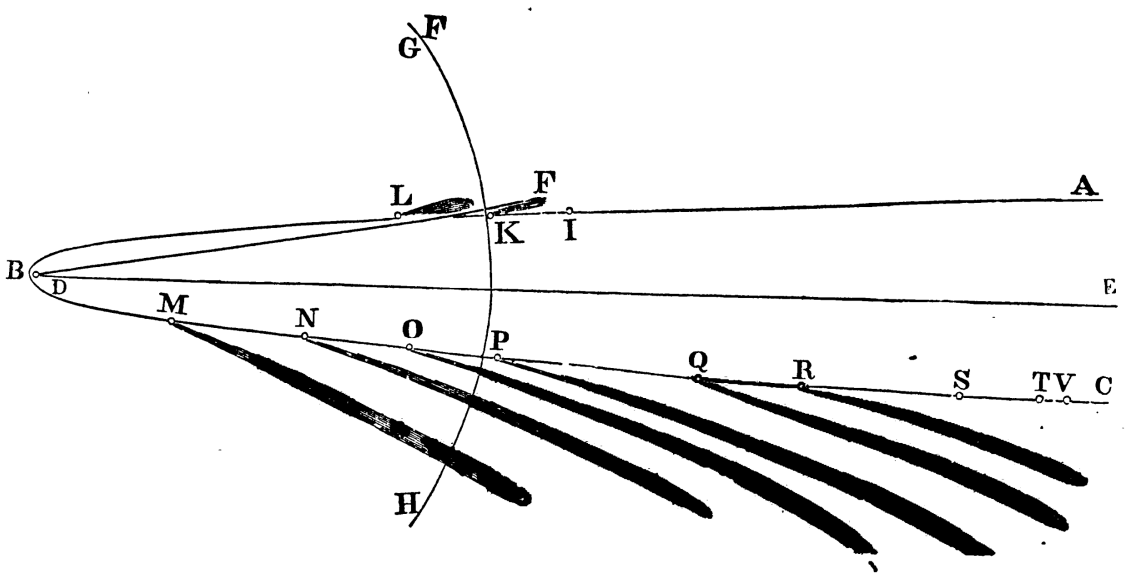

Figure 2.1 Orbit of the Great Comet of 1680

An illustration of the nearly parabolic orbit of the Great Comet of 1680 from Newton's *Philosophiæ Naturalis Principia Mathematica* (Newton, 1726 p. 358-359). Isaac Newton was the first to explain that the paths of comets (and all heavenly bodies) are conic sections, and that such shapes are the result of his law of universal gravitation. The tail of the Great Comet of 1680 obviously pointed away from the Sun, when its observed orientation was drawn in the appropriate location on the comet's path.

survived traveling through the solar atmosphere (Newton, 1726 p. 385), he concluded that comets must be durable, solid, and very dense (Heidarzadeh, 2008 p. 94-96). Newton realized that the optical theories of comet tails are inconsistent with observations. As Henry Pemberton later summarized Newton's logic:

> Of [the appearance of comet tails] there are several opinions; our author reduces them to three...The first is, that they arise from a beam of light transmitted through the head of the comet, in like manner as a stream of light is discerned, when the sun shines into a darkened room through a small hole. This opinion, as Sir ISAAC NEWTON observes, implies the authors of it wholly unskilled in the principles of optics; for that stream of light, seen in a darken'd room, arises from the reflection of the sun beams by the dust and motes floating in the air: for the rays of light themselves are not seen, but by their being reflected to the eye from some substance, upon which they fall. The next opinion examined by our author is that of the celebrated DES CARTES, who imagins these tails to be the light of the comet refracted in its passage to us, and thence affording an oblong representation; as the light of the sun does, when refracted by the prism in that noted experiment […] But this opinion is at once overturned from this consideration only, that the planets could be no more free from this refraction than the comets; nay ought to have larger or brighter tails, than they, because the light of the planets is strongest...And besides, when the light in its passage from different comets to the earth describes the same path through the heavens, the refraction of it should of necessity be in all respects the same. But this is contrary to observation; for the comet in 1680, the 28th day of December, and a former comet in the year 1577, the 29th day of December, appear'd in the same place of the heavens, that is, were seen adjacent to the same fixed stars, the earth

> likewise being in the same place at both times; yet the tail of the latter comet deviated from the opposition to the sun a little to the northward, and the tail of the former comet declined from the opposition of the sun five times as much southward. (Pemberton, 1728)

Newton's own theory on the tails of comets is based on his observation of the relationship between heliocentric distance and the length of a comet's tail, and that comet tails are curved (Newton, 1726 p. 365):

> It is plain that the phænomena of the tails of Comets, depend upon the motions of their heads, and by no means upon the places of the heavens in which their heads are seen, and that therefore the tails of Comets do not proceed from the refraction of the heavens, but from their own heads, which furnish the matter that forms the tail. For, as in our air, the smoak of a heated body ascends, wither perpendicularly if the body is at rest, or obliquely, if the body is mov'd obliquely; so in the heavens, where all bodies gravitate towards the Sun, smoak and vapour must (as we have already said) ascend from the Sun, and either rise perpendicularly, if the smoaking body is at rest; or obliquely, if the body, in all the progress of its motion, is always leaving those places from which the upper or heigher parts of the vapour had risen before. And that obliquity will be least, where the vapour ascends with most velocity, to wit near the smoaking body, when that is near the Sun. But because the obliquity varies, the column of vapour will be incurvated; and because the vapour in the preceding side is something more recent, that is, has ascended something more late from the body, it will therefore be something more dense on that side, and must on that account reflect more light, as well as be better defin'd. (Newton, 1726 p. 365-366)

Thus, Newton's theory that comet tails are a smoke-like material explained why comet tails are brightest near the head, are oriented away from the Sun, and curved.

The Newtonian model of comets as massive objects with thick atmospheres was a drastic change from theories that came before, and was remarkably successful in explaining a host of cometary and planetary motions and behaviors. This model was quite persistent, and even served as the basis for works of science fiction. For example, in Jules Verne's 1877 *Hector Servadac*, which tells of a group of people that find themselves living on a comet after one collides with the Earth (Verne, 1877). Even today, it is remarkably still recognizable as the basis of all comet theories that came afterwards. Newton even postulated that comets can serve as a mechanism to deliver volatile materials to the planets.

While his deduction that comet nuclei were dense, planet-sized durable objects surrounded by thick atmospheres was quite logical, Newton did notice problems with this theory. He realized that the gravitational perturbations of such massive comets would destabilize the Solar System over time. He therefore proposed that the Creator of the Solar System would have to periodically intervene and "restore" the Solar System. Thus, Isaac Newton invoked divine intervention to solve problems with his theories.

Furthermore, the newtonian model of comets could not explain why planet-sized comets with thick atmospheres have tails at heliocentric distances comparable to the terrestrial planets, while the planets themselves do not have tails. As Henry Pemberton described:

> [A] difference is found between the planets and comets. The atmospheres of the planets are of so fine and subtile a substance, as hardly to be discerned at any

> distance, by reason of the small quantity of light which they reflect...But the atmospheres which surround the comets are so gross and thick, as to reflect light very copiously. (Pemberton, 1728 p.237)

Thus, the rarified nature of planetary atmospheres, when compared to those of the comets, prevents them from reflecting more light to the observer. Moreover, Pemberton cites differences between the material composing planetary and cometary atmospheres

> if we consider, that [comets] do not send out those fumes merely by their near approach to the sun; but are framed of a texture, which disposes them in a particular manner to fume in that sort: for the earth, without emitting any such steam, is more than half the year at a less distance from the sun, than the comet of 1664 and 1665 approached it, when nearest; likewise the comets of 1682 and 1683 never approached the sun much above a seventh part nearer than Venus, and were more than half as far again from the sun as Mercury; yet all these emitted tails. (Pemberton, 1728 p. 245)

Thus, Pemberton attempted to explain away the lack of planetary tails by claiming that the different "textures" of the cometary and planetary atmospheres result in only comets forming tails (Hidarzideh, 208 p. 140-141).

William Whiston, who succeeded Isaac Newton as the Lucasian Professor at Cambridge, found Newton's explanation for the formation of comet tails incomplete. Whereas Newton proposed that the vapors of the comet tail rise from the Sun due to heat and interactions with the æther, Whiston adopted the Keplerian view that the rays of the Sun exert a pressure on these materials that drive them antisunward (Heidarzadeh, 2008 p.129-135). As he described in his book *A new theory of the Earth*, comets tails form from the "Atmosphere rarified by the Sun's Heat; which becoming thereby, if not

specifically lighter than the Æther, or Atmosphere encompassing the Sun, yet as least so rare an light as to yield to the Sun's Rays, and to be carry'd away by them, and so rise in a Mist or Steam of Vapours towards the Parts opposite to the Sun" (Whiston, 1755 p. 52). Leonhard Euler later eliminated any interaction with æther, stating that tails are formed solely by interaction with the Sun's rays (Heidarzadeh, 2008 p.159-164).

Edmund Halley, a contemporary and colleague of Isaac Newton, used Newton's theory of gravity and observations of all known well-measured comets to break their motions down into orbital elements (Halley, 1705), and conducted the first dynamical studies of their population. He discovered that the observed population of comets is nearly isotropic: "tis apparent, their Orbits are dispos'd in no manner of Order; nor can they, as the Planets are, be comprehended within a Zodiack, but move indifferently every Way, as well Retrograde as Direct" (Halley, 1705). This population is now known as the Nearly Isotropic Comets (NICs). Halley also proposed that there may be a great many number of comets that we do not see due to their lack of activity: "the Distances in the Perihelium's are sometimes greater, sometimes less; which makes me suspect, there may be a far greater Number of them, which moving in Regions more remote from the Sun, become very obscure; and wanting Tails, pass by us unseen." (Halley, 1705)

However, Edmund Halley is most famous for proposing that the comets are not onetime apparitions, but rather that they return. He noted that none of the known comets have been observed to follow hyperbolic motion, and thus no observed comet is unbound to the Sun. He therefore concluded that Newton's parabolic path for the comets is merely an approximation for very eccentric orbits with very long periods. He then commented on how a comet with nearly the same set of orbital elements appears every ~76 years:

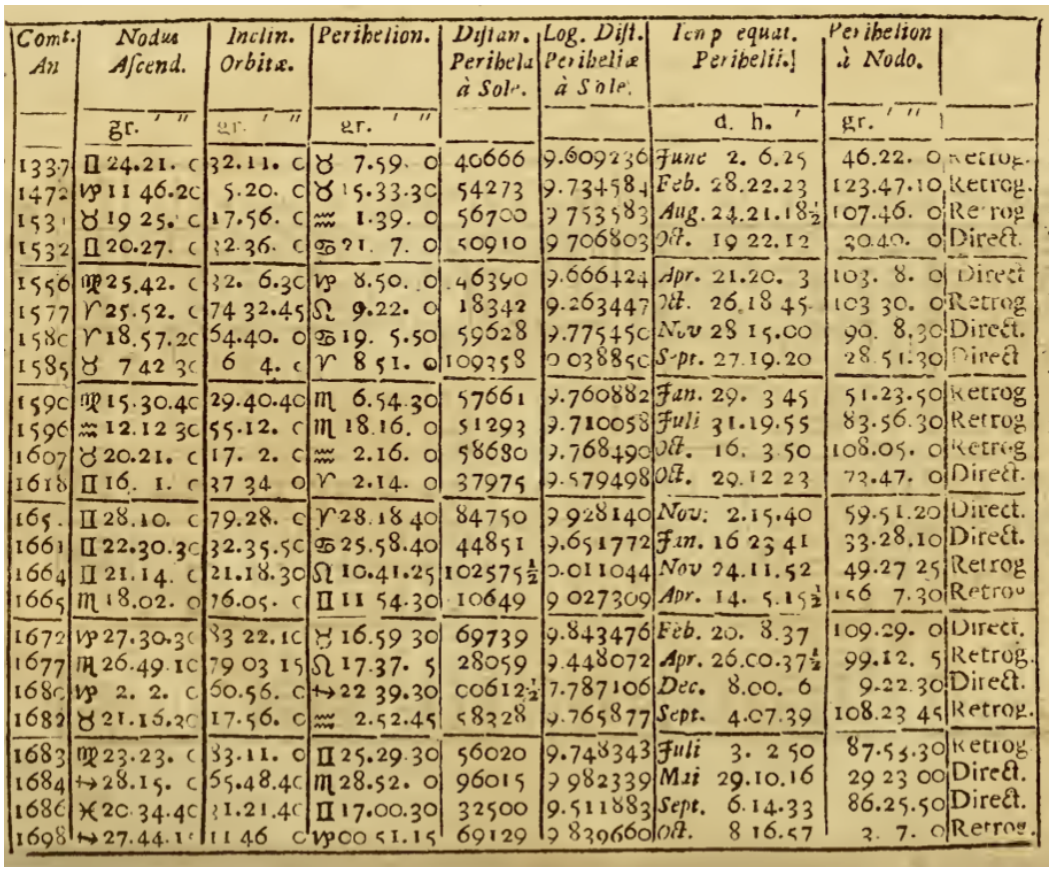

Comt. An	Nodus Ascend.	Inclin. Orbitæ.	Perihelion.	Distan. Perihel. à Sole.	Log. Dist. Perihel. à Sole.	Temp equat. Perihelii.	Perihelion à Nodo.	
	gr. ′ ″	gr. ′ ″	gr. ′ ″			d. h. ′	gr. ′ ″	
1337	♊ 24.21. c	32.11. c	♉ 7.59. 0	40666	9.609236	*June* 2. 6.25	46.22. 0	Retrog.
1472	♍ 11 46.2c	5.20. c	♉ 15.33.3c	54273	9.734584	*Feb.* 28.22.23	123.47.10	Retrog.
1531	♉ 19 25. c	17.56. c	♒ 1.39. 0	56700	9 753583	*Aug.* 24.21.18½	107.46. 0	Retrog
1532	♊ 20.27. c	32.36. c	♋ 21. 7. 0	50910	9 706803	*Oct.* 19 22.12	30.40. 0	Direct.
1556	♌ 25.42. c	32. 6.3c	♍ 8.50. 0	46390	9.666424	*Apr.* 21.20. 3	103. 8. 0	Direct
1577	♈ 25.52. c	74 32.45	♎ 9.22. 0	18342	9.263447	*Oct.* 26.18 45	103 30. 0	Retrog
1580	♈ 18.57.2c	54.40. 0	♋ 19. 5.50	59628	9.775450	*Nov* 28 15.00	90. 8.30	Direct.
1585	♉ 7 42 3c	6 4. c	♈ 8 51. 0	109358	0 038850	*Sept.* 27.19.20	28 51.30	Direct
1590	♌ 15.30.4c	29.40.4c	♏ 6.54.30	57661	9.760882	*Jan.* 29. 3 45	51.23.50	Retrog
1596	♒ 12.12 3c	55.12. c	♏ 18.16. 0	51293	9.710058	*Juli* 31.19.55	83.56.30	Retrog
1607	♉ 20.21. c	17. 2. c	♒ 2.16. 0	58680	9.768490	*Oct.* 16. 3.50	108.05. 0	Retrog
1618	♊ 16. 1. c	37 34 0	♈ 2.14. 0	37975	9.579498	*Oct.* 29.12 23	72.47. 0	Direct.
165.	♊ 28.10. c	79.28. c	♈ 28.18 40	84750	9 928140	*Nov.* 2.15.40	59.51.20	Direct.
1661	♊ 22.30.3c	32.35.5c	♋ 25.58.40	44851	9.651772	*Jan.* 16 23 41	33.28.10	Direct.
1664	♊ 21.14. c	21.18.3c	♎ 10.41.25	102575½	0.011044	*Nov* 24.11.52	49.27 25	Retrog
1665	♏ 18.02. 0	76.05. c	♊ 11 54.30	10649	9 027309	*Apr.* 14. 5.15½	156 7.30	Retrog
1672	♍ 27.30.3c	83 22.1c	♑ 16.59 30	69739	9.843476	*Feb.* 20. 8.37	109.29. 0	Direct.
1677	♏ 26.49.1c	79 03 15	♎ 17.37. 5	28059	9.448072	*Apr.* 26.20.37½	99.12. 5	Retrog.
1680	♍ 2. 2. c	60.56. c	♑ 22 39.30	20612½	7.787106	*Dec.* 8.00. 6	9.22.30	Direct.
1682	♉ 21.15.3c	17.56. c	♒ 2.52.45	58328	9.765877	*Sept.* 4.07.39	108.23 45	Retrog.
1683	♌ 23.23. c	83.11. 0	♊ 25.29.30	56020	9.748343	*Juli* 3. 2 50	87.55.30	Retrog
1684	♑ 28.15. c	55.48.4c	♏ 28.52. 0	96015	9 982339	*Mai* 29.10.16	29 23 00	Direct.
1686	♐ 20.34.4c	31.21.4c	♊ 17.00.30	32500	9.511883	*Sept.* 6.14.33	86.25.50	Direct.
1698	♑ 27.44.1c	11 46 c	♍ 00 51.15	69129	9 839660	*Oct.* 8 16.57	3. 7. 0	Retrog.

Figure 2.2 Edmund Halley's Table of Cometary Orbital Elements.

Edmund Halley computed this table of the orbital elements of the comets from all sufficiently and reliably observed comets. This table, printed in his 1705 publication *Astronomiae Cometicae Synopsis*, shows that the comets of 1531, 1607, and 1682 share the same orbital elements, and are therefore the same object. The units of the table "needs little Explication", except that "the Perihelium Distances, are estimated in such Parts, as the Middle Distance of the Earth from the Sun, contains 100000." (Halley, 1705)

> there are many Things which make me believe that the Comet which Apian observ'd in the Year 1531. was the same with that which Kepler and Longomontanus took Notice of and describ'd in the Year 1607. and which I my self have seen return, and observ'd in the Year 1682. All the Elements agree, and nothing seems to contradict thismy Opinion, besides the Inequality of the Periodick Revolutions: Which Inequality is not so great neither, as that it may not be owing to Physical Causes. For the Motion of Saturn is so disturbed by the rest of the Planets, especially Jupiter, that the Periodick Time of that Planet is uncertain for some whole Days together. How much more therefore will a Comet be subject to such like Errors, which rises almost Four times higher than Saturn, and whose Velocity, tho' encreased by a very little, would be sufficient to change its Orbit, from an Elliptical to a Parabolical one. This, moreover, confirms me in my Opinion of its being the same; that in the Year 1456. in the Summer time, a Comet was seen passing Retrograde between the Earth and the Sun, much after the same Manner: Which, tho' no Body made Observations upon it, yet from its Period, and the Manner of its Transit, I cannot think different from these I have just now mention'd. Hence I dare venture to foretell, That it will return again in the Year 1758. And, if it should then return, we shall have no Reason to doubt but the rest must return too: Therefore Astronomers have a large Field to exercise themselves in for many Ages, before they will be able to know the Number of these many and great Bodies revolving about the common Center of the Sun. (Halley, 1705)

Halley could not have known that the comet he predicted to return (now known as Comet 1P/Halley) has a period so much shorter than the other NICs, nor that the giant planets (Jupiter in particular) do in fact excite incoming comets with highly eccentric

elliptical orbits to hyperbolic escape trajectories. It therefore seemed reasonable to add observed comets to a table and look for the return of previous comets until all the comets are discovered. Nevertheless, his discovery that comets can have elliptical orbits opened up a new avenue for studying the dynamics of comets and comet populations.

All proposed theories of comets generally only attempted to explain the observed motion and behavior of comets, rather than their formation. Immanuel Kant proposed one of the first theories of comet formation. He proposed that the bodies of the Solar System formed through accretion of protoplanetary materials, which were organized such that the densest materials were closer to the Sun, forming denser bodies (Heidarzadeh, 2008 p. 164-168). Further, the resulting bodies followed orbits that became progressively more eccentric with increasing heliocentric distance (Heidarzadeh, 2008 p. 164-168). Thus, in Kant's theory, comets were merely planets that formed from materials beyond Saturn (the most distant known planet at that time) into highly elliptical planetary bodies, an idea that is still recognizable in current theories of comet formation.

In mid-June 1770, a bright new comet was discovered by Charles Messier that passed within 0.015 AU of the Earth, the closest perigee of a comet in recorded history (Stén, 2014 p.86-91). Anders Johan Lexell tried to fit the observations of the orbit to a parabolic orbit, but found that the best fit was of an elliptical orbit with a period of 5.58 years (Stén, 2014 p.86-91). No comet had ever before had such a short orbital period (Stén, 2014 p.86-91). Even more strangely, such a short orbital period suggested that this comet, now known as Lexell's Comet, should have been observed on previous orbits. Although the following apparition of Lexell's comet in 1776 possessed poor viewing geometry, the 1781 apparition had good viewing geometry, but the comet was never

observed (Stén, 2014 p.86-91). Lexell integrated the comet's orbit forward and backward, and determined that the comet had had a close approach with Jupiter, which had reduced the comet's perihelion and rendered the comet visible in 1770 (Laplace, 1824 p. 215). Furthermore, forward integrating the orbit revealed that the comet had had another close encounter with Jupiter in 1779 that had changed its orbit and rendered the comet "forever invisible" (Stén, 2014 p.86-91). Although the comet has never been recovered (Stén, 2014 p.86-91), Lexell's Comet turned out to be the first known member of an entirely new class of comet, the Jupiter Family Comets (JFCs).

In the early 1800's Pierre-Simon Marquis De Laplace realized that the mass of a comet should have gravitationally perturbed the orbits of the Earth and Moon, as well as that of the satellites of Jupiter. While Laplace determined that the Earth had decreased the orbital period of Lexell's Comet by 2 days, he found that the period of the Earth had not changed by a detectable amount (Heidarzadeh, 2008 p. 197-199). Laplace therefore concluded:

> De toutes les comètes observées, celle-ci a le plus approche de la terre qui, par conséquent, aurait dû en éprouver une action sensible, si la masse de cet astre était comparable à celle du globe terrestre. En supposant ces deux masses égales, l'action de la comète aurait accru de 11612'', la durée de l'année sidérale. Nous sommes certains par les nombreuses comparaisons des observations, que MM. Delambre et Burckhardt ont faites pour construire leurs Tables du Soleil, que depuis 1770, l'année sidérale n'a pas augmenté de 3''; la masse de la comète n'est donc pas 1/5000 de celle de la terre, et si l'on considere que cet astre en 1767 et 1779, a traversé le système des satellites de Jupiter, sans y causer le plus léger trouble; on verra qu'elle est moindre encore. La petitesse des masses des

> comètes est généralement indiqueé par leur influence insensible sur les mouvemens du système planétaire (Laplace, 1824 p. 215-216).

Thus, Laplace showed that the mass of Lexell's Comet had to be significantly less than 1/5000th that of the Earth, and therefore has a negligible effect on the motions of the planets and the moons of Jupiter. This unexpected result showed that the comets are not planet-mass objects, but rather they are at most a tiny fraction of a lunar mass (Heidarzadeh, 2008 p. 198). Laplace further concluded that comets must be mostly composed of an extremely rarified atmosphere with only small amounts of condensed material contained within:

> Ces astres que l'on nomme comètes, sont preque toujours accompagnés d'une nébulosité qui en croissant, se termine quelquefois dans une queue d'une grande étendue, et qui doit être d'une rareté extrême; puisque l'on voit les étoiles à travers son immense profondeur. (Laplace, 1808 p. 51)

William Herschel, who was observing nebulae around that time, noted that they have a "resemblance to telescopic comets, however, is very apt to suggest the idea, that possibly such small telescopic comets as often visit our neighbourhood may be composed of nebulous matter" (Heidarzadeh, 2008 p. 190). He later calculated the comet of 1807 to have a coma ~1 million km across with a nucleus less than 1,000 km in diameter (Heidarzadeh, 2008 p. 190), a result consistent with the cometary mass computation of Laplace.

Laplace later speculated on the composition and nature of comets in his work *Exposition du système du monde* by considering the nature of their comae (atmospheres):

> There are bodies which cannot be reduced to a state of fluidity, by the greatest heat which we can produce. There are others which the greatest cold experienced on earth is unable to reduce to a solid State: such are the fluids which compose our atmosphere, and which, notwithstanding the pressure and cold to which they have been subjected, have still maintained themselves in the state of vapours. But their analogy with aeriform fluids, to which we can reduce a great number of substances by the application of heat, and their condensation by compression and cold, leaves no doubt but that the atmospheric fluids are extremely volatile bodies, which an intense cold would reduce to a solid state. To make them assume this state, it would be, sufficient to remove the earth farther from the sun, as it would be sufficient in order that water and several other bodies should enter into our atmosphere, to bring the earth nearer to the sun. These great vicissitudes take place in the comets, and principally on those which approach very near to the sun in their perihelion. The nebulosities which surround them, being the effect of the vaporisation of fluids at their surface, the cold which follows ought to moderate the excessive heat which is produced by their proximity to the sun; and the condensation of the same vaporised fluids when they recede from it, repairs in part the diminution of temperature, which this remotion ought to produce, so that the double effect of the vaporisation and condensation of fluids, makes the difference between the extreme heat and cold, which the comets experience at each revolution, much less than it would otherwise be. (Heidarzadeh, 2008 p.203)

Thus, Laplace proposed that comets are small, ice-covered bodies that form comae as the nucleus approaches the sun and volatilizes the ices. Although this passage was later removed from all editions of the *Exposition du système du monde* after the 4th edition

(Heidarzadeh, 2008 p.202-203), this model of comets is the first hint of what would later be referred to as the "dirty snowball" model of comet nuclei.

Following in the footsteps of Edmund Halley, Johann Franz Encke computed the orbits of the comets of 1786 I, 1795, 1805, and 1819, and determined that they were all the same comet with a period of 3.3 years (Heidarzadeh, 2008 p. 212). He then ventured to predict the return in 1822 of the comet now known as Comet Encke (Heidarzadeh, 2008 p. 212). Encke was using a new method of computing orbits that had recently been developed by Carl Friedrich Gauss, and his calculations showed that Comet Encke's orbital period was lengthening during each apparition (Heidarzadeh, 2008 p. 212). Encke proposed that this motion was the result of drag with a medium that pervades the Solar System, the æther (Heidarzadeh, 2008 p. 212).

A decade later, Friedrich Bessel was making observations of the 1835 apparition of Comet Halley, when he noticed that the coma was structured, containing what we now call dust jets (Heidarzadeh, 2008 p. 214). He observed that the coma exhibited an enhancement of activity on the sunward side of the nucleus that appeared to oscillate about the sunward axis (Heidarzadeh, 2008 p. 214-215). Bessel deduced that the nucleus of the comet was somehow ejecting material in the direction of the Sun. Furthermore, he deduced that the recoil force from such an ejection pushes the nucleus in the opposite direction "like a burning rocket", which can strongly affect the keplerian motion of the nucleus:

> die Ausströmung des *Halley*'schen Kometen, ohngefähr in der Richtung der Sonne, gab ihm, wie ich schon in der Beschreibung seines Ansehens angeführt habe, das Ansehen einer brennenden Rakete. Sie muss auch dieselbe Wirkung

> auf seine Bewegung gehabt haben, welche das Brennen einer Rakete auf die ihrige hat; sie muss ihm eine, ihrer eigenen entgegengesetzte Geschwindigkeit ertheilt haben. Denn nicht der Schwerpunkt des Kometen selbst, sondern nur der gemeinschaftliche Schwerpunt des Kometen und der Ausströmung, kann, in jedem Augenblicke, eine Kegelschnitt nach den *Kepler*schen Gesetzen beschreiben; da die Ausströmung sich in jedem Augenblicke erneueren, oder sich als eine beschleunigende Kraft zeigen. Der Anblick der Lebhaftigkeit der Ausströmung, oder vielmehr das anscheinende Verhältniss ihrer Masse zu der Masse des Kerns, muss die Meinung erzeugen, dass die daraus hervorgehende störende Kraft der elliptischen Bewegung des Kometen merklich sein könne. (Bessel, 1836)

Thus, Bessel discovered how sublimating volatiles from the surface of comet nuclei affects their dynamical evolution, without invoking the æther.

Bessel then discussed the meaning of this volatile nature of comets in regard to their structure and composition. He argued that comets, unlike the planets, are not solid bodies. He noted that the cores of comets are not opaque, and do not show a clear boundary. Additionally, the small masses of comets, which must somehow fill the very large volume of the comet, is consistent with a warmed vapor heated by the sun:

> Mehrere Beobachter haben frühere Kometen über Sterne hinweggehen sehen und diese nicht aus dem Gesichte verloren. Wenn ein Vorübergang wirklich central gewesen ist und wenn die Atmosphäre des Kometen keine Strahlenbrechung besessen hat, so begründet diese Beobachtung den Schluss, dass der Kern des Kometen kein undurchsichtiger Körper gewesen ist. Ich glaube zwar nicht, dass man die völlige Ueberzeugung hat erlangen können, dass die beobachteten

Bedeckungen central waren; auch bin ich der Meinung, dass die Behauptung der gänzlichen Abwesenheit einer Strahlenbrechung, auf Beobachtungen gegründet werden müsste, durch welche der scheinbare Ort eines Sterns, in noch grösserer Nähe bei dem Mittelpunkte des Kometen bestimmt wird, als durch meine, im vorigen Artikel mitgetheilte Beobachtung der Fall ist. Demohngeachtet aber halte ich für wahrscheinlich, dass der Kern des Kometen kein eigentlich fester Körper ist; d.h. kein fester Körper der Art wie die Erde, der Mond und die Planeten. Er muss in der That leicht in den Zustand der Verflüchtigung übergehen können, während die eben genannten Körper diese Eigenschaft nicht, oder wenigstens in einem geringen Grade besitzen: indem seine Oberfläche keine feste Begränzung zeigt, scheint sie sich in diesem Zustande zu befinden; der fast unbegreiflich grosse Raum, welcher durch die Schweife vieler Kometen gefüllt wird, verbunden mit der wahrscheinlichen äufsersten Kleinheit ihrer Massen, zeigt gleichfalls, dass die Materie der Kometen die Eigenschaft erlangt, sich unbegrenzt auszudehnen. Allein diese Eigenschaft kann die Masse des Kometen ursprünglich nicht besitzen; wenigstens kann sie keine Materie sein, welche keine Dichtigkeit hat, wenn sie keinen Druck erleidet, denn seine solche Materie würde sich offenbar gänzlich zerstreuen. Ich sehe aber keine Schwierigkeit der Annahme, dass die Kometen aus Theilen bestehen, welchen nur noch wenig and der Wärme, oder einer anderen repulsirenden Eigenschaft fehlt, welche sie besitzen müssen um flüchtig zu werden. Dass die Verflüchtigung sich an dem der Sonne gerade zugewandten Theile der Oberfläche am frühesten zeigt, auch dass sie sich durch grössere Annäherung an die Sonne und durch längere Dauer ihrer Wirkung vermehrt und über einen, immer grösser werdenden Theil der Oberfläche erstreckt, ist nach dieser Ansicht zu erwarten, so wie auch mit den

> Beobachtungen übereinstimmend. Dass die Verflüchtigung, durch den mit ihr verbundenen Wärmeverlust, das Mittel werden kann, durch welches ein Theil der Kometenmasse vor der Zerstreuung geschützt wird, ist, wenn ich nicht irre, schon von Laplace bemerkt worden. (Bessel, 1836)

A decade after Bessel observed Comet Halley, astronomers anticipated the 1846 return of the third known Jupiter Family Comet, Comet 3P/Biela. Although the comet was discovered by J.L. Montaigne of France (Jenniskens & Vaubaillon, 2007), it was named after Wilhelm von Biela, who was the first to calculate its 6.75 year orbit in 1826 (Jenniskens & Vaubaillon, 2007). Astronomers first spotted Comet Biela as a faint, nebulous object on 26 November 1846 (Heidarzadeh, 2008 p. 217). Further observations soon revealed that the comet had fragmented into two separate comets, each with its own tail, and exhibited significant brightening events throughout the apparition (Jenniskens & Vaubaillon, 2007). Additionally, the primary (brighter) fragment appeared to shed further pieces during the apparition (Jenniskens & Vaubaillon, 2007). The two fragments did not appear to exert any significant gravitational influence on one another, in spite of a separation of only ~250,000 km, further evidence that the mass of comets are tiny (Heidarzadeh, 2008 p. 218). The two fragments were again recovered during the following 1852 apparition, but failed to appear at any subsequent apparitions (Heidarzadeh, 2008 p. 219). However, during an 1872 search for the comet, a very prominent and unexpected meteor shower appeared, with a peak intensity of 3000 hr^{-1} (Heidarzadeh, 2008 p. 219). Furthermore, the radiant of the meteor shower was in the constellation Andromeda, along the very path the Comet Biela was expected to follow

(Heidarzadeh, 2008 p. 219). Thus, astronomers realized that comet dust produces meteor showers, and that Comet Biela had fragmented into dust.

In 1858, Comet Donati appeared in the sky, exhibiting three tails, two of which were thin, linear features tangent to the main dust tail (Heidarzadeh, 2008 p. 219). The two thin linear tails, called streamers, are now known to be the result of instantaneous ejections of dust from the nucleus (Sekanina & Kracht, 2014). However, Comet Donati's most novel feature were the shells of material surrounding the head of the nucleus, which expanded with time (Heidarzadeh, 2008 p.220-221). These shells led George Bond to conclude that a dust jet was building up these shells on each revolution of the nucleus as it swept through space (Heidarzadeh, 2008 p. 221), which expanded over time due to momentum. He further realized that this ejection was controlled by the sun (Heidarzadeh, 2008 p. 221), which explained why no section of a shell was visible on the antisunward side of the nucleus (see Figure 2.3). Thus, Comet Donati was the first comet to provide evidence of a rotating nucleus, and strengthened Bessel's observation of cometary dust jets.

A coherent picture of comet tail formation was beginning to emerge. Comet Biela showed that comets can fragment into fine pieces, while Comets Halley and Donati revealed that such materials could be ejected sunward from the head of the nucleus. While Leonard Euler had first suggested that an interaction with Sun's rays could push cometary material antisunward, the mechanics of such an effect was poorly understood.

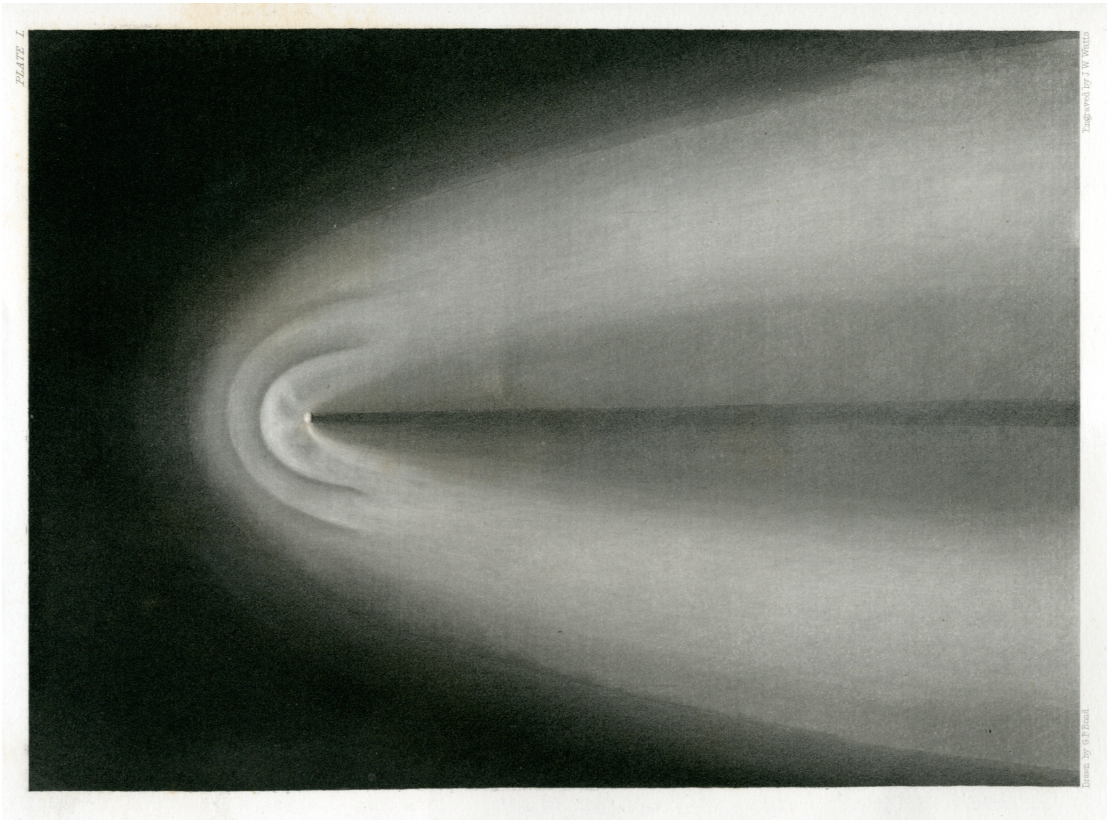

Figure 2.3 Drawing of the Head of Comet Donati by George Bond.

Comet Donati exhibited prominent shells of material that expanded away from the nucleus on the sunward side of the nucleus. This engraving of Comet Donati was sketched by George Bond on 2 October 1858. (Bond & Watts, 1858)

James Clerk Maxwell first described the nature of such a radiation pressure in *A treatise on Electricity and Magnetism*, the same work in which he described the fundamental equations of electromagnetism:

> ...the combined effect of the electrostatic and the electrokinetic stresses is a *pressure*[…] in the direction of the propagation of the wave.[...] Hence in a medium in which waves are propagated there is a pressure in the direction normal to the waves, and numerically equal to the energy in unit of volume. (Maxwell, 1954 p. 440-441)

He further quantified the magnitude of this pressure based on his newly-developed "Maxwell's Equations" of electricity and magnetism (Maxwell, 1954 p. 440-441).

Shortly thereafter, William Crookes showed qualitatively that radiation has the expected repulsive effect. He used the newly-invented Sprengel Pump, which consists of drops of mercury falling through a narrow tube, trapping bubbles of air to be evacuated from the system, and removes it from the system as it reaches the bottom of the tube (Sprengel, 1865). Crookes found that the Sprengel pump could just barely get the test apparatus to the required "evacuation", and used chemical absorption of the remaining gases to further reduce the pressure of his test chamber (Crookes, 1874). In his evacuated chamber, he constructed a balance out of straw, which he experimentally determined to be the most ideal material available, attached two weights made of pith, and balanced the apparatus by charring the ends of the straw until the system reached equilibrium (Crookes, 1874). He then experimented with light and heat, and found that both always repelled the mass, which a piece of ice attracted it (Crookes, 1874). Lastly, he experimented with sunlight scattered through a prism, and found that "extreme visible

red" produced the strongest effect (Crookes, 1874). Crookes concluded by discussing the possible application of radiation pressure to unsolved problems in celestial mechanics:

> In the sun's radiation passing through the quasi vacuum of space we have the radial repulsive force, possessing successive propagation, required to account for the changes of form in the lighter matter of comets and nebulæ; and we may learn by that action, which is rapid and apparently fitful, to find the cause in those rapid bursts which take place in the central body of our system; but until we measure the force more exactly we shall be unable to say how much influence it may have in keeping the heavenly bodies at their respective distances. (Crookes, 1874)

Later, Svante Arrhenius used Maxwell's theory to calculate that comet dust must be ~1 μm across for radiation pressure to balance solar gravity (and therefore significantly affect dust motions), and Karl Schwarzschild computed that the solar radiation pressure can be up to 20 times stronger than solar gravity (Heidarzadeh, 2008 p. 229-230). Finally, the strength of radiation pressure on 1 μm grains was confirmed experimentally by Ernest Nichols and Gordon Hull (Heidarzadeh, 2008 p.230). Thus, the formation of cometary dust tails was largely understood.

Meanwhile, the developing techniques of spectroscopy started being applied to comet observations in the mid-19th century. Arthur Wright identified CO and CO_2 gases trapped inside a freshly-fallen meteorite, and later passed an arc through this sample and noted that three bright spectral lines were produced, which matched the spectral bands of comets (Heidarzadeh, 2008 p. 234). Thus, Arthur Wright identified two of the three most prevalent volatile species present in comets. Later, W.A. Norton used the recent

experimental and theoretical results of Michael Faraday and Claude Servais Mathias Pouillet to conclude that CO_2 exists in a condensed phase on the surface of comet nuclei (Heidarzadeh, 2008 p. 234). In the 1940's, Polydore F. Swings discovered that H_2O was also present in comets (Heidarzadeh, 2008 p. 238), and is now known to be the most abundant cometary volatile ice. Spectroscopy also uncovered many other, more minor volatile species generally composed of the elements Carbon, Hydrogen, Oxygen, and Nitrogen (or CHON) (Bockelée-Morvan et al. 2004).

While the composition of comets was now being understood through spectroscopy, the structural nature of comets was still poorly understood. Some believed that comets were merely coherent collections of dust in mutual orbits about the Sun (e.g. Lyttleton, 1948) (so-called "sandbank" model), an idea that seemed consistent with cometary meteor streams and the fragility of splitting comets (Whipple, 1961). However, Whipple (1961) convincingly demonstrated that, were one to consider the surface area required to reflect the observed quantity of light toward the observer, and then considered the thickness of a coating of volatiles that would be required to cover this surface area to produce the observed quantities of volatiles leaving a comet (he focused specifically on the CO^+ ion in particular), the "dust" would need to be coated in at least a meter of ice, and therefore a comet cannot be primarily composed of dust (Whipple, 1961). Whipple then showed that these sandbank models are at least two orders of magnitude too low in their predicted gas-to-dust ratios compared to observations (Whipple, 1961). Whipple also pointed out that sandbank models cannot explain the secular changes in the motions of comets, are inconsistent with sungrazing comets, whose close approaches would

vaporize any grain smaller than 30 cm, and that some tensile strength is required for a comet to survive tidal breakup (Whipple, 1961).

Fred Whipple proposed an icy conglomerate model of comets (commonly known as the "dirty snowball" model) in two seminal papers (Whipple, 1950; 1951), in which a comet contains a small solid nucleus of ice and dust a few kilometers across. He showed that, as these nuclei sublimate, the escaping gases carry away dust and form a coma (Whipple, 1950). Additionally, he showed that the reaction force from sublimating gases can account for the secular motion of comets Encke, d'Arrest, and Wolf 1 (Whipple, 1950). Finally, an icy conglomerate continuously refreshes both the gas and "meteoric" materials in the nucleus, accounting for the observed gas-to-dust ratios (Whipple, 1951).

Whipple's icy conglomerate model of comets was proven correct when the Giotto spacecraft imaged the nucleus of Comet Halley in 1986 (Keller, 1986). The nature of comets was finally known. Over the following three decades, spacecraft would investigate another five comet nuclei *in situ*, all of which are Jupiter Family Comets: 19P/Borrelley, 9P/Tempel 1, 81P/Wild 2, 103P/Hartley 2, and 67P/Churyumov-Gerasimenko.

In the middle of the twentieth century, astronomers were beginning to devote significant effort to understand the reservoirs of the comets. Although Edmund Halley first noted the parabolic shapes of comet orbits and speculated that a large number of comets exists at great heliocentric distance (Halley, 1705), Jan Oort first studied the distance to these comets. He noted that Long-Period comets typically have aphelia between 50,000 AU and 150,000 AU, and noted that very few have aphelia smaller than 10,000 AU, and noted that these distances denote the inner and outer radii of "a general

cloud of comets" surrounding the Sun (Oort, 1950). Oort proposed that his eponymous Oort Cloud was formed from objects scattered by Jupiter to great heliocentric distance (Oort, 1950). Later, it was proposed that the Oort cloud formed from icy planetesimals that were scattered to large heliocentric distance during migration of the giant planets (a.k.a. the Nice Model) (Gomes et al. 2005; Morbidelli et al. 2005; Tsiganis et al. 2005).

Meanwhile, Fred Whipple noted the similarity in composition of comets with Uranus and Neptune, and proposed the existence of a belt of comets beyond the orbit of Neptune akin to the asteroid belt between Mars and Jupiter (Whipple, 1964). This belt is named after Gerhard Kuiper (the Kuiper Belt), even though Kuiper ironically predicted that such a belt would be dynamically unstable and should therefore not exist (Kuiper, 1951). Later, it was proposed that a separate population of comets scattered outward by Neptune during planet migration (Gomes et al. 2008) have been slowly leaking into the giant planet region of the Solar System on billion-year timescales (Duncan & Levison, 1997). These comets then migrate through the giant planet region on timescales of ~10 million years before entering the Jupiter Family of Comets (Duncan & Levison, 1997).

Thus, the general structure, composition, dynamics, and origin of the comets became known by the time I began graduate school.

References

Aristotle; *Meteorology*. Translated 1952, Webster, E.B. (350a B.C.E.)

Aristotle, *On the Heaven.* Translated 1922, Stocks, J.L. (350b B.C.E.)

Bessel, F.W.; Beobachtungen über die physische Beschaffenheit des *Halley*'schen Kometen und dadurch veranlasste Bemerkungen. *Astronomische Nachrichten* **13**, 184-232 (1836)

Bockelée-Morvan, D.; Crovisier, J.; Mumma, M.J.; Weaver, H.A.; "The Composition of Cometary Volatiles" In *Comets II*, Editors: Festou, M.; Keller, H.U.; Weaver, H.A. University of Arizona Press: Tucson, AZ, p. 391-423 (2004)

Bond, G. P.; Watts, J.W.; *An Account of Donati's Comet of 1858*. Sketch by Bond, G.P., engraved by Watts, J.W. 1858. retrieved from University of Cambridge online repository on 22 October 2015. https://www.repository.cam.ac.uk/handle/1810/219106

Crookes, W.; On Attraction and Repulsion Resulting from Radiation. *Philosophical Transactions Royal Society London* **164**, 501-527 (1874)

Duncan, M.J. & Levison, H.F.; A disk of scattered icy objects and the origin of Jupiter-family comets. *Science* **276**, 1670-1672 (1997)

Gingerich, O.; Tycho Brahe and the Nova of 1572. *ASP Conference Series* **342** (2005)

Gomes, R., Levison, H.F., Tsiganis, K., Morbidelli, A. Origin of the cataclysmic Late Heavy Bombardment period of the terrestrial planets. *Nature* **435**, 466-469 (2005)

Gomes, R.S. et al. "The Scattered Disk: Origins, Dynamics, and End States" in *The Solar System Beyond Neptune*. Editors: Barucci, M.A.; Boehnhardt, H.; Cruikshank, D.P.; Morbidelli, A. University of Arizona Press: Tucson, AZ. p. 259-273 (2008)

Halley, E.; A Synopsis of the Astronomy of Comets. *Philosophical Transactions* **24**, 1882-1899. Translated from original: Astronomiae Cometicae Synopsis. Printed for John Senex. (1705)

Heidarzadeh,T. A history of Physical Theories of Comets, from Aristotle to Whipple. *Archimedes: New Studies in the History of Science and Technology* **19**. Springer Science + Business Media. (2008)

Jenniskens, P. & Vaubaillon, J.; 3D/Biela and the Andromedids: Fragmenting versus Sublimating Comets; *AJ* **134**, 1037-1045 (2007)

JPL Solar System Dynamics - comet orbital elements. http://ssd.jpl.nasa.gov/dat/ELEMENTS.COMET. retrieved 16 October 2015

Keller, H.U. et al. First Halley Multicolour Camera imaging results from Giotto. *Nature* **321**, 320-326 (1986)

Kuiper, G.P. "Origin of the Solar system" in *Astrophysics: A Topical Symposium*. editor: Hynek, J.A. New York: McGraw-Hill (1951)

Lyttleton, R.A. Comets and their origin. *MNRAS* **108**, 465 - 475 (1948)

Lowry, S.; Fitzsimmons, A.; Lamy, P.; Weissamn, P.; "Kuiper Belt Objects in the Planetary Region: The Jupiter-Family Comets" in *The Solar System Beyond Neptune* Editors: Barucci, M.A.; Boehnhardt, H.; Cruikshank, D.P.; Morbidelli, A.. University of Arizona Press: Tucson, AZ (2008) p. 397-210

Laplace, P.S., marquis de. *Exposition du Système du Mond*. 3rd ed. Paris. (1808)

Laplace, P.S., marquis de. *Exposition du Système du Monde*. 5th ed. Bachelier: Paris (1824)

Maxwell, J.C.; *A Treatise on Electricity and Magnetism*. vol 2. 3rd edition. Dover Publications: New York (1954)

Morbidelli, A., Levison, H.F., Tsiganis, K., Gomes, R. Chaotic capture of Jupiter's Trojan asteroids in the early Solar System. *Nature* **435**, 462-465 (2005)

Newton, I. *Philosophiæ Naturalis Principia Mathematica*. vol 3. 3rd edition. 1726. Translated into English by Andrew Motte 1729. Printed by Benjamin Motte: London (1726)

Oort, J.H. The structure of the cloud of comets surrounding the solar system, and a hypothesis concerning its origin. *BAN* **11**(408), 91- 110 (1950)

Pemberton, H. *A view of Sir Isaac Newton's philosophy*. London: Printed by S. Palmer. p. 238-239 (1728)

Sekanina, Z. & Kracht, R.; disintegration of Comet C/2012 S1 (ISON) shortly before perihelion: evidence from independent data sets. *arXiv* 1404.5968v6 (2014)

Sprengel, H. Researches on the Vacuum. *Journal Chem. Society London* **18**, 9-21 (1865)

Stén, J. C.-E.; A Comet of the Enlightenment: Anders Johan Lexell's Life and Discoveries. Edited by Martin Matmüller. Springer International: Switzerland (2014)

Thorndike, L.; Albumasar in Sadan. *Isis* **45**, (1954)

Tsiganis, K., Gomes, R., Morbidelli, A., Levison, H.F. Origin of the orbital architecture of the giant planets of the Solar System. *Nature* **435**, 459-461 (2005)

Verne, J. *Hector Servadac*. published by P.-J. Hetzel, 1877

Whipple, F.L. A comet model I. the acceleration of Comet Encke. *ApJ* **111**, 375-394 (1950)

Whipple, F.L. A comet model II. Physical relations for comets and meteors. *ApJ* **113**, 464-474 (1951)

Whipple, F.L. Problems of the cometary nucleus. *AJ* **66**(8), (1961)

Whipple, F.L. Evidence for a comet belt beyond Neptune. *PNAS* **51**(5), 711-718 (1964)

Whiston, W., *A New Theory of the Earth, from its Original, to the Consummation of All Things, Where the Creation of the World in Six Days, the Universal Deluge, And the General Conflagration, As laid down in the Holy Scriptures, Are Shown to be perfectly agreeable to Reason and Philosophy*, 6th edition, London: printed for J. Whiston and B. White. (1755)

Yeomans, D.K.; Great Comets in History. http://ssd.jpl.nasa.gov/?great_comets. (2007) retrieved 16 October 2015.

"200 degrees in the sunlight, minus 200 in the shade, canyons of razor-sharp rock, unpredictable gravitational conditions, unexpected eruptions..."

"...That's all you gotta say, scariest environment imaginable"

-Armageddon (1998)

CHAPTER 3. SUBLIMATION PRESSURE

Sublimation is a defining process of comet nuclei. The release of volatile gases generates a momentum flux (units of pressure) that pushes nuclei, leading to non-keplerian motion of the comet. Despite the importance of this process, methods to compute the magnitude of this reaction pressure have been limited to empirical fits of volatile sublimation experiments, which are only available for some cometary volatiles. I develop a theoretical model of volatile sublimation that requires significantly less empirical data to accurately model volatile sublimation.

I then devise a novel model of cometary disruption, in which sublimative momentum flux induces differential stresses within the nucleus. If these stresses exceed the material strength of the nucleus, it will undergo brittle failure and fragment. I then show that this model is consistent with the fragmentation of Comet C/2012 S1 (ISON). Through this model, I estimate the strength of Comet ISON's nucleus to be 0.2-0.5 Pa, ad the strength of the resulting fragments to be 0.6-9 Pa.

The following manuscript was published in *Icarus* (volume 258, p. 430-437) in 2015 as "Dynamic sublimation pressure and the catastrophic breakup of Comet ISON", coauthored by Brandon C. Johnson, Timothy Bowling, H. Jay Melosh, David Minton, Carey M. Lisse, and Karl Battams.

3.1 Introduction

On November 12, 2013 sungrazing comet C/2012 S1 (ISON) unexpectedly disrupted into fragments. This occurred at a heliocentric distance of 145 solar radii ($R_\odot$) (0.68 AU), prior to reaching perihelion (Combi et al. 2014; Boehnhardt et al. 2013; Steckloff et al. 2015). Subsequent disruption events occurred on November 21 and 26 at 88 $R_\odot$ (0.41 AU) and 36 $R_\odot$ (0.17 AU) respectively (Knight & Battams, 2014; Steckloff et al. 2015). While there is nothing seemingly special about these heliocentric distances, currently known sungrazing comet disruption mechanisms seem inadequate to explain ISON's demise. ISON's disruptions occurred much too far from the Sun to have been caused by ablation or chromospheric impact, which disrupt nuclei within a heliocentric distance (q) of 1.01 $R_\odot$ (Brown et al. 2011). Tidal stresses can disrupt the nucleus only within the fluid Roche Limit (q < ~2 $R_\odot$) (Knight & Walsh, 2013). Additionally, ISON's effective radius of ~600-700 m (Delamere et al. 2013; Lamy et al. 2014) was too large to have lost all its ice through complete sublimation and then disintegrated, a process that may only disrupt nuclei less than ~200-350 m in radius (Knight & Walsh, 2013; Sekanina, 2003). Finally, ISON's 10.4 hour rotation period at 210 $R_\odot$ on November 1 (Lamy et al. 2014) was too long for nongravitational torques to spin the body up to

fragmentation (~2.2 hour period) (Pravec et al. 2006) by the time it reached 145 $R_{\odot}$ less than 2 weeks later on November 13 (Samarasinha & Mueller, 2013). However, it has been implied that sublimating gases are linked to the disruption of sungrazing comets (Sekanina 2003). Here we introduce a new break-up mechanism that readily explains Comet ISON's series of disruptions.

As illustrated in Figure 3.1, gas sublimating on the sunward side of the nucleus transfers momentum to the nucleus, exerting a dynamic sublimation pressure on its illuminated hemisphere. The sublimation pressure on the surface generates differential stresses within the nucleus that may exceed ISON's material strength, ultimately disrupting the comet into fragments (Brown et al. 2011; Borovička et al. 2013). Based on the timing of disruption events we can estimate the bulk unconfined crushing strength of Comet ISON's nucleus.

3.2 Theory/calculation

Investigating our proposed disruption mechanism requires an accurate computation of the sublimation pressure (itself a function of both thermal gas velocity and mass loss rate) acting at the surface of the nucleus as a function of heliocentric distance. Previous computations of cometary sublimation rely heavily upon either empirical fits to observed volatile mass loss rates (e.g. Marsden et al. 1973; Cowan & A'Hearn 1979; Sekanina, 1992), or on the theoretical dependence of mass loss rates on temperature (Delsemme & Swings, 1952) rather than the dependence of sublimation pressure on heliocentric distance. We choose instead to construct a versatile thermodynamic model of the sublimation pressure acting upon a cometary surface. In our

calculations, the heliocentric dependence of the sublimation pressure of a particular volatile species is fully described by six known quantities: heliocentric distance (r_{helio}), molar mass (m_{molar}), heat of sublimation (L), sublimation coefficient (α) and a laboratory measurement of vapor pressure (P_{ref}) at a known temperature (T_{ref}).

Comets consist of intimate mixtures of refractory materials (silicates, metal sulfide dust, organics) and volatile ices (primarily H_2O, CO_2, and CO [Bockleé-Morvan et al. 2004]). The phase-change behavior of mixtures of volatiles can be significantly more complicated than that of a single, pure volatile species. In particular, if cometary CO is mostly trapped within amorphous H_2O ice, then the release of significant quantities of CO may require the amorphous H_2O ice to crystallize (Bar-Nun et al. 2013), which is a highly exothermic and potentially explosive phase transition (Mastrapa et al., 2013). Moreover, the presence of amorphous ice in comets is contentious (Lisse et al. 2013). However, Comet ISON's CO content is only a few percent of its H_2O content (Weaver et al., 2014) and produced an order of magnitude less CO_2 than H_2O (McKay et al. 2014). Therefore, we may assume that the sublimation pressure acting on Comet ISON's surface is dominated by the sublimation of pure H_2O ice, which avoids the complications of the sublimation of mixed materials and species more volatile than H_2O ice. However, we include the cases in which pure CO_2 and CO ice sublimates for the sake of comparison, which admittedly ignores the complications of how one would trap significant quantities of CO ice in the first place.

Typical bond albedos measured for Jupiter Family Comet (JFC) nuclei are very low (0.03-0.06) (Li et al. 2013a; Li et al. 2013b; Capaccioni et al. 2015), and when JFCs approach the Sun, most of the incident radiation (94-97%) is absorbed at the surface and

drives the sublimation of volatile ices (an active comet's dominant cooling mechanism). We explore the case in which Comet ISON's albedo is similar to that of JFCs, and assume that all incident radiation is absorbed (bond albedo of 0). However, because dynamically new comets have never been thermally processed by the Sun, it is plausible that their surfaces are significantly richer in ices than JFCs, which could lead to a much higher albedo. Moreover, there are no high-resolution observations of dynamically new comet nuclei, which would constrain their albedos. We therefore also explore the case in which Comet ISON has a bond albedo of 0.5, which is similar to that of the dwarf planet Pluto.

Observations of JFC nuclei suggest that cometary thermal inertia is very low (Gulkis et al. 2015; Davidsson et al. 2013; Groussin et al. 2013; Lisse et al. 2005; Lamy et al. 2008), meaning that little daytime heat is stored by the surface to be later released when it rotates into night. This naturally explains their highly asymmetric dayside-nightside distribution of sublimating gases (Feaga et al. 2007; Gulkis et al. 2015). Similarly, Comet ISON's activity is concentrated on its illuminated hemisphere (Li et al. 2013c). Since cometary activity is driven by volatile sublimation, we assume that effectively all volatile emission occurs on Comet ISON's illuminated hemisphere, causing a sublimation pressure that only acts on the illuminated parts of its nucleus. Indeed, it has been known for decades that nongravitational forces push predominantly on the sunward hemispheres of comet nuclei (Marsden et al. 1973). While observations show that the unilluminated side of comet nuclei can emit volatiles, emission on the unilluminated side is usually less than half of the emission of the illuminated side (Feaga

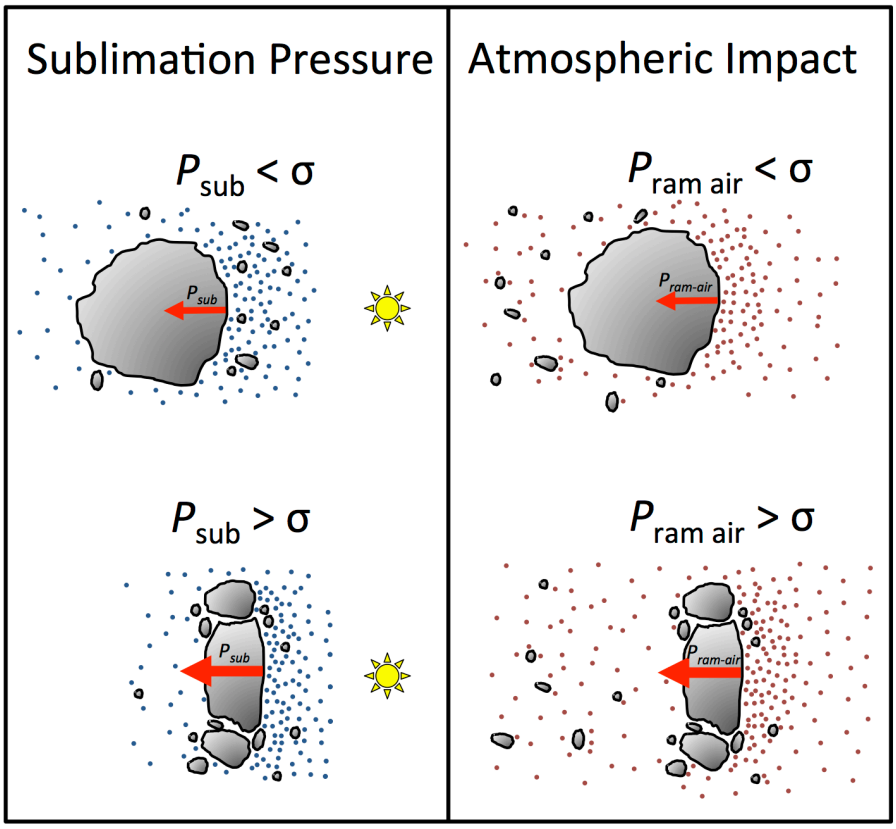

Figure 3.1 Schematic of Dynamic Sublimation Pressure Disruption Mechanism and Comparison to Atmospheric Impact.

(Left) We assume that the dynamic pressure is zero on the dark side of the nucleus, while the peak dynamic pressure on the illuminated side (P_{sub}) becomes comparable to the unconfined static crushing strength of the nucleus (σ). When P_{sub} exceeds σ, the nucleus disrupts catastrophically. (Right) This is analogous to the nucleus impacting a planetary atmosphere. A ram pressure (P_{ram}) builds up on the leading edge of the nucleus as it travels through the atmosphere. If P_{ram} exceeds σ, then the nucleus breaks up into fragments (Borovička et al. 2013).

et al. 2007; Gulkis et al. 2015). Therefore, our sunward emission assumption is valid for our purpose of obtaining an order of magnitude estimate of ISON's strength.

While the nuclei of highly thermally evolved comets (like JFCs) emit dust and gas from only a small fraction of their surfaces (Ververka et al. 2013, Samarasinha & Mueller, 2013), ISON's high H_2O production rate prior to disruption suggests that nearly the entire surface of its nucleus was active (Combi et al. 2014), consistent with a thermally primitive, dynamically new comet. This implies that volatile ices are located within the thermal skin depth of the comet's surface. We therefore assume that volatile ices sublimate from the entire illuminated surface of ISON, and that a negligible amount of incident solar energy is thermally radiated into space from a mantle of material covering the volatile ices.

The dynamic pressure exerted by sublimating volatiles on the surface of the nucleus is equal to the momentum flux of the departing material, and is computed by multiplying the volatile's mass flux by its thermal velocity. Assuming that volatile ices are at or near the surface, we estimate Comet ISON's volatile mass flux by equating the absorbed solar energy to the energy required to sublime each ice species, as first described by Fred Whipple (Whipple, 1950). We assume that volatile ices and refractory materials are intimately mixed, such that heat is rapidly transferred from refractory materials to volatile ices. We ignore the amount of energy required to warm the ices from their initial low temperatures (perhaps 10 K for dynamically new comets such as ISON) to the equilibrium sublimation temperature. Such heating consumes less than ~10%, ~25%, and ~25% of the total incident solar energy for H_2O, CO_2, and CO ice respectively, and is therefore negligible for our order of magnitude estimates. For

simplicity, we treat each volatile species individually, while acknowledging that multiple species may sublime simultaneously from different depths below the surface.

3.2.1 Computing Mass Flux, Force, Temperature, and Sublimation Pressure

The incident solar radiation intensity at the location of the comet is given by

$$I_{solar} = \frac{L_{solar}}{4\pi r_h^2} \tag{3.1}$$

where L_{solar} is the solar luminosity (3.846 x 10^{26} W), and r_h is the heliocentric distance. We assume that all solar radiation incident upon an area element of the surface of the nucleus (dA) is used to overcome the latent heat of sublimation of these volatile ices (Whipple, 1950) to determine each species' mass flux

$$\dot{m} = (1 - A)\frac{I_{solar}}{\lambda(T)}\cos\phi = (1 - A)\frac{L_{solar}}{4\pi r_h^2 \lambda(T)}\cos\phi \tag{3.2}$$

where A is the albedo of the sublimating surface, $\lambda(T)$ is the temperature-dependent latent heat of sublimation of a volatile ice species and ϕ is the angle between the comet-Sun line and the vector normal to the area element (local phase angle). For a sphere, ϕ is equivalently the azimuth angle of the area element from the subsolar point. While the latent heat of sublimation for water is temperature-dependent, it varies so little over the temperature range of interest (Feistel & Wagner, 2007) that treating it as a constant makes a negligible difference in our results. We therefore assume that the latent heat of sublimation is a constant.

We determine the thermal velocity of the dominant sublimating volatile using the kinetic theory of gases. We assume that the speeds of sublimating gas molecules obey a

Maxwell-Boltzmann distribution, where the mean of the magnitude of the molecule velocities escaping from a given area element (dA) is

$$v_{thermal} = \sqrt{\frac{8RT}{\pi m_{mol}}} \tag{3.3}$$

where m_{mol} is the molar mass of the species, T is the gas temperature, and R is the ideal gas constant. The gas diffusing through the cometary pores has a Knudsen number of Kn~10^2-10^5, which allows us to assume that the sublimating volatile molecules are sufficiently rarefied to be emitted from a porous regolith according to Lambert's cosine law (Gombosi, 1994, pp. 227-230). Thus, the number of molecules emitted in a particular direction from an area element ($d\dot{N}(\theta)$) is proportional to the cosine of the angle of that direction with respect to the vector normal to that area element

$$d\dot{N}(\theta) = \frac{\dot{N}_{dA}}{\pi}\cos\theta \tag{3.4}$$

where $\dot{N}_{dA}$ is the number flux of molecules through area element dA, and θ is the angle made with the vector normal to area element dA. We compute the net force on a given area element from sublimating gas molecules by multiplying this particle density distribution by both $v_{thermal}$ and the mass of a particle, and then integrate over all solid angles. Since the particle density distribution depends solely on the angle with respect to the vector normal to the area element, this computation is axisymmetric. Thus, the components of the force tangential to the surface of area element dA cancel out, allowing us to consider only the component of the force normal to the surface. Integrating over all solid angles above the ground

$$F_{element} = \frac{2}{3}\, v_{thermal}\, \dot{m}\, dA \tag{3.5}$$

and the mass flux from the area element ($\dot{m}$) is

$$\dot{m} = \frac{m_{molar}}{N_{av}} \frac{\dot{N}_{dA}}{dA} \tag{3.6}$$

where m_{molar} is the molar mass of the sublimating gas and N_{av} is Avogadro's constant. Combining equations (3.2), (3.3), and (3.5)

$$F_{element} = \frac{2}{3}(1 - A)\frac{L_{solar}}{4\pi r_h^2 \lambda}\sqrt{\frac{8RT}{\pi m_{mol}}}\cos\phi \, dA \tag{3.7}$$

We compute the appropriate temperature (T) in Equation (3.7) by joining the Langmuir-Knudsen (Langmuir, 1913) equation of sublimation rates with the Clausius-Clapyron relation of equilibrium partial pressure and temperature of an ideal gas

$$\dot{m} = \alpha(T)\sqrt{\frac{m_{mol}}{2\pi RT}}P(T) \tag{3.8}$$

$$\frac{dP}{dT} = \frac{P}{T^2}\frac{\lambda}{R} \tag{3.9}$$

where $\alpha(T)$ is the temperature-dependent sublimation coefficient (e.g. Gundlach et al. 2011) and $P(T)$ is the temperature-dependent partial pressure of the molecular species, which results in the following expression for the temperature as a function of the mass flux:

$$\dot{m} = \alpha(T)\sqrt{\frac{m_{mol}}{2\pi RT}}P_{ref}e^{\frac{\lambda}{R}\left(\frac{1}{T_{ref}}-\frac{1}{T}\right)} \tag{3.10}$$

where P_{ref} and T_{ref} are an experimentally measured reference pressure and temperature of the species. We use the empirical fit to the temperature dependence of the sublimation coefficient $\alpha(T)$ for H_2O from Gundlach et al. (2011), which produces a small improvement in the computation of water's sublimation pressure over setting the

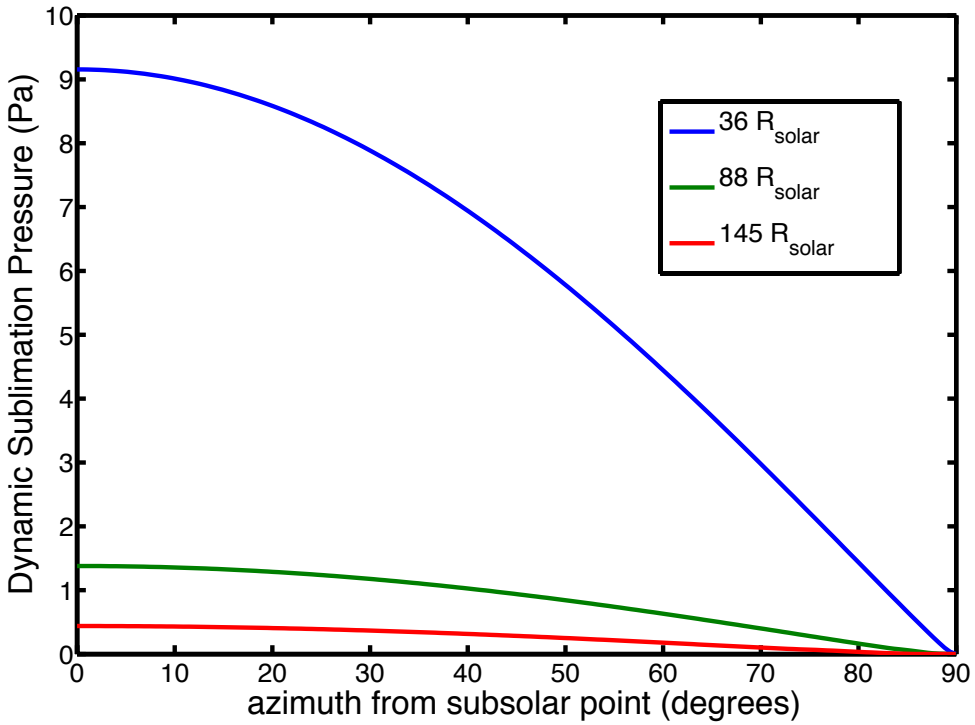

Figure 3.2 Azimuthal Dependence of Dynamic Sublimation Pressure

A plot of the azimuthal dependence of the dynamic sublimation pressure for three separate heliocentric distances for the case of a bond albedo of 0. Azimuthal angle is the angle between the subsolar point and the vector normal to the surface of an idealized, spherical nucleus. While the real nucleus is not necessarily spherical, it will have a subsolar point and a limb, where the dynamic sublimation pressures will be at a maximum and zero respectively. The differential stress that results from this pressure difference is ultimately responsible for fragmenting the nucleus.

sublimation coefficient to 1. We set the sublimation coefficient $\alpha(T)$ for all other species to 1. Combining equations (3.2) and (3.10)

$$(1-A)\frac{L_{solar}}{4\pi r_h^2 \lambda}\cos\phi = \alpha(T)\sqrt{\frac{m_{mol}}{2\pi RT}}P_{ref}e^{\frac{\lambda}{R}\left(\frac{1}{T_{ref}}-\frac{1}{T}\right)} \tag{3.11}$$

Note that this is a transcendental equation, which does not have an analytical solution. Thus, we solve for this temperature numerically. Lastly, since pressure is a force applied over an area, we rearrange equation (3.7) to describe the dynamic sublimation pressure exerted on the surface of a nucleus

$$P_{sub}(r_h,\phi) = \frac{2}{3}(1-A)\frac{L_{solar}}{4\pi r_h^2 \lambda}\sqrt{\frac{8RT}{\pi m_{mol}}}\cos\phi \tag{3.12}$$

We approximate a comet as a sphere, and plot the dependence of the dynamic sublimation pressure on the azimuth from the subsolar point (ϕ) for the sublimation of H_2O at heliocentric distances of 36 $R_\odot$, 88 $R_\odot$, and 145 $R_\odot$ (see Figure 3.2).

3.2.2 Differential Stress

Computing differential stresses with ISON's nucleus is essential to our analysis, because differential stresses can lead to its disruption. A compressive differential stress will cause a brittle material to deform, but the material will remain intact deforming elastically as long as the differential stress remains below the material's strength. However, when the differential stress exceeds a brittle material's strength, the material will fail and fracture. In the case of a comet, when the dynamic sublimation pressure causes material failure, the nucleus will subsequently fragment.

Because the sublimation pressure drops to zero at a 90-degree azimuth from the subsolar point (the limb of the nucleus) and remains near zero on the unilluminated side,

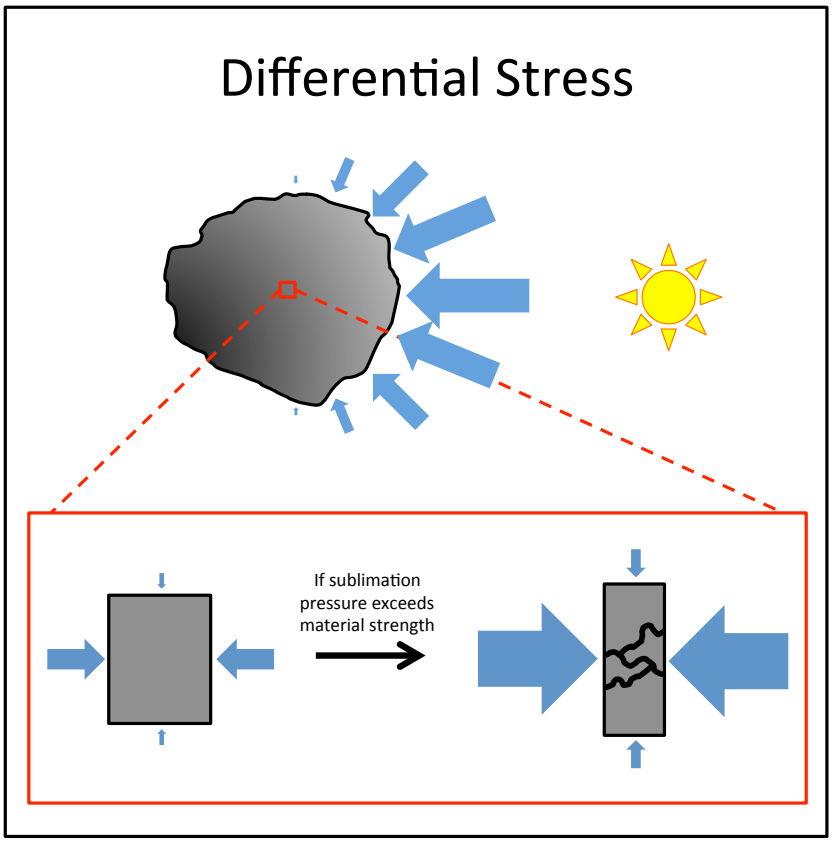

Figure 3.3 Schematic of how Sublimation Pressure Induces Differential Stresses.

(top) dynamic sublimation pressure acts upon the sunward hemisphere of the nucleus. Sublimation pressure peaks at the subsolar point, but drops off to zero toward the limb. As the nucleus approaches the Sun, the sublimation pressure increases. (bottom inset) We illustrate the stresses acting on a parcel of material within the nucleus after subtracting off the hydrostatic pressure. The distribution of the sublimation pressure acting on the surface of the nucleus induces unequal stresses on the parcel of material, with stresses greatest along the comet-Sun axis. As the nucleus approaches the Sun, the stresses on the parcel grow. If the difference in stresses between the maximum stress and minimum stress axis (the differential stress) exceeds the strength of the material, then the parcel fails and fragments.

the maximum differential stress within the nucleus is similar in magnitude to the sublimation pressure at the subsolar point (the maximum sublimation pressure). Therefore, when we compute the dynamic sublimation pressure at the subsolar point as a function of heliocentric distance, we are approximating the maximum differential stresses within the nucleus (see Figure 3.3).

Gundlach et al. (2012) proposed a related mechanism, in which a sublimation pressure that pressed equally on all parts of the nucleus may have allowed Comet C/2011 W3 (Lovejoy) to survive through its perihelion of 1.2 $R_{\odot}$. Within ~10 $R_{\odot}$ of the Sun, the coma of a comet with a ~1 km nucleus becomes optically thick (Drahus et al. 2014), causing light of equal intensity to fall upon all parts of the nucleus, which results in a uniform sublimation pressure being exerted on all parts of its surface. Unlike our proposed mechanism, such a phenomenon would generate no new differential stresses within the interior of the nucleus. However, it would induce a confining pressure on its surface, which can increase the strength of porous, granular materials (Alkire & Andersland, 1973). If this increase in strength were sufficiently large, then volatile sublimation near the Sun could allow C/2011 W3 (Lovejoy) to resist the strong solar tidal forces that exist within the Roche Limit that would otherwise disrupt the nucleus (Gundlach et al. 2012).

The Whipple model for ice sublimation (Whipple, 1950), combined with our model of ISON as a sublimating sphere of ice 680 m in radius (Lamy et al. 2014), predicts a mass loss rate from Comet ISON's nucleus for H_2O at 214 $R_{\odot}$ (1 AU) of $q_{water}=2.75\text{x}10^{28}$ s^{-1}, in agreement with the observed production rate of $q_{water} = 2.30(\pm0.71)\text{x}10^{28}$ s^{-1} (Combi et al. 2014). Measurements of Comet ISON's *Afρ* parameter

as a function of aperture radius (ρ) flattened out and approached a constant value as ISON approached the Sun, suggesting that icy grains ceased to contribute significantly to ISON's volatile production by late October (Knight & Schleicher, 2015). We therefore find that such close agreement between the expected and measured production rates generally support our assumption that the entire illuminated hemisphere is sublimating. Although Combi et al. (2014) deconvolved the observations with a model to obtain a daily average water production rate, their observed production rate of q_{water}=1.99(±0.32)x10^{28} s^{-1} at 0.98 AU is consistent with the measured rate of q_{water} = 1.6x10^{28} s^{-1} (±25%) at 0.98 AU (Bodewits et al. 2013), and their observed production rate of q_{water}=1.79(±0.35)x10^{28} s^{-1} at 0.88 AU is within a factor of 2 of q_{OH} = 8.14(±2.31)x10^{27} s^{-1} at 0.89 AU (Opitom et al. 2013a). These observations, which demonstrate remarkable agreement across various instruments, are consistent with a highly active, intact nucleus.

However, after November 12th, the amount of active surface required to match the observed H_2O production increased permanently by a factor of ~25, implying that the nucleus had then disrupted into a swarm of fragments (Combi et al. 2014). This is consistent with the observation of arc-like wings in the coma of ISON, which suggest the presence of multiple fragments (Boehnhardt et al. 2013). Other analysis determined that the radius of ISON's nucleus (or nucleus fragments) decreased too much during this event to be solely the result of sublimative surface erosion, further implying a disruption event at 145 $R_{\odot}$ (Steckloff et al. 2015). We therefore interpret this first event to be the complete breakup of the nucleus into a swarm dominated by large fragments ~100 m in radius (see Discussion section). The swarm (or specific large fragments within it) was

later observed to undergo two further significant disruption events on November 21st and November 26th Knight & Battams, 2014; Steckloff et al. 2015).

Escaping fragments and lofted grains do not directly contribute to the reaction force on the comet's nucleus because their velocity is so slow near the nucleus relative to the sublimating gases that they carry a negligible amount of momentum away from the nucleus. However, they can reflect some fraction of the sublimated gas molecules back onto the nucleus, further increasing the dynamic pressure. This effect can only increase the peak dynamic pressure by a factor of π (in the unlikely limit that every gas molecule bounces indefinitely between the nucleus and icy grains), to equal the gas vapor pressure. We adopt the conservative stance of neglecting this uncertain (but positive) backpressure, which can only add to the dynamic sublimation pressure, and which will introduce only small errors into our estimate.

3.3 Results

Motivated by observations of high H_2O production (Combi et al. 2014; Opitom et al. 2013a, 2013b, 2013c), we assume that volatile sublimation is dominated by H_2O as ISON approached perihelion. We compute the maximum dynamic H_2O sublimation pressure (and thus estimate the bulk cometary unconfined crushing strength) when Comet ISON disrupted at heliocentric distances of 36, 88, and 145 $R_\odot$ (Combi et al. 2014; Boehnhardt et al. 2013; Knight & Battams, 2014; Steckloff et al. 2015)]. We find strengths of 9, 1, and 0.5 Pa, respectively, for the case where ISON has a bond albedo of 0. If we instead assume a bond albedo of 0.5, we find strengths of 4, 0.6, and 0.2 Pa respectively (see Figure 3.4). These strengths are comparable to estimates of the strengths

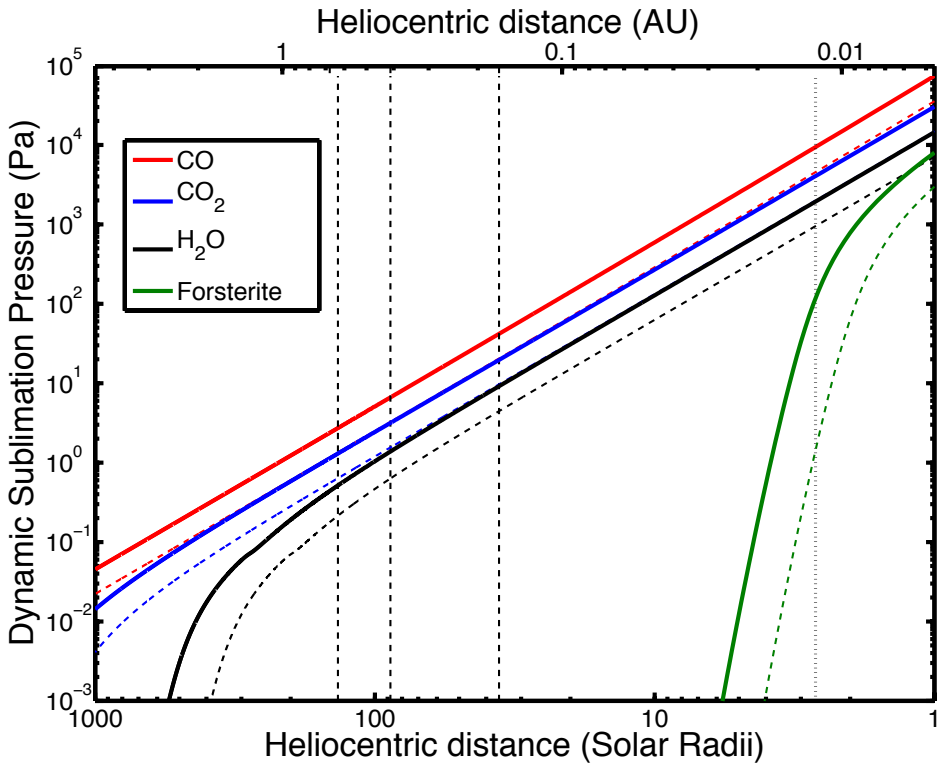

Figure 3.4 Dynamic Gas Sublimation Pressures for Major Volatile Species.

A plot of dynamic gas pressures for pure H_2O, CO_2, and CO as a function of heliocentric distance, measured in both Solar Radii ($R_\odot$) and Astronomical Units (AU). We include the mineral fosterite (Nagahara et al. 1994) as a proxy for refractory cometary materials, which only becomes dominant in the absence of volatiles very near the Sun. Solid curves denote sublimation pressures if the nucleus has zero bond albedo while the dashed curves are for an assumed bond albedo of 0.5. For a bond albedo between these two values, the sublimation pressure will lie between these two curves. The thin, dashed vertical lines at 36, 88[2], and 145[1] $R_\odot$ mark where Comet ISON disrupted into fragments (Combi et al. 2014; Knight & Battams, 2014), while the dotted line at 2.66 $R_\odot$ denote Comet ISON's perihelion distance.

of Jupiter Family Comets (JFCs) (Asphaug & Benz, 1996; Bowling et al. 2014; Melosh, 2011; Sekanina & Yeomans, 1985; Thomas et al. 2015). If Comet ISON's true bond albedo is between these two values, then the maximum dynamic pressure and bulk unconfined crushing strength estimates will also lie between the corresponding values. Such a hierarchy of strengths is consistent with studies of the strength of geologic materials, which depend inversely on the size of the sample (Brace, 1961), and is consistent with evidence suggesting that comet nuclei are composed of pieces that are heterogeneous in strength (Sekanina, 2003). The lowest of these strength estimates (0.2 and 0.5 Pa depending on bond albedo) corresponds to the first disruption event (at 145 $R_{\odot}$), and therefore represents the bulk unconfined crushing strength of ISON's intact nucleus (prior to any significant fragmentation). The higher strength estimates correspond to the later disruption events at 88 $R_{\odot}$ and 36 $R_{\odot}$, and therefore represent the strengths of fragments of ISON's nucleus.

3.4 Discussion

After a fragmentation event, the size of the resulting fragments may have an observable effect on the motion of the comet or morphology of the nucleus. The sublimation pressure acting on the illuminated surfaces of the nucleus provides a net antisunward force, with the net motion of the nucleus dependent on this sublimation force and the solar gravitational force. Since the sublimation force depends on surface area, while the gravitation force depends on volume, larger bodies (smaller surface-area-to-volume ratio) are less susceptible to the sublimation force than smaller bodies (larger surface-area-to-volume ratio). Therefore, if the nucleus produced fragments of

substantially unequal sizes, smaller fragments would appear to drift antisunward of the larger fragments, which would cause the central condensate of the comet's coma to elongate and even break up. However, Comet ISON maintained a strong central condensate (a compact region of peak coma brightness) up until only a few hours before perihelion (Knight & Battams, 2014; Opitom et al. 2013b, 2013c), and this central condensate only began to noticeably elongate a few days before perihelion (Steckloff et al. 2015). Thus, either the first fragmentation event broke Comet ISON into a swarm of equally sized fragments, or into differently sized fragments that were still each large enough to limit the relative drift between fragments and the resulting observable changes to the morphology of the coma.

Steckloff et al. (2015) conducted a preliminary study to estimate the sizes of the dominant fragments of Comet ISON. They measured the deviation of Comet ISON's position using the SCUBA-2 instrument on the James Clerk Maxwell Telescope from JPL Horizon's ephemeris solution #53, and estimated fragment sizes by assuming that this deviation is entirely due to H_2O sublimation pressure. From this, they determined that the first fragmentation event reduced the effective radius of Comet ISON from an approximately 680 m for the intact nucleus to fragments on the order of ~100 m. Such fragments would require approximately half of a week to traverse a single pixel of the SCUBA-2 instrument and a few days more for the larger pixels of the TRAPPIST telescope. This provides a rough estimate of the timescale over which coma morphology would noticeably elongate from the release of a single fragment from a much larger parent nucleus. This timescale would be longer if the fragments are closer in size, since they would drift together. Since no change in coma morphology was detected during the

9 days between the first and second fragmentation events, it is unlikely that ISON only released a single ~100 m fragment from the nucleus during the first fragmentation event. Rather, it is more likely that the first fragmentation event broke up ISON's nucleus into a swarm of large fragments with radii on the order of ~100 meters.

Because the coma may have started to elongate between the second and third fragmentation events, it is unclear whether the second fragmentation event was the result of a single fragment or multiple fragments disrupting. However, the elongation of the central condensate after the third fragmentation event (Steckloff et al. *in prep.*) suggests that a large range of fragment sizes were present after the third fragmentation event.

3.4.1 Supervolatiles and Amorphous Ice

Samarasinha (2001) proposed that the buildup of pore pressure within the nucleus from the sublimation of super-volatile species could lead to its disruption. This mechanism requires that the thermal skin depth of the comet be large enough to reach pockets of deeply seated volatiles. The thermal skin depth (h_{skin}) describes the characteristic length scale over which the amplitude of a heat pulse conducting (without sublimating volatiles) into an infinite half-space of material with a fixed boundary location and temperature drops by a factor of *e*, and is given by the equation

$$h_{skin} = \sqrt{\mathcal{H}\tau} \tag{3.13}$$

where $\mathcal{H}$ is a material's thermal diffusivity (typically on the order of 10^{-6} m^2 s^{-1} for dense rocks or ice) and τ is the duration since the onset of the thermal pulse. The longer a material is exposed to a heat pulse, the deeper the heat can penetrate. The rate at which

the thermal skin depth advances into a material is obtained by differentiating equation (13) with respect to time (τ)

$$v_{skin} = \frac{dh_{skin}}{d\tau} = \frac{1}{2}\sqrt{\frac{\mathcal{H}}{\tau}} \tag{3.14}$$

$$= \frac{\mathcal{H}}{2h_{skin}} \tag{3.15}$$

Thus, as the time of exposure (τ) and thermal skin depth (h_{skin}) increases, the rate of growth of the thermal skin depth (v_{skin}) decreases.

If the fixed-temperature boundary is receding at a constant rate, the thermal skin depth (h_{skin}) will either grow or shrink until v_{skin} is equal to this rate of recession, and the thermal skin depth will maintain a fixed depth relative to the surface. However, because heat takes time to conduct from the surface to the thermal skin depth, the distance between the thermal skin depth (h_{skin}) and the receding surface will be less than what equation (3.13) provides. Also, the rate of surface recession on a comet nucleus is not constant, but rather accelerates as the nucleus approaches the Sun, which further reduces the distance between the surface and h_{skin}. Additionally, moving boundaries, changing boundary conditions, and sublimation make the actual temperature profile of a comet nucleus significantly more complicated than that which results from simple heat conduction. However, if we assume that the H_2O sublimation front, whose temperature is largely determined by heliocentric distance, is some distance h_{sub} below the surface of the nucleus and that h_{skin} is measured from the sublimation front, then the quantity $h_{skin} + h_{sub}$ (computed using equations (3.13) and (3.15)) will be a conservative overestimate of Comet ISON's orbital thermal skin depth.

Because Comet ISON's activity occurred predominantly on the sunward hemisphere (Li et al. 2013c), the volatiles driving this activity had to respond to the day-night (diurnal) cycle of the nucleus, and could therefore be no deeper below the surface than a depth comparable to the diurnal skin depth. Based on a ~10.4 hour rotation period for the nucleus of Comet ISON (Lamy et al. 2014), the sublimation front of H_2O (h_{sub}) is no more than ~20 cm below the surface. Since sublimation is a comet's dominant cooling mechanism in the inner Solar System, we estimate the rate of the sublimation front's recession into the nucleus at the time of the Lamy et al. (2014) observations by dividing the mass-loss rate equation (equation 3.2) by the bulk density of a typical comet, and find that it is on the order of ~10^{-6} m/s. Noting that the rate of sublimation front recession and thermal skin depth recession (v_{skin}) are in equilibrium, we set v_{skin} to ~10^{-6} m/s, and find that h_{skin} is on the order of ~0.5 m. Thus, $h_{skin} + h_{sub}$ is on the order of meters, and therefore cold, Oort Cloud conditions persist in the primordial materials of Comet ISON only a few meters at most below the surface of the nucleus.

Because the orbital thermal skin depth is so shallow, if the thermal wave were to reach a pocket of supervolatile ices or trigger the crystallization of amorphous ice, they would release fragments from the surface with sizes comparable to the orbital thermal skin depth. Thus, if the first fragmentation event were the result of the rapid sublimation of supervolatile species, one would expect to see an outburst that released debris up to an order of ~1 m in size, leaving the nucleus largely intact. If the nucleus is composed of amorphous water ice whose crystallization was triggered by the propagation of the thermal wave into the interior, the crystallization front will propagate into the amorphous ice until the cold interior of the nucleus absorbs the exothermic heat of the phase

transition and quenches the crystallization process. Because the thermal wave is near the surface, the temperature gradient near the sublimation front is very steep (dropping to primordial temperatures over a distance on the order of the orbital thermal skin depth), and would quench the crystallization of the amorphous ice very quickly. Therefore, even if the exothermic crystallization of amorphous ice caused the first fragmentation event, one would still only expect to see an outburst that released similarly small debris.

Such small debris from a surface layer is inconsistent with the drastic reduction in the size of the nucleus after the first fragmentation event (Steckloff et al. 2015) and the observation of coma wings (Boehnhardt et al. 2013), which may indicate the presence of multiple large fragments. Additionally, such small debris would dissipate quickly, which is inconsistent with the sustained increase in water production (Combi, 2014). Therefore, while a direct application of the Samarasinha (2001) model may explain the disruption of highly thermally evolved comet nuclei, it appears that its direct application is inconsistent with the disruption of Comet ISON.

We cannot rule out a modification of the Samarasinha (2001) model, in which sublimating gases can penetrate into the pores of the nucleus and recondense (thus transporting heat into the cometary interior by releasing their heats of sublimation). If voids are present within the interior of the nucleus, then a sublimation front and thermal skin depth would be created within the walls of these voids akin to the situation at the surface. The Second Law of Thermodynamics limits the maximum temperature of the void walls achievable through this mechanism to the surface temperature of the nucleus (although the actual temperature would likely be much lower). Gas must be able to readily diffuse through the nucleus for a significant amount of heat to be transported into

the cometary interior in this manner, which greatly restricts the ability of sublimating volatiles to build up a gas pressure as though the comet were a sealed vessel. As the walls of the void recede through sublimation, the thermal wave may encounter supervolatile ices or amorphous ice. The sublimation of supervolatiles within a void would produce pressures that could be no greater than those that would be present at the surface, but probably significantly less. If these low pressures lead to the destruction of the nucleus, then our strength estimates would be an upper bound to the strength of the nucleus. However, were the thermal wave to trigger the crystallization of amorphous ice, this exothermic phase transition could cause a very rapid buildup of gas pressure within the void, potentially faster than the gases may diffuse out, and could potentially lead to a catastrophic explosion of the nucleus. We therefore cannot rule out this modified mechanism. This mechanism requires special diffusive, compositional, and structural conditions to disrupt the nucleus, which seems less likely to lead to ISON's disruption than sublimation pressure at the surface. However, a detailed exploration of the relevant physics of diffusion, sublimation, and phase transitions is beyond the scope of this paper.

3.4.2 Hydrostatic Pressure and Fragmentation Timescale

Our crushing strength computation ignores the internal hydrostatic pressure due to self-gravity of comet ISON, which is up to ~10 Pa for a 680m spherical nucleus (Lamy et al. 2014) with a density of 400 kg m^{-3} (Richardson & Melosh, 2013). If the nucleus were to uniformly disrupt in a single event, the dynamic sublimation pressure would have to overcome this overburden pressure in the comet's interior. In reality, the nucleus probably disrupted piecewise, in a process where the dynamic sublimation pressure first

overcomes the crushing strength and disperses the material near the surface of the nucleus, where the hydrostatic pressure is low. This reduces the hydrostatic pressure throughout the remaining nucleus, where this process repeats until the entire cometary nucleus is dispersed. We estimate the timescale of this dispersion by computing the time needed for the surface of the comet to accelerate across the diameter of the nucleus from sublimation pressure alone, assuming typical cometary densities of around 400 kg m^{-3} (Richardson & Melosh, 2013; Richardson & Bowling, 2014; Thomas et al. 2015). This results in a dispersion timescale for Comet ISON of only a few hours at 145 $R_{\odot}$, allowing us to ignore the effects of hydrostatic pressure and treat the cometary disruption effectively as an instantaneous event in the comet's orbit.

Our sublimation pressure disruption mechanism assumes that the nucleus is rotating slowly enough that the maximum dynamic sublimation pressure at the sub-solar region has enough time to fragment the nucleus before rotating significantly away from the sub-solar point and reducing the sublimation pressure on that area element. The critical timescale for fragmenting the nucleus is the amount of time needed for a crack, once started, to propagate across the nucleus. The growing tip of a crack travels at the Rayleigh surface wave velocity, which are typically on the order of ~100 m/s for granular materials, and higher for more coherent materials (Lawn & Wilshaw, 1975). Thus, the time needed for a crack to travel across the nucleus (and therefore the timescale of fragmentation) is on the order of a few seconds. Since the rotation period of a comet nucleus is limited to be no shorter than a few hours before fragmenting rotationally (Snodgrass et al. 2006; Pravec et al. 2006), the timescale of fragmentation is negligible and our assumption holds.

3.4.3 Strengths of Other Comets

We compare our crushing strength estimate to observationally constrained estimates of the bulk, tensile, and shear strengths of other comets, which are related to the bulk crushing strength by small factors on the order of unity (Price, 1968). The crushing strength of Comet ISON is consistent with Comet Shoemaker-Levy 9's bulk tensile strength of <6.5 Pa (Asphaug & Benz, 1996); Comet Brooks 2's bulk tensile strength of <2 Pa (Sekanina & Yeomans, 1985); within an order of magnitude of Comet Wild 2's shear strength of >17 Pa (Melosh, 2011); and Comet Churyumov-Gerasimenko's cohesive strength of ~2-16 Pa (Bowling et al. 2014), and tensile strength of <20 Pa (Thomas et al. 2015). Thus, if Comet ISON is representative of thermally unprocessed comets, then the low bulk strength of comets is a primordial property that is unaltered by thermal processing.

We consider other strength estimates of comets, and note that they are not applicable to our mechanism. The 1-10 kPa effective target strength of Comet 9P/Tempel 1 from the Deep Impact experiment (Richardson & Melosh, 2013) is a measurement of dynamic strength (which does not adhere to the weakest link model of material failure). Therefore, we expect this estimate to be several orders of magnitude larger than a measurement of static strength, which is applicable to our disruption mechanism. Comet Hyakutake's tensile strength was estimated to be ~100 Pa from the strength required to hold the comet together from rotational fragmentation (Lisse et al. 1999). However, this estimate assumed a bulk density for Comet Hyakutake of 100 kg m^{-3}, which is now known to be unreasonably low: a more typical cometary density of 270 kg m^{-3} or greater allows the nucleus to be held together by gravity alone. Indeed the

known rotation rates of JFCs and Kuiper Belt Objects are consistent with effectively strengthless bodies with densities less than 600 kg m^{-3} (Snodgrass et al. 2006) in a manner analogous to the asteroid rubble pile "spin barrier" (Pravec et al. 2006).

All of these upper bounds of comet strength require that the nucleus structurally fail in some way. Thus, these strength estimates may be biased toward weaker nuclei, which would structurally fail more easily. Indeed, many comets survive perihelion passage despite having orbits that take them to smaller heliocentric distances than those corresponding to Comet ISON's fragmentation events (Bortle, 1991), consistent with stronger nuclei. If comets are effectively rubble piles held together by van der Waal's forces, then they may possess strengths similar to rubble pile asteroids of ~25 Pa (Sánchez & Scheeres, 2014). Such strengths would allow comet nuclei to survive the differential stresses induced by H_2O sublimation to within 20 $R_\odot$ (0.1 AU) of the Sun. Thus, the survival/non-survival of near-Sun comets is consistent with different comet nuclei having strengths that span more than an order of magnitude.

Additionally, short-period comets with small perihelia (when compared to where ISON fragmented) may survive multiple orbits as a result of their unique dynamical and thermophysical evolution. Jupiter Family Comets like 2P/Encke and 96P/Machholz originate in the Kuiper Belt and Scattered Disk until an encounter with Neptune sends them into the Outer Planet region of the Solar System, where they are reclassified as Centaurs (Duncan et al. 2004). Typically, an encounter with Jupiter after a few million years (the dynamical lifetime of a Centaur) either ejects the object from the Solar System or sends it into the Jupiter Family of comets (Duncan et al. 2004). During this inward migration process, a Jupiter Family Comet is also undergoing thermophysical evolution.

As its orbit evolves ever closer the Sun, the comet loses volatile ices through sublimation, which may result in the build up of a lag deposit (or dust mantle) on its surface. These deposits are very good insulators (Gulkis et al. 2015; Davidsson et al. 2013; Groussin et al. 2013; Lisse et al. 2005; Lamy et al. 2008), and even a thin coating would restrict volatile sublimation to a small fraction of the surface. Therefore, when this inhibited sublimation activity is averaged over the surface, we expect JFCs to experience significantly lower sublimation pressures than the pristine icy surfaces that we have modeled in this work. Thus, the survival of JFCs with small perihelia is consistent with our work, even without allowing for larger material strengths.

3.5 Conclusions

We have shown that existing mechanisms of comet disruption have difficulty explaining Comet ISON's fragmentation. We proposed a new mechanism of comet disruption in which sublimating gases exert a dynamic pressure on the sunward hemisphere of a nucleus and induce differential stresses within the nucleus, which may fracture and fragment the nucleus if they exceed its material strength. Using a versatile thermodynamic model of volatile sublimation, we find Comet ISON has a material strength similar to JFCs. For the case that the nucleus of Comet ISON has a bond albedo of 0, we estimate its bulk unconfined crushing strength to be 0.5 Pa, and the bulk unconfined crushing strength of resulting fragments at 1-9 Pa. If Comet ISON's nucleus has a bond albedo of 0.5, then these strength estimates drop to 0.2 Pa for the intact nucleus and 0.6-4 Pa for its fragments.

References

Alkire, B.D. & Andersland, O.B.; The Effect of Confining Pressure on the Mechanical Properties of Sand-Ice Materials. *Journal of Glaciology* **12**(66), 469-481 (1973)

Asphaug, E. & Benz, W.; Size, Density, and Structure of Comet Shoemaker-Levy 9 Inferred from the Physics of Tidal Breakup. *Icarus* **121**, 225-248 (1996).

Bar-Nun, A.; Laufer, D.; Rebolledo, O.; Malyk, S.; Reisler, H.; Wittig, C.; Gas Trapping in Ice and Its Release upon Warming. In *The Science of Solar System Ices*, 487 - 499. Editors: Gudipati, M.S. & Castillo-Rogez, J.; Springer Publishing: New York (2013)

Bockelée-Morvan, D.; Crovisier, J.; Mumma, M.J.; Weaver, H.A.; The Composition of Cometary Volatiles. In *Comets II*, 391-423. Editors: Festou, M.C.; Keller, H.U.; Weaver, H.A. University of Arizona Press: Tuscon (2004)

Bodewits, D.; Farnham, T.; A'Hearn, M.F.; *Central Bureau Electronic Telegrams (CBET)* **3718** (2013)

Boehnhardt, H.; Tubiana, C.; Oklay, N.; Vincent, J.B.; *Central Bureau Electronic Telegrams (CBET)* **3715** (2013)

Borovička, J. et al.; The trajectory, structure and origin of the Chelyabinsk asteroidal impactor. *Nature* **503**, 235-237 (2013)

Bortle, J.E.; Post-perihelion Survival of Comets with Small q. *International Comet Quarterly* **13**, 89-91 (1991)

Bowling, T.B.; Steckloff, J.K.; Melosh, H.J.; Graves, K.J.; The Strength of Comet 67P/Churyumov-Gerasimenko. *American Astronomical Society – Division of Planetary Science Meeting #46*, Abstract #100.03 (2014)

Brace, W.F.; Dependence of fracture strength of rocks on grain size. *Penn State University Mineral Expt. State Bulletin* **76**, 99-103 (1961)

Brown, J.C. et al. Mass loss, destruction and detection of Sun-grazing and –impacting cometary nuclei. *A&A* **535**, A71, 12pp (2011).

Capaccioni, F. and 77 coauthors. The organic-rich surface of comet 67P/Churyumov-Gerasimenko as seen by VIRTIS/Rosetta. *Science* **347**, (2015). DOI: 10.1126/science.aaa0628

Combi, M.R et al.; Unusual water production activity of Comet C/2012 S1 (ISON): Outbursts and continuous fragmentation. *Ap. J.* **788**:L7-L11 (2014)

Cowan, J.J. and A'Hearn, M.F.; Vaporization of comet nuclei: Light curves and life times. *The Moon and the Planets* **21**, 155-171 (1979)

Davidsson, B.J.R. et al. Thermal inertia and surface roughness of Comet 9P/Tempel 1. *Icarus* **224**, 154-171 (2013).

Delamere, W.A.; McEwan, A.S.; Li, J.-Y.; Lisse, C.M. *Central Bureau Electronic Telegrams* **3720** (2013)

Delsemme, A.H. and Swings, P.; Hydrates de gaz dans les noyaux cométaires et les grains interstellaires. *Annales d'Astrophysique* **15**(1), 1-6 (1952)

Drahus, M. Rotational Disruption of Comets with Parabolic Orbits. *AAS/Division for Planetary Sciences Meeting Abstracts 46*, #200.04 (2014)

Duncan, M.; Levison, H.; Dones, L.; Dynamical Evolution of Ecliptic Comets. In *Comets II*, 193 – 204. Editors: Festou, M.C.; Keller, H.U.; Weaver, H.A.; The University of Arizona Press: Tuscon (2004)

Feaga, L.M.; A'Hearn, M.F.; Sunshine, J.M.; Groussin, O.; Farnham, T.L. Asymmetries in the distribution of H_2O and CO_2 in the inner coma of Comet 9P/Tempel 1 as observed by Deep Impact. *Icarus* **190** 345-356 (2007)

Feistel, R.; and Wagner, W.; Sublimation pressure and sublimation enthalpy of H_2O ice Ih between 0 and 273.16 K. *Geochimica et Cosmochimica Acta* **71**, 36-45 (2007)

Gombosi, T.I.; Free molecular aerodynamics. In *Gaskinetic Theory*. Edn. 1. Cambridge University Press: Cambridge, UK. (1994)

Groussin, O. et al. The temperature, thermal inertia, roughness and color of the nuclei of Comets 103P/Hartley 2 and 9P/Tempel 1. *Icarus* **222**, 580-594. (2013)

Gulkis, S. et al. Subsurface properties and early activity of comet 67P/Churyumov-Gerasimenko. *Science* **347**, (2015) DOI: 10.1126/science.aaa0709

Gundlach, B.; Skorov, Y.V.; Blum, J.; Outgassing of icy bodies in the Solar System – I. The sublimation of hexagonal water ice through dust layers. *Icarus* **213**, 710-719 (2011)

Gundlach, B.; Blum, J.; Skorov, V.; Keller, H.U.; A note on the survival of the sungrazing comet C/2012 W3 (Lovejoy) within the Roche limit.; arxiv.org/abs/1203.1808 (2012)

Knight, M.M. and Battams, K.; Preliminary analysis of *SOHO*/*STEREO* observations of sungrazing Comet ISON (C/2012 S1) around perihelion. *Ap J. Letters.* **782**:L37 (5 pp) (2014)

Knight, M.M. & Walsh, K.J.; Will Comet ISON (C/2012 S1) survive perihelion? *Ap J.* **776**, 776:L5, 5pp (2013)

Knight, M.M.; Schleicher, D.G.; Observations of Comet ISON (C/2012 S1) from Lowell Observatory. *AJ* **149**:19 (15 pp) doi:10.1088/0004-6256/149/1/19

Lamy, P.L.; Toth, I.; Groussin, O.; Jorda, L.; Kelley, M.S.; Stansberry, J.A.; Spitzer Space Telescope observations of the nucleus of comet 67P/Churyumov-Gerasimenko. *A&A* **489**, 777-785 (2008)

Lamy, P.L.; Toth, I.; Weaver, H.A.; *Hubble Space Telescope* Observations of the nucleus of Comet C/2012 S1 (ISON). *ApJL* **794**, L9 (2014)

Langmuir, I. The vapor pressure of metallic tungsten. *Phys. Rev.* **vol. II, no. 5**, 329-342 (1913).

Lawn, B.R.; Wilshaw, T.R.; *Fracture of Brittle Solids*. Cambridge University Press, Cambridge, U.K. (1975)

Li, J.-Y. et al. Photometric properties of the nucleus of Comet 9P/Tempel1 from Stardust-NExT flyby and the implications. *Icarus* **222**, 467-476 (2013a).

Li, J.-Y. et al. Photometric properties of the nucleus of Comet 103P/Hartley 2 *Icarus* **222**, 559-570 (2013b)

Li, J.-Y. et al.; Characterizing the dust coma of Comet C/2012 S1 (ISON) at 4.15 AU from the Sun. *Ap. J. L.* **779**, L3 (2013c)

Lisse, C.M. et al.; The Nucleus of Comet Hyakutake (C/1996 B2). *Icarus* **140**, 189-204 (1999)

Lisse, C.M.; A'Hearn, M.F.; Groussin, O.; Fernandez, Y.R.; Belton, M.J.S.; van Cleve, J.E.; Charmandaris, V.; Meech, K.J.; McGleam, C.; rotationally resolved 8-35 micron *Spitzer Space Telescope* observations of the nucleus of Comet 9P/Tempel 1. *The Ap. J.* **625** L139-L142 (2005)

Lisse, C.; Bar-Nun, A.; Laufer, D.; Belton, M.; Harris, W.; Hsieh, H.; Jewitt, D.; Cometary Ices. In *The Science of Solar System Ices*, 455 – 485. Editors: Gudipati, M.S. & Castillo-Rogez, J.; Springer Publishing: New York.(2013)

Marsden, B.G., Sekanina, Z.; Yeomans, D.K.; Comets and nongravitational forces. V. *Astronomical Journal* **78**(2), 211-225 (1973)

Mastrapa, R.M.E.; Grundy, W.M.; Gudipati. Amorphous and Crystalline H_2O-Ice. In *The Science of Solar System Ices*, 371 - 408. Editors: Gudipati, M.S. & Castillo-Rogez, J.; Springer Publishing: New York.(2013)

McKay, A.; Cochran, A.; Dello Russo, N.; Weaver, H.; Vervack, R.; Harris, W.; Kawakita, H.; DiSanti, M.; Chanover, N.; Tsvetanov, Z.; Evolution of fragment-species production in comet C/2012 S1 (ISON) from 1.6 au to 0.4 au. *Asteroids, Comets, Meteors 2014*, 365 (2014)

Melosh, H.J.; Slopes and mass movement. In *Planetary Surface Processes* Edn. 1 (Cambridge University Press, Cambridge, UK 2011)

Nagahara, H.; Kushiro, I.; Mysen, B.O.; Evaporation of olivine: Low pressure phase relations of the olivine system and its implication for the origin of chondritic components in the solar nebula. *Geochimica et Cosmochimica Acta* **58**(8), 1951-1963 (1994)

Opitom, C.; Jehin, E.; Manfroid, J.; Gillon, M.; *Central Bureau Electronic Telegrams (CBET)* **3693** (2013a)

Opitom, C.; Jehin, E.; Manfroid, J.; Gillon, M.; *Central Bureau Electronic Telegrams (CBET)* **3711** (2013b)

Opitom, C.; Jehin, E.; Manfroid, J.; Gillon, M.; *Central Bureau Electronic Telegrams (CBET)* **3719** (2013c)

Pravec, P. et al.; Photometric survey of binary near-Earth asteroids. *Icarus* **181**, 63-93 (2006)

Price, N.J. In *FAULT AND JOINT DEVELOPMENT IN BRITTLE AND SEMI BRITTLE ROCK*. Editor Rhodes, F.H.T. Edn.1 reprint (Pergamon Press, Oxford, UK 1968)

Richardson, J.E.; Bowling, T.J.; Investigating the combined effects of shape, density, and rotation on small body surface slopes and erosion rates. *Icarus* **234**, 53-65 (2014)

Richardson, J.E.; Melosh, H.J.; An examination of the Deep Impact collision site on Comet Tempel 1 via Stardust-NExT: Placing further constraints on cometary surface properties. *Icarus* **222**, 492-501 (2013)

Samarasinha, N.H.; A model for the breakup of Comet LINEAR (C/1999 S4). *Icarus* **154**, 540-544 (2001).

Samarasinha, N.H. and Mueller, B.E.A.; Relating changes in cometary rotation to activity: Current status and applications to Comet C/2012 S1 (ISON). *ApJL* **775**, L10 6pp (2013).

Sánchez, P.; Scheeres, D.J.; The strength of regolith and rubble pile asteroids. *M&PS* **49**(5), 788-811 (2014)

Sekanina, Z.; Sublimation rates of Carbon Monoxide at Carbon Dioxide from comets at large heliocentric distances. *Asteroids, Comets, Meteors 1991*, 545-548 (1992)

Sekanina, Z.; Erosion model for the sungrazing comets observed with the Solar and Heliospheric Observatory. *Ap J.* **597**, 1237-1265 (2003)

Sekanina, Z. & Yeomans, D.K.; orbital motion, nucleus precession, and splitting of periodic comet Brooks 2. *Astron. J.* **90**, 2335-2352 (1985)

Snodgrass, C.; Lowry, S.C.; Fitzsimmons, A.; Photometry of cometary nuclei: rotation rates, colours, and a comparison with Kuiper Belt Objects. *Monthly Notices of the Royal Astronomical Society* **373**, 1590-1602 (2006)

Steckloff, J.K. et al.; The size and fragmentation of the nucleus of Comet C/2012 S1 (ISON). *LPSC XLVI,* Abstract #2723 (2015)

Thomas, N. and 58 coauthors; The morphological diversity of comet 67P/Churyumov-Gerasimenko. *Science* **347**, (2015) DOI: 10.1126/science.aaa0440

Ververka, J.; Klaasen, K;, A'Hearn, M.; Belton, M.; Brownlee, D.; Chesley, S.; Clark, B.; Economou, T.; Farquhar, R.; Green, S.F.; Groussin, O.; Harris, A.; Kissel, J.; Li, J.-Y.; Meech, K.; Melosh, J.; Richardson, J.; Schultz, P.; Silen, J.; Sunshine, J.; Thomas, P.; Bhaskaran, S.; Bodewits, D.;Carcich, B.; Cheuvront, A.; Farnham, T.; Sackett, S.; Wellnitz, D.; Wolf, A.; Return to Comet Tempel 1: Overview of Stardust-NExT results. *Icarus* **222**, 424-435 (2013)

Weaver, H.; A'Hearn, M.; Feldman, P.; Bodewits, D.; Combi, M.; Dello Russo, N.; McCandliss, S.; Ultraviolet spectroscopy of comet ISON (2012 S1). *Asteroids, Comets, Meteors 2014*, 604 (2014)

Whipple, F.L.; A comet model. I. The acceleration of Comet Encke. *The Ap. J.* **111** 375–394 (1950)

"I came in with Halley's Comet in 1835.
It is coming again next year, and I expect to go out with it.
It will be the greatest disappointment of my life if I don't go out with
Halley's Comet."

-Mark Twain (1909)

CHAPTER 4. A SUBLIMATIVE ANALOGUE TO THE YORP EFFECT

Sublimating volatiles can also generate sublimative torques that alter the rotation state of the nucleus. Traditionally, one requires detailed knowledge of the shape and activity of an icy body to compute the effects of sublimative torques. However, this information is only available for the few comet nuclei visited by spacecraft, limiting the study of sublimative torques to a handful of objects. I remedied this by developing a novel framework to study the average effects of sublimative torques on large populations of cometary bodies, rather than individual objects. This SYORP framework is based on the YORP Effect, which computes the torques resulting from the nonisotropic emission of thermal photons from an asymmetric body. Because surfaces emit both thermal photons and sublimating molecules in a functionally similar manner, I developed the necessary scaling relationships that allow the YORP torque equations to accurately describe sublimative torques. Because the YORP effect parameterizes the net effect of shape and albedo into a single numerical constant, SYORP similarly replaces the detailed information required to traditionally compute sublimative torques with simple numerical

constants (or statistical distributions of these parameters). The activity parameters can be estimated from measurements of cometary outgassing, observations of coma structures, or computed directly from detailed knowledge of a comet's activity.

I then use this framework to explain the formation of dust striae (rare, Sun-aligned linear dust features in the tails of some comets), which has remained an enigma for more than a century. Specifically, I apply this model to the stria system of Comet West (C/1975 V1). It is generally accepted that stria formation is a two-step process in which a nucleus ejects a coherent mass of material that later breaks up and disperses far from the nucleus. However, proposed formation mechanism either can not get enough material to drift coherently away from the nucleus or are thermodynamically implausible. I show that ~10-100 m chunks of material, which are observed being ejected from comet nuclei, experience sublimative torques that spin them up to the point of disruption, naturally forming the observed striae.

The following manuscript was published in *Icarus* (volume 264, p. 160-171) in 2015 as "The formation of striae within cometary dust tails by a sublimation-driven YORP-like effect" coauthored by Seth A. Jacobson.

4.1 Introduction

Linear features sometimes form within the dust tails of "great comets" from the Oort Cloud such as Comet West (C/1975 V1) (Sekanina & Farrell 1978, 1980), Comet Hale-Bopp (C/1995 O1) (Pittichová et al. 1997), Comet McNaught (C/2006 P1), and Comet PANSTARRS (C/2011 L4) (Jones & Battams 2014). These features are generally aligned with either the nucleus of the comet (synchrones) or with the Sun (striae) (e.g.

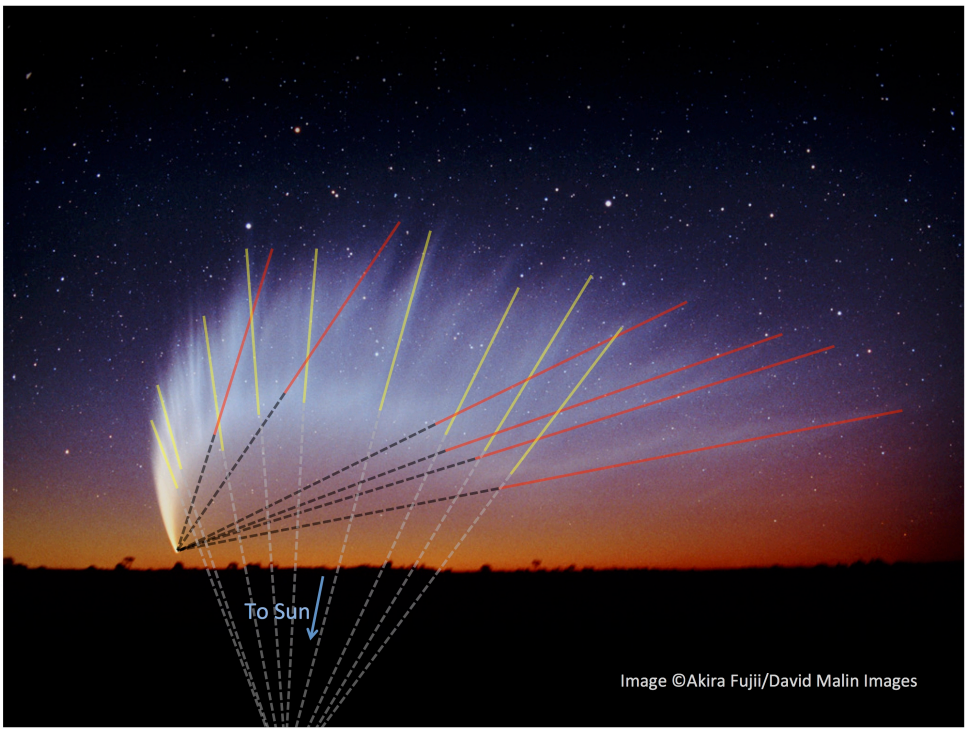

Figure 4.1 Illustrating Stria and Synchrones.

An image of Comet McNaught (C/2006 P1) shows long linear structures within the tail of the comet. We have overlain lines to highlight the linear features in the cometary tail. Note how these features line up with either the head of the comet (synchrones) or with the Sun (striae). Image ©Akira Fujii/David Malin Images reproduced with permission, with annotations and markings added by authors

Comet McNaught [C/2006 P1] in Figure 4.1). Synchrones are believed to form from ~1-100 μm dust released nearly simultaneously or diurnally from active areas of the comet's surface, which drifts away from the nucleus due to solar radiation pressure (Karchuk & Korsun 2010). In contrast, the mechanism that creates striae is poorly understood.

Sekanina & Farrell (1980) observed that "striae seem to fit synchronic formations whose sources of emission are located in the area of the dust tail rather than in the nucleus," and postulated three conditions that need to be met by the "parent" materials that form a stria: (1) these materials must be ejected simultaneously from the nucleus; (2) they must experience identical repulsive accelerations from the Sun and (3) these parent objects must break up and disperse simultaneously (listed at the beginning of Section II in Sekanina & Farrell 1980). Some proposed mechanisms assume that (3) occurs as a single, short-lived event (Sekanina & Farrell, 1980; Fröhlich & Notni, 1998), while other mechanisms model (3) as a relatively long-lived fragmentation cascade (Nishioka 1998, Jones & Battams 2014). Regardless of the exact details of (3), these three conditions ensure that the pre-stria materials arrive at the source location of a stria as a single unit, where the parent materials are then transformed into a daughter fragment size distribution that creates the narrow lineaments oriented towards the Sun via anti-sunward acceleration.

4.2 Radiation Pressure

Sekanina & Farrell (1980) and subsequent authors (e.g. Fröhlich & Notni, 1988; Pittichová et al, 1997) considered that solar radiation pressure was solely responsible for

the parent materials' repulsive acceleration (second condition above). Sunlight, like gravity, obeys an inverse square law and solar radiation pressure is oriented antiparallel to the solar gravitational acceleration force (to leading order). Thus, its strength can be parameterized by the dimensionless constant β, which is the ratio of the force of solar radiation pressure to the solar gravitational force acting upon a particular object. Since the force of gravity depends on an objects volume ($\sim R^3$) while force of radiation depends on an objects surface area ($\sim R^2$), β is a size-dependent parameter. For Comet West, the β parameter for the parent materials released from the nucleus was estimated at $\beta_p = 0.55 – 1.10$, while the β parameter for the dust fragments within the striae was $\beta_f = 0.6 – 2.7$ (Sekanina & Farrell, 1980). Such high beta parameters require that both parent and daughter grains be small (~ 0.1 μm), such that a small parent grain is most likely capable of creating only ~10 daughter grains (Sekanina & Farrell, 1980). Alternatively, the parent grains could be extremely elongated such that they have a Sun-facing cross-section of a ~0.1 μm grain (Sekanina & Farrell, 1980). Since Comet West's striae are estimated to contain $\sim 10^6$ kg of material (Sekanina & Farrell 1980), such extreme elongation is unlikely, and more recent research has focused instead on exploring mechanisms that allow a swarm of small-sized parent grains to travel together.

Fröhlich & Notni (1988) propose that such a swarm could travel away from the nucleus in a coherent, optically thick parcel of grains with a narrow range of β-values. The breadth of this range depends on the swarm's optical thickness (with optically thin swarms incapable of remaining together), with β values above this range receiving enough illumination to surge ahead and leave the swarm, while grains with β values below this range lag behind the coherent swarm. Fröhlich & Notni (1988) propose that

swarms on the order of ~1000 km across become optically thin in the cometary tail and disperse, forming striae. However, to maintain an optically thick swarm the grains must not have any significant transverse velocity (motion perpendicular to the direction of solar gravity/radiation pressure), a condition that is thermodynamically very unlikely without a mechanism for laterally confining the dust.

Neither of these proposed mechanisms is satisfactory. Meeting Sekanina & Farrell's (1980) second condition with radiation pressure requires small parent grains, but then it is difficult to meet the third condition while creating a large enough mass of daughter grains. If an alternative to radiation pressure can be found, then these issues may disappear.

Lastly, observations show that comets with perihelia <6AU form striae between near-perihelion and ~1 AU of the Sun (Pittichová et al, 1997), which suggests that the mechanism driving stria formation must turn off beyond ~1 AU and somehow prevent the formation of observable striae until after the comet has approached the near-perihelion part of its orbit. Since the intensity of solar irradiation decreases smoothly as the inverse-square of heliocentric distance, there is no heliocentric distance at which the solar radiation pressure drops off precipitously. Therefore, if solar radiation pressure drives stria formation, then striae should form at all heliocentric distances, with differences in solar radiation pressure manifesting itself as an increase in the duration of the stria formation process with increasing heliocentric distance.

4.3. Sublimation-Driven Stria Formation Model

In this paper, we propose a sublimation-driven stria formation mechanism that allows for relatively large, volatile-rich chunks of ejected cometary materials to drift into the cometary dust tail and fragment quickly into fine dust, forming cometary dust tail striae. This mechanism also naturally restricts the formation of observable stria until the comet reaches the near- or post-perihelion portion of its orbit and is inactive beyond ~1 AU. We show, through careful consideration of the timescale of stria formation, that this mechanism is consistent with the observed striae of Comet West.

The sublimation of volatile ices is enough to both accelerate the parent chunk anti-sunward relative to the cometary nucleus and spin up the parent chunk to fragmentation, (i.e. rotational fission.) Because the sublimation pressure exerted on the illuminated hemisphere of a volatile rich body is many orders of magnitude greater than radiation pressure, this mechanism is able to affect chunks that are many orders of magnitude larger than previous radiation pressure-driven only mechanisms. We envision that the formation of a stria occurs in five steps (see Figure 4.2): (1) a parent chunk is released from the nucleus of a comet, (2) sublimation pressure causes the parent chunk to drift anti-sunward relative to the nucleus while simultaneously increasing its spin rate, (3) parent chunk spins up to the point of fission, (4) the resulting daughter chunks repeat steps 2 and 3 at an ever-increasing rate, resulting in a fragmentation cascade that (5) stops when the materials become small (micron-sized grains) and devolatilized, at which point radiation pressure dominates the behavior of grains which stream out to form a stria.

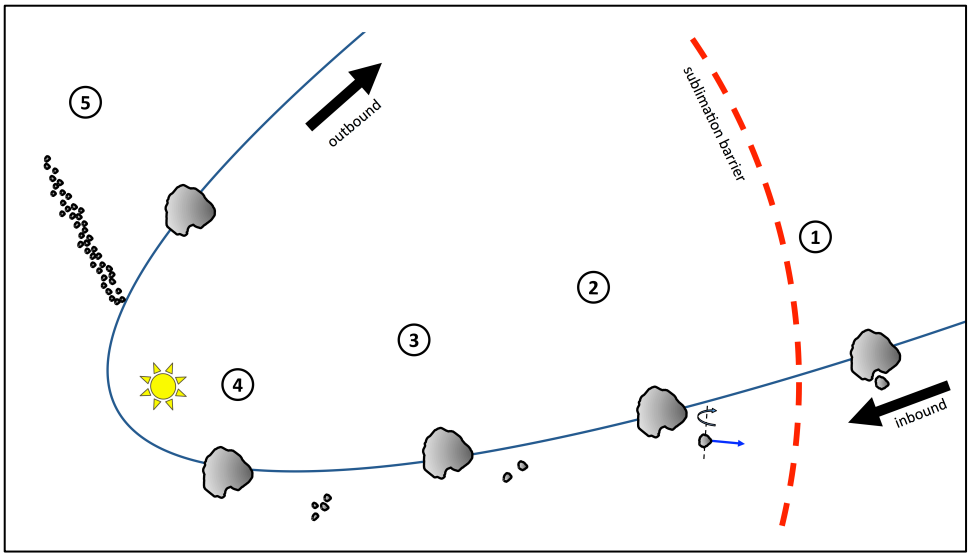

Figure 4.2: A Cartoon of SYORP-induced Stria Formation.

The five steps of stria formation are illustrated above including (1) parent chunk release, (2) sublimation-driven anti-sunward drift and rotational acceleration, (3) rotational fission, (4) fragmentation cascade, and (5) transition from sublimation to radiation pressure domination of anti-sunward drift. After step 5, the stream of small micron-sized chunks appears observationally as a stria.

Previous studies of the effects of the reactive torques due to sublimating gas on the rotation state of cometary nuclei have focused on the reactive torques from jets either observed or inferred on the surface (e.g. Wilhelm, 1987; Peale & Lissauer, 1989; Julian, 1990; Samarasinha & Belton, 1995; Neishtadt et al, 2002, 2003; Gutiárrez et al., 2003; Sidorenko et al., 2008). These jets may be the dominant rotation state torques for large cometary nuclei (Meech et al., 2011; Belton et al., 2011; Chesley et al., 2013), but the relatively small cometary chunks discussed below are assumed to not possess the ability to create jets (Belton, 2010, 2013; Bruck Syal et al., 2013), although jet production is itself poorly understood. In this work, we propose that it is the background sublimation that torques the cometary chunk. This sublimation is nearly isotropic in the sense that it is emitted from every heated surface element but is very sensitive to the shape and illumination of the chunk. A similar model for an entire comet nuclei has been considered in the past, but it was preliminary (Szegö et al,. 2001), considered only an ellipsoidal shape (Mysen, 2004; 2007), or focused on matching different observational phenomena (Rodionov et al., 2002; Gutiárrez et al., 2007).

4.3.1 Step 1: Parent chunks leave comet

We propose that a single ejected (parent) chunk contains all of the material that later becomes a stria. Sekanina & Farrell (1980) illustrated a method of obtaining an order of magnitude estimate of the volume of a stria for Comet West. Assuming that the dust of a stria has a typical Jupiter Family Comet (JFC) albedo of ~0.03 (Hammel et al. 1987;Brownlee et al. 2004; Lamy et al. 2004; Oberst et al. 2004; Li et al. 2007; Li et al. 2013a; Sierks et al. 2015), is comprised of ~0.1-1 micron particles (Green et al. 2004),

and that it originated from an initial parent chunk that was half water ice (McDonnell et al. 1987), then we expect the initial parent chunks to have radii on the order of ~10-100 m. We assume that these parent chunks have a density of ~400 kg/m^3, which is typical of JFCs (Sierks et al. 2015; Thomas et al. 2013; Richardson et al. 2007).

Such house- or building-sized (~10-100 m) chunks of material have been observed in the debris of comets 57P/du Toit-Neujmin-Delporte (Fernández, 2009), 73P/Schwassmann-Wachmann 3 (Fuse et al. 2007; Reach et al. 2009), and C/1999 S4 (LINEAR) (Weaver et al. 2001); were observed within the coma of 17P/Holmes following its massive 2007 outburst (Stevenson et al. 2010); and was possibly detected by the *Giotto* spacecraft within a few hundred kilometer of Comet 26P/Grigg-Skjellerup's nucleus (McBride et al. 1997). Most applicably, comet C/1996 B2 (Hyakutake) ejected ~10-100 m chunks, which drifted antisunward relative to the nucleus via sublimation pressure (Desvoivres et al. 2000; Schleicher & Woodney, 2003).

The frequency of striae is likewise consistent with the frequency of ejected ~10-100 m chunks. While a direct measurement of this frequency is difficult due to observational limitations, it is expected to be intermediate to the frequencies of ejection of larger and smaller chunks. Centaur comet 174P/Echeclus ejected a fragment a few kilometers in size (Rousselot, 2008), the only known ejection of such a large fragment. Meanwhile, high-resolution images from spacecraft have revealed that ~1/3 of Jupiter Family Comets (JFCs) eject a large number of decimeter to meter scale chunks into their inner comae at speeds near their escape velocities (~1 m/s) (Hermalyn et al. 2013; Rotundi et al. 2015). Because striae occur more frequently than the ejection of kilometer-scale fragments yet less frequently than the detection of decimeter to meter scale chunks,

it is reasonable that the parent bodies that form them are likewise intermediate in size (~10-100 m).

While we do not propose a model for the ejection of these suggested house-sized parent chunks from the nuclei of striated comets, we speculate that perhaps cometary outbursts (Pittichová et al. 1997; Rousselot, 2008) or supervolatile-driven activity may be responsible for launching these parent chunks at greater than escape velocity. Such activity would eject parent chunks with a distribution of initial velocities, and the Rosetta spacecraft observed indirect evidence for the ejection of ~10-100 m chunks from the surface of Comet 67P/Churyumov-Gerasimenko at less than escape velocity that later reimpacted its surface (Thomas et al. 2015). We assume that these parent chunks are rich in water ice throughout, including near the surface of the chunk (relative to the thermal skin depth). If this is not the case, then sublimation pressure will not be able to drive the chunk away from the nucleus (see *Step 2*), due to the inability of the ices to respond to the parent chunk's diurnal thermal cycle.

4.3.2 Step 2: Sublimation Pressure instead of Radiation Pressure

We propose that the reaction force (or equivalently, the sublimative momentum flux) on a volatile-rich parent chunk from the ejection of sublimating gas molecules is enough to both accelerate the parent chunk anti-sunward relative to the cometary nucleus (discussed below) and spin up the parent chunk to fragmentation (discussed in Step 3). Sublimating gasses exert an anti-sunward acceleration on volatile-rich cometary material (Whipple, 1950; Marsden et al. 1973; Steckloff et al. 2015a). Near the Sun, the magnitude of this acceleration behaves similarly to radiation pressure, since it

approximates the same inverse square law. Thus, it provides the repulsive acceleration necessary to form striae. However, since the sublimation pressure for H_2O ice is up to 4-5 orders of magnitude stronger than radiation pressure, it can transport chunks of material into the cometary tail that are 4-5 orders of magnitude larger in radius than those transported by radiation pressure alone for a given acceleration of the material relative to the nucleus.

We model parent chunks as balls of pure H_2O ice with such low albedos, that they effectively absorb all incident solar radiation, similar to Steckloff et al. (2015a). We note that these assumptions certainly do no accurately describe the real composition and structure of the parent chunks, which are likely complicated agglomerates of ices and refractory materials with albedos of only a few percent. However, these assumptions illustrate the conditions under which sublimation pressure is maximized, and therefore, define the upper bound of the sublimation pressure acting upon parent chunks. Assuming that the subliming gas is in thermal equilibrium with its source ice and that all incident solar radiation is either re-radiated to space or applied toward overcoming the ice's latent heat of sublimation (Whipple 1950), Steckloff et al. (2015a) show that the sublimation pressure acting on a surface element of cometary material is determined by the following two equations

$$(1-A)\frac{L_{solar}}{4\pi r_h^2 \lambda}\cos\phi = \alpha_{(T)}\sqrt{\frac{m_{mol}}{2\pi RT}}P_{ref}e^{\frac{\lambda}{R}\left(\frac{1}{T_{ref}}-\frac{1}{T}\right)} \tag{4.1}$$

$$P_{sub\,(r_h,\phi)} = \frac{2}{3}(1-A)\frac{L_{solar}}{4\pi r_h^2 \lambda}\sqrt{\frac{8RT}{\pi m_{mol}}}\cos\phi \tag{4.2}$$

where A is the bond albedo of the material, $\alpha_{(T)}$ is the temperature-dependent sublimation coefficient of the volatile species, L_{solar} is the Sun's luminosity, r_{helio} is the

heliocentric distance of the object, λ is the ice's latent heat of sublimation, ϕ is the solar phase of the element of surface relative to the subsolar point, m_{mol} is the molar mass of the ice species, R is the ideal gas constant, T is the temperature of the sublimating gas (assumed to be in thermal equilibrium with its source ice), and P_{ref} is an experimentally determined vapor pressure at temperature T_{ref}. Since equation (4.1) is transcendental, we solve for temperature (T) numerically, then insert it into equation (4.2) to determine the sublimation pressure of a given surface area element. This formulation assumes that the coma around the volatile-rich body is optically thin (Steckloff et al. 2015), which is valid for heliocentric distances greater than ~0.05 AU for cometary bodies up to ~1 km (Drahus, 2014). This method of computing sublimation pressures provides similar results to previous methods of computing sublimative forces on comet nuclei (e.g. Whipple, 1950; Marsden et al. 1973; Sekanina, 2003), but is instead based on the theoretical (rather than empirical) relationship between vapor pressure and temperature, and is therefore useful for volatile species for which limited empirical data exists (Steckloff et al. 2015a). We plot this dynamic sublimation pressure at the subsolar point in Figure 4.3. To compute the net force acting upon a volatile-rich object, we integrate equation 4.2 over the surface of the object.

Once a parent chunk is broken up into small grains and devolatilized, following the remaining steps detailed below, radiation pressure dominates the non-gravitational behavior of the grains. At this point, radiation pressure streams the chunks into a long lineament as in Sekanina & Farrell (1980), creating the observed striae. However, sublimation pressure is responsible for moving the bulk mass of stria material to the location of stria formation.

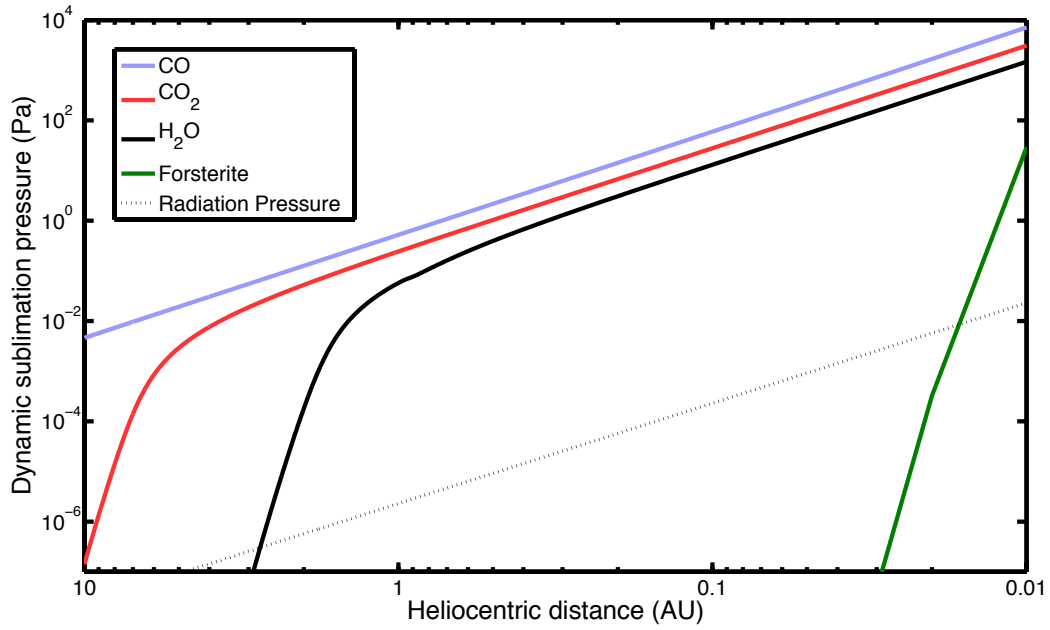

Figure 4.3 Peak Sublimation Pressure as a Function of Heliocentric Distance

We adopted *figure 4* from Steckloff et al. (2015a) to show the variation in peak sublimation pressure for an assumed albedo of 0 as a function of heliocentric distance for common cometary volatile species (H_2O, CO_2, and CO) and the mineral Forsterite, which was found in the coma of comet Wild 2 (Zolensky et al. 2006). For the formation of striae, we focus on the H_2O sublimation curve, as we are positing that H_2O sublimation is responsible for stria formation. Clearly visible is the point (~1 AU) beyond which the sublimation pressure drops off much more quickly. Strength of radiation pressure is added for reference.

4.3.3 Step 2 continued: Rotational acceleration due to SYORP

The back-reaction from anisotropic volatile emission rotationally accelerates striae parent chunks. As a gas molecule escapes from the surface of a parent chunk, it transports angular momentum relative to the center of mass of the parent chunk. The sum of the individual torques from each gas molecule sublimating off of the parent chunk creates a net rotational acceleration of the nucleus (unless that comet possesses perfect symmetry). Thus, in addition to changing the linear motion of a chunk's center of mass, diurnal sublimation can also change a chunk's rotation about its center of mass. We assess the strength of this angular acceleration by analogizing this effect to the well-studied YORP effect (Rubincam, 2000; Bottke et al., 2002; Vokrouhlicky & Capek, 2002; Capek & Vokrouhlicky, 2004; Scheeres, 2007; Rozitis & Green, 2013).

Gas molecules sublimate near the surface of a parent chunk and diffuse through its porous structure, where the gas mean free path is significantly larger than the pores of the cometary material. Eventually these molecules reach the surface, where the last scattering of each gas molecule can be treated independently and the gas emission profile is Lambertian (the probability of being ejected in any given direction is proportional to the cosine of the angle made between that direction and a vector normal to the local surface of the parent chunk [pp. 227-230 in Gombosi, 1994]). Since gas molecules and photons are emitted in a nearly identical fashion, we are able to utilize the theory developed for the photon-driven YORP effect to quantify these sublimation-driven torques.

4.3.3.1 The YORP Effect

Since the numerous instantaneous torques acting on a body are infinitesimal in duration and may be oriented in opposing directions, the YORP effect is a time-averaged phenomenon. The secular rotational acceleration rate due to the YORP effect for an object of radius R and density ρ is (Scheeres, 2007):

$$\frac{d\omega}{dt} = \left(\frac{G_1}{a_{\odot}^2 \sqrt{1-e_{\odot}^2}} \right) \frac{3\, C_Y}{4\pi \rho R^2} \tag{4.3}$$

where $a_{\odot}$ and $e_{\odot}$ are the object's heliocentric semi-major axis and eccentricity, C_Y is a shape-dependent coefficient with typical values between 10^{-3} and 10^{-2} (Scheeres, 2007; Rozitis & Green, 2013), and $G_1 \approx 10^{14}$ kg km s^{-2} is related to the speed of light c and the solar constant $W_{\odot}$ = 1.361 kW m^{-2}, which is defined at 1 AU:

$$\frac{G_1}{(1\ \mathrm{AU})^2} = \frac{W_{\odot}}{c} \tag{4.4}$$

Note that the magnitude of the rotational acceleration scales inversely with surface area and density, and scales linearly with the absolute strength of the solar radiation pressure at the object's location and with its shape-dependent coefficient C_Y, which is defined independent of size (Scheeres, 2007). The coefficient C_Y is determined by the thermally emitted photons, since the absorbed solar radiation contributes no net torque (Rubincam & Paddack, 2010).

4.3.3.2 The SYORP Effect

Since gas molecules carry significantly more momentum than photons, the instantaneous torques acting upon the body are much greater than for the YORP effect.

We parameterize this sublimation-driven YORP (SYORP) effect by modifying the YORP effect rotational acceleration equations (equations 4.3 and 4.4). Since sublimating gas molecules behave like photons at the surface of the parent chunk, sublimation-driven angular acceleration should depend on the shape of the object in the same manner as emitted photon-driven angular acceleration. Therefore, the shape dependent coefficient for sublimation C_S should be the same as that for photons C_Y. Physically, the coefficient C_S represents the fraction of the spin and orbit averaged sublimative momentum flux that contributes a torque due to shape asymmetry. Thus we assume that $C_Y \approx C_S$ for the purposes of our order of magnitude considerations, and should have a value that lies in the range 10^{-3} – 10^{-2} based on asteroid shapes (Scheeres, 2007; Rozitis & Green, 2013), which should be representative of the shapes of cometary nuclei to first order. This is consistent with recent work that implies the values of C_S for cometary nuclei may lie within a small range of values (Samarasinha & Mueller, 2013).

The absolute strength of the gas sublimation pressure P_S is very different than thermal emission pressure

$$P_Y = G_1/{a_\odot}^2\sqrt{1-e_\odot^2}. \tag{4.5}$$

We parameterize this difference with a quantity γ, which is the ratio of the sublimation pressure to the radiation pressure:

$$\gamma = P_S/P_Y \tag{4.6}$$

The angular acceleration associated with SYORP is directly analogous to the angular acceleration associated with YORP:

$$\frac{d\omega}{dt} = \frac{3P_S C_S}{4\pi\rho R^2} = \frac{3\gamma P_Y C_Y}{4\pi\rho R^2} \tag{4.7}$$

where we have taken advantage of both the new parameter γ and the equivalence between the two shape factors C_S and C_γ.

Since a subliming gas molecule carries significantly more momentum than an emitted thermal photon, we might naively expect γ to be greater than one. However, if gas emission is significantly reduced relative to thermal emission, γ may be less than one. We use equations 4.5 and 4.2 for the radiation P_γ and sublimation P_S pressures respectively to compute the ratio γ as a function of heliocentric distance. Near the Sun, the chunk is cooled predominantly through sublimative cooling and energy is lost primarily through overcoming a species latent heat of sublimation. Since the incident solar energy flux scales as the inverse square of heliocentric distance, the sublimative mass-loss rate and resulting sublimation pressures (and therefore gamma) scale approximately (but not exactly) as an inverse square law with heliocentric distance. Further from the Sun, however, the chunk is predominantly cooled by blackbody radiation, and the sublimative mass-loss rates fall far short of the inverse square law, resulting in a steep drop off in gamma with increasing heliocentric distance. This leads to a shape of the gamma curves in which they rise steeply with decreasing heliocentric distance until reaching an approximately constant value (see Figure 4.4).

4.3.4 Step 3: Critical failure of the body

We define a critical rotation rate ω_{crit}, above which the centripetal acceleration required to hold the body together overcomes the tensile strength of the body, leading to fragmentation. Since these chunks survived ejection from the cometary nucleus intact, they are necessarily stronger than their parent nucleus, which typically have strengths on

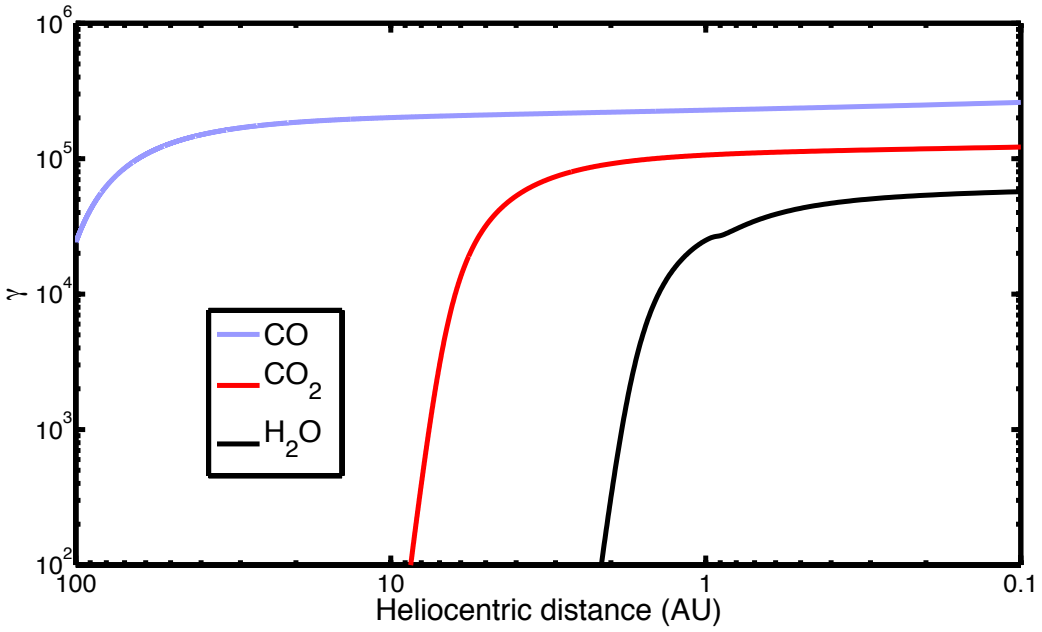

Figure 4.4 A plot of the gamma factor for various species.

Above is a plot of γ (ratio of sublimation pressure to radiation pressure) versus heliocentric distance for various volatiles. We computed these values based on a planar surface element composed purely of the respective volatile, with the Sun located at the zenith. Sublimation pressure data for all volatiles obtained from Steckloff et al. (2015a). We observe that the volatiles activate at larger heliocentric distances, building up the sublimation pressure as the sublimating object moves inward. Closer to the Sun the volatile becomes fully activated, and nearly scale with $\propto 1/r_{helio}^2$, causing the γ-gamma curves to flatten out to a nearly a constant value.

the order of a few Pascals (Sekanina & Yeomans, 1985; Asphaug & Benz, 1996; Melosh, 2011; Bowling et al. 2014; Steckloff et al. 2015a, Thomas et al. 2015). For these icy chunks, self-gravitational forces are dominated by even this weak strength limit. Thus gravity has a negligible effect in holding these icy parent chunks together. To estimate ω_{crit}, we approximate the icy parent chunks as rectangular prisms, where the long axis ($a = 2R$) is twice the length of the other two sides, which we assume to be equal in length ($b = c = R$). The maximum tensile force exerted along the long axis of the body due to strength is then

$$F_{tensile} = A\sigma_t = R^2\sigma_t \tag{4.8}$$

where A is the cross-sectional area perpendicular to the long axis, and σ_t is the material tensile strength. The centripetal force at which the body fails (fragments) under principal axis rotation is

$$F_{cent} = ma_{cent} = \tfrac{1}{2}\rho\omega^2 R^4 \tag{4.9}$$

At the critical rotation rate, $F_{tensile} = F_{cent}$, thus the critical rotation rate (above which the object fragments) is

$$\omega_{crit} = \sqrt{\frac{2\sigma_t}{\rho R^2}} \tag{4.10}$$

We estimate the SYORP timescale by assuming that the parent chunk starts at rest and compute the amount of time required to spin the chunk up to ω_{crit}. We integrate the expression for angular acceleration (equation 4.7) with respect to time (τ), set the constant of integration to zero (for chunks starting at rest), and set this resulting expression for angular velocity (ω) equal to ω_{crit}

$$\tau_S = \frac{R\sqrt{32\rho\sigma_t}}{\gamma P_Y C_Y} \tag{4.11}$$

This timescale defines the duration of an SYORP cycle.

4.3.5 Step 4: Runaway Fragmentation Cascade

We now consider the fragmentation of the parent chunk. Since the chunk slowly spins up to the point of fragmentation, the parent clump likely fragments along a single plane of weakness[1], resulting in two roughly equal-sized daughter chunks. If we assume that the two daughter chunks are equal in mass, and that the total volume of material is preserved, then the daughter chunks will have a radius $\sqrt[3]{1/2}$ of the parent chunk. Such a size decrease is associated with a corresponding increase in the tensile strength of the daughter chunk. According to Griffith Crack Theory (Brace 1961) and assuming a Weibull distribution of flaws within the material, the strength scales approximately as $\sim\sqrt{1/s}$, where *s* is the size of the object. Thus, the daughter clumps will have a tensile strength that is approximately $\sqrt[6]{2} \approx 1.12$ times the tensile strength of the parent chunk.

After fragmentation, the daughter chunks will be rotating approximately at a rate $\omega_{crit,p}$ (the critical rotation rate of its parent chunk), with the exact value depending on geometry. Thus, instead of starting at rest (as is assumed for the initial parent chunk), the daughter chunks already are rotating at a significant fraction of their own ω_{crit}

[1] As opposed to a sudden shock of the material, which may result in many forked fractures and numerous fragments if the shock is traveling faster than the velocity of Raleigh surface waves within the material (order of ~100 m/s)

$$\omega_0 = \omega_{crit,p} \tag{4.12}$$

$$= \sqrt{\frac{1}{\sqrt[3]{2^2}\sqrt[6]{2}}}\,\omega_{crit} \tag{4.13}$$

$$C = \frac{\omega_0}{\omega_{crit}} \approx 0.75 \tag{4.14}$$

which reduces the time needed for the daughter chunks to spin up to fragmentation proportionally. Therefore, the timescales to fragmentation for all chunks (except for the initial parent chunk) are (1-*C*) ≈ 25% of the time to rotational fission from rest. Therefore, while the initial parent chunk will require the full τ_S to spin up to fragmentation, all ensuing daughter chunks will only require $(1-C)\tau_S$ to spin up to ω_{crit}.

If we compute the ratio of the SYORP timescales (equation 4.11) for the daughter clump versus the parent clump, we find that

$$\frac{\tau_{daughter}}{\tau_{parent}} = \frac{(1-C)R_{daughter}\sqrt{\sigma_{daughter}}}{(1-C)R_{parent}\sqrt{\sigma_{parent}}} \tag{4.15}$$

$$= \sqrt[3]{1/2}\sqrt[12]{2} \tag{4.16}$$

$$= \sqrt[12]{\frac{1}{8}} \approx 0.84 \tag{4.17}$$

assuming that ρ and C_s are the same for parent and daughter chunks. Since this ratio of SYORP timescales is less than 1, each successive generation of chunks will have a shorter lifetime than the previous generation, leading to a runaway cascade of fragmentation. Such a cascade is consistent with the modeling of Nishioka (1998) and Jones & Battams (2014) for the creation of dust necessary to explain striae.

We next estimate the duration of the entire cascade of fragmentation events, which is equivalent to the elapsed time between parent chunk ejection from the nucleus and the onset of stria formation. We first compute the number of fragmentation steps needed to fragment a parent chunk into micron-sized dust, which is the suspected size of stria grains (Sekanina & Farrell, 1980). Since daughter chunks have a radius $1/\sqrt[3]{2}$ times the size of their parent chunks, the radius of a chunk in the n^{th} generation is

$$R_n = R_0 2^{-\frac{n}{3}} \tag{4.18}$$

where R_0 is the size of the initial parent chunk ejected from the nucleus. Thus, the number of generations needed to reach size R_n is

$$n = -3\frac{\log_{10}(R_n) - \log_{10}(R_0)}{\log_{10}(2)} \tag{4.19}$$

Therefore, a parent chunk of ~10-100 m in radius requires ~70-80 generations to produce micron sized dust.

Since the SYORP timescale decreases with each subsequent generation, we can analytically solve for the total amount of time needed for a parent chunk to fragment into the n^{th} generation

$$T_n = \tau_0 + \tau_0(1 - C)\sum_{i=1}^{n}\left(\frac{\tau_n}{\tau_{n-1}}\right)^i \approx \tau_0 + 0.25\tau_0\sum_{i=1}^{n}(0.84)^i \tag{4.20}$$

where τ_0 is the SYORP timescale of the initial parent chunk and $C = \omega_0/\omega_{crit}$, which accounts for the nonzero initial rotation of the daughter chunks. The first ~10 generations, which together reduce parent chunk radii by an order of magnitude, dominate this total timescale, occupying over 90% of the time needed to reach sufficiently small fragments. Thus, the time required for an ejected parent chunk to

fragment into micron-sized stria grains (and therefore the duration of the stria-forming fragmentation cascade) is effectively independent of the size of the final grain

$$T_{fragmentation} \approx T_n \approx 2.31\tau_0 \approx 2.31 \frac{R_0\sqrt{32\rho\sigma_{t,0}}}{\gamma P_Y C_Y} \quad (4.21)$$

where $\sigma_{t,0}$ is the tensile strength of the parent chunk.

After each fragmentation event, classical YORP theory predicts that, on average, half of the daughter chunks will continue to spin up to ω_{crit}, while the other half will spin down towards a stationary state. For those chunks that spin down to a low velocity rotation state, the literature is currently inconclusive as to whether or not they will be captured into a low velocity tumbling state (Vokrouhlický & Capek, 2002; Cicalo & Scheeres, 2010; Breiter et al., 2011). If the chunk is not captured in a tumbling state, then it will pass through a low velocity rotation state and emerge accelerating with the opposite sense of rotation. This has been a standard and successful assumption in the literature matching both near-Earth and main asteroid belt spin period distributions (Rossi et al., 2009; Marzari et al., 2011). After making this assumption, then nominally half the chunks take 175% of the SYORP timescale τ_S to fragment while the other half take 25% of τ_S. This factor of a few difference of the fragmentation timescale is smaller than the expected order of magnitude variations of the SYORP shape coefficient C_S.

When the chunks are large and the SYORP fragmentation timescales are relatively long, the chunks that fragment much faster or much slower than the average chunk could drift away from the pack contributing to background dust production and possibly form separate mini-striae. As the SYORP fragmentation cascade progresses and the fragmentation timescales decrease, even chunks with very different fragmentation

timescales will be unable to drift appreciably apart from one another. If only half the initial parent chunk's mass ends up in the stria, then the initial parent chunks must be approximately ¼ larger in radius to account for the mass that fails to form striae. While a sublimative analogue to the Tangential YORP Effect will increase the fraction of chunks that accelerate in the direction of their rotation (Golubov & Krugly, 2012; Golubov et al. 2014) and therefore contribute to stria formation, we conservatively neglect this contribution.

4.3.6 Step 5: Onset of Stria Formation

As the fragmentation cascade continues, the resulting fragments become not only smaller, but also increasingly devolatilized. At some point, the resulting grains within the fragment swarm are so small and devolatilized, that solar radiation pressure dominates their behavior, and they stream anti-sunward as in previous models. While we assume that all daughter chunks are of an equal size and have an idealized distribution of flaws, rotational fragmentation will create chunks that are only approximately equal. While these different sizes will not produce large separations between chunks during earlier generations, variations in size during the final generations will cause the grains to separate from one another via solar radiation pressure according to their differing β values, forming a stria (Sekanina & Farrell, 1980). We therefore consider the point at which a parent chunk completes its fragmentation cascade to be the onset of stria formation

4.3.7 Modeling and Constraints on Stria Formation

We now estimate the constraints of SYORP-driven stria formation on Comet West. We approximate Comet West's orbit as a parabola with a perihelion of 0.197 AU, and numerically investigate the heliocentric and cometocentric distances of stria formed from our scheme as a function of the heliocentric distance of parent chunk ejection. We numerically integrate the motion of hypothetical parent chunks ejected from the nucleus between 180 days pre-perihelion to 90 days post-perihelion, and record their heliocentric and cometocentric distances at which they complete their fragmentation cascades. We assume that parent chunks that have not completed their fragmentation cascades by the time they reached a post-perihelion heliocentric distance of 10 AU will not form stria because this distance is much greater than the heliocentric distance beyond which water ice sublimation shuts down. We assume the separation between the comet and the parent chunk is small compared to their heliocentric distances, which allows us to approximate the change in the cometocentric distance (d_{comet}) of the parent chunk by assuming that its cometocentric drift is due entirely to the effects of dynamic sublimation pressure

$$\Delta d_{comet} = \tfrac{1}{2} a_{(r_{helio})} \Delta t^2 + vt = \frac{3P_{sub\,(r_{helio})}}{8\rho R} \Delta t^2 + v\Delta t \qquad (4.22)$$

where $a_{(r_{helio})}$ is the acceleration of the parent chunk due to sublimation pressure, $P_{sub\,(r_{helio})}$ is the heliocentric distance dependent sublimation pressure, ρ is the density of the parent chunk, and v is the parent chunk's cometocentric velocity. We assume that this distance montonically increases. This is an admittedly simplified model, which accounts only for a one-dimensional change in the cometocentric distance. However, the largest sources of error are likely the uncertainties in the physical properties of the parent

grains. This one-dimensional model is therefore sufficient for our purpose of understanding the order of magnitude behavior of parent chunks, and we reserve two or three-dimensional modeling of stria formation with a deeper study of parent chunk properties for another paper.

Our assumed initial velocity of the parent chunk (~1 m/s) relative to the nucleus is negligible compared to the average velocity needed to move a parent chunk from the nucleus to the cometocentric location of stria formation (~100-1,000 m/s) in the weeks between passing the sublimation barrier (the heliocentric distance within which H_2O sublimation becomes the dominant cooling mechanism of the nucleus) and forming a stria. Therefore, we can treat the parent chunks as though they were initially at rest. Additionally, because the parent chunks have an initial velocity comparable to the comet's escape velocity, the parent chunk will quickly move several nucleus radii away from the nucleus, to a point where the cometary gravity is negligible compared to solar gravity or sublimation pressure (while still being relatively close to the nucleus when compared to the cometocentric distance of stria formation). We therefore ignore the negligible effects of cometary gravity on this calculation. We assume that that parent chunk has a tensile strength of 10 Pa, which is the expected order of magnitude when the ~1 Pa strength of ~1 km comet nuclei (Sekanina & Yeomans, 1985; Asphaug & Benz, 1996; Bowling et al. 2014; Thomas et al. 2015; Steckloff et al. 2015a) is scaled to a ~10 m chunk using a $\sqrt{1/s}$ strength scaling law (Brace, 1961). We use a time step of 6 hours in the numerical modeling.

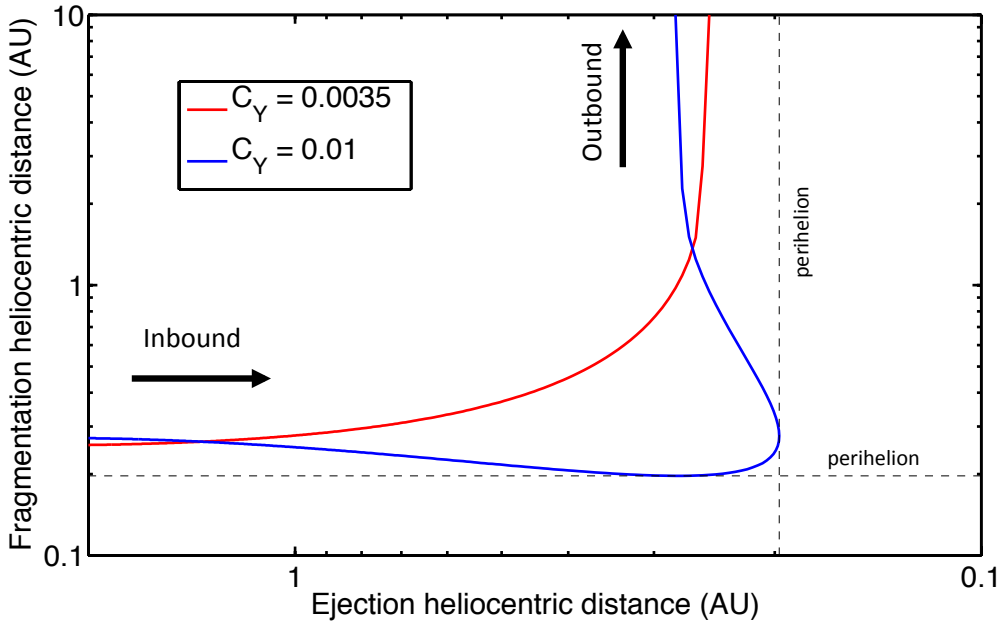

Figure 4.5: Comet West stria formation heliocentric distance versus parent chunk ejection heliocentric distance

We plot the heliocentric distance of fragmentation for each simulated 10m parent chunk ejected from Comet West at 6 hour invervals as a function of the heliocentric distance of parent chunk ejection for two values of the SYORP coefficient C_Y = 0.01 and 0.0035. This plot reveals that the overwhelming majority of ejected parent chunks would produce stria between 0.2 and 0.3 AU (near perihelion), consistent with observations (Sekanina & Farrell 1980). Additionally, parent chunks ejected beyond the sublimation barrier (~1 AU) form striae at near the same heliocentric distance (the stria barrier), leading to the asymtotic behavior of the inbound part of the curves. Meanwhile, few chunks ejected after the sublimation barrier have time to fragment before passing back beyond the sublimation barrier, leading to the asymptotic behavior of the outbound part of the curves.

In Figure 4.5, we plot the heliocentric distance of the onset of stria formation (the point at which the fragmentation cascade is complete) as a function of the heliocentric distance of ejection of a 10 m parent chunk for a comet with the orbit of Comet West. We plot two different cases of the SYORP coefficient C_S, which illustrate two different behaviors in Figure 4.5: one in which the parent chunk parameters restrict all striae formation to post-perihelion (C_S=0.0035), and another in which the parent chunk parameters allow for the formation of some pre-perihelion striae (C_S=0.01), which puts a bulge in the curve near perihelion.

For the case where C_S=0.01 (which is the upper bound of the expected range of SYORP coefficients, and therefore represents the strongest expected response to SYORP), we find that the heliocentric distance of stria formation has little dependence on the heliocentric distance of parent chunk ejection, with the vast majority of parent chunks forming striae within a narrow window of heliocentric distances (for a given parent chunk size and SYORP coefficient). Because of the sublimation barrier, any parent chunk ejected beyond ~1 AU will experience neither a significant SYORP effect nor sublimation pressure until it reaches the sublimation barrier. After crossing the sublimation barrier, the rapid increase in SYORP torques that peak at perihelion will induce a peak in the number of parent chunks completing their fragmentation cascades, and would therefore cause a burst of stria formation near- and post-perihelion. Meanwhile, Figure 4.5 reveals that very few parent chunks ejected post-perihelion have sufficient time to undergo the SYORP fragmentation cascade (Step 5) to form striae before passing back across the sublimation barrier, and is only possible for parent chunks

that have a very strong response to SYORP torques (i.e. smaller radii and larger SYORP coefficients).

Thus, our model predicts that large, Comet West-like stria should preferentially form after the comet reaches near-perihelion and ~1 AU (water sublimation barrier), with a large burst of striae forming near perihelion, consistent with observations of striae (Sekanina & Farrell, 1980; Pittichová et al. 1997). This is not to suggest that no striae can form prior to perihelion. Striated comet nuclei likely eject a population of parent chunks with a distribution of sizes and SYORP coefficients. Because the SYORP response is size-dependent, our model predicts that smaller parent chunks will be able to respond quickly enough to the weaker pre-perihelion SYORP torques to form striae (assuming that SYORP coefficients are independent of size.) However, these early striae would contain significantly less material than the larger striae that form later, and may therefore be unobservable. Thus, while our SYORP model of stria suggests that any comet capable of ejecting icy chunks could form striae, they may not stand out above background dust emission. Therefore, a careful pre-perihelion study of striated comets could confirm this aspect of SYORP theory.

4.4. Striae of Comet West

We lastly apply our model to the striae of Comet West as a proof of concept of the SYORP model. We use this rudimentary one-dimensional model to estimate the sizes and SYORP coefficients of the initial parent chunks needed to match the estimated heliocentric and cometocentric distances of its striae (Sekanina & Farrell, 1980). Sekanina & Farrell (1980) obtain these distances by modeling the motion of devolatilized

dust under the effects of solar gravity and radiation pressure. Although the Sekanina & Farrell (1980) model of stria formation differs from the model presented in this paper, both models of dust behavior post-formation are identical. Therefore, the heliocentric and cometocentric distances of stria formation that were obtained by post-formation stria dust modeling are applicable to our model.

We list the heliocentric and cometocentric distances of stria formation for the observed stria of Comet West from Sekanina & Farrell (1980), along with our parent chunk radii and SYORP coefficients (C_S) that best fit those distances in Table 4.1. Each heliocentric and cometocentric distance pair have two unique solutions for parent chunk radius and SYORP coefficient: one solution for the pre-perihelion portion of the comet's orbit, and a second solution for the post-perihelion portion of the orbit. Because the striae in Sekanina & Farrell (1980) were observed post-perihelion, we restrict ourselves to this set of solutions.

The best-fit parent chunks' SYORP coefficients (C_S) lie between 0.00029 – 0.00126, and their best-fit radii lie between 15-110 m. These SYORP coefficients are on the low size of their expected range of ~0.001-0.01 (Scheeres, 2007; Rozitis & Green, 2013), which is based on repurposing YORP coefficients to SYORP. While this may be a result of model assumptions, we acknowledge that it may be indicative of a fundamental difference between the YORP and SYORP effects. The YORP and SYORP coefficients are shape-dependent parameters that describe the second order torques that arise from asymmetries in the shape of the object. Unlike the YORP effect, SYORP depends on the loss of material from the surface of the object that can eliminate asymmetries in its shape over time, particularly at smaller size scales.

Table 4.1 Heliocentric and Cometocentric locations of stria formation for Comet West and their best-fit parent chunks

Heliocentric Distance (AU)[1]	Cometocentric Distance (Gm)[1]	Best Fit Parent Radius (m) (error $R_{-27\%}^{+10\%}$)	Best Fit Parent C_S (error $C_{S\,-2\%}^{+6\%}$)
0.2284	2.56	32.5	0.00056
0.2924	7.58	16.4	0.00029
0.2696	5.34	20.5	0.000355
0.2581	4.2	24	0.000406
0.2606	4.1	24.75	0.000415
0.2535	3.27	30.5	0.000493
0.2683	4.06	26.5	0.000433
0.2506	2.8	35	0.000555
0.2592	2.92	34	0.000530
0.2517	2.14	47	0.000688
0.2543	1.97	50	0.000715
0.2785	2.94	37	0.000544
0.2769	2.29	49	0.00067
0.2624	1.1	95	0.00114
0.2685	0.96	110	0.00126
0.2841	1.12	105	0.00118

[1]Sekanina & Farrell (1980)

This table lists the modeled heliocentric and cometocentric distances of formation for 16 striae of Comet West (Sekanina & Farrell, 1980). These distances were obtained by modeling the post-formation dynamics of the dust that composed each stria. This table also lists our best fit radius and SYORP coefficient for each stria.

If the object becomes more symmetrical, its SYORP coefficient will drop over time. Therefore, time-averaged SYORP coefficients may be, as a whole, smaller than their YORP counterparts. While our model assumes a static SYORP coefficient, these best-fit SYORP coefficients are more representative of an average value. Therefore, while the initial SYORP coefficient of a parent chunk may be comparable to its YORP coefficient, the loss of mass required by SYORP may result in a lower average SYORP coefficient than the average YORP coefficient (were the chunk not sublimating.)

The best-fit radii of the parent chunks fall within the expected ~10-100 m range. The estimated error in the size of the radii of the parent chunks is a result of uncertainly in the magnitude of the average dynamic sublimation pressure. Steckloff et al. (2015a) estimate the uncertainly in the sublimation pressure to be up to ~10% for pure H_2O ice sublimation. Additionally, we use a dynamically new comet C/2012 S1 (ISON), which is a reasonable analogue to the predicted pristine parent chunks, to estimate uncertainties associated with sublimation contributions from less common but more volatile species and the active fraction of the parent chunks' surfaces. We estimate that the small contributions from less common sublimating volatile species (CO_2, CO, etc.) to be up to ~10%, based on their relative abundances (McKay et al. 2014; Weaver et al. 2014) and relative volatilities (Steckloff et al. 2015a). Unlike JFC nuclei which have only small fractions of their nuclei that are active, the entire surface of Comet ISON appeared to be active (Steckloff et al. 2015b), which is consistent with the thermally primitive nature of long-period comets. While this would suggest that fragments of such a nucleus (i.e. stria parent chunks) would similarly be active all over, we do not understand what mechanism may be responsible for their ejection. We consider the case in which the ejection

mechanism lofts a partially exposed chunk of material, and conservatively estimate that the exposed region of that chunk (perhaps 20% of its surface) is devolatilized and inactive (or equivalently, that a larger portion of its surface is partially devolatilized). Because we do not currently have a well-studied ejection mechanism that we could use to better constrain these uncertainties, we adopt the conservative estimate of 20% as the uncertainly in the active area.

These errors are not symmetrical about our best fit solution. Our model assumes the maximum possible sublimation pressure and active area, and uncertainties in their values can only revise them downward. We therefore end up with an asymmetrical error in the average sublimation pressure of $P_{sub}{}_{-25\%}^{+10\%}$ from propagation of errors. We run these uncertainties through our model to estimate the uncertainties in the radii of the parent chunks of the striae from Sekanina & Farrell (1980) to be $\varepsilon R = R_{-27\%}^{+10\%}$, and the uncertainty in the corresponding SYORP coefficients to be $\varepsilon C_S = C_S{}_{-2\%}^{+6\%}$.

With 16 parent chunks, we can generate a Size-Frequency Distribution (SFD), which plots the number of chunks larger than a particular size (see Figure 4.6). We neglect to include parent clumps smaller than 20 m in this power law fit, as the power law shows a break in the trend, which likely indicates observational bias near the limit of detection. The cumulative-SFD represents the number of chunks greater than a given size, and appears to follow a clear power law ($N(> R) \propto R^q$) with a best-fit power law index (q) of -1.4. However, a power law index between -2.0 and -1.1 is consistent with the estimated errors in our model, and power law indexes between -1.1 and -4.0 are consistent with the estimated errors of the chunks up to 50 m in radius. This cumulative-

SFD power-law index is consistent with the index of q=-1.92±0.20 for Jupiter Family Comets (JFCs) with radii larger than 1.25 km (Snodgrass et al. 2011), but is only marginally consistent with the index of ~-1 that describes the impactor population (<~2km) in the young terrains of Europa (Bierhaus et al. 2012).

The differential Size-Frequency Distribution (differential-SFD) is generated by taking a derivative of the cumulative-SFD with respect to object radius generates the differential Size-Frequency Distribution (differential-SFD). The differential-SFD for all parent chunks has a power-law slope of -2.4 (-3.0- -2.1), but values between -2.1 and -5 are consistent with the estimated errors of the chunks up to 50 m in radius. This is consistent with the differential-SFD index of the fragments of Comet 73P/Schwassmann-Wachmann 3 Nucleus B of -2.11 (Fuse et al. 2007) or -2.56 (large fragments F > 10mJy) (Reach et al. 2009), but inconsistent with its small fragments (F < 10 mJy) index of -1.84 (Reach et al. 2009). This range of differential-SFD power-law indexes for all parent chunks of Comet West is inconsistent with the differential-SFD indexes of -4.7 to -6.6 (Kelley et al. 2013) and -3 to -4 (Rotundi et al. 2015) that describe the chunks and grains in the inner comae of comets 103P/Hartley 2 and 67P Churyumov-Gerasimenko respectively. However, the two latter populations are for small chunks (up to ~1 m in radius), and the differential-SFD power-law slope for parent chunks of Comet West up to 50 m in radius is consistent with both of these populations. It is presently unclear whether these similar power law indexes indicate a similar origin, composition, or evolution of these different populations, and further study is warranted to place these cometary populations into a common context and explore how evolutionary and ejection processes may alter these SFDs.

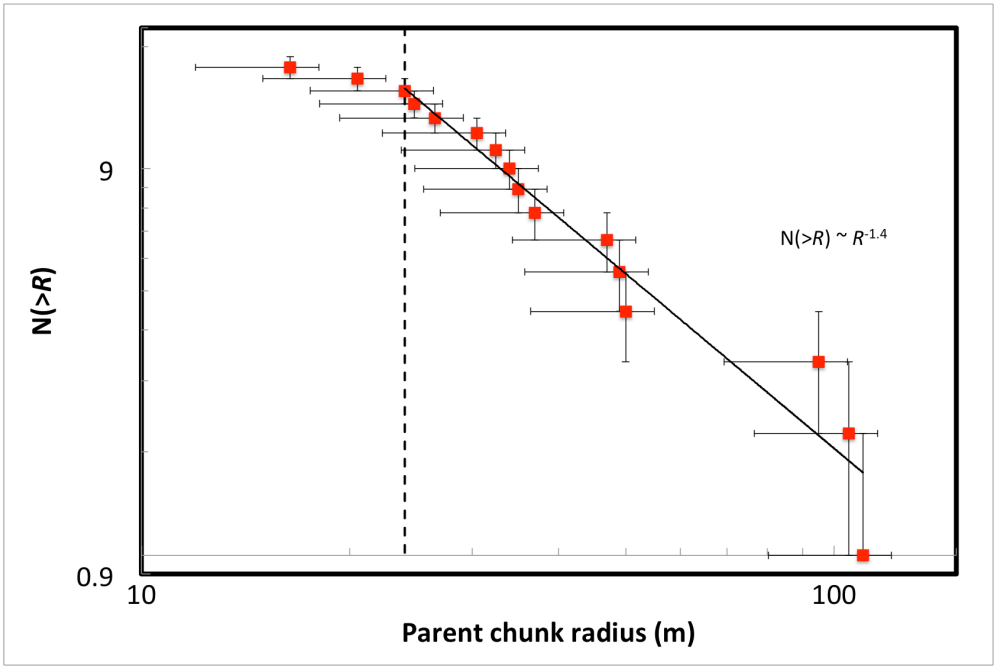

Figure 4.6: Cumulative Size-frequency distribution of the best-fit parent chunks of Comet West's striae. Here we plot the number of chunks larger than a given parent chunk size. Vertical error bars are $\sqrt{N}$, while horizontal error bars are the estimated $\sim^{+10\%}_{-27\%}$ uncertainly in parent chunk radius. Vertical dashed line represents a break in the size-frequency distribution, which we belive is due to observational bias.

4.5. Discussion

Thus far our analysis has assumed that the sublimation fronts for the volatile ices are located at the surface of the chunks, rather than below. Comet ISON's dust activity, which is a proxy for gas sublimation, was located predominantly on the sunward side of the nucleus (Li et al. 2013b). This is common for comet nuclei (Whipple, 1950; Keller et al. 1986; Feaga et al. 2007; Belton, 2013; Gulkis et al. 2015), and suggests that the volatile sublimation front is close enough to the surface of the nucleus to respond to the diurnal thermal wave (Steckloff et al. 2015a), such that the time required for a pulse of heat at the surface to propagate to the sublimating volatiles is short compared to the rotation period. This behavior is consistent with the low thermal inertias of cometary material (Lisse et al. 2005; Lamy et al. 2008; Davidsson et al. 2013; Groussin et al. 2013; Gulkis et al. 2015). However, if the rotation period of a parent chunk were to become comparable to this thermal lag time during SYORP spin up, then the chunk's gas emissions would begin to lose their sunward directionality, and sublimation pressure would begin to cease driving the chunk anti-sunward.

Shutting down the anti-sunward sublimation-driven acceleration would not affect the SYORP torques, which, like the YORP effect, only depends on the shape of the chunk. Therefore a chunk in this situation would cease to accelerate heliocentrically, but would drift cometocentrically at a constant rate and continue to spin up to the point of fragmentation, at which point this cycle would repeat with the daughter chunks. Because the antisunward acceleration would episodically shut down, the resulting cometocentric distance of stria formation would be reduced. However, since neither the thermal lag time between the nuclear surface and the volatile ices nor the depth of the volatile ices of

Oort Cloud comets is known, these considerations are currently merely unconstrained speculation.

The SYORP mechanism, while explaining why most observed striae form near- or post-perihelion, predicts that striae may also form pre-perihelion within ~1 AU of the Sun. However, the parent chunks that would form these earlier striae would have to undergo their fragmentation cascades in a shorter period of time, and would therefore be significantly smaller than the parent chunks that form post-perihelion striae. Because these smaller parent chunks would form striae that contain less material than the post-perihelion striae, these earlier striae are expected to be faint and likely to remain undetected. A careful pre-perihelion study of comets that produce post-perihelion striae may be able to confirm this aspect of the SYORP theory.

Additionally, we assume that H_2O sublimation is driving the stria formation process. However, if more volatile species such as CO_2 or CO are driving striae formation, then striae may form further from the Sun, form faster, and contain more material. Additionally, if parent chunks are ejected via sublimation of supervolatile species from a discrete location of the nucleus, then parent chunks may be diurnally ejected. If this process occurs within the sublimation barrier of the driving species, then it may lead to the formation of striae that are regularly spaced within the cometary tail, and that form at an interval approximating the rotation period of the nucleus.

Our model relies on the ability of comet nuclei to eject ~10-100 m sized chunks at escape velocity (~1 m/s). Long-period comet C/1992 B2 (Hyakutake) experienced an outburst that ejected chunks consistent with the parent chunks in our model (Desvoivres et al. 2000; Schleicher & Woodney, 2003). However, it is unclear whether or not the

comet formed striae due to limited observations of the comet post-perihelion. Similarly, Jupiter Family Comet 17P/Holmes produced fragments consistent with parent chunks (Stevenson et al. 2010), however its distant perihelion of 2 AU would likely prevent the vigorous sublimation that is necessary in our model to form striae. Spacecraft flybys of comet nuclei (such as Giotto, Deep Space 1, Deep Impact, Stardust, DIXI, and Stardust-NExT) would be very unlikely to resolve the ejection of parent-sized chunks of material due to their limited time of encounter, and would almost certainly require a Rosetta-style mission to observe the nucleus of a striated comet for an extended period of time.

The Rosetta spacecraft itself has observed decimeter to meter-sized chunks of material moving at near escape velocity at Comet 67P/Churyumov-Gerasimenko (Rotundi et al. 2015) and would certainly be able to detect the ejection of objects as large as parent chunks. However, because striae are a rare phenomenon and Jupiter Family Comets are so thermally processed, we would not necessarily expect that 67P/Churyumov-Gerasimenko would be able to eject parent chunks at escape velocity, which is required to form striae. Indeed, Rosetta has discovered ~10-100 m chunks of material that may have been ejected from the nucleus of 67P/Churyumov-Gerasimenko, but lacked sufficient velocity to escape the nucleus' gravity (Thomas et al. 2015). Direct observation of the ejection of ~10-100 m chunks of material would be much more likely by a spacecraft at a long period comet or active centaur. However, failure to detect the ejection of ~10-100 m chunks of material at these bodies would not necessarily invalidate this theory, since it predicts that only some bodies are capable of ejecting these chunks.

It is plausible that a particularly active comet could eject parent chunks at velocities an order or two of magnitude greater than the comet's escape velocity. Such

parent chunks could drift significantly farther from the nucleus than other parent chunks, and would form striae far from the cometary tail. However, if these parent chunks are ejected sufficiently far from the Sun in the centaur region, they may drift so far from the nucleus that they would form dust features too far from the nucleus to be easily associated with the comet. The Rosetta spacecraft currently in orbit around the nucleus of comet 67P/Churyumov-Gerasimenko may be able to directly observe the ejection of large chunks of material from the nucleus during perihelion, and perhaps even obtain a velocity profile of the ejected population.

Additionally, our model may predict observable intermediate stages of stria formation. Because we begin with a single parent chunk, the initial stages of stria formation would be unobservable. We have already shown that daughter chunks with radii that are comparable to the initial parent chunk predominantly occupy the duration of the SYORP fragmentation cascade. Thus, as the daughter chunks drift away from the nucleus, they remain unobservable. However, as the runaway fragmentation cascade nears completion, a very large number of small chunks are produced very rapidly. Thus, immediately prior to the onset of stria formation, an observable cloud of material may appear in the tail of the comet that then streams outward into a stria.

While we assume that each step of the SYORP fragmentation cascade produces two identical daughter chunks (size and shape), it is likely that these two chunks vary from one another. If this variation is small, then the fragmentation cascade would be insignificantly affected and the daughter chunks will still complete their fragmentation cascades at approximately the same time. However, if this variation is large, then one daughter chunk may undergo a significantly faster fragmentation cascade, and complete

its fragmentation before drifting a significant distance from the nucleus. This would manifest itself as a source of fine-grained debris in the tail of the comet located between the nucleus and the striae. Additionally, if the fragmentation of the larger daughter chunks (early stages of the fragmentation cascade) is messy and produces fine-grained debris, then it would also manifest itself as an additional source of fine-grained material between the nucleus and striae. In either of these cases, one may see a diffuse or wispy tail of material distinct from the striae or the rest of the dust tail. However, if the fragmentation cascade is more ideal, or if the dust tail is bright, then this feature may not be visible or even existent.

Lastly, while we have only applied SYORP to parent chunks on the order of ~10-100 m in radius, there is no reason why SYORP would not affect much larger icy objects within the Solar System. Indeed, the SYORP mechanism should be able to change the spin state of icy objects of all sizes. The limiting factor for SYORP is heliocentric distance, as the effect shuts down beyond the sublimation barrier of the driving volatile species. While we have here only considered the sublimation of water ice (which shuts down beyond ~1 AU), CO_2-driven SYORP would be active out to ~10 AU, while CO-driven SYORP would remain active out to ~100 AU! Therefore, as long as the appropriate volatile species is present and abundant, SYORP can provide torques to objects throughout the observable Solar System.

4.6. Summary & Conclusions

We have proposed a new sublimation-driven model for the formation of striae within the tails of comets that provides a natural explanation for why comets with

perihelia within 0.6 AU only form striae within ~1 AU of the Sun after reaching the near-perihelion portion of their orbits. Our model easily allows a large amount of material to be transported as a single unit to the location of stria formation, a major weakness of existing stria formation schemes. As part of our driving mechanism, we describe a new, sublimation-driven analogue to the YORP effect (SYORP), which allows large (~10-100 m) parent chunks to fragment quickly enough to form stria within the inner Solar System. If large numbers of parent chunks with similar sizes and shapes are ejected prior to the comet passing within the sublimation barrier, then these parent chunks should produce a sudden burst of striae. However, the ejection of parent chunks with a range of sizes and shapes is more likely.

We apply our model to the striae of Comet West, and find that parent chunks with radii between 15 m and 110 m ($^{+10\%}_{-27\%}$), which are consistent with expected sizes. The sizes of these parent chunks follow a power-law cumulative size-frequency distribution (cumulative-SFD) with a power-law index of $-1.4^{+0.3}_{-0.6}$ ($-1.5^{+0.4}_{-2.5}$ for parent chunks less than 50 m radius), which is consistent with the index of -1.92±0.20 for Jupiter Family Comets with radii larger than 1.25 km (Snodgrass et al. 2011) and marginally consistent with the index of ~-1 for the impactor population into the young terrains of Europa (Bierhaus et al. 2012). The differential Size-Frequency Distribution (differential-SFD) of $-2.4^{+0.3}_{-0.6}$ is consistent with 73P/Schwassmann-Wachmann 3 Nucleus B's large fragments (Reach et al. 2009) or all fragments (Fuse et al. 2007). The differential-SFD for parent chunks less than 50 m in radius of $-2.5^{+0.4}_{-2.5}$ is consistent with the differential-SFD indexes of the particles in the inner comae of comets 103P/Hartley 2 (Kelley et al. 2013) and 67P/Churyumov-Gerasimenko (Rotundi et al. 2015). The mechanism responsible for

lofting these parent chunks off of the surface of the nucleus is unknown, but we speculate that it may be the resulting gas drag from a cometary outburst, consistent with the observed parent-sized chunks of comet 17P/Holmes (Stevenson et al. 2010) and comet C/1996 B2 (Hyakutake) (Desvoivres et al. 2000; Schleicher & Woodney, 2003). The SYORP coefficients (C_S) of Comet West's parent chunks are 0.00029 – 0.00126 ($^{+6\%}_{-2\%}$), which is on the low side of the expected range of ~0.001-0.01 (Scheeres, 2007; Rozitis & Green, 2013). This may be due to the loss of surface material that is inherent in the SYORP mechanism, and which may remove the asymmetries in the shape of the body that generate the sublimative torques that create the SYORP effect.

We also predict that fainter, potentially observable striae may form earlier than the larger easily observable striae. However, these early striae would tend to form from smaller parent chunks, and would therefore be harder to detect. Additionally, our mechanism suggests that any comet capable of ejecting icy chunks can produce striae, which may or may not be large enough to be observable. Lastly, we speculate on possible intermediate stages of stria formation in our mechanism that may be observable. One would appear as a cloud of material present immediately prior to stria formation, which may or may not be visible above the background of the dust tail. The other depends on imperfections during the SYORP fragmentation cascade, and may appear as a faint wispy tail-like feature located in the dust tail between the nucleus and the striae if the fragmentation is sufficiently imperfect and the dust tail is sufficiently dim.

References

Asphaug, E. & Benz, W. Size, density, and structure of Comet Shoemaker-Levy 9 inferred from the physics of tidal breakup. *Icarus* **121**, 225-248, (1996)

Belton, M.J.S. 2010. Cometary activity, active areas, and a mechanism for collimated outflows on 1P, 9P, 19P, and 81P. *Icarus* **210**, 881-897 (2010)

Belton, M. J. S., Meech, K. J., Chesley, S., Pittichová, J., Carcich, B., Drahus, M., Harris, A., Gillam, S., Veverka, J., Mastrodemos, N., Owen, W., A'Hearn, M. F., Bagnulo, S., Bai, J., Barrera, L., Bastien, F., Bauer, J. M., Bedient, J., Bhatt, B. C., Boehnhardt, H., Brosch, N., Buie, M., Candia, P., Chen, W.-P., Chiang, P., Choi, Y.-J., Cochran, A., Crockett, C. J., Duddy, S., Farnham, T., Fernández, Y. R., Gutiárrez, P., Hainaut, O. R., Hampton, D., Herrmann, K. A., Hsieh, H., Kadooka, M. A., Kaluna, H., Keane, J., Kim, M.-J., Klaasen, K., Kleyna, J., Krisciunas, K., Lara, L. M., Lauer, T. R., Li, J.-Y., Licandro, J., Lisse, C. M., Lowry, S. C., McFadden, L., Moskovitz, N., Mueller, B., Polishook, D., Raja, N. S., Riesen, T., Sahu, D. K., Samarasinha, N., Sarid, G., Sekiguchi, T., Sonnett, S., Suntzeff, N. B., Taylor, B. W., Thomas, P., Tozzi, G. P., Vasundhara, R., Vincent, J.-B., Wasserman, L. H., Webster-Schultz, B., Yang, B., Zenn, T., Zhao, H. Stardust-NExT, Deep Impact, and the accelerating spin of 9P/Tempel 1. *Icarus* **213**, 345-368 (2011)

Belton, M.J.S. The sources of the unusual dust jets seen in Comet 103P/Hartley 2. *Icarus* **222**, 653-661 (2013)

Bierhaus, E.B.; Dones, L.; Alvarellos, J.L.; Zahnle, K.; The role of ejecta in the small crater populations on the mid-sized Saturnian satellites. *Icarus* **218**, 602-621 (2012)

Bottke, W. F., Jr., Vokrouhlicky, D., Rubincam, D. P., Broz, M. The Effect of Yarkovsky Thermal Forces on the Dynamical Evolution of Asteroids and Meteoroids. *Asteroids III* 395-408 (2002)

Bowling, T.B.; Steckloff, J.K.; Melosh, H.J.; Graves, K.J. The strength of Comet 67P/Churyumov-Gerasimenko. *American Astronomical Society – Division of Planetary Science Meeting #46*, Abstract #100.03 (2014)

Brace, W.F.; Dependence of fracture strength of rocks on grain size. *Penn State University Mineral Expt. State Bulletin* **76**, 99-103 (1961)

Breiter, S., Rozek, A., Vokrouhlicky, D.. 2011. Yarkovsky-O'Keefe-Radzievskii-Paddack effect on tumbling objects. Monthly Notices of the Royal Astronomical Society 417, 2478-2499

Brownlee, D.E. et al.; Surface of young Jupiter Family Comet 81P/Wild 2: View from the Stardust Spacecraft. *Science* **304**(5), 1764-1769 (2004)

Bruck Syal, M., Schultz, P. H., Sunshine, J. M., A'Hearn, M. F., Farnham, T. L., Dearborn, D. S. P. Geologic control of jet formation on Comet 103P/Hartley 2. *Icarus* **222**, 610-624 (2013)

Capek, D., Vokrouhlicky, D. The YORP effect with finite thermal conductivity. *Icarus* **172**, 526-536 (2004)

Chesley, S.R.; Belton, M.J.S.; Carcish, B.; Thomas, C.; Pittichová, J.; Klaasen, K.P.; Li, J.-Y.; Farnham, T.L.; Gillam, S.D.; Harris, A.W. An updated rotational model for Comet 9P/Tempel 1. *Icarus* **222**, 516-525 (2013)

Cicalo S., Scheeres, D. J.. 2010. Averaged rotational dynamics of an asteroid in tumbling rotation under the YORP torque. Celestial Mechanics and Dynamical Astronomy 106, 301-337

Davidsson, B.J.R. et al. Thermal inertia and surface roughness of Comet 9P/Tempel 1. *Icarus* **224**, 154-171 (2013).

Desvoivres, E.; Kinger, J.; Levasseur-Regourd, A.C.; Jones, G.H.; Modeling the Dynamics of Cometary Fragments: Application to Comet C/1996 B2 Hyakutake. *Icarus* **144**, 172-181 (2000)

Drahus, M. Rotational Disruption of Comets with Parabolic Orbits. *AAS/Division for Planetary Sciences Meeting Abstracts 46*, #200.04 (2014)

Feaga, L.M.; A'Hearn, M.F.; Sunshine, J.M.; Groussin, O.; Farnham, T.L. Asymmetries in the distribution of H_2O and CO_2 in the inner coma of Comet 9P/Tempel 1 as observed by Deep Impact. *Icarus* **190** 345-356 (2007)

Fernández, Y.R.; That's the way the comet crumbles: Splitting Jupiter-family comets. *PSS* **57**, 1218-1227 (2009)

Froehlich, H.-E., Notni, P. Radiation pressure - A stabilizing agent of dust clouds in comets?. *Astronomische Nachrichten* **309**, 147-155 (1988)

Fuse, T.; Yamamoto, N.; Kinoshita, D.; Furusawa, H.; Watanabe, J.; Observations of Fragments Split from Nucleus B of Comet 73P/Schwassmann-Wachmann 3 with Subaru Telescope; *PASJ* **59**, 381-386 (2007)

Golubov, O. and Krugly, Y.N. Tangential component of the YORP effect. *Ap. J.* **752**, L11-L15 (2012) doi: 10.1088/2041-8205/752/1/L11

Golubov, O.; Scheeres, D.J.; Krugly, Y.N.; A three-dimensional model of tangential YORP. *Ap. J.* **794**, 22-30 (2014) doi:10.1088/0004-637X/794/1/22

Gombosi, T.I. 1994. Free molecular aerodynamics. In *Gaskinetic theory*. Edn. 1 (Cambridge University Press, Cambridge, UK)

Green, S.F. et al. The dust mass distribution of comet 81P/Wild 2. *JGR* **109**, E12S04 (2004) doi:10.1029/2004JE002318

Groussin, O. et al. The temperature, thermal inertia, roughness and color of the nuclei of Comets 103P/Hartley 2 and 9P/Tempel 1. *Icarus* **222**, 580-594. (2013)

Gulkis, S. et al. Subsurface properties and early activity of comet 67P/Churyumov-Gerasimenko. *Science* **347**, (2015) DOI: 10.1126/science.aaa0709

Gutiárrez, P. J., Jorda, L., Ortiz, J. L., Rodrigo, R. Long-term simulations of the rotational state of small irregular cometary nuclei. *Astronomy and Astrophysics* **406**, 1123-1133 (2003)

Gutiárrez, P. J., Davidsson, B. J. R. Non-gravitational force modeling of Comet 81P/Wild 2. II. Rotational evolution. *Icarus* **191**, 651-664 (2007)

Hammel, H.B.; Telesco, C.M.; Campins, H.; Decher, R.; Storrs, A.D.; Cruikshank, D.P.; Albedo maps of comets P/Halley and P/Giacobini-Zinner. *Astron. Astrophys.* **187**, 665-668 (1987)

Hermalyn, B. and 11 coauthors. The detection, localization, and dynamics of large icy particles surrounding Comet 103P/Hartley 2. *Icarus* **222**, 625-633 (2013)

Jones, G., Battams, K. Dust tail striae: Lessons from recent comets. *Asteroids, Comets, Meteors* 2014 249- (2014)

Julian, W.H. The Comet Halley nucleus – Random jets. *Icarus* **88**, 355-371 (1990)

Keller, H.U. et al.; First Halley multicolour camera imaging results from Giotto. *Nature* **321**, 320-326 (1986)

Kelley, M.S. et al. A distribution of large particles in the coma of Comet 103P/Hartley 2. *Icarus* **222**, 634-652 (2013)

Kharchuk, S.V. & Korsun, P.P. Striated features in the dust tail of Comet C/2006 P1 (McNaught). *Kinematics and Physics of Celestial Bodies* **26**(6), 322-325 (2010)

Lamy, P.L.; Toth, I.; Fernández, Y.R.; Weaver, H.A.; The Sizes, Shapes, Albedos, and Colors of Cometary Nuclei. In *Comets II*. Editors: Festou, M.; Keller, H.U.; Weaver, H.A. University of Arizona Press-Tucson, AZ (2004)

Lamy, P.L.; Toth, I.; Groussin, O.; Jorda, L.; Kelley, M.S.; Stansberry, J.A.; Spitzer Space Telescope observations of the nucleus of comet 67P/Churyumov-Gerasimenko. *A&A* **489**, 777-785 (2008)

Li, J.-Y. et al.; Deep Impact photometry of Comet 9P/Tempel 1. *Icarus* **191**, 161-175 (2007)

Li, J.-Y. et al.; Photometric properties of the nucleus of Comet 103P/Hartley 2. *Icarus* **222**, 559-570 (2013a)

Li, J.-Y. et al.; Characterizing the dust coma of Comet C/2012 S1 (ISON) at 4.15 AU from the Sun. *Ap. J. L.* **779**, L3 (2013b)

Lisse, C.M.; A'Hearn, M.F.; Groussin, O.; Fernandez, Y.R.; Belton, M.J.S.; van Cleve, J.E.; Charmandaris, V.; Meech, K.J.; McGleam, C.; rotationally resolved 8-35 micron *Spitzer Space Telescope* observations of the nucleus of Comet 9P/Tempel 1. *The Ap. J.* **625** L139-L142 (2005)

Marsden, B.G., Sekanina, Z.; Yeomans, D.K.; Comets and nongravitational forces. V. *Astronomical Journal* **78**(2), 211-225 (1973)

Marzari, F., Rossi, A., Scheeres, D. J.. 2011. Combined effect of YORP and collisions on the rotation rate of small Main Belt asteroids. Icarus 214, 622-631

McBride, N.;Green, S.F.; Levasseur-Regourd, A.C.; Goidet-Devel, B.; Renard, J.-B.; The inner dust coma of Comet 26P/Grigg-Skjellerup: multiple jets and nucleus fragments? *MNRAS* **289**, 535-553 (1997)

McDonnell, J. A. M., Evans, G. C., Evans, S. T., Alexander, W. M., Burton, W. M., Firth, J. G., Bussoletti, E., Grard, R. J. L., Hanner, M. S., Sekanina, Z. The dust distribution within the inner coma of comet P/Halley 1982i - Encounter by Giotto's impact detectors. *Astronomy and Astrophysics* **187**, 719-741 (1987)

McKay, A.; Cochran, A.; Dello Russo, N.; Weaver, H.; Vervack, R.; Harris, W.; Kawakita, H.; DiSanti, M.; Chanover, N.; Tsvetanov, Z.; Evolution of fragment-species production in comet C/2012 S1 (ISON) from 1.6 au to 0.4 au. *Asteroids, Comets, Meteors 2014*, 365 (2014)

Meech, K. J., Pittichová, J., Yang, B., Zenn, A., Belton, M. J. S., A'Hearn, M. F., Bagnulo, S., Bai, J., Barrera, L., Bauer, J. M., Bedient, J., Bhatt, B. C., Boehnhardt, H., Brosch, N., Buie, M., Candia, P., Chen, W.-P., Chesley, S., Chiang, P., Choi, Y.-J., Cochran, A., Duddy, S., Farnham, T. L., Fernández, Y., Gutiárrez, P., Hainaut, O. R., Hampton, D., Herrmann, K., Hsieh, H., Kadooka, M. A., Kaluna, H., Keane, J., Kim, M.-J., Kleyna, J., Krisciunas, K., Lauer, T. R., Lara, L., Licandro, J., Lowry, S. C., McFadden, L. A., Moskovitz, N., Mueller, B. E. A., Polishook, D., Raja, N. S., Riesen, T., Sahu, D. K., Samarasinha, N. H., Sarid, G., Sekiguchi, T., Sonnett, S., Suntzeff, N., Taylor, B., Tozzi, G. P., Vasundhara, R., Vincent, J.-B., Wasserman, L., Webster-Schultz, B., Zhao, H. Deep Impact, Stardust-NExT and the behavior of Comet 9P/Tempel 1 from 1997 to 2010. *Icarus* **213**, 323-344 (2011)

Melosh, H.J. 2011. Slopes and mass movement. In *Planetary Surface Processes*. Edn. 1 (Cambridge University Press, Cambridge, UK)

Mysen, E. Rotational dynamics of subsolar sublimating triaxial comets. *Planetary and Space Science* **52**, 897-907 (2004)

Mysen, E. The dynamics of globally active triaxial comets, with applications to asteroid rotation. *Monthly Notices of the Royal Astronomical Society* **381**, 301-307, (2007)

Neishtadt, A. I., Scheeres, D. J., Sidorenko, V. V., Vasiliev, A. A. Evolution of Comet Nucleus Rotation. *Icarus* **157**, 205-218 (2002)

Neishtadt, A. I., Scheeres, D. J., Sidorenko, V. V., Stooke, P. J., Vasiliev, A. A. The Influence of Reactive Torques on Comet Nucleus Rotation. *Celestial Mechanics and Dynamical Astronomy* **86**, 249-275 (2003)

Nishioka, K. Finite Lifetime Fragment Model 2 for Synchronic Band Formation in Dust Tails of Comets. *Icarus* **134**, 24-34, (1998)

Oberst, J. et al. The nucleus of Comet Borrelly: a study of morphology and surface brightness. *Icarus, **167*** (2004), 70-79

Peale, S.J.; Lissauer, J.J. Rotation of Halley's comet. *Icarus* **79**, 396-430 (1989)

Pittichová, J.; Sekanina Z.; Birkle, K.; Boehnhardt, H.; Engels, D.; Keller, P.; An early investigation of the striated tail of comet Hale-Bopp (C/1995 O1). *Earth, Moon and Planets* **78**, 329-338. (1997)

Reach, W.T.; Vaubaillon, J.; Kelley, M.S.; Lisse, C.M.; Sykes, M.V.; Distribution and properties of fragments and debris from the split Comet 73P/Schwassmann-Wachmann 3 as revealed by *Spitzer* Space Telescope. *Icarus* **203**, 571-588 (2009)

Richardson, J.E.; Melosh, H.J.; Lisse, C.M.; Carcich, B.; A ballistics analysis of the Deep Impact ejecta plume: Determining Comet Tempel 1's gravity, mass, and density. *Icarus*, **190**, 357-390 (2007)

Rodionov, A. V., Crifo, J.-F., Szegö;, K., Lagerros, J., Fulle, M. An advanced physical model of cometary activity. *Planetary and Space Science* **50**, 983-1024 (2002)

Rossi, A., Marzari, F., Scheeres, D. J.. 2009. Computing the effects of YORP on the spin rate distribution of the NEO population. Icarus 202, 95-103

Rotundi, A. et al. Dust measurements in the coma of comet 67P/Churyumov-Gerasimenko inbound to the Sun. *Science* **347**, (3pp) (2015)

Rousselot, P. 174P/Echeclus: a strange case of outburst, *A&A* **480**(2), 543-550 (2008)

Rozitis, B. & Green, S.F., The influence of global self-heating on the Yarkovsky and YORP Effects. *MNRAS* **433**(1), 603-621 (2013)

Rubincam, D. P. Radiative Spin-up and Spin-down of Small Asteroids. *Icarus* **148**, 2-11, (2000)

Rubincam, D.P. & Paddack, S.J., Zero secular torque on asteroids from impinging solar photons in the YORP effect: A simple proof. *Icarus* **209**(2), 863-865 (2010)

Samarasinha, N.H.; Belton, M.J.S. Long-term evolution of rotational stress and nongravitational effects for Halley-like cometary nuclei. *Icarus* **116**, 340-358 (1995)

Samarasinha, N.H. & Mueller, B.E.A. Relating changes in cometary rotation to activity: current status and applications to comet C/2012 S1 (ISON). *Ap. J. Letters* **775**:L10 (6pp) (2013)

Scheeres, D. J. The dynamical evolution of uniformly rotating asteroids subject to YORP. *Icarus* **188**, 430-450 (2007)

Scheeres, D. J., Hartzell, C. M., Sánchez, P., Swift, M. Scaling forces to asteroid surfaces: The role of cohesion. *Icarus* **210**, 968-984 (2010)

Schleicher, D.G. & Woodney, L.M.; Analyses of dust coma morphology of Comet Hyakutake (1996 B2) near perigee: outburst behavior, jet motion, source region locations, and nucleus pole orientation.; *Icarus* **162**, 190-213 (2003)

Sekanina, Z., Farrell, J. A. Comet West 1976. VI - Discrete bursts of dust, split nucleus, flare-ups, and particle evaporation. *The Astronomical Journal* **83**, 1675-1680 (1978)

Sekanina, Z., Farrell, J. A. The striated dust tail of Comet West 1976 VI as a particle fragmentation phenomenon. *The Astronomical Journal* **85**, 1538-1554 (1980)

Sekanina, Z. & Yeomans, D.K. Orbital motion, nucleus precession, and splitting of periodic comet Brooks 2. *Astron. J.* **90**, 2335-2352 (1985)

Sekanina, Z.; Erosion model for the sungrazing comets observed with the Solar and Heliospheric Observatory. *Ap. J.* **597**, 1237-1265 (2003)

Sidorenko, V. V., Scheeres, D. J., Byram, S. M. On the rotation of comet Borrelly's nucleus. *Celestial Mechanics and Dynamical Astronomy* **102**, 133-147 (2008)

Sierks, H. and 65 coauthors. On the nucleus structure and activity of comet 67P/Churyumov-Gerasimenko, *Science***,** **347**, (2015). DOI: 10.1126/science.aaa1044

Snodgrass, C.; Fitzsimmons, A.; Lowry, S.C.; Weissman, P.; The size distribution of Jupiter Family comet nuclei. *MNRAS* **414**, 458-469 (2011)

Steckloff, J.K.; Johnson, B.C.; Bowling, T.; Melosh, H.J.; Minton, D.; Lisse, C.M.; Battams, K. Dynamic sublimation pressure and the catastrophic breakup of Comet ISON. *Icarus* **258**, 430-437 (2015a) doi:10.1016/j.icarus.2015.06.032

Steckloff, J.K. et al.; The size and fragmentation of the nucleus of Comet C/2012 S1 (ISON). *LPSC XLVI,* Abstract #2723 (2015b)

Stevenson, R.; Kleyna, J.; Jewitt, D.; Transient Fragments in Outbursting Comet 17P/Holmes. *AJ* **139**, 2230-2240 (2010)

Szegö, K.; Crifo, J.F.; Földy, L.; Lagerros, J.S.V.; Rodionov, A.V. Dynamical effects of comet P/Halley gas production. *A&A* **370**, L35-L38 (2001)

Thomas, N. et al. The morphological diversity of comet 67P/Churyumov-Gerasimenko. *Science* **347**, (2015) DOI: 10.1126/science.aaa0440

Thomas, P.C.; A'Hearn, M.F.; Veverka, J.; Belton, M.J.S.; Kissel, J.; Klaasen, K.P.; McFadden, L.A.; Melosh, H.J.; Schultz, P.H.; Besse, S.; Carcich, B.T.; Farnham, T.L.; Groussin, O.; Bermalyn, B.; Li, J.-Y.; Lindler, D.J.; Lisse, C.M.; Meech, K.; Richardson, J.E. Shape, density, and geology of the nucleus of Comet 103P/Hartley 2. *Icarus* **222**, 550-558 (2013)

Vokrouhlicky D., Capek, D. YORP-Induced Long-Term Evolution of the Spin State of Small Asteroids and Meteoroids: Rubincam's Approximation. *Icarus* **159**, 449-467 (2002)

Weaver, H.A. et al. HST and VLT Investigations of the Fragments of Comet C/1999 S4 (LINEAR). *Science* **292**, 1329-1333 (2001)

Weaver, H.; A'Hearn, M.; Feldman, P.; Bodewits, D.; Combi, M.; Dello Russo, N.; McCandliss, S.; Ultraviolet spectroscopy of comet ISON (2012 S1). *Asteroids, Comets, Meteors 2014*, 604 (2014)

Wilhelm, K. Rotation and precession of comet Halley. *Nature* **327**, 27-30 (1987)

Whipple, F.L. A comet model. I. The acceleration of Comet Encke. *Ap. J.* **111**, 375-394 (1950)

Zolensky, M.E. + 74 colleagues. Mineralogy and petrology of Comet 81P/Wild 2 nucleus samples. *Science* **314**, 1735-1739 (2006)

"Rocket science is difficult. Spacecraft exploration of comets is even more so."
-Richard P. Binzel

CHAPTER 5. ROTATIONALLY INDUCED AVALANCHES AND THE ACTIVATION OF COMET HARTLEY 2

When sublimative torques spin up comet nuclei, the effects on the geomorphology and activity of the nucleus can be profound, potentially causing massive avalanches that excavate buried supervolatile ices. The activity of Comet 103P/Hartley 2 is dominated by CO_2 driven sublimation at the tip of its bilobate nucleus. This CO_2 ice responds to the nucleus's diurnal cycle, and must therefore be very near the surface. However, CO_2 ices were expected to have receded deep below Hartley 2's surface during its ~10 million year migration from the Kuiper Belt to the Jupiter Family, suggesting that these ices were somehow brought to the surface. I map the gravitational slopes of Hartley 2's surface as a function of rotation period, and show that large avalanches capable of excavating these CO_2 ices set in at a rotation period of ~11 hours, and are entirely confined to the regions of the nucleus exhibiting CO_2 driven activity. This suggests that a period of fast rotation activated this CO_2 activity. At the rate of spin-down observed by EPOXI, this avalanche likely occurred between 1984 and 1991, and would have significantly brightened the comet, consistent with its discovery in 1986. Furthermore, this mechanism allows me

date nearly all terrains imaged by EPOXI, a first for a comet. Finally, this mechanism may be the sought-after mechanism for reactivating dormant comet nuclei.

The following manuscript was submitted to *Icarus* in Octoboer 2015 as "Rotationally Induced Surface Slope Instabilities and the Activation of CO_2 Activity on Comet 103P/Hartley 2", and is coauthored by Kevin Graves, Masatoshi Hirabayashi, H. Jay Melosh, and James E. Richardson.

5.1 Introduction

The DIXI (Deep Impact eXtended Investigation) flyby of comet 103P/Hartley 2 on November 4, 2010, revealed the nucleus to be a small, bilobate, but highly active world (A'Hearn et al. 2011). The majority of Hartley 2's activity is restricted to a region at the tip of its small lobe, and is diurnally driven by CO_2 sublimation (A'Hearn et al. 2011). While bilobate comet nuclei are fairly common (Keller et al. 1986; Oberst et al. 2004; Harmon et al. 2010; A'Hearn et al. 2011; Sierks et al. 2015), diurnal control of CO_2 sublimation has never before been observed by spacecraft in situ.

Diurnal control requires that Hartley 2's CO_2 ices are located within the diurnal skin depth of the nucleus, which extends no more than a few centimeters below the surface. However, this is unexpected of a Jupiter Family Comet (JFC) like Hartley 2, which spend typically ~45 million years as a Centaur object (Duncan et al. 2004) before migrating into the Jupiter family. In the Centaur region of the Solar System carbon monoxide and carbon dioxide ices sublimate vigorously enough to drive cometary activity in this region of space (Sekanina, 1992; Steckloff & Jacobson, 2016).

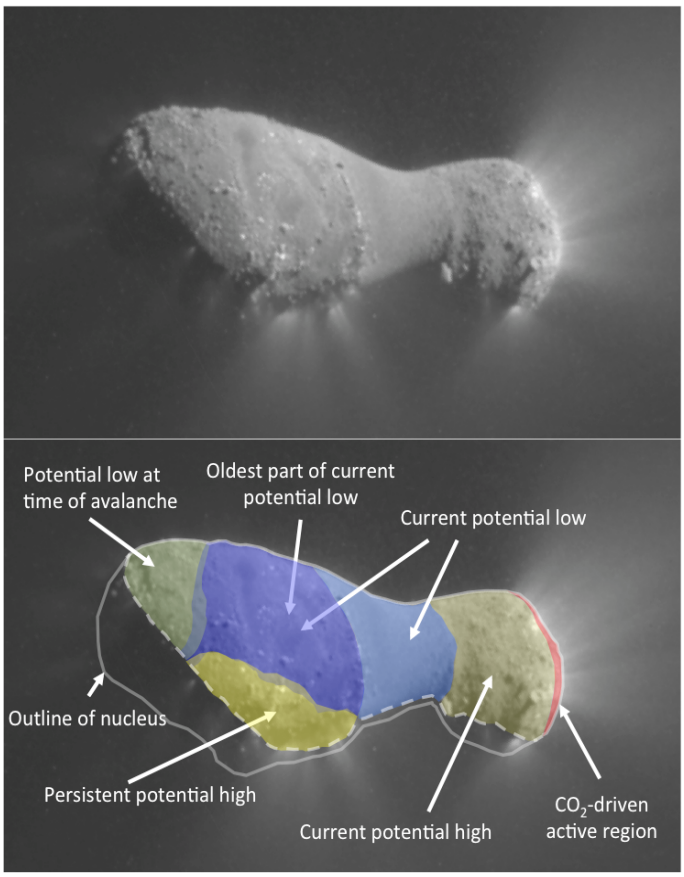

Figure 5.1 Overview of relevant regions of comet 103P/Hartley 2

The nucleus of comet Hartley 2 exhibits various terrain types visible in this original and annotated image from the DIXI flyby (MRI-VIS frame 5004052). Although the CO_2-driven active region was only obliquely imaged by the Deep Impact spacecraft, the entire tip of the small lobe is dominated by CO_2 activity. The rest of the nucleus surface is a combination of knobby, hummocky terrain and smooth regions. As a result of this work, we have determined the location of current and former locations of low net potential (gravitational plus rotational potential), where materials will preferentially settle. The migration of these potential lows over time as the nucleus rotation period lengthens to the observed period during the DIXI flyby implies the following relative ages for the terrains denoted above (oldest to youngest): persistent potential high, CO_2-driven region and potential low at time of avalanche (contemporaneous), oldest part of current potential low, and current potential low.

Volatile sublimation over such a long dynamical lifetime should produce a chemical stratification of the surface layers of the nucleus, with more volatile ices receding into the interior of the nucleus, while less volatile ices such as water ice remain closer to the surface. Thus, the diurnal activity of a JFC is expected to be driven by near-surface H_2O sublimation, consistent with high-resolution spacecraft observations of JFCs (Feaga et al. 2007; Gulkis et al. 2015; Sierks et al. 2015).

For Hartley 2 to exhibit diurnally controlled CO_2 sublimation, Hartley 2 must either have had an unusually short migration through the Centaur region into the Jupiter Family that limited the thermophysical evolution of the surface layers of the nucleus, or some mechanism must have recently removed the thermally evolved surface layers that are expected to overlie CO_2-rich layers. Here we show that an episode of fast rotation in the recent past of Hartley 2 could have generated surface slope instabilities that exposed buried CO_2-rich ices in the region of the observed activity.

At the time of the Deep Impact flyby, the nucleus of Hartley 2 was in a tumbling rotation state (A'Hearn et al. 2011; Knight & Schliecher, 2011; Samarasinha et al. 2011), with a rotation period about its principal axis of 18.3 hours (A'hearn et al. 2011; Drahus et al. 2011) and rotation period about its long axis of 27.79 hours (A'Hearn et al. 2011). However, sublimative torques can change comet spin periods, and during the Deep Impact flyby, Hartley 2's rotation period about its principal axis was lengthening at an estimated rate of 1.3±0.2 min/day based on DIXI flyby imagery (Belton et al. 2013) or 1.00±0.15 min/day from ground-based observations (Drahus et al. 2011), while its rotation period about the long axis (the rolling motion of the nucleus) first increased before decreasing again during the encounter (Belton et al. 2013). Other ground-based

observations are consistent with these rapid changes in the rotation state of the nucleus (Knight & Schleicher, 2011; Meech et al. 2011; Samarasinha et al. 2011; Knight et al. 2015).

This suggests that Hartley 2 was likely spinning much faster about its principal axis in the recent past. At the rate of angular deceleration observed during the DIXI encounter, Hartley 2 would have been spinning fast enough to break apart (disrupt) only ~20 orbits in the past (Drahus et al. 2011). However, this assumes that the nucleus would survive to the disruption limit of a gravity-dominated ellipsoid (Pravec & Harris, 2000). Consideration of the rotationally-induced stresses that concentrate at the waist of Hartley 2's bilobate structure suggests that its nucleus would fission into two lobes at rotation periods shorter than ~8 hours. Thus, Hartley 2 would have been rotating at its disruption limit only ~10 orbits in the past. This suggests that the CO_2 activity driving Hartley 2's sublimative torques is either less than ~70 years old, or that its nucleus migrated unusually quickly through the Centaur region, such that the nucleus did not significantly thermophysically evolve.

In the case of rapid migration, Hartley 2's orbit would need to have evolved from a perihelion outside of ~10 AU into the Jupiter Family of comets in a timespan on the order of centuries or shorter for its CO_2 activity to remain diurnally controlled and the nucleus to remain intact. However, this is exceedingly unlikely when compared to the typical migration timescale through the centaur region of ~45 million years (Duncan et al. 2004). Even if we assume that Hartley 2 migrated through the Centaur region in negligible time and was directly injected into the Jupiter Family, the median dynamical lifetime of a JFC is ~325,000 years (Duncan et al. 2004) and CO_2 sublimates vigorously

throughout the JFC region of space (Steckloff et al. 2015; Steckloff & Jacobson, 2016), making it exceedingly unlikely (~0.02%) that Hartley 2 has been in the Jupiter Family for less than this ~70 year maximum age of activity.

Instead, we investigate the alternative, that comet Hartley 2's CO_2 activity is young, and thus was a relatively dormant comet that was reactivated in the recent past. We propose that rotationally-induced avalanches preferentially exposed buried CO_2-rich materials on the surface of Hartley 2's small lobe, where solar radiation could diurnally controls CO_2 sublimation, generating the observed activity of the nucleus. We explore this case numerically.

5.2 Methods

We explore the effects of spin rate changes on the surface of Hartley 2's nucleus by computing the stability of its slopes at rotation periods between four hours (where the nucleus is unstable and breaks apart) and its rotation period of 18.34 hours at the time of the DIXI flyby. Although Hartley 2 is in a tumbling rotation state (A'Hearn et al. 2011; Knight & Schliecher, 2011; Samarasinha et al. 2011), we ignore the slower rotation about its long axis (period of 27.79 hours at the time of the flyby [A'Hearn et al. 2011]), and assume principal axis rotation.

We assume that avalanches, which remove surface materials while leaving underlying materials undisturbed, are responsible for exposing CO_2-rich ices on the surface of the nucleus. Avalanches occur when the slope angle of a surface exceeds its angle of repose (Lambe & Whitman, 1969). We compute the surface slope angles of Hartley 2 by first computing the net acceleration vector (the sum of the gravitational and

centrifugal acceleration) at the center of each facet of the Thomas et al. (2013) shape model of Hartley 2 using the GRAVMAP code, which is based on the method of Werner (1994). We then compute the angle between the net acceleration vector and the vector normal to the facet of the shape model to obtain the surface slope angle of the facet. We next identify facets of the shape model with slope angles that exceed the angle of repose of Hartley 2's regolith, an unstable condition that precedes landslides and avalanches.

Critical to this method is the density of the nucleus, which is assumed to be uniform. The high relative encounter velocity of the Deep Impact spacecraft with Hartley 2's small nucleus prevented a direct measurement of its density from gravitational deflection of the spacecraft (A'Hearn et al. 2011). However, A'Hearn et al. (2011) considered that the smooth waist of the nucleus is likely a ponded depositional feature, which requires a density of at least 220 kg/m³ for this region to occupy a gravitational low. Richardson & Bowling (2014) considered that the waist is likely the result of a fluidized flow, and would therefore approximate an equipotential surface. By minimizing the variance of the effective potential (gravitational plus rotational) for the observed portion of the waist at the principal rotation period during the Deep Impact flyby, they estimated the nucleus density to be ρ= 200 (140-520) kg/m³. Thomas et al. (2013) further considered the changing rotation state of the nucleus to refine this estimate to ρ= 300 (200-400) kg/m³.

The angle of repose (α) of a surface (the maximum stable slope angle) depends on the angle of internal friction (ϕ), pore pressure of fluids within the material (p_{pore}), material density (ρ), cohesive strength (σ_c), and the local gravity field ($\boldsymbol{g}$) of the body

$$\sigma_S = \sigma_c + (\sigma_n - p_{pore}) tan\ \phi \tag{5.1}$$

$$\sigma_S = \rho g h \sin \alpha \quad (5.2)$$

$$\sigma_n = \rho g h \cos \alpha \quad (5.3)$$

where h is the thickness of the unstable layer (Melosh, 2011). The angles of internal friction for geologic materials are remarkable uniform, typically ~30°-45° (Lambe & Whitman, 1969). We conservatively assume that pore pressure (p_{pore}) within the regolith of Hartley 2 is negligible, which will result in more stable surfaces and higher angles of repose.

We also assume that the surface regolith of Hartley 2 is non-cohesive, based on the presence of the smooth waist of Hartley 2 that is believed to be a flow deposit that fluidized by H_2O sublimation (A'Hearn et al. 2011; Thomas et al. 2013; Richardson & Bowling, 2014). Because this regolith would fail to fluidize if its cohesive strength were greater than the vapor pressure of the sublimating H_2O, the vapor pressure of H_2O provides a maximum constraint to the cohesive strength of the regolith. If H_2O ice were located right at the surface of the smooth waist (as opposed to mixed within it), its vapor pressure at perihelion with the Sun at the zenith would be ~0.1 Pa (Steckloff et al. 2015; Steckloff & Jacobson, 2016), however this constraint would only allow for the onset of fluidization for a very brief moment of Hartley 2's orbit. If we assume that the waist is able to fluidize for a few months preceding perihelion, then the constraint on the cohesive strength of the regolith drops by nearly an order of magnitude, and if we assume that the sublimating H_2O ice deposits are located within the regolith (rather than on top of it), the constraint on cohesive strength drops even further. It is therefore reasonable to assume that the regolith of Hartley 2 has such weak cohesion, that it effectively behaves as a non-cohesive material.

In this case of regolith without significant pore pressure or cohesion, the angle of repose (α) in equations (5.2)-(5.3) becomes equal to the angle of internal friction (ϕ), and is therefore expected to lie between 30°-45°. We conservatively choose to only consider slopes less than 30° to be stable, and slopes exceeding 45° to be unstable. It is unclear if surface slopes between 30° and 45° are stable or unstable without a more thorough understanding of the structural properties of Hartley 2's regolith. We vary the principal axis rotation period of Hartley 2 in 1 hour increments, compute the resulting surface slope angles, and identify unstable regions of the nucleus surface for each rotation period.

5.3 Results

We find that the surface of comet Hartley 2 is generally very stable during the DIXI flyby (spin period of 18.34 hours), with all the surface (except for a single scarp on the large lobe) possessing a surface slope angle less than 20°, and therefore stable. The surface slopes of the large lobe's scarp are maximally between 30° and 45°, leaving unclear the stability of its surface. However, this feature is associated with a dust jet (Bruck Syal et al. 2013), and so it is plausible that this scarp is unstable or was unstable in the recent past.

As we spin up the nucleus of Hartley 2 to a rotation period of 13 hours, a ring of terrain outlining the CO_2-driven activity of the small lobe steepens to surface slope angles of 30° to 45° degrees (see Figure 2). While this does not necessarily indicate that the tip of the small lobe becomes unstable and prone to avalanches, it does suggest that the tip of the small lobe is trending toward slope instability as the nucleus is spun up. Interestingly, the rest of the nucleus outside of the scarp on the large lobe remains relatively flat, with

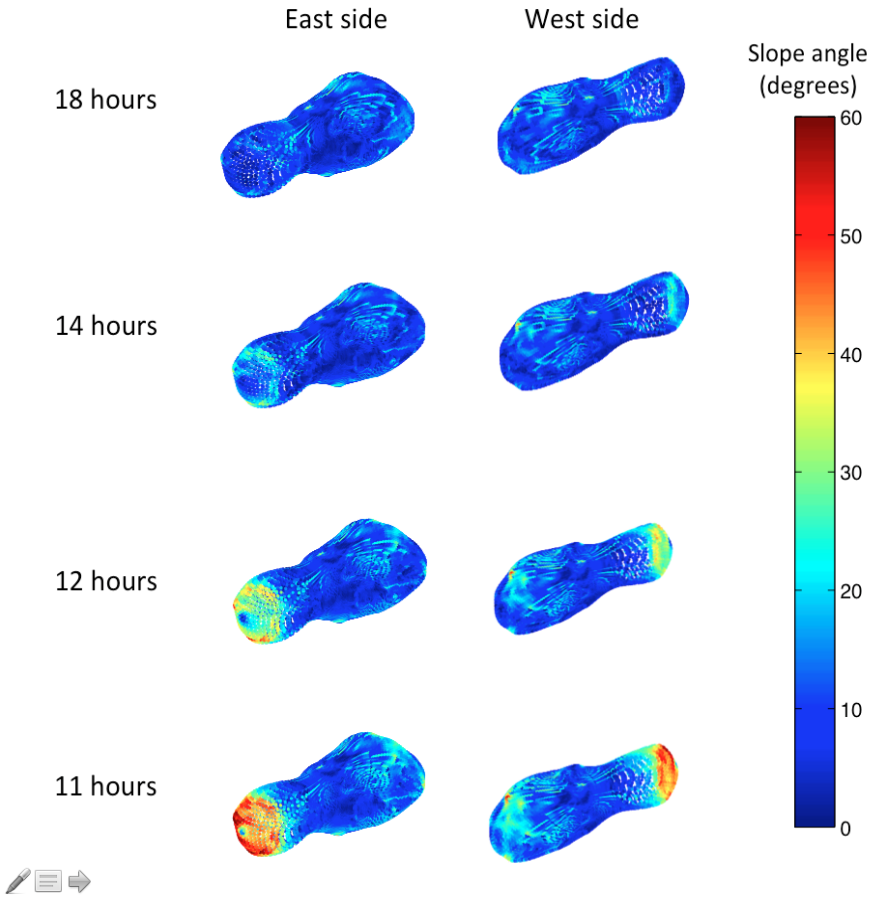

Figure 5.2: Surface slopes of 103P/Hartley 2 under different rotation rates

As the nucleus of comet 103P/Hartley 2 is spun up from it's DIXI flyby rotation period of 18.34 hours, the slopes on the tip of the small lobe of the nucleus increase significantly more than any other place on the nucleus, and become highly unstable (above 45°) at a rotation period of 11 hours. This suggests that, at an 11 hour rotation period, avalanches would set in on the tip of the small lobe, excavating buried CO_2 ices and activating this region of the nucleus. Interestingly, the rest of the nucleus remains at roughly the same slope, regardless of rotation period, and would not experience avalanches.

surface slopes less than ~20°. At a 13 hour rotation period, the scarp on the large lobe steepens to a slope angle of ~45° indicating that it is likely unstable without cohesion.

At a rotation period of 11 hours, the surface slopes of the source region of the CO_2-driven activity at the tip of the small lobe exceed 45° and become clearly unstable. Under these conditions, avalanches will excavate buried materials, and surface materials will flow downhill, toward the tip of the small lobe. Interestingly, these avalanches are almost exclusively restricted to the active region of the small lobe, as the rest of the nucleus outside of the scarp on the large lobe and a few isolated facets remains stable with surface slope angles less than 20°. The remarkable geographic correlation between surface slope instabilities and the CO_2-driven active terrains on the small lobe of Hartley 2 strongly suggest that the nucleus recently experienced an episode of fast rotation (with a period of ~11 hours), which excavated buried CO_2 ices to the surface of the nucleus where they currently drive activity.

This result is robust against uncertainties in the bulk density of the nucleus. While our previous computations assume a nucleus bulk density (ρ) of 300 kg/m³ (Thomas et al. 2013), a decrease in the nucleus bulk density makes the surface slopes more prone to change under rotational spin up, while an increase in density makes the surface slopes more resistant to change. As a result, when we run the same analysis and vary the nucleus bulk density (ρ), we find that surface slope instabilities set in at the tip of the small lobe at a rotation period of ~13 hours for a bulk nucleus density of 200 kg/m^3, and at a rotation period of ~10 hours for a bulk nucleus density of 400 kg/m^3. However, the distribution of surface slopes is effectively unchanged under these differing

densities, and the same regions and isolated facets of the nucleus shape model remain stable/unstable across the uncertainty in the nucleus bulk density.

Although we assume the regolith of the comet to be cohesionless, the underlying, non-thermally evolved materials likely possess significant strength. We use finite element model (FEM) analysis (Hirabayashi & Scheeres, 2015) to compute the internal stress state of Hartley 2's nucleus and determine the minimum strength required to maintain the interior structural stability of the nucleus at the onset of surface slope instabilities on the small lobe. We input the Thomas et al. (2013) shape model into ANSYS FEM software and assume that the nucleus deforms plastically. At the DIXI flyby rotation period of 18.34 hours, the nucleus experiences entirely compressional stresses, but does not fail compressionally (structurally stable). However, at the onset of surface slope instabilities, the waist of Hartley 2 enters a tensile state (while the two lobes of the nucleus remain compressional), and requires a tensile strength of at least 2.8 (2.0 - 4.0) Pa to remain structurally stable (see Figure 5.3).

We compare this to known bulk strength estimates of comet nuclei and find that it is consistent with the constraints on the tensile strength of comets Shoemaker-Levy 9 (D/1993 F2) and Brooks 2 (16P) of <6.5 Pa (Asphaug & Benz, 1996) and <2 Pa (Sekanina & Yeomans, 1985) respectively. This constraint is also consistent with estimates of comet Churyumov-Gerasimenko's (67P's) cohesive strength of 1-16 Pa (Bowling et al. 2015) and tensile strength of 3-15 Pa (Groussin et al. 2015) and 20 Pa (Thomas et al. 2015). It is also consistent with the ~1 Pa order unconfined crushing strength of Comet ISON (C/2012 S1) (Steckloff et al. 2015) and >17 Pa cohesive strength of Comet Wild 2 (81P) (Melosh 2011; Steckloff et al. 2015).

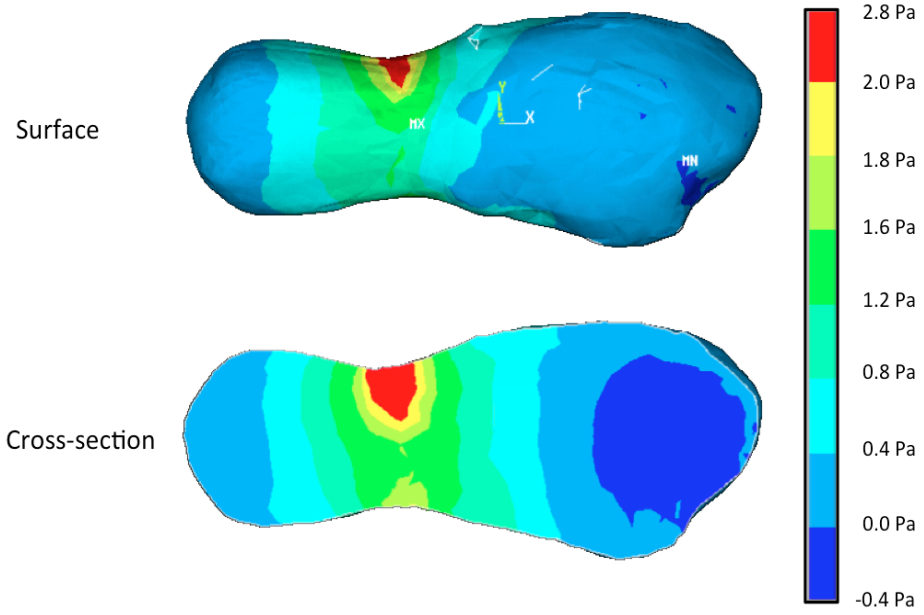

Figure 5.3: Finite Element Model (FEM) Analysis of Plastic Stresses in the body of Hartley 2 at Critical Rotation Period.

We model the internal stress state of Hartley 2's nucleus at the critical rotation period at which surface slope instabilities and their resulting avalanches set in on the small lobe (11 hour period for a bulk density of 300 kg/m^3). We assume plastic deformation of the nucleus material, and compute the highest stresses experienced by the nucleus material. Although we assume that a non-cohesive regolith covers the nucleus, the interior of the nucleus must have ~2.8 Pa of cohesive strength to prevent the nucleus from breaking, consistent with strengths of other cometary nuclei (Sekanina & Yeomans, 1985; Asphaug & Benz, 1996; Melosh, 2011; Bowling et al. 2015; Thomas et al. 2015; Steckloff et al. 2015).

5.4 Discussion

Small, isolated jets appear on the large lobe of the nucleus (Bruck Syal et al. 2013), and it is conceivable that the scattered, isolated facets of the large lobe that experience surface slope instabilities at faster spin rates may be associated with jets. However, the contribution of these jets to the overall production of the nucleus is likely very minor, otherwise the light curve amplitude during DIXI's approach to Hartley 2 (A'Hearn et al. 2011) would not be a drastic). Additionally, these unstable facets were on the unilluminated side of the nucleus during the DIXI flyby, where jets are less likely to be active or observed, and where the shape of the nucleus is relatively poorly constrained. It is therefore possible that the surface slope instabilities of these facets are artifacts of imperfections in the Thomas et al. (2013) shape model. Furthermore, although the sources of the small jets are associated with geologic features of the nucleus (Bruck Syal et al. 2013), these source areas are smaller than, or comparable to, the 2 degree (~10-44 m) resolution of the Thomas et al. (2013) shape model. Because our method is limited by the resolution of the shape model, studying the activation of these isolated jets, or the effects of isolated unstable facets of the shape model, is difficult and unreliable. We therefore restrict our analysis to large-scale regional trends on the surface of Hartley 2's nucleus, which are unlikely to be the result of errors in the shape model.

The unstable scarp on the large lobe is not associated with activity on its face, although it does have a dust jet at its base (Bruck Syal et al. 2013). This suggests that this region did not recently experience avalanches that exposed interior ices preceding the flyby or during previous episodes of fast rotation. However, the instability of this region at all studied spin periods implies that any non-cohesive regolith would slide off of this

surface, keeping underlying cohesive materials exposed at the surface. This scarp region may therefore be an outcrop of cohesive materials that generally underlie the cometary regolith, similar to the Hathor terrain on comet Churyumov-Gerasimenko (67P) (Sierks et al. 2015; Thomas et al. 2015). However, its lack of observed CO_2 activity suggests that it has long been exposed at the surface, allowing CO_2 ices to recede below the diurnal thermal skin depth.

Although the principal rotation period of Hartley 2's nucleus was increasing by ~1 minute/day during the DIXI encounter (Drahus et al. 2011, Belton et al. 2013), this rate is not maintained during an entire orbit (Knight et al. 2015). Drahus et al. (2013) estimated the orbitally-averaged decrease in the principal axis rotation frequency to be ~0.012 hr^{-1} per orbit. At this rate, Hartley 2 would have been spinning fast enough (period of 11 hours) to induce surface slope instabilities ~3-4 orbits prior to the DIXI encounter. This suggests that Hartley 2 was reactivated between 1984 and 1991. Interestingly, this coincides with the discovery of the comet by Malcolm Hartley in 1986, and activation of the small lobe of the nucleus would have certainly facilitated the discovery of the comet. Such a recent activation is consistent with observations that suggest the activity of the nucleus has been diminishing over time since systematic observations of Hartley 2 began during its 1991 apparition (Meech et al. 2011; Knight & Schleicher, 2013), as would be expected as the exposed surface of the nucleus evolves thermophysically. It is therefore quite likely that Hartley 2 was a relatively dormant comet that reactivated shortly before its discovery, possibly during its 1985 perihelion passage.

During the rotationally-induced avalanches, material flows downhill toward the tip of the small lobe. If the CO_2 ices were located at a similar depth as they are on Tempel 1 (9P), then the thickness of the avalanching material is equal to the ~10m orbital thermal skin depth (Sarid et al. 2005) of Tempel 1's seasonally-active CO_2 (Feaga et al. 2007). Hartley 2 has a surface area of 5.24 km^2 (Thomas et al. 2013), ~16% of which is sublimating CO_2 (Samarasinha & Mueller, 2013). If we assume that all of this CO_2 activity is located on the small lobe, then surface material covering ~0.8 km^2 (~$2.4x10^{10}$ kg) would avalanche toward the tip of the small lobe, severely restricting cometary activity. However, since DIXI observed this region to be highly active (A'Hearn et al. 2011), this material needs to be removed from the surface.

At a spin period of 11 hours, the component of net acceleration normal to the surface at the tip of the small lobe is ~$5x10^{-6}$ m/s^2, which is a factor of 5 smaller than during the DIXI flyby (due to the faster spin rate). Thus, it would have been easier to remove material from the surface through gas drag during periods of fast rotation. If we assume that the CO_2 ices, once exposed to sunlight during the avalanches, quickly warmed up and reached a sublimative equilibrium, then the sublimating CO_2 would exert a dynamic sublimation pressure between 0.001 Pa (at aphelion) and 0.1 Pa (at perihelion) (Steckloff et al. 2015; Steckloff & Jacobson, 2016) on the surface materials. This pressure is great enough to loft chunks between ~0.5 - 50 m off the surface of the small lobe! Some of the smaller pieces of this material would reach escape velocity and be visible as a sizeable outburst of the comet. However, the larger pieces of material would fall back onto the nucleus, and may be the source of the ~20-40 m mounds and rough surface terrains observed by the DIXI mission (Thomas et al. 2013).

We replotted the Thomas et al. (2013) binned size distribution data of these mounds on the surface of Hartley 2, and found that their cumulative size-frequency distribution (SFD) has a power-law index of -4.1. This is consistent with the range of indices of -5.6 - -3.7 for the differential SFD of the chunks of material found in Hartley 2's inner coma (Kelley et al. 2013) and with the index of -4.0±0.3 from *WISE/NEOWISE* observations of Hartley 2 (Bauer et al. 2011), suggesting that an ejection and fallback origin of these mounds is plausible. (See Figure 4). In any case, it is quite likely that the avalanching surface materials would leave the surface of the region of CO_2-driven activity on the small lobe, and may end up being deposited on the rest of the nucleus.

We computed the net specific potential (gravitational plus rotational potential per unit mass) of Hartley 2's surface at various spin periods. Since materials are preferentially deposited in potential minima, we consider the location of the potential minima at the time of Hartley 2's avalanche to determine where the materials are preferentially deposited. We find that the potential minima are located at the tips of each lobe. However, since the avalanche activated CO_2 activity that can prevent this material from settling on the surface, the avalanche debris is most likely to settle at the tip of the large lobe. Thus, our model of Hartley 2's activation predicts that a rough, hummocky avalanche debris deposit should be located at the tip of the large lobe, consistent with observations of hummocky terrain at this location (see Figure 1). Furthermore, our model predicts the existence of other depositional terrains as the location of potential lows migrates about the nucleus during the lengthening of the principal rotation period of the nucleus from ~11 hours at the time of the avalanche to the 18.34 hour period during the DIXI flyby (see Figure 5.5).

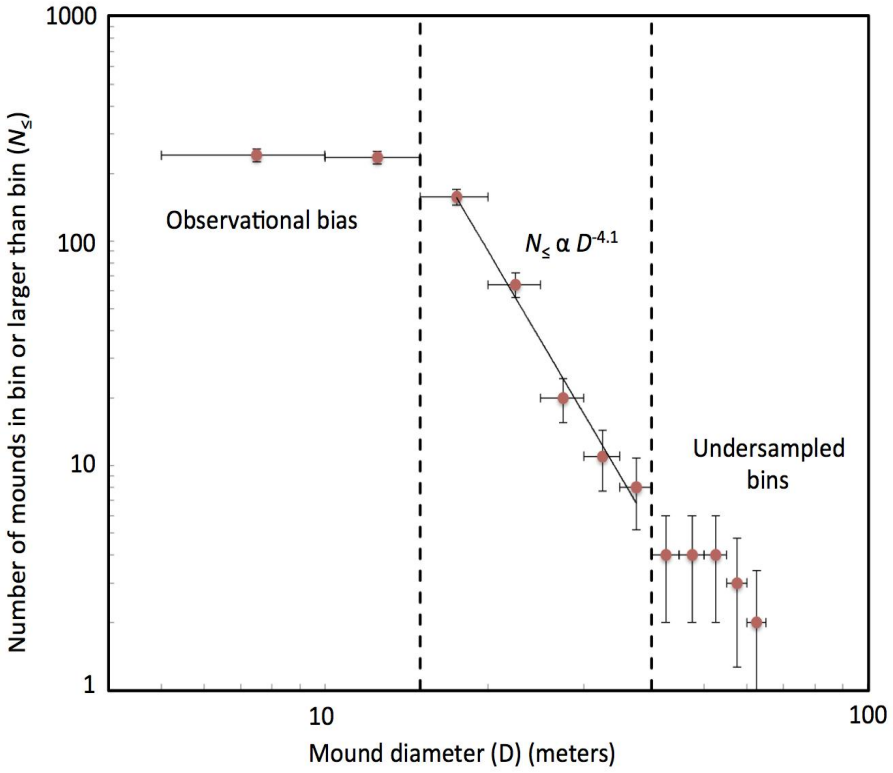

Figure 5.4 Size-Frequency Distribution of Mounds on Nucleus of Hartley 2.

We replotted the binned size-frequency data of mounds on the surface of Hartley 2 from Thomas et al. (2013) to compute their cumulative size frequency distribution (cumulative SFD). Thomas et al. (2013) placed the data in 5 meter bins (the source of the horizontal error bars). Vertical error bars are standard square-root of *N*. Because data is binned, large bins become undersampled due to low probability of mound having a large size. We exclude these bins, which would otherwise skew the power-law fit to the SFD. We exclude the smallest-sized bins, which are near the resolution of the Deep Impact MRI, and therefore exhibit observational bias. We find that the mounds follow a power-law cumulative SFD, with a power-law index of -4.1, consistent with the SFD of icy chunks in the inner coma of Hartley 2 during the DIXI flyby (Kelley et al. 2013)

At spin periods longer than ~14 hours, the potential low of the nucleus migrates from the tips of the lobes to the large region on the center of the imaged portion of the large lobe (denoted by Bruck-Syal et al. [2013] as a "central mound"). During this episode of intermediate spin periods, the surface of the nucleus is stable (slope angles below the angle of repose), inhibiting the formation of large-scale hummocky avalanche deposits. However, the CO_2-driven activity at the tip of the small lobe is ejecting grains composed of H_2O ice and dust (A'Hearn et al. 2011), some of which settle back onto the surface. As these grains warm up, the H_2O ice sublimates, forming a fluidized flow (Belton & Melosh, 2009) that settles in the potential well. Thus, our avalanche theory predicts the formation of a smooth terrain that approximates an equipotential surface on the central mound, consistent with observations. At a spin period longer than ~16 hours, the waist region of the nucleus joins this potential low, where fluidized icy grains should flow and settle, forming a smooth, equipotential surface (A'Hearn et al. 2011; Thomas et al. 2013; Richardson & Bowling, 2014), consistent with observations. Finally, we note that the unstable scarp on the large lobe is part of a region that is a persistent location of high potential at all studied spin periods. It is unlikely that material would settle in this terrain rather than move downhill. Thus, we most expect an unstable scarp be located in this region, where the cohesive interior of the nucleus is most likely to be outcropped at the surface, rather than covered with regolith.

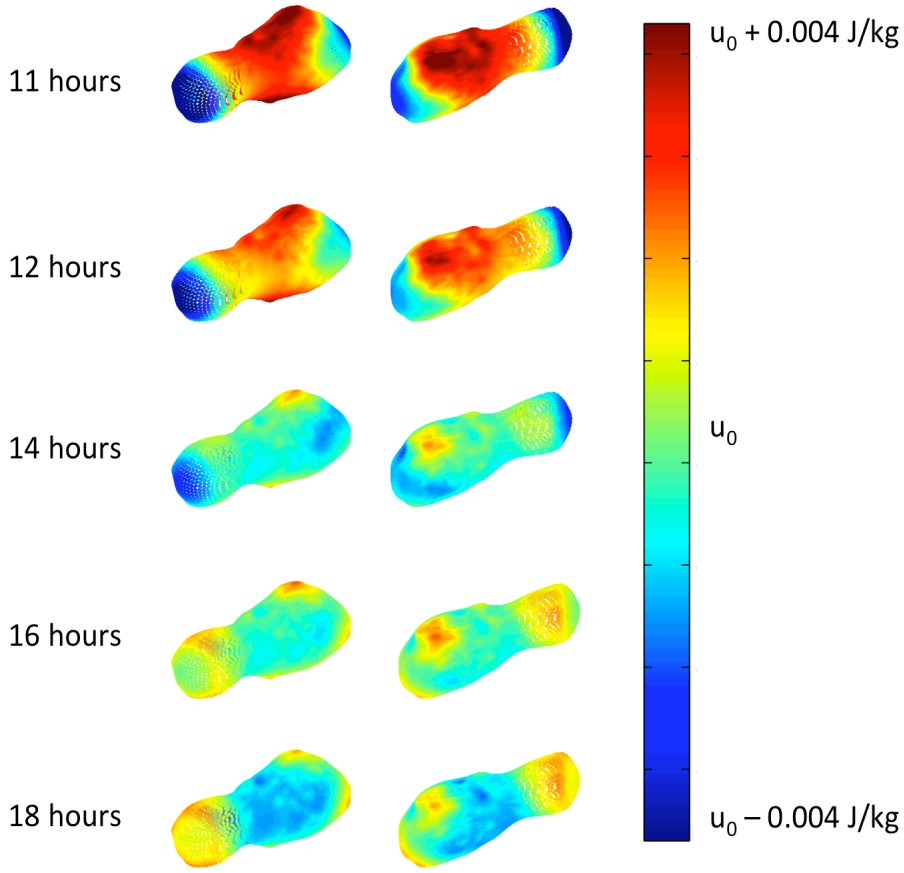

Figure 5.5: Specific Potential Map of Hartley 2 at Various Spin Period

We compute the net specific potential (gravitational plus rotational potential per unit mass) for various rotation periods. Because we only care about potential differences we plot each case with a color bar that spans 0.008 J/kg, roughly centered about the median specific potential of the surface (u_0). We clearly see that the regions of low specific potential migrate over the surface of the nucleus as the spin period increases. At the time of avalanche that excavated the small lobe, the potential lows were located at the tips of the lobes, migrating to waist and central mound of the nucleus by the time of the DIXI flyby.

From this sequence of events, we can place relative ages on most of the imaged surface of Hartley 2. The region of persistent potential high is likely the oldest terrain on the surface, with the unstable scarp representing an outcrop of the nucleus on the surface. The CO_2-driven active region and hummocky terrain at the tip of the large lobe, which formed simultaneously ~1984-1991 are the oldest terrains formed since the avalanche. The smooth terrain of the central mound formed next, when the rotation period was longer than ~14 hours. This terrain developed over time, as fallback material accumulated on the surface of the nucleus and fluidized. Finally, the smooth waist region joined the potential low at spin periods longer than ~16 hours, and formed most recently as fluidized fallback material settled.

It is likely that surface slope instabilities across the small lobe did not set in simultaneously. More likely, a series of smaller avalanches excavated buried CO_2 ices, rather than one large avalanche, causing a more gradual brightening of the comet (gradual, long-lived outburst). As this outburst faded, the comet would dim, but would settle to a much brighter magnitude than before the outburst due to the activation of CO_2-driven activity on the small lobe. The CO_2-driven regions would resist being covered by an avalanche because their activity would be able to loft this material off the surface, preventing it from settling.

At the ~11 hour rotation period at which surface slope instabilities set in, the waist of the nucleus enters a tensile state. Although only a small amount of cohesion (~2.8 Pa) is needed to hold the nucleus together, the waist may still experience a slow creep of the nucleus material, which may lead to an elongation of the neck, and could contribute to the formation of the bilobate shape of the nucleus. The rest of the nucleus

remains in compression, with most of the large and small lobes experiencing very small stresses (~1 Pa) at all rotation periods between 11 and 18 hours. This lack of significant compression or change in stress state would allow the nucleus to remain uncompacted, and may explain why the nucleus of comet Hartley 2 appears to be significantly less dense than other observed comet nuclei (Richardson et al. 2007; Thomas et al. 2013; Sierks et al. 2015).

In proposing that the activity of Hartley 2 is the result of rotationally-induced avalanches, we require a mechanism to spin up the nucleus to the onset of surface-slope instabilities. Although we suggest that Hartley 2 was relatively dormant prior to reactivation, it may still have exhibited some activity, which can generate sublimation torques. To induce enough sublimation torque to spin up Hartley 2 to the onset of surface slope instabilities within a typical ~3 x 10^5 year dynamical lifetime of a Jupiter Family Comet (Duncan et al. 2004), only ~0.01% of the total solar heat incident on Hartley 2 over its orbit needs to reach the buried ices (according to SYORP theory [Steckloff & Jacobson, 2016]). If we assume that sublimation cooling dominated the 5% of comet Tempel 1 (9P) that is active (Samarasinha et al. 2013), then a dormant nucleus would need to have at least ~1% of the activity of Tempel 1 to be capable of inducing surface slope instabilities during a typical dynamical JFC lifetime. It is therefore plausible that even very weak activity could have spun up the nucleus of a dormant Hartley 2 and activate the activity on the small lobe.

Our work suggests that comet Hartley 2 was recently a dormant comet, a class of comets that recent work suggests exists (Kresak, 1987; Levison et al. 2006). While dormancy may be a common phase of Jupiter Family Comets, their mechanisms of

reactivation are poorly understood. Bruck-Syal et al. (2013) show that a rapid release of energy into the subsurface of comet Hartley 2 can trigger the formation of well-collimated jets. However, whereas Bruck Syal et al. (2013) propose that amorphous ice crystallization could provide the energy required to initiate jet formation, amorphous ice has yet to be detected on a comet (Huebner, 2009; Lisse et al. 2013), and another explosive source of heat on comet nuclei has not been identified. We have shown that rotationally-induced avalanches can excavate ices and reactivate a comet.

5.5 Conclusions

We have shown that the distribution of the activity of comet 103P/Hartley 2, which is driven by diurnally controlled carbon dioxide sublimation, is consistent with rotationally-induced surface slope instabilities from a recent episode of fast rotation. At a rotation period of ~11 (10-13) hours, the region of Hartley 2's surface that is bounded by its carbon dioxide activity becomes unstable and avalanches toward the tip of the small lobe, excavating buried materials beneath. These avalanched materials would likely be lofted off the surface of the nucleus at less than escape velocity and be redeposited on other parts of the nucleus, forming hummocky terrains. We further show that spinning up the nucleus from its DIXI encounter spin period of 18.34 hours to this faster spin period does not induce surface slope instabilities on any other part of the nucleus prior to generating instabilities at the tip of the small lobe. Additionally, we have shown that the stresses within the nucleus are small enough in magnitude that the shape of the nucleus can be maintained if it possesses a bulk cohesive strength of at least 2.8 (2.0-4.0) Pa, which is consistent with strength estimates of other comet nuclei (Sekanina & Yeomans,

1985; Asphaug & Benz, 1996; Melosh, 2011; Bowling et al. 2015; Groussin et al. 2015; Thomas et al. 2015; Steckloff et al. 2015). We therefore conclude that rotational spin up is responsible for either initiating or maintaining the diurnally-controlled carbon dioxide driven activity of comet Hartley 2, and may have formed the observed knobby, hummocky terrains in the process. Our model of activating Hartley 2 predicts the formation of smooth fluidized terrains on the central mound and waist as the nucleus rotation period lengthened to the 18.34 hours of the DIXI flyby, consistent with observations. We discuss how this mechanism can potentially reactivate dormant comet nuclei, and how the shape of Hartley 2 may be responsible for its unusually low density by limiting the internal stresses of the nucleus.

References

A'Hearn et al., EPOXI at Comet Hartley 2, Science 332,1396 (2011)

Asphaug, E. & Benz, W. Size, density, and structure of Comet Shoemaker-Levy 9 inferred from the physics of tidal breakup. Icarus 121, 225-248 (1996)

Bauer, J.M. et al., 2011. WISE/NEOWISE observations of Comet 103P/Hartley 2. Astrophys. J. 738, 171.

Belton, M.J.S. & Melosh, H.J.; Fluidization and multiphase transport of particulate cometary material as an explanation of the smooth terrains and repetitive outbursts on 9P/Tempel 1. Icarus 200, 280-291 (2009)

Belton, M.J.S. et al.; The complex spin state of 103P/Hartley 2: kinematics orientation in space. Icarus 222, 595-609 (2013)

Bowling, T.B.; Steckloff, J.K.; Melosh, H.J.; Graves, K.J.; The Strength of Comet 67P/Churyumov-Gerasimenko. *American Astronomical Society – Division of Planetary Science Meeting #46*, Abstract #100.03 (2014)

Bruck Syal, M.; Schultz, P.H.; Sunshine, J.M.; A'Hearn, M.F.; Farnham, T.L.; Dearborn, D.S.P; Geologic control of jet formation on Comet 103P/Hartley 2. Icarus 222, 610-624 (2013)

Drahus, M. et al.; Rotation state of comet 103P/Hartley 2 from radio spectroscopy at 1 mm. Ap. J. L. 734:L4 (6pp) (2011)

Duncan, M.; Levison, H.; Dones, L.; "Dynamical Evolution of Ecliptic Comets" in Comets II Editors: Festou, M, Keller, H.U., Weaver, H.A.; University of Arizona Press-Tucson, AZ. p. 193-204 (2004)

Groussin, O. et al. ; Gravitational slopes, geomorphology, and material strengths of the nucleus of comet 67P/Churyumov-Gerasimenko from OSIRIS observations. A & A, in press. (2015)

Gulkis, S. et al.; Subsurface properties and early activity of comet 67P/Churyumov-Gerasimenko. Science 347, (2015) doi: 10.1126/science.aaa0709

Harmon, J.K. et al.; Radar observations of 8P/Tuttle: A contact-binary comet. Icarus 207, 499-502 (2010)

Hirabayashi, M. & Scheeres, D.J., Stress and failure analysis of rapidly rotating asteroid (29075) 1950 DA. Ap. J. L. 798.1, L8 (2015)

Huebner, W.F. Origins of cometary materials. In: Origin and Early Evolution of Comet Nuclei, p. 5 - 25. Editors: Balsiger, H., Altwegg, K., Huebner, W., Owen, T., Schulz, R. (2009)

Keller, H.U. et al.; First Halley Multicolour camera imaging results from Giotto. Nature 321, 320-326 (1986)

Kelley, M.S. et al. A distribution of large particles in the coma of Comet 103P/Hartley 2. Icarus 222, 634-652 (2013)

Knight, M.M. & Schleicher, D.G.; CN Morphology studies of comet 103P/Hartley 2; AJ 141, 183 (2011)

Knight, M.M. & Schleicher, D.G.; The highly unusual outgassing of Comet 103P/Hartley 2 from narrowband photometry and imaging of the coma. Icarus 222, 691-706 (2013)

Knight, M.M.; Bueller, B.E.A.; Samarasinha, N.H.; Schleicher, D.G.; A Further Investigation of Apparent Periodicities and the Rotational State of Comet 103P/Hartley 2 from Combined Coma Morphology and Light Curve Data Sets. AJ 150:22, 14 pp. (2015)

Kresák, L.; Dormant phases in the aging of periodic comets.; A & A 187, 906-908 (1987)

Lambe, T.W. & Whitman, R.v.; Soil Mechanics. John Wiley & Sons: New York. (1969)

Levison, H.F. et al.; ON the origin of the unusual orbit of Comet 2P/Encke. Icarus 182, 161-168 (2006)

Lisse, C.; Bar-Nun, A.; Laufer, D.; Belton, M.; Harris, W.; Hsieh, H.; Jewitt, D.; Cometary Ices. In *The Science of Solar System Ices*, 455 – 485. Editors: Gudipati, M.S. & Castillo-Rogez, J.; Springer Publishing: New York. (2013)

Meech, K.J. et al.; EPOXI: Comet 103P/Hartley 2 observations from a worldwide campaign; Ap. J. L. 734:L1 (9pp) (2011)

Melosh, H.J.; Slopes and mass movement. In *Planetary Surface Processes* Edn. 1; Cambridge University Press: Cambridge, UK. p326-345 (2011)

Oberst, J. et al.; The nucleus of Comet Borrelly: a study of morphology and surface brightness. Icarus 167, 70-79 (2004)

Pravec, P. & Harris, A.W.; Fast and slow rotation of asteroids. Icarus 148, 12-20 (2000)

Richardson, J.E.; Melosh, H.J.; Lisse, C.M.; Carcich, B.; A ballistics analysis of the Deep Impact ejecta plume: Determining Comet Tempel 1's gravity, mass, and density. Icarus 190, 357-390 (2007)

Richardson, J.E. & Bowling, T.J., Investigating the combined effect of shape, density, and rotation on small body surface slopes and erosion rates., Icarus 234, 53-65 (2014)

Samarasinha, N. H. & Mueller, B.E.A. Relating changes in cometary rotation to activity: Current status and applications to comet C/2012 S1 (ISON). Ap. J. L. 775:L10 (2013)

Sarid, G. et al.; Thermal evolution and activity of Comet 9P/Tempel 1 and simulation of a deep impact. PASP 117, 796-809 (2005)

Sekanina, Z.; Sublimation rates of carbon monoxide and carbon dioxide from comets at large heliocentric distances. *Asteroids, Comets, Meteors 1991*, 545-548 (1992)

Sekanina, Z. & Yeomans, D.K.; orbital motion, nucleus precession, and splitting of periodic comet Brooks 2. *Astron. J.* **90**, 2335-2352 (1985)

Sierks, H. et al.; On the nucleus structure and activity of comet 67P/Churyumov-Gerasimenko. Science 347 (2015) DOI:10.1126/science.aaa1044

Steckloff, J.K. et al., Dynamic sublimation pressure and the catastrophic breakup of Comet ISON. Icarus 258, 430-437 (2015)

Steckloff, J.K. & Jacobson, S.A.; The formation of striae within cometary dust tails by a sublimation-driven YORP-like effect. Icarus 264, 160-171 (2016)

Thomas, P.C. et al. Shape, density, and geology of the nucleus of comet 103P/Hartley 2. Icarus 222, 550-558 (2013)

Thomas, N. and 58 coauthors; The morphological diversity of comet 67P/Churyumov-Gerasimenko. *Science* **347**, (2015) DOI: 10.1126/science.aaa0440

Werner, R.A., The gravitational potential of a homogeneous polyhedron or don't cut corners. Celest. Mech. Dynam. Astron. 59, 253-278 (1994)

VITA

VITA

Jordan Steckloff was born in Detroit, Michigan. During high school, he was dual-enrolled in Oakland Community College, and completed the coursework for his Associate of Science degree within two months of graduating from Harrison High School in Farmington Hills, Michigan. He graduated from the University of Michigan with a Bachelor of Science degree in 2009 with majors in Physics, Economics, and German (which included a year abroad at Albert-Ludwigs Universität, Freiburg im Breisgau, Germany). Jordan began his graduate studies at Purdue University in the Department of Physics in the fall of 2009, and earned a Master of Science degree in 2012.

PUBLICATIONS

Icarus 258 (2015) 430–437

Contents lists available at ScienceDirect

Icarus

journal homepage: www.elsevier.com/locate/icarus

Dynamic sublimation pressure and the catastrophic breakup of Comet ISON

Jordan K. Steckloff [a,*], Brandon C. Johnson [b], Timothy Bowling [c], H. Jay Melosh [a,c,d], David Minton [c], Carey M. Lisse [e], Karl Battams [f]

[a] Purdue University, Department of Physics and Astronomy, 525 Northwestern Avenue, West Lafayette, IN 47907, United States
[b] Massachusetts Institute of Technology, Department of Earth, Atmospheric, and Planetary Sciences, 77 Massachusetts Avenue, Cambridge, MA 02139, United States
[c] Purdue University, Department of Earth, Atmospheric, and Planetary Sciences, 550 Stadium Mall Drive, West Lafayette, IN 47907, United States
[d] Purdue University, Department of Aeronautical and Astronautical Engineering, 701 W. Stadium Avenue, West Lafayette, IN 47907, United States
[e] John Hopkins University – Applied Physics Laboratory, 11100 Johns Hopkins Road, Laurel, MD 20723, United States
[f] Naval Research Laboratory, 4555 Overlook Avenue, Washington, DC 20375, United States

ARTICLE INFO

Article history:
Received 5 February 2015
Revised 18 June 2015
Accepted 21 June 2015
Available online 27 June 2015

Keywords:
Comets, dynamics
Comets, nucleus
Ices

ABSTRACT

Previously proposed mechanisms have difficulty explaining the disruption of Comet C/2012 S1 (ISON) as it approached the Sun. We describe a novel cometary disruption mechanism whereby comet nuclei fragment and disperse through dynamic sublimation pressure, which induces differential stresses within the interior of the nucleus. When these differential stresses exceed its material strength, the nucleus breaks into fragments. We model the sublimation process thermodynamically and propose that it is responsible for the disruption of Comet ISON. We estimate the bulk unconfined crushing strength of Comet ISON's nucleus and the resulting fragments to be 0.5 Pa and 1–9 Pa, respectively, assuming typical Jupiter Family Comet (JFC) albedos. However, if Comet ISON has an albedo similar to Pluto, this strength estimate drops to 0.2 Pa for the intact nucleus and 0.6–4 Pa for its fragments. Regardless of assumed albedo, these are similar to previous strength estimates of JFCs. This suggests that, if Comet ISON is representative of dynamically new comets, then low bulk strength is a primordial property of some comet nuclei, and not due to thermal processing during migration into the Jupiter Family.

1. Introduction

On November 12, 2013 sungrazing comet C/2012 S1 (ISON) unexpectedly disrupted into fragments. This occurred at a heliocentric distance of 145 solar radii ($R_\odot$) (0.68 AU), prior to reaching perihelion (Combi et al., 2014; Boehnhardt et al., 2013; Steckloff et al., 2015). Subsequent disruption events occurred on November 21 and 26 at 88 $R_\odot$ (0.41 AU) and 36 $R_\odot$ (0.17 AU) respectively (Knight and Battams, 2014; Steckloff et al., 2015). While there is nothing seemingly special about these heliocentric distances, currently known sungrazing comet disruption mechanisms seem inadequate to explain ISON's demise. ISON's disruptions occurred much too far from the Sun to have been caused by ablation or chromospheric impact, which disrupt nuclei within a heliocentric distance (q) of 1.01 $R_\odot$ (Brown et al., 2011). Tidal stresses can disrupt the nucleus only within the fluid Roche Limit ($q < \sim 2\ R_\odot$) (Knight and Walsh, 2013). Additionally, ISON's effective radius of ~600–700 m (Delamere et al., 2013; Lamy et al., 2014) was too large to have lost all its ice through complete sublimation and then disintegrated, a process that may only disrupt nuclei less than ~200–350 m in radius (Knight and Walsh, 2013; Sekanina, 2003). Finally, ISON's 10.4 h rotation period at 210 $R_\odot$ on November 1 (Lamy et al., 2014) was too long for nongravitational torques to spin the body up to fragmentation (~2.2 h period) (Pravec et al., 2006) by the time it reached 145 $R_\odot$ less than 2 weeks later on November 13 (Samarasinha and Mueller, 2013). However, it has been implied that sublimating gases are linked to the disruption of sungrazing comets (Sekanina, 2003). Here we introduce a new break-up mechanism that readily explains Comet ISON's series of disruptions.

As illustrated in Fig. 1, gas sublimating on the sunward side of the nucleus transfers momentum to the nucleus, exerting a dynamic sublimation pressure on its illuminated hemisphere. The sublimation pressure on the surface generates differential stresses within the nucleus that may exceed ISON's material strength, ultimately disrupting the comet into fragments (Brown et al., 2011; Borovička et al., 2013). Based on the timing of

* Corresponding author.
E-mail address: jstecklo@purdue.edu (J.K. Steckloff).

http://dx.doi.org/10.1016/j.icarus.2015.06.032
0019-1035/

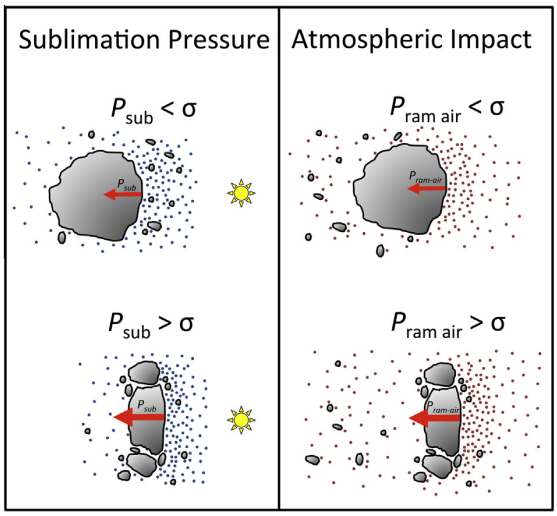

Fig. 1. Schematic of Dynamic Sublimation Pressure Disruption Mechanism and Comparison to Atmospheric Impact. (Left) We assume that the dynamic pressure is zero on the dark side of the nucleus, while the peak dynamic pressure on the illuminated side (P_{sub}) becomes comparable to the unconfined static crushing strength of the nucleus (σ). When P_{sub} exceeds σ, the nucleus disrupts catastrophically. (Right) This is analogous to the nucleus impacting a planetary atmosphere. A ram pressure (P_{ram}) builds up on the leading edge of the nucleus as it travels through the atmosphere. If P_{ram} exceeds σ, then the nucleus breaks up into fragments (Borovicka et al., 2013).

disruption events we can estimate the bulk unconfined crushing strength of Comet ISON's nucleus.

2. Theory/calculation

Investigating our proposed disruption mechanism requires an accurate computation of the sublimation pressure (itself a function of both thermal gas velocity and mass loss rate) acting at the surface of the nucleus as a function of heliocentric distance. Previous computations of cometary sublimation rely heavily upon either empirical fits to observed volatile mass loss rates (e.g. Marsden et al., 1973; Cowan and A'Hearn, 1979; Sekanina, 1992), or on the theoretical dependence of mass loss rates on temperature (Delsemme and Swings, 1952) rather than the dependence of sublimation pressure on heliocentric distance. We choose instead to construct a versatile thermodynamic model of the sublimation pressure acting upon a cometary surface. In our calculations, the heliocentric dependence of the sublimation pressure of a particular volatile species is fully described by six known quantities: heliocentric distance (r_{helio}), molar mass (m_{molar}), heat of sublimation (L), sublimation coefficient (α) and a laboratory measurement of vapor pressure (P_{ref}) at a known temperature (T_{ref}).

Comets consist of intimate mixtures of refractory materials (silicates, metal sulfide dust, organics) and volatile ices (primarily H_2O, CO_2, and CO [Bockelée-Morvan et al., 2004]). The phase-change behavior of mixtures of volatiles can be significantly more complicated than that of a single, pure volatile species. In particular, if cometary CO is mostly trapped within amorphous H_2O ice, then the release of significant quantities of CO may require the amorphous H_2O ice to crystallize (Bar-Nun et al., 2013), which is a highly exothermic and potentially explosive phase transition (Mastrapa et al., 2013). Moreover, the presence of amorphous ice in comets is contentious (Lisse et al., 2013). However, Comet ISON's CO content is only a few percent of its H_2O content (Weaver et al., 2014) and produced an order of magnitude less CO_2 than H_2O (McKay et al., 2014). Therefore, we may assume that the sublimation pressure acting on Comet ISON's surface is dominated by the sublimation of pure H_2O ice, which avoids the complications of the sublimation of mixed materials and species more volatile than H_2O ice. However, we include the cases in which pure CO_2 and CO ice sublimates for the sake of comparison, which admittedly ignores the complications of how one would trap significant quantities of CO ice in the first place.

Typical bond albedos measured for Jupiter Family Comet (JFC) nuclei are very low (0.03–0.06) (Li et al., 2013a,b; Capaccioni et al., 2015), and when JFCs approach the Sun, most of the incident radiation (94–97%) is absorbed at the surface and drives the sublimation of volatile ices (an active comet's dominant cooling mechanism). We explore the case in which Comet ISON's albedo is similar to that of JFCs, and assume that all incident radiation is absorbed (bond albedo of 0). However, because dynamically new comets have never been thermally processed by the Sun, it is plausible that their surfaces are significantly richer in ices than JFCs, which could lead to a much higher albedo. Moreover, there are no high-resolution observations of dynamically new comet nuclei, which would constrain their albedos. We therefore also explore the case in which Comet ISON has a bond albedo of 0.5, which is similar to that of the dwarf planet Pluto.

Observations of JFC nuclei suggest that cometary thermal inertia is very low (Gulkis et al., 2015; Davidsson et al., 2013; Groussin et al., 2013; Lisse et al., 2005; Lamy et al., 2008), meaning that little daytime heat is stored by the surface to be later released when it rotates into night. This naturally explains their highly asymmetric dayside–nightside distribution of sublimating gases (Feaga et al., 2007; Gulkis et al., 2015). Similarly, Comet ISON's activity is concentrated on its illuminated hemisphere (Li et al., 2013c). Since cometary activity is driven by volatile sublimation, we assume that effectively all volatile emission occurs on Comet ISON's illuminated hemisphere, causing a sublimation pressure that only acts on the illuminated parts of its nucleus. Indeed, it has been known for decades that nongravitational forces push predominantly on the sunward hemispheres of comet nuclei (Marsden et al., 1973). While observations show that the unilluminated side of comet nuclei can emit volatiles, emission on the unilluminated side is usually less than half of the emission of the illuminated side (Feaga et al., 2007; Gulkis et al., 2015). Therefore, our sunward emission assumption is valid for our purpose of obtaining an order of magnitude estimate of ISON's strength.

While the nuclei of highly thermally evolved comets (like JFCs) emit dust and gas from only a small fraction of their surfaces (Ververka et al., 2013; Samarasinha and Mueller, 2013), ISON's high H_2O production rate prior to disruption suggests that nearly the entire surface of its nucleus was active (Combi et al., 2014), consistent with a thermally primitive, dynamically new comet. This implies that volatile ices are located within the thermal skin depth of the comet's surface. We therefore assume that volatile ices sublimate from the entire illuminated surface of ISON, and that a negligible amount of incident solar energy is thermally radiated into space from a mantle of material covering the volatile ices.

The dynamic pressure exerted by sublimating volatiles on the surface of the nucleus is equal to the momentum flux of the departing material, and is computed by multiplying the volatile's mass flux by its thermal velocity. Assuming that volatile ices are at or near the surface, we estimate Comet ISON's volatile mass flux by equating the absorbed solar energy to the energy required to sublime each ice species, as first described by Whipple (1950). We assume that volatile ices and refractory materials are intimately mixed, such that heat is rapidly transferred from refractory materials to volatile ices. We ignore the amount of energy required to warm the ices from their initial low temperatures (perhaps 10 K for dynamically new comets such as ISON) to the equilibrium

sublimation temperature. Such heating consumes less than ~10%, ~25%, and ~25% of the total incident solar energy for H_2O, CO_2, and CO ice respectively, and is therefore negligible for our order of magnitude estimates. For simplicity, we treat each volatile species individually, while acknowledging that multiple species may sublime simultaneously from different depths below the surface.

2.1. Computing mass flux, force, temperature, and sublimation pressure

The incident solar radiation intensity at the location of the comet is given by

$$I_{solar} = \frac{L_{solar}}{4\pi r_h^2} \tag{1}$$

where L_{solar} is the solar luminosity (3.846×10^{26} W), and r_h is the heliocentric distance. We assume that all solar radiation incident upon an area element of the surface of the nucleus (dA) is used to overcome the latent heat of sublimation of these volatile ices (Whipple, 1950) to determine each species' mass flux

$$\dot{m} = (1-A)\frac{I_{solar}}{\lambda(T)}\cos\phi = (1-A)\frac{L_{solar}}{4\pi r_h^2 \lambda(T)}\cos\phi \tag{2}$$

where A is the albedo of the sublimating surface, $\lambda(T)$ is the temperature-dependent latent heat of sublimation of a volatile ice species and ϕ is the angle between the comet–Sun line and the vector normal to the area element (local phase angle). For a sphere, ϕ is equivalently the azimuth angle of the area element from the subsolar point. While the latent heat of sublimation for water is temperature-dependent, it varies so little over the temperature range of interest (Feistel and Wagner, 2007) that treating it as a constant makes a negligible difference in our results. We therefore assume that the latent heat of sublimation is a constant.

We determine the thermal velocity of the dominant sublimating volatile using the kinetic theory of gases. We assume that the speeds of sublimating gas molecules obey a Maxwell–Boltzmann distribution, where the mean of the magnitude of the molecule velocities escaping from a given area element (dA) is

$$v_{thermal} = \sqrt{\frac{8RT}{\pi m_{mol}}} \tag{3}$$

where m_{mol} is the molar mass of the species, T is the gas temperature, and R is the ideal gas constant. The gas diffusing through the cometary pores has a Knudsen number of $Kn \sim 10^2$–10^5, which allows us to assume that the sublimating volatile molecules are sufficiently rarefied to be emitted from a porous regolith according to Lambert's cosine law (Gombosi, 1994, pp. 227–230). Thus, the number of molecules emitted in a particular direction from an area element ($d\dot{N}(\theta)$) is proportional to the cosine of the angle of that direction with respect to the vector normal to that area element

$$d\dot{N}(\theta) = \frac{\dot{N}_{dA}}{\pi}\cos\theta \tag{4}$$

where $\dot{N}_{dA}$ is the number flux of molecules through area element dA, and θ is the angle made with the vector normal to area element dA. We compute the net force on a given area element from sublimating gas molecules by multiplying this particle density distribution by both $v_{thermal}$ and the mass of a particle, and then integrate over all solid angles. Since the particle density distribution depends solely on the angle with respect to the vector normal to the area element, this computation is axisymmetric. Thus, the components of the force tangential to the surface of area element dA cancel out, allowing us to consider only the component of the force normal to the surface. Integrating over all solid angles above the ground

$$F_{element} = \frac{2}{3} v_{thermal}\, \dot{m}\, dA \tag{5}$$

and the mass flux from the area element ($\dot{m}$) is

$$\dot{m} = \frac{m_{molar}}{N_{av}}\frac{\dot{N}_{dA}}{dA} \tag{6}$$

where m_{molar} is the molar mass of the sublimating gas and N_{av} is Avogadro's constant. Combining Eqs. (2), (3) and (5)

$$F_{element} = \frac{2}{3}(1-A)\frac{L_{solar}}{4\pi r_h^2 \lambda}\sqrt{\frac{8RT}{\pi m_{mol}}}\cos\phi\, dA \tag{7}$$

We compute the appropriate temperature (T) in Eq. (7) by joining the Langmuir–Knudsen (Langmuir, 1913) equation of sublimation rates with the Clausius–Clapeyron relation of equilibrium partial pressure and temperature of an ideal gas

$$\dot{m} = \alpha(T)\sqrt{\frac{m_{mol}}{2\pi RT}}P(T) \tag{8}$$

$$\frac{dP}{dT} = \frac{P}{T^2}\frac{\lambda}{R} \tag{9}$$

where $\alpha(T)$ is the temperature-dependent sublimation coefficient (e.g. Gundlach et al., 2011) and $P(T)$ is the temperature-dependent partial pressure of the molecular species, which results in the following expression for the temperature as a function of the mass flux:

$$\dot{m} = \alpha(T)\sqrt{\frac{m_{mol}}{2\pi RT}}P_{ref}\, e^{\frac{\lambda}{R}\left(\frac{1}{T_{ref}}-\frac{1}{T}\right)} \tag{10}$$

where P_{ref} and T_{ref} are an experimentally measured reference pressure and temperature of the species. We use the empirical fit to the temperature dependence of the sublimation coefficient $\alpha(T)$ for H_2O from Gundlach et al. (2011), which produces a small improvement in the computation of water's sublimation pressure over setting the sublimation coefficient to 1. We set the sublimation coefficient $\alpha(T)$ for all other species to 1. Combining Eqs. (2) and (10)

$$(1-A)\frac{L_{solar}}{4\pi r_h^2 \lambda}\cos\phi = \alpha(T)\sqrt{\frac{m_{mol}}{2\pi RT}}P_{ref}\, e^{\frac{\lambda}{R}\left(\frac{1}{T_{ref}}-\frac{1}{T}\right)} \tag{11}$$

Note that this is a transcendental equation, which does not have an analytical solution. Thus, we solve for this temperature numerically. Lastly, since pressure is a force applied over an area, we rearrange Eq. (7) to describe the dynamic sublimation pressure exerted on the surface of a nucleus

$$P_{sub}(r_h,\phi) = \frac{2}{3}(1-A)\frac{L_{solar}}{4\pi r_h^2 \lambda}\sqrt{\frac{8RT}{\pi m_{mol}}}\cos\phi \tag{12}$$

We approximate a comet as a sphere, and plot the dependence of the dynamic sublimation pressure on the azimuth from the subsolar point (ϕ) for the sublimation of H_2O at heliocentric distances of 36, $R_\odot$ 88, $R_\odot$ and 145 $R_\odot$ (see Fig. 2).

2.2. Differential stress

Computing differential stresses with ISON's nucleus is essential to our analysis, because differential stresses can lead to its disruption. A compressive differential stress will cause a brittle material to deform, but the material will remain intact deforming elastically as long as the differential stress remains below the material's strength. However, when the differential stress exceeds a brittle material's strength, the material will fail and fracture. In the case of a comet, when the dynamic sublimation pressure causes material failure, the nucleus will subsequently fragment.

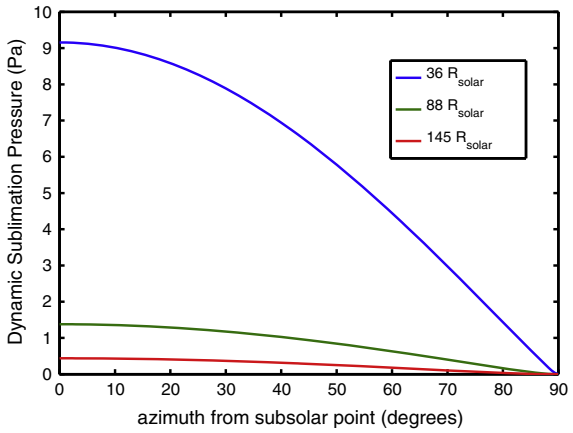

Fig. 2. Azimuthal dependence of dynamic sublimation pressure. A plot of the azimuthal dependence of the dynamic sublimation pressure for three separate heliocentric distances for the case of a bond albedo of 0. Azimuthal angle is the angle between the subsolar point and the vector normal to the surface of an idealized, spherical nucleus. While the real nucleus is not necessarily spherical, it will have a subsolar point and a limb, where the dynamic sublimation pressures will be at a maximum and zero respectively. The differential stress that results from this pressure difference is ultimately responsible for fragmenting the nucleus.

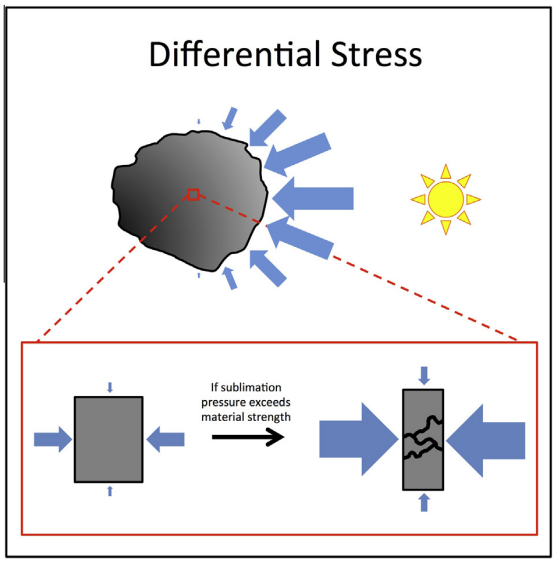

Fig. 3. Schematic of how sublimation pressure induces differential stresses. (top) Dynamic sublimation pressure acts upon the sunward hemisphere of the nucleus. Sublimation pressure peaks at the subsolar point, but drops off to zero toward the limb. As the nucleus approaches the Sun, the sublimation pressure increases. (bottom inset) We illustrate the stresses acting on a parcel of material within the nucleus after subtracting off the hydrostatic pressure. The distribution of the sublimation pressure acting on the surface of the nucleus induces unequal stresses on the parcel of material, with stresses greatest along the comet–Sun axis. As the nucleus approaches the Sun, the stresses on the parcel grow. If the difference in stresses between the maximum stress and minimum stress axis (the differential stress) exceeds the strength of the material, then the parcel fails and fragments.

Because the sublimation pressure drops to zero at a 90-degree azimuth from the subsolar point (the limb of the nucleus) and remains near zero on the unilluminated side, the maximum differential stress within the nucleus is similar in magnitude to the sublimation pressure at the subsolar point (the maximum sublimation pressure). Therefore, when we compute the dynamic sublimation pressure at the subsolar point as a function of heliocentric distance, we are approximating the maximum differential stresses within the nucleus (see Fig. 3).

Gundlach et al. (2012) proposed a related mechanism, in which a sublimation pressure that pressed equally on all parts of the nucleus may have allowed Comet C/2011 W3 (Lovejoy) to survive through its perihelion of 1.2 $R_\odot$. Within ~10 $R_\odot$ of the Sun, the coma of a comet with a ~1 km nucleus becomes optically thick (Drahus, 2014), causing light of equal intensity to fall upon all parts of the nucleus, which results in a uniform sublimation pressure being exerted on all parts of its surface. Unlike our proposed mechanism, such a phenomenon would generate no new differential stresses within the interior of the nucleus. However, it would induce a confining pressure on its surface, which can increase the strength of porous, granular materials (Alkire and Andersland, 1973). If this increase in strength were sufficiently large, then volatile sublimation near the Sun could allow C/2011 W3 (Lovejoy) to resist the strong solar tidal forces that exist within the Roche Limit that would otherwise disrupt the nucleus (Gundlach et al., 2012).

The Whipple model for ice sublimation (Whipple, 1950), combined with our model of ISON as a sublimating sphere of ice 680 m in radius (Lamy et al., 2014), predicts a mass loss rate from Comet ISON's nucleus for H_2O at 214 $R_\odot$ (1 AU) of $q_{water} = 2.75 \times 10^{28}$ s^{-1}, in agreement with the observed production rate of $q_{water} = 2.30(\pm0.71) \times 10^{28}$ s^{-1} (Combi et al., 2014). Measurements of Comet ISON's $Af\rho$ parameter as a function of aperture radius (ρ) flattened out and approached a constant value as ISON approached the Sun, suggesting that icy grains ceased to contribute significantly to ISON's volatile production by late October (Knight and Schleicher, 2015). We therefore find that such close agreement between the expected and measured production rates generally support our assumption that the entire illuminated hemisphere is sublimating. Although Combi et al. (2014) deconvolved the observations with a model to obtain a daily average water production rate, their observed production rate of $q_{water} = 1.99(\pm0.32) \times 10^{28}$ s^{-1} at 0.98 AU is consistent with the measured rate of $q_{water} = 1.6 \times 10^{28}$ s^{-1} (±25%) at 0.98 AU (Bodewits et al., 2013) and their observed production rate of $q_{water} = 1.79(\pm0.35) \times 10^{28}$ s^{-1} at 0.88 AU is within a factor of 2 of $q_{OH} = 8.14(\pm2.31) \times 10^{27}$ s^{-1} at 0.89 AU (Opitom et al., 2013a). These observations, which demonstrate remarkable agreement across various instruments, are consistent with a highly active, intact nucleus.

However, after November 12th, the amount of active surface required to match the observed H_2O production increased permanently by a factor of ~25, implying that the nucleus had then disrupted into a swarm of fragments (Combi et al., 2014). This is consistent with the observation of arc-like wings in the coma of ISON, which suggest the presence of multiple fragments (Boehnhardt et al., 2013). Other analysis determined that the radius of ISON's nucleus (or nucleus fragments) decreased too much during this event to be solely the result of sublimative surface erosion, further implying a disruption event at 145 $R_\odot$ (Steckloff et al., 2015). We therefore interpret this first event to be the complete breakup of the nucleus into a swarm dominated by large fragments ~100 m in radius (see Discussion section). The swarm (or specific large fragments within it) was later observed to undergo two further significant disruption events on November 21st and November 26th Knight and Battams, 2014; Steckloff et al., 2015).

Escaping fragments and lofted grains do not directly contribute to the reaction force on the comet's nucleus because their velocity is so slow near the nucleus relative to the sublimating gases that they carry a negligible amount of momentum away from the nucleus. However, they can reflect some fraction of the sublimated gas molecules back onto the nucleus, further increasing the dynamic pressure. This effect can only increase the peak dynamic

pressure by a factor of π (in the unlikely limit that every gas molecule bounces indefinitely between the nucleus and icy grains), to equal the gas vapor pressure. We adopt the conservative stance of neglecting this uncertain (but positive) backpressure, which can only add to the dynamic sublimation pressure, and which will introduce only small errors into our estimate.

3. Results

Motivated by observations of high H_2O production (Combi et al., 2014; Opitom et al., 2013a,b,c), we assume that volatile sublimation is dominated by H_2O as ISON approached perihelion. We compute the maximum dynamic H_2O sublimation pressure (and thus estimate the bulk cometary unconfined crushing strength) when Comet ISON disrupted at heliocentric distances of 36, 88, and 145 $R_\odot$ (Combi et al., 2014; Boehnhardt et al., 2013; Knight and Battams, 2014; Steckloff et al., 2015)]. We find strengths of 9, 1, and 0.5 Pa, respectively, for the case where ISON has a bond albedo of 0. If we instead assume a bond albedo of 0.5, we find strengths of 4, 0.6, and 0.2 Pa respectively (see Fig. 4). These strengths are comparable to estimates of the strengths of Jupiter Family Comets (JFCs) (Asphaug and Benz, 1996; Bowling et al., 2014; Melosh, 2011; Sekanina and Yeomans, 1985; Thomas et al., 2015). If Comet ISON's true bond albedo is between these two values, then the maximum dynamic pressure and bulk unconfined crushing strength estimates will also lie between the corresponding values. Such a hierarchy of strengths is consistent with studies of the strength of geologic materials, which depend inversely on the size of the sample (Brace, 1961), and is consistent with evidence suggesting that comet nuclei are composed of pieces that are heterogeneous in strength (Sekanina, 2003). The lowest of these strength estimates (0.2 and 0.5 Pa depending on bond albedo) corresponds to the first disruption event (at 145) $R_\odot$, and therefore represents the bulk unconfined crushing strength of ISON's intact nucleus (prior to any significant fragmentation). The higher strength estimates correspond to the later disruption events at 88 $R_\odot$ and 36, $R_\odot$ and therefore represent the strengths of fragments of ISON's nucleus.

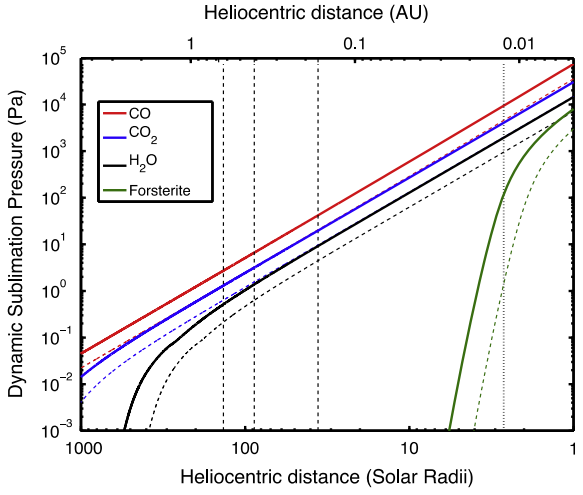

Fig. 4. Dynamic gas sublimation pressures for major volatile species. A plot of dynamic gas pressures for pure H_2O, CO_2, and CO as a function of heliocentric distance, measured in both Solar Radii ($R_\odot$) and Astronomical Units (AU). We include the mineral fosterite (Nagahara et al., 1994) as a proxy for refractory cometary materials, which only becomes dominant in the absence of volatiles very near the Sun. Solid curves denote sublimation pressures if the nucleus has zero bond albedo while the dashed curves are for an assumed bond albedo of 0.5. For a bond albedo between these two values, the sublimation pressure will lie between these two curves. The thin, dashed vertical lines at 36, 88[2], and 145[1] $R_\odot$ mark where Comet ISON disrupted into fragments (Combi et al., 2014; Knight and Battams, 2014), while the dotted line at 2.66 $R_\odot$ denote Comet ISON's perihelion distance.

4. Discussion

After a fragmentation event, the size of the resulting fragments may have an observable effect on the motion of the comet or morphology of the nucleus. The sublimation pressure acting on the illuminated surfaces of the nucleus provides a net antisunward force, with the net motion of the nucleus dependent on this sublimation force and the solar gravitational force. Since the sublimation force depends on surface area, while the gravitation force depends on volume, larger bodies (smaller surface-area-to-volume ratio) are less susceptible to the sublimation force than smaller bodies (larger surface-area-to-volume ratio). Therefore, if the nucleus produced fragments of substantially unequal sizes, smaller fragments would appear to drift antisunward of the larger fragments, which would cause the central condensate of the comet's coma to elongate and even break up. However, Comet ISON maintained a strong central condensate (a compact region of peak coma brightness) up until only a few hours before perihelion (Knight and Battams, 2014; Opitom et al., 2013b,c), and this central condensate only began to noticeably elongate a few days before perihelion (Steckloff et al., 2015). Thus, either the first fragmentation event broke Comet ISON into a swarm of equally sized fragments, or into differently sized fragments that were still each large enough to limit the relative drift between fragments and the resulting observable changes to the morphology of the coma.

Steckloff et al. (2015) conducted a preliminary study to estimate the sizes of the dominant fragments of Comet ISON. They measured the deviation of Comet ISON's position using the SCUBA-2 instrument on the James Clerk Maxwell Telescope from JPL Horizon's ephemeris solution #53, and estimated fragment sizes by assuming that this deviation is entirely due to H_2O sublimation pressure. From this, they determined that the first fragmentation event reduced the effective radius of Comet ISON from an approximately 680 m for the intact nucleus to fragments on the order of ~100 m. Such fragments would require approximately half of a week to traverse a single pixel of the SCUBA-2 instrument and a few days more for the larger pixels of the TRAPPIST telescope. This provides a rough estimate of the timescale over which coma morphology would noticeably elongate from the release of a single fragment from a much larger parent nucleus. This timescale would be longer if the fragments are closer in size, since they would drift together. Since no change in coma morphology was detected during the 9 days between the first and second fragmentation events, it is unlikely that ISON only released a single ~100 m fragment from the nucleus during the first fragmentation event. Rather, it is more likely that the first fragmentation event broke up ISON's nucleus into a swarm of large fragments with radii on the order of ~100 m.

Because the coma may have started to elongate between the second and third fragmentation events, it is unclear whether the second fragmentation event was the result of a single fragment or multiple fragments disrupting. However, the elongation of the central condensate after the third fragmentation event (Steckloff et al., in prep.) suggests that a large range of fragment sizes were present after the third fragmentation event.

4.1. Supervolatiles and amorphous ice

Samarasinha (2001) proposed that the buildup of pore pressure within the nucleus from the sublimation of super-volatile species could lead to its disruption. This mechanism requires that the

thermal skin depth of the comet be large enough to reach pockets of deeply seated volatiles. The thermal skin depth (h_{skin}) describes the characteristic length scale over which the amplitude of a heat pulse conducting (without sublimating volatiles) into an infinite half-space of material with a fixed boundary location and temperature drops by a factor of e, and is given by the equation

$$h_{skin} = \sqrt{\mathcal{H}\tau} \tag{13}$$

where $\mathcal{H}$ is a material's thermal diffusivity (typically on the order of 10^{-6} m^2 s^{-1} for dense rocks or ice) and τ is the duration since the onset of the thermal pulse. The longer a material is exposed to a heat pulse, the deeper the heat can penetrate. The rate at which the thermal skin depth advances into a material is obtained by differentiating Eq. (13) with respect to time (τ)

$$v_{skin} = \frac{dh_{skin}}{d\tau} = \frac{1}{2}\sqrt{\frac{\mathcal{H}}{\tau}} \tag{14}$$

$$= \frac{\mathcal{H}}{2h_{skin}} \tag{15}$$

Thus, as the time of exposure (τ) and thermal skin depth (h_{skin}) increases, the rate of growth of the thermal skin depth (v_{skin}) decreases.

If the fixed-temperature boundary is receding at a constant rate, the thermal skin depth (h_{skin}) will either grow or shrink until v_{skin} is equal to this rate of recession, and the thermal skin depth will maintain a fixed depth relative to the surface. However, because heat takes time to conduct from the surface to the thermal skin depth, the distance between the thermal skin depth (h_{skin}) and the receding surface will be less than what Eq. (13) provides. Also, the rate of surface recession on a comet nucleus is not constant, but rather accelerates as the nucleus approaches the Sun, which further reduces the distance between the surface and h_{skin}. Additionally, moving boundaries, changing boundary conditions, and sublimation make the actual temperature profile of a comet nucleus significantly more complicated than that which results from simple heat conduction. However, if we assume that the H_2O sublimation front, whose temperature is largely determined by heliocentric distance, is some distance h_{sub} below the surface of the nucleus and that h_{skin} is measured from the sublimation front, then the quantity $h_{skin} + h_{sub}$ (computed using Eqs. (13) and (15)) will be a conservative overestimate of Comet ISON's orbital thermal skin depth.

Because Comet ISON's activity occurred predominantly on the sunward hemisphere (Li et al., 2013c), the volatiles driving this activity had to respond to the day-night (diurnal) cycle of the nucleus, and could therefore be no deeper below the surface than a depth comparable to the diurnal skin depth. Based on a ~10.4 h rotation period for the nucleus of Comet ISON (Lamy et al., 2014), the sublimation front of H_2O (h_{sub}) is no more than ~20 cm below the surface. Since sublimation is a comet's dominant cooling mechanism in the inner Solar System, we estimate the rate of the sublimation front's recession into the nucleus at the time of the Lamy et al. (2014) observations by dividing the mass-loss rate equation (Eq. (2)) by the bulk density of a typical comet, and find that it is on the order of ~10^{-6} m/s. Noting that the rate of sublimation front recession and thermal skin depth recession (v_{skin}) are in equilibrium, we set v_{skin} to ~10^{-6} m/s, and find that h_{skin} is on the order of ~0.5 m. Thus, $h_{skin} + h_{sub}$ is on the order of meters, and therefore cold, Oort Cloud conditions persist in the primordial materials of Comet ISON only a few meters at most below the surface of the nucleus.

Because the orbital thermal skin depth is so shallow, if the thermal wave were to reach a pocket of supervolatile ices or trigger the crystallization of amorphous ice, they would release fragments from the surface with sizes comparable to the orbital thermal skin depth. Thus, if the first fragmentation event were the result of the rapid sublimation of supervolatile species, one would expect to see an outburst that released debris up to an order of ~1 m in size, leaving the nucleus largely intact. If the nucleus is composed of amorphous water ice whose crystallization was triggered by the propagation of the thermal wave into the interior, the crystallization front will propagate into the amorphous ice until the cold interior of the nucleus absorbs the exothermic heat of the phase transition and quenches the crystallization process. Because the thermal wave is near the surface, the temperature gradient near the sublimation front is very steep (dropping to primordial temperatures over a distance on the order of the orbital thermal skin depth), and would quench the crystallization of the amorphous ice very quickly. Therefore, even if the exothermic crystallization of amorphous ice caused the first fragmentation event, one would still only expect to see an outburst that released similarly small debris.

Such small debris from a surface layer is inconsistent with the drastic reduction in the size of the nucleus after the first fragmentation event (Steckloff et al., 2015) and the observation of coma wings (Boehnhardt et al., 2013), which may indicate the presence of multiple large fragments. Additionally, such small debris would dissipate quickly, which is inconsistent with the sustained increase in water production (Combi et al., 2014). Therefore, while a direct application of the Samarasinha (2001) model may explain the disruption of highly thermally evolved comet nuclei, it appears that its direct application is inconsistent with the disruption of Comet ISON.

We cannot rule out a modification of the Samarasinha (2001) model, in which sublimating gases can penetrate into the pores of the nucleus and recondense (thus transporting heat into the cometary interior by releasing their heats of sublimation). If voids are present within the interior of the nucleus, then a sublimation front and thermal skin depth would be created within the walls of these voids akin to the situation at the surface. The Second Law of Thermodynamics limits the maximum temperature of the void walls achievable through this mechanism to the surface temperature of the nucleus (although the actual temperature would likely be much lower). Gas must be able to readily diffuse through the nucleus for a significant amount of heat to be transported into the cometary interior in this manner, which greatly restricts the ability of sublimating volatiles to build up a gas pressure as though the comet were a sealed vessel. As the walls of the void recede through sublimation, the thermal wave may encounter supervolatile ices or amorphous ice. The sublimation of supervolatiles within a void would produce pressures that could be no greater than those that would be present at the surface, but probably significantly less. If these low pressures lead to the destruction of the nucleus, then our strength estimates would be an upper bound to the strength of the nucleus. However, were the thermal wave to trigger the crystallization of amorphous ice, this exothermic phase transition could cause a very rapid buildup of gas pressure within the void, potentially faster than the gases may diffuse out, and could potentially lead to a catastrophic explosion of the nucleus. We therefore cannot rule out this modified mechanism. This mechanism requires special diffusive, compositional, and structural conditions to disrupt the nucleus, which seems less likely to lead to ISON's disruption than sublimation pressure at the surface. However, a detailed exploration of the relevant physics of diffusion, sublimation, and phase transitions is beyond the scope of this paper.

4.2. Hydrostatic pressure and fragmentation timescale

Our crushing strength computation ignores the internal hydrostatic pressure due to self-gravity of Comet ISON, which is up to

~10 Pa for a 680 m spherical nucleus (Lamy et al., 2014) with a density of 400 kg m^{-3} (Richardson and Melosh, 2013). If the nucleus were to uniformly disrupt in a single event, the dynamic sublimation pressure would have to overcome this overburden pressure in the comet's interior. In reality, the nucleus probably disrupted piecewise, in a process where the dynamic sublimation pressure first overcomes the crushing strength and disperses the material near the surface of the nucleus, where the hydrostatic pressure is low. This reduces the hydrostatic pressure throughout the remaining nucleus, where this process repeats until the entire cometary nucleus is dispersed. We estimate the timescale of this dispersion by computing the time needed for the surface of the comet to accelerate across the diameter of the nucleus from sublimation pressure alone, assuming typical cometary densities of around 400 kg m^{-3} (Richardson and Melosh, 2013; Richardson and Bowling, 2014; Thomas et al., 2015). This results in a dispersion timescale for Comet ISON of only a few hours at 145, $R_\odot$ allowing us to ignore the effects of hydrostatic pressure and treat the cometary disruption effectively as an instantaneous event in the comet's orbit.

Our sublimation pressure disruption mechanism assumes that the nucleus is rotating slowly enough that the maximum dynamic sublimation pressure at the sub-solar region has enough time to fragment the nucleus before rotating significantly away from the sub-solar point and reducing the sublimation pressure on that area element. The critical timescale for fragmenting the nucleus is the amount of time needed for a crack, once started, to propagate across the nucleus. The growing tip of a crack travels at the Rayleigh surface wave velocity, which are typically on the order of ~100 m/s for granular materials, and higher for more coherent materials (Lawn and Wilshaw, 1975). Thus, the time needed for a crack to travel across the nucleus (and therefore the timescale of fragmentation) is on the order of a few seconds. Since the rotation period of a comet nucleus is limited to be no shorter than a few hours before fragmenting rotationally (Snodgrass et al., 2006; Pravec et al., 2006), the timescale of fragmentation is negligible and our assumption holds.

4.3. Strengths of other comets

We compare our crushing strength estimate to observationally constrained estimates of the bulk, tensile, and shear strengths of other comets, which are related to the bulk crushing strength by small factors on the order of unity (Price, 1968). The crushing strength of Comet ISON is consistent with Comet Shoemaker-Levy 9's bulk tensile strength of <6.5 Pa (Asphaug and Benz, 1996); Comet Brooks 2's bulk tensile strength of <2 Pa (Sekanina and Yeomans, 1985); within an order of magnitude of Comet Wild 2's shear strength of >17 Pa (Melosh, 2011); and Comet Churyumov–Gerasimenko's cohesive strength of ~2–16 Pa (Bowling et al., 2014), and tensile strength of <20 Pa (Thomas et al., 2015). Thus, if Comet ISON is representative of thermally unprocessed comets, then the low bulk strength of comets is a primordial property that is unaltered by thermal processing.

We consider other strength estimates of comets, and note that they are not applicable to our mechanism. The 1–10 kPa effective target strength of Comet 9P/Tempel 1 from the Deep Impact experiment (Richardson and Melosh, 2013) is a measurement of dynamic strength (which does not adhere to the weakest link model of material failure). Therefore, we expect this estimate to be several orders of magnitude larger than a measurement of static strength, which is applicable to our disruption mechanism. Comet Hyakutake's tensile strength was estimated to be ~100 Pa from the strength required to hold the comet together from rotational fragmentation (Lisse et al., 1999). However, this estimate assumed a bulk density for Comet Hyakutake of 100 kg m^{-3}, which is now known to be unreasonably low: a more typical cometary density of 270 kg m^{-3} or greater allows the nucleus to be held together by gravity alone. Indeed the known rotation rates of JFCs and Kuiper Belt Objects are consistent with effectively strengthless bodies with densities less than 600 kg m^{-3} (Snodgrass et al., 2006) in a manner analogous to the asteroid rubble pile "spin barrier" (Pravec et al., 2006).

All of these upper bounds of comet strength require that the nucleus structurally fail in some way. Thus, these strength estimates may be biased toward weaker nuclei, which would structurally fail more easily. Indeed, many comets survive perihelion passage despite having orbits that take them to smaller heliocentric distances than those corresponding to Comet ISON's fragmentation events (Bortle, 1991), consistent with stronger nuclei. If comets are effectively rubble piles held together by van der Waal's forces, then they may possess strengths similar to rubble pile asteroids of ~25 Pa (Sánchez and Scheeres, 2014). Such strengths would allow comet nuclei to survive the differential stresses induced by H_2O sublimation to within 20 $R_\odot$ (0.1 AU) of the Sun. Thus, the survival/non-survival of near-Sun comets is consistent with different comet nuclei having strengths that span more than an order of magnitude.

Additionally, short-period comets with small perihelia (when compared to where ISON fragmented) may survive multiple orbits as a result of their unique dynamical and thermophysical evolution. Jupiter Family Comets like 2P/Encke and 96P/Machholz originate in the Kuiper Belt and Scattered Disk until an encounter with Neptune sends them into the Outer Planet region of the Solar System, where they are reclassified as Centaurs (Duncan et al., 2004). Typically, an encounter with Jupiter after a few million years (the dynamical lifetime of a Centaur) either ejects the object from the Solar System or sends it into the Jupiter Family of comets (Duncan et al., 2004). During this inward migration process, a Jupiter Family Comet is also undergoing thermophysical evolution. As its orbit evolves ever closer the Sun, the comet loses volatile ices through sublimation, which may result in the build up of a lag deposit (or dust mantle) on its surface. These deposits are very good insulators (Gulkis et al., 2015; Davidsson et al., 2013; Groussin et al., 2013; Lisse et al., 2005; Lamy et al., 2008), and even a thin coating would restrict volatile sublimation to a small fraction of the surface. Therefore, when this inhibited sublimation activity is averaged over the surface, we expect JFCs to experience significantly lower sublimation pressures than the pristine icy surfaces that we have modeled in this work. Thus, the survival of JFCs with small perihelia is consistent with our work, even without allowing for larger material strengths.

5. Conclusions

We have shown that existing mechanisms of comet disruption have difficulty explaining Comet ISON's fragmentation. We proposed a new mechanism of comet disruption in which sublimating gases exert a dynamic pressure on the sunward hemisphere of a nucleus and induce differential stresses within the nucleus, which may fracture and fragment the nucleus if they exceed its material strength. Using a versatile thermodynamic model of volatile sublimation, we find Comet ISON has a material strength similar to JFCs. For the case that the nucleus of Comet ISON has a bond albedo of 0, we estimate its bulk unconfined crushing strength to be 0.5 Pa, and the bulk unconfined crushing strength of resulting fragments at 1–9 Pa. If Comet ISON's nucleus has a bond albedo of 0.5, then these strength estimates drop to 0.2 Pa for the intact nucleus and 0.6–4 Pa for its fragments.

Acknowledgments

This research project was internally funded through the startup funds of H. Jay Melosh (Purdue University). We thank Nalin Samarasinha and an anonymous referee for helpful comments.

References

Alkire, B.D., Andersland, O.B., 1973. The effect of confining pressure on the mechanical properties of sand–ice materials. J. Glaciol. 12 (66), 469–481.
Asphaug, E., Benz, W., 1996. Size, density, and structure of Comet Shoemaker-Levy 9 inferred from the physics of tidal breakup. Icarus 121, 225–248.
Bar-Nun, A. et al., 2013. Gas trapping in ice and its release upon warming. In: Gudipati, M.S., Castillo-Rogez, J. (Eds.), The Science of Solar System Ices. Springer Publishing, New York, pp. 487–499.
Bockelée-Morvan, D. et al., 2004. The composition of cometary volatiles. In: Festou, M.C., Keller, H.U., Weaver, H.A. (Eds.), Comets II. University of Arizona Press, Tucson, pp. 391–423.
Bodewits, D., Farnham, T., A'Hearn, M.F., 2013. Central Bureau Electronic Telegrams (CBET), 3718.
Boehnhardt, H. et al., 2013. Central Bureau Electronic Telegrams (CBET), 3715.
Borovička, J. et al., 2013. The trajectory, structure and origin of the Chelyabinsk asteroidal impactor. Nature 503, 235–237.
Bortle, J.E., 1991. Post-perihelion Survival of Comets with Small q. Int. Comet Quart. 13, 89–91.
Bowling, T.B. et al., 2014. The strength of Comet 67P/Churyumov–Gerasimenko. American Astronomical Society, Division of Planetary Science Meeting #46. Abstract #100.03.
Brace, W.F., 1961. Dependence of fracture strength of rocks on grain size. Penn State Univ. Miner. Expt. State Bull. 76, 99–103.
Brown, J.C. et al., 2011. Mass loss, destruction and detection of Sun-grazing and –Impacting cometary nuclei. Astron. Astrophys. 535, 71–82.
Capaccioni, F. et al., 2015. The organic-rich surface of Comet 67P/Churyumov–Gerasimenko as seen by VIRTIS/Rosetta. Science 347. http://dx.doi.org/10.1126/science.aaa0628.
Combi, M.R. et al., 2014. Unusual water production activity of Comet C/2012 S1 (ISON): Outbursts and continuous fragmentation. Astrophys. J. 788, L7–L11.
Cowan, J.J., A'Hearn, M.F., 1979. Vaporization of comet nuclei: Light curves and life times. Moon Planets 21, 155–171.
Davidsson, B.J.R. et al., 2013. Thermal inertia and surface roughness of Comet 9P/Tempel 1. Icarus 224, 154–171.
Delamere, W.A. et al., 2013. Central Bureau Electronic Telegrams, 3720.
Delsemme, A.H., Swings, P., 1952. Hydrates de gaz dans les noyaux cométaires et les grains interstellaires. Ann. Astrophys. 15 (1), 1–6.
Drahus, M., 2014. Rotational disruption of comets with parabolic orbits. AAS/Division for Planetary Sciences Meeting. Abstracts 46, #200.04.
Duncan, M., Levison, H., Dones, L., 2004. Dynamical evolution of ecliptic comets. In: Festou, M.C., Keller, H.U., Weaver, H.A. (Eds.), Comets II. The University of Arizona Press, Tucson, pp. 193–204.
Feaga, L.M. et al., 2007. Asymmetries in the distribution of H_2O and CO_2 in the inner coma of Comet 9P/Tempel 1 as observed by Deep Impact. Icarus 190, 345–356.
Feistel, R., Wagner, W., 2007. Sublimation pressure and sublimation enthalpy of H_2O ice Ih between 0 and 273.16 K. Geochim. Cosmochim. Acta 71, 36–45.
Gombosi, T.I., 1994. Free molecular aerodynamics. In: Gaskinetic Theory, first ed. Cambridge University Press, Cambridge, UK.
Groussin, O. et al., 2013. The temperature, thermal inertia, roughness and color of the nuclei of Comets 103P/Hartley 2 and 9P/Tempel 1. Icarus 222, 580–594.
Gulkis, S. et al., 2015. Subsurface properties and early activity of Comet 67P/Churyumov–Gerasimenko. Science 347. http://dx.doi.org/10.1126/science.aaa0709.
Gundlach, B., Skorov, Y.V., Blum, J., 2011. Outgassing of icy bodies in the Solar System – I. The sublimation of hexagonal water ice through dust layers. Icarus 213, 710–719.
Gundlach, B. et al., 2012. A note on the survival of the sungrazing Comet C/2012 W3 (Lovejoy) within the Roche limit. Earth Planet. Astrophys. Available from: arXiv: 1203.1808.
Knight, M.M., Battams, K., 2014. Preliminary analysis of SOHO/STEREO observations of sungrazing Comet ISON (C/2012 S1) around perihelion. Astrophys. J. 782, L37–L41.
Knight, M.M., Schleicher, D.G., 2015. Observations of Comet ISON (C/2012 S1) from Lowell Observatory. Astron. J. 149, 19. http://dx.doi.org/10.1088/0004-6256/149/1/19 (15 pp).
Knight, M.M., Walsh, K.J., 2013. Will Comet ISON (C/2012 S1) survive perihelion? Astrophys. J. 776, L5–L9.
Lamy, P.L. et al., 2008. Spitzer Space Telescope observations of the nucleus of Comet 67P/Churyumov–Gerasimenko. Astron. Astrophys. 489, 777–785.
Lamy, P.L., Toth, I., Weaver, H.A., 2014. Hubble Space Telescope observations of the nucleus of Comet C/2012 S1 (ISON). Astrophys. J. 794, L9–L14.
Langmuir, I., 1913. The vapor pressure of metallic tungsten. Phys. Rev. II (5), 329–342.
Lawn, B.R., Wilshaw, T.R., 1975. Fracture of Brittle Solids. Cambridge University Press, Cambridge, UK.
Li, J.-Y. et al., 2013a. Photometric properties of the nucleus of Comet 9P/Tempel1 from Stardust-NExT flyby and the implications. Icarus 222, 467–476.
Li, J.-Y. et al., 2013b. Photometric properties of the nucleus of Comet 103P/Hartley 2. Icarus 222, 559–570.
Li, J.-Y. et al., 2013c. Characterizing the dust coma of Comet C/2012 S1 (ISON) at 4.15 AU from the Sun. Astrophys. J. 779, L3–L7.
Lisse, C.M. et al., 1999. The nucleus of Comet Hyakutake (C/1996 B2). Icarus 140, 189–204.
Lisse, C.M. et al., 2005. Rotationally resolved 8–35 micron Spitzer Space Telescope observations of the nucleus of Comet 9P/Tempel 1. Astrophys. J. 625, L139–L142.
Lisse, C. et al., 2013. Cometary ices. In: Gudipati, M.S., Castillo-Rogez, J. (Eds.), The Science of Solar System Ices. Springer Publishing, New York, pp. 455–485.
Marsden, B.G., Sekanina, Z., Yeomans, D.K., 1973. Comets and nongravitational forces. V. Astron. J. 78 (2), 211–225.
Mastrapa, R.M.E., Grundy, W.M., Gudipati, 2013. Amorphous and crystalline H_2O-ice. In: Gudipati, M.S., Castillo-Rogez, J. (Eds.), The Science of Solar System Ices. Springer Publishing, New York, pp. 371–408.
McKay, A. et al., 2014. Evolution of fragment-species production in Comet C/2012 S1 (ISON) from 1.6 au to 0.4 au. Asteroids Comets Meteors 365.
Melosh, H.J., 2011. Slopes and mass movement. In: Planetary Surface Processes, first ed. Cambridge University Press, Cambridge, UK.
Nagahara, H., Kushiro, I., Mysen, B.O., 1994. Evaporation of olivine: Low pressure phase relations of the olivine system and its implication for the origin of chondritic components in the solar nebula. Geochim. Cosmochim. Acta 58 (8), 1951–1963.
Opitom, C. et al., 2013a. Central Bureau Electronic Telegrams (CBET), 3693.
Opitom, C. et al., 2013b. Central Bureau Electronic Telegrams (CBET), 3711.
Opitom, C. et al., 2013c. Central Bureau Electronic Telegrams (CBET), 3719.
Pravec, P. et al., 2006. Photometric survey of binary near-Earth asteroids. Icarus 181, 63–93.
Price, N.J., 1968. In: Rhodes, F.H.T. (Ed.), Fault and Joint Development in Brittle and Semi Brittle Rock. Pergamon Press, Oxford, UK (1 reprint).
Richardson, J.E., Bowling, T.J., 2014. Investigating the combined effects of shape, density, and rotation on small body surface slopes and erosion rates. Icarus 234, 53–65.
Richardson, J.E., Melosh, H.J., 2013. An examination of the Deep Impact collision site on Comet Tempel 1 via Stardust-NExT: Placing further constraints on cometary surface properties. Icarus 222, 492–501.
Samarasinha, N.H., 2001. A model for the breakup of Comet LINEAR (C/1999 S4). Icarus 154, 540–544.
Samarasinha, N.H., Mueller, B.E.A., 2013. Relating changes in cometary rotation to activity: Current status and applications to Comet C/2012 S1 (ISON). Astrophys. J. 775, L10–L15.
Sánchez, P., Scheeres, D.J., 2014. The strength of regolith and rubble pile asteroids. Meteorit. Planet Sci. 49 (5), 788–811.
Sekanina, Z., 1992. Sublimation rates of carbon monoxide at carbon dioxide from comets at large heliocentric distances. Asteroids Comets Meteors 1991, 545–548.
Sekanina, Z., 2003. Erosion model for the sungrazing comets observed with the Solar and Heliospheric Observatory. Astrophys. J. 597, 1237–1265.
Sekanina, Z., Yeomans, D.K., 1985. Orbital motion, nucleus precession, and splitting of periodic Comet Brooks 2. Astron. J. 90, 2335–2352.
Snodgrass, C., Lowry, S.C., Fitzsimmons, A., 2006. Photometry of cometary nuclei: rotation rates, colours, and a comparison with Kuiper Belt Objects. Mon. Not. Roy. Astron. Soc. 373, 1590–1602.
Steckloff, J.K. et al., 2015. The size and fragmentation of the nucleus of Comet C/2012 S1 (ISON). Lunar Planet. Sci. XLVI. Abstract #2723.
Thomas, N. et al., 2015. The morphological diversity of Comet 67P/Churyumov–Gerasimenko. Science 347. http://dx.doi.org/10.1126/science.aaa0440.
Ververka, J. et al., 2013. Return to Comet Tempel 1: Overview of Stardust-NExT results. Icarus 222, 424–435.
Weaver, H. et al., 2014. Ultraviolet spectroscopy of Comet ISON (2012 S1). Asteroids Comets Meteors, 604.
Whipple, F.L., 1950. A comet model. I. The acceleration of Comet Encke. Astrophys. J. 111, 375–394.

Icarus 264 (2016) 160–171

Contents lists available at ScienceDirect

Icarus

journal homepage: www.journals.elsevier.com/icarus

The formation of striae within cometary dust tails by a sublimation-driven YORP-like effect

Jordan K. Steckloff [a,*], Seth A. Jacobson [b,c]

[a] Purdue University, Department of Physics and Astronomy, 525 Northwestern Avenue, West Lafayette, IN 47907, United States
[b] Observatoire de la Côte d'Azur, Laboratoire Lagrange, CS 34429, 06304 Nice Cedex 4, France
[c] Universtät Bayreuth, Bayerisches Geoinstitut, 95440 Bayreuth, Germany

ARTICLE INFO

Article history:
Received 3 April 2015
Revised 11 September 2015
Accepted 11 September 2015
Available online 25 September 2015

Keywords:
Comets
Comets, dust
Comets, dynamics
Comets, nucleus

ABSTRACT

Sublimating gas molecules scatter off of the surface of an icy body in the same manner as photons (Lambertian Scattering). This means that for every photon-driven body force, there should be a sublimation-driven analog that affects icy bodies. Thermal photons emitted from the surfaces of asymmetrically shaped bodies in the Solar System generate net torques that change the spin rates of these bodies over time. The long-term averaging of this torque is called the YORP effect. Here we propose a sublimation-driven analog to the YORP effect (Sublimation-YORP or SYORP), in which sublimating gas molecules emitted from the surfaces of icy bodies in the Solar System also generate net torques on the bodies. However, sublimating gas molecules carry $\sim 10^4$–10^5 times more momentum away from the body than thermal photons, resulting in much greater body torques. Previous studies of sublimative torques focused on emissions from highly localized sources on the surfaces of Jupiter Family Comet nuclei, and have therefore required extensive empirical observations to predict the resulting behavior of the body. By contrast, SYORP applies to non-localized emissions across the entire body, which likely dominates sublimation-drive torques on small icy chunks and dynamically young comets outside the Jupiter Family, and can therefore be applied without high-resolution spacecraft observations of their surfaces. Instead, we repurpose the well-tested mathematical machinery of the YORP effect to account for sublimation-driven torques. We show how an SYORP-driven mechanism best matches observations of the rarely observed, Sun-oriented linear features (striae) in the tails of comets, whose formation mechanism has remained enigmatic for decades. The SYORP effect naturally explains why striae tend to be observed between near-perihelion and ~1 AU from the Sun for comets with perihelia less than 0.6 AU, and solves longstanding problems with moving enough material into the cometary tail to form visible striae. We show that the SYORP mechanism can form striae that match the striae of Comet West, estimate the sizes of the stria-forming chunks, and produce a power-law fit to these parent chunks with a power law index of $-1.4^{+0.3}_{-0.6}$. Lastly, we predict potential observables of this SYORP mechanism, which may appear as clouds or material that appear immediately prior to stria formation, or as a faint, wispy dust feature within the dust tail, between the nucleus and the striae.

1. Introduction

Linear features sometimes form within the dust tails of "great comets" from the Oort Cloud such as Comet West (C/1975 V1) (Sekanina and Farrell, 1978, 1980), Comet Hale-Bopp (C/1995 O1) (Pittichová et al., 1997), Comet McNaught (C/2006 P1), and Comet PANSTARRS (C/2011 L4) (Jones and Battams, 2014). These features are generally aligned with either the nucleus of the comet (synchrones) or with the Sun (striae) (e.g. Comet McNaught [C/2006 P1] in Fig. 1). Synchrones are believed to form from ~1 to 100 μm dust released nearly simultaneously or diurnally from active areas of the comet's surface, which drifts away from the nucleus due to solar radiation pressure (Kharchuk and Korsun, 2010). In contrast, the mechanism that creates striae is poorly understood.

Sekanina and Farrell (1980) observed that "striae seem to fit synchronic formations whose sources of emission are located in the area of the dust tail rather than in the nucleus," and postulated three conditions that need to be met by the "parent" materials that form a stria: (1) these materials must be ejected simultaneously from the nucleus; (2) they must experience identical repulsive accelerations from the Sun and (3) these parent objects must break

* Corresponding author.

http://dx.doi.org/10.1016/j.icarus.2015.09.021
0019-1035/

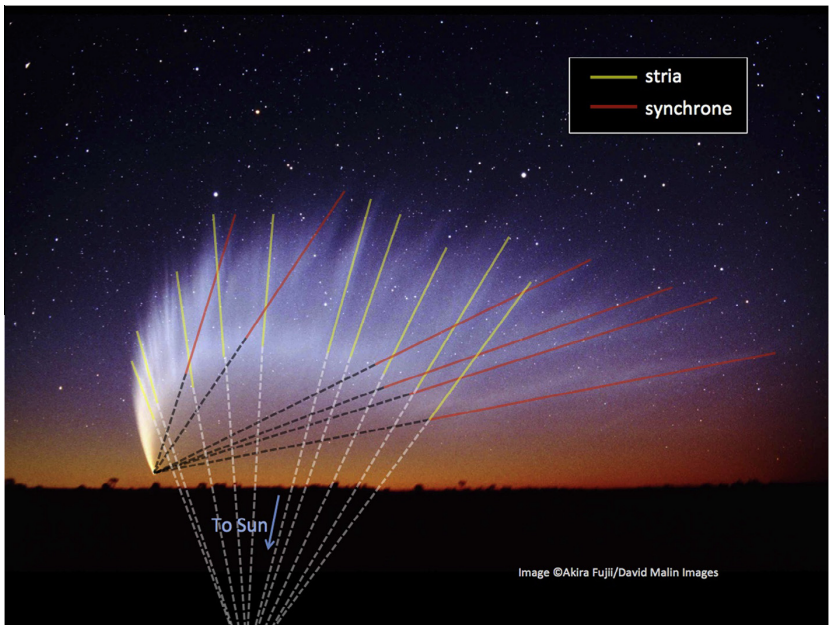

Fig. 1. *Illustrating Stria and Synchrones.* An image of Comet McNaught (C/2006 P1) shows long linear structures within the tail of the comet. We have overlain lines to highlight the linear features in the cometary tail. Note how these features line up with either the head of the comet (synchrones) or with the Sun (striae). Image ©Akira Fujii/David Malin Images reproduced with permission, with annotations and markings added by authors.

up and disperse simultaneously (listed at the beginning of Section 2 in Sekanina and Farrell, 1980). Some proposed mechanisms assume that (3) occurs as a single, short-lived event (Sekanina and Farrell, 1980; Froehlich and Notni, 1988), while other mechanisms model (3) as a relatively long-lived fragmentation cascade (Nishioka, 1998; Jones and Battams, 2014). Regardless of the exact details of (3), these three conditions ensure that the pre-stria materials arrive at the source location of a stria as a single unit, where the parent materials are then transformed into a daughter fragment size distribution that creates the narrow lineaments oriented towards the Sun via anti-sunward acceleration.

2. Radiation pressure

Sekanina and Farrell (1980) and subsequent authors (e.g. Froehlich and Notni, 1988; Pittichová et al., 1997) considered that solar radiation pressure was solely responsible for the parent materials' repulsive acceleration (second condition above). Sunlight, like gravity, obeys an inverse square law and solar radiation pressure is oriented antiparallel to the solar gravitational acceleration force (to leading order). Thus, its strength can be parameterized by the dimensionless constant β, which is the ratio of the force of solar radiation pressure to the solar gravitational force acting upon a particular object. Since the force of gravity depends on an objects volume ($\sim R^3$) while force of radiation depends on an objects surface area ($\sim R^2$), β is a size-dependent parameter. For Comet West, the β parameter for the parent materials released from the nucleus was estimated at $\beta_p = 0.55–1.10$, while the β parameter for the dust fragments within the striae was $\beta_f = 0.6–2.7$ (Sekanina and Farrell, 1980). Such high beta parameters require that both parent and daughter grains be small (∼0.1 μm), such that a small parent grain is most likely capable of creating only ∼10 daughter grains (Sekanina and Farrell, 1980). Alternatively, the parent grains could be extremely elongated such that they have a Sun-facing cross-section of a ∼0.1 μm grain (Sekanina and Farrell, 1980). Since Comet West's striae are estimated to contain $\sim 10^6$ kg of material (Sekanina and Farrell, 1980), such extreme elongation is unlikely, and more recent research has focused instead on exploring mechanisms that allow a swarm of small-sized parent grains to travel together.

Froehlich and Notni (1988) propose that such a swarm could travel away from the nucleus in a coherent, optically thick parcel of grains with a narrow range of β-values. The breadth of this range depends on the swarm's optical thickness (with optically thin swarms incapable of remaining together), with β values above this range receiving enough illumination to surge ahead and leave the swarm, while grains with β values below this range lag behind the coherent swarm. Froehlich and Notni (1988) propose that swarms on the order of ∼1000 km across become optically thin in the cometary tail and disperse, forming striae. However, to maintain an optically thick swarm the grains must not have any significant transverse velocity (motion perpendicular to the direction of solar gravity/radiation pressure), a condition that is thermodynamically very unlikely without a mechanism for laterally confining the dust.

Neither of these proposed mechanisms is satisfactory. Meeting Sekanina and Farrell's (1980) second condition with radiation pressure requires small parent grains, but then it is difficult to meet the third condition while creating a large enough mass of daughter grains. If an alternative to radiation pressure can be found, then these issues may disappear.

Lastly, observations show that comets with perihelia <6 AU form striae between near-perihelion and ∼1 AU of the Sun (Pittichová et al., 1997), which suggests that the mechanism driving stria formation must turn off beyond ∼1 AU and somehow prevent the formation of observable striae until after the comet has approached the near-perihelion part of its orbit. Since the intensity of solar irradiation decreases smoothly as the inverse-square of heliocentric distance, there is no heliocentric distance at which the solar radiation pressure drops off precipitously. Therefore, if solar radiation pressure drives stria formation, then striae should

form at all heliocentric distances, with differences in solar radiation pressure manifesting itself as an increase in the duration of the stria formation process with increasing heliocentric distance.

3. Sublimation-driven stria formation model

In this paper, we propose a sublimation-driven stria formation mechanism that allows for relatively large, volatile-rich chunks of ejected cometary materials to drift into the cometary dust tail and fragment quickly into fine dust, forming cometary dust tail striae. This mechanism also naturally restricts the formation of observable stria until the comet reaches the near- or post-perihelion portion of its orbit and is inactive beyond ~1 AU. We show, through careful consideration of the timescale of stria formation, that this mechanism is consistent with the observed striae of Comet West.

The sublimation of volatile ices is enough to both accelerate the parent chunk anti-sunward relative to the cometary nucleus and spin up the parent chunk to fragmentation (i.e. rotational fission.) Because the sublimation pressure exerted on the illuminated hemisphere of a volatile rich body is many orders of magnitude greater than radiation pressure, this mechanism is able to affect chunks that are many orders of magnitude larger than previous radiation pressure-driven only mechanisms. We envision that the formation of a stria occurs in five steps (see Fig. 2): (1) a parent chunk is released from the nucleus of a comet, (2) sublimation pressure causes the parent chunk to drift anti-sunward relative to the nucleus while simultaneously increasing its spin rate, (3) parent chunk spins up to the point of fission, (4) the resulting daughter chunks repeat steps 2 and 3 at an ever-increasing rate, resulting in a fragmentation cascade that (5) stops when the materials become small (micron-sized grains) and devolatilized, at which point radiation pressure dominates the behavior of grains which stream out to form a stria.

Previous studies of the effects of the reactive torques due to sublimating gas on the rotation state of cometary nuclei have focused on the reactive torques from jets either observed or inferred on the surface (e.g. Wilhelm, 1987; Peale and Lissauer, 1989; Julian, 1990; Samarasinha and Belton, 1995; Neishtadt et al., 2002, 2003; Gutiárrez et al., 2003; Sidorenko et al., 2008). These jets may be the dominant rotation state torques for large cometary nuclei (Meech et al., 2011; Belton et al., 2011; Chesley et al., 2013), but the relatively small cometary chunks discussed below are assumed to not possess the ability to create jets (Belton, 2010, 2013; Bruck Syal et al., 2013), although jet production is itself poorly understood. In this work, we propose that it is the background sublimation that torques the cometary chunk. This sublimation is nearly isotropic in the sense that it is emitted from every heated surface element but is very sensitive to the shape and illumination of the chunk. A similar model for an entire comet nuclei has been considered in the past, but it was preliminary (Szegö et al., 2001), considered only an ellipsoidal shape (Mysen, 2004, 2007), or focused on matching different observational phenomena (Rodionov et al., 2002; Gutiárrez and Davidsson, 2007).

3.1. Step 1: Parent chunks leave comet

We propose that a single ejected (parent) chunk contains all of the material that later becomes a stria. Sekanina and Farrell (1980) illustrated a method of obtaining an order of magnitude estimate of the volume of a stria for Comet West. Assuming that the dust of a stria has a typical Jupiter Family Comet (JFC) albedo of ~0.03 (Hammel et al., 1987; Brownlee et al., 2004; Lamy et al., 2004; Oberst et al., 2004; Li et al., 2007, 2013a; Sierks et al., 2015), is comprised of ~0.1–1 μm particles (Green et al., 2004), and that it originated from an initial parent chunk that was half water ice (McDonnell et al., 1987), then we expect the initial parent chunks to have radii on the order of ~10–100 m. We assume that these parent chunks have a density of ~400 kg/m^3, which is typical of JFCs (Sierks et al., 2015; Thomas et al., 2013; Richardson et al., 2007).

Such house- or building-sized (~10–100 m) chunks of material have been observed in the debris of Comets 57P/du Toit-Neujmin-Delporte (Fernández, 2009), 73P/Schwassmann-Wachmann 3 (Fuse et al., 2007; Reach et al., 2009), and C/1999 S4 (LINEAR) (Weaver et al., 2001); were observed within the coma of 17P/Holmes following its massive 2007 outburst (Stevenson et al., 2010); and was possibly detected by the *Giotto* spacecraft within a few hundred kilometer of Comet 26P/Grigg-Skjellerup's nucleus (McBride et al., 1997). Most applicably, Comet C/1996 B2 (Hyakutake) ejected ~10–100 m chunks, which drifted antisunward relative to the nucleus via sublimation pressure (Desvoivres et al., 2000; Schleicher and Woodney, 2003).

The frequency of striae is likewise consistent with the frequency of ejected ~10–100 m chunks. While a direct measurement of this frequency is difficult due to observational limitations, it is expected to be intermediate to the frequencies of ejection of larger and smaller chunks. Centaur Comet 174P/Echeclus ejected a fragment a few kilometers in size (Rousselot, 2008), the only known ejection of such a large fragment. Meanwhile, high-resolution images from spacecraft have revealed that ~1/3 of Jupiter Family Comets (JFCs) eject a large number of decimeter to meter scale chunks into their inner comae at speeds near their escape velocities (~1 m/s) (Hermalyn et al., 2013; Rotundi et al., 2015). Because striae occur more frequently than the ejection of kilometer-scale fragments yet less frequently than the detection of decimeter to meter scale chunks, it is reasonable that the parent bodies that form them are likewise intermediate in size (~10–100 m).

While we do not propose a model for the ejection of these suggested house-sized parent chunks from the nuclei of striated comets, we speculate that perhaps cometary outbursts (Pittichová et al., 1997; Rousselot, 2008) or supervolatile-driven activity may be responsible for launching these parent chunks at greater than escape velocity. Such activity would eject parent chunks with a distribution of initial velocities, and the Rosetta spacecraft observed indirect evidence for the ejection of ~10–100 m chunks from the surface of Comet 67P/Churyumov-Gerasimenko at less than escape velocity that later reimpacted its surface (Thomas et al., 2015). We assume that these parent chunks are rich in water ice throughout, including near the surface of the chunk (relative to the thermal skin depth). If this is not the case, then sublimation pressure will not be able to drive the chunk away from the nucleus (see Section 3.2), due to the inability of the ices to respond to the parent chunk's diurnal thermal cycle.

3.2. Step 2: Sublimation pressure instead of radiation pressure

We propose that the reaction force (or equivalently, the sublimative momentum flux) on a volatile-rich parent chunk from the ejection of sublimating gas molecules is enough to both accelerate the parent chunk anti-sunward relative to the cometary nucleus (discussed below) and spin up the parent chunk to fragmentation (discussed in Section 3.4). Sublimating gasses exert an anti-sunward acceleration on volatile-rich cometary material (Whipple, 1950; Marsden et al., 1973; Steckloff et al., 2015a). Near the Sun, the magnitude of this acceleration behaves similarly to radiation pressure, since it approximates the same inverse square law. Thus, it provides the repulsive acceleration necessary to form striae. However, since the sublimation pressure for H_2O ice is up to 4–5 orders of magnitude stronger than radiation pressure, it can transport chunks of material into the cometary tail that are 4–5

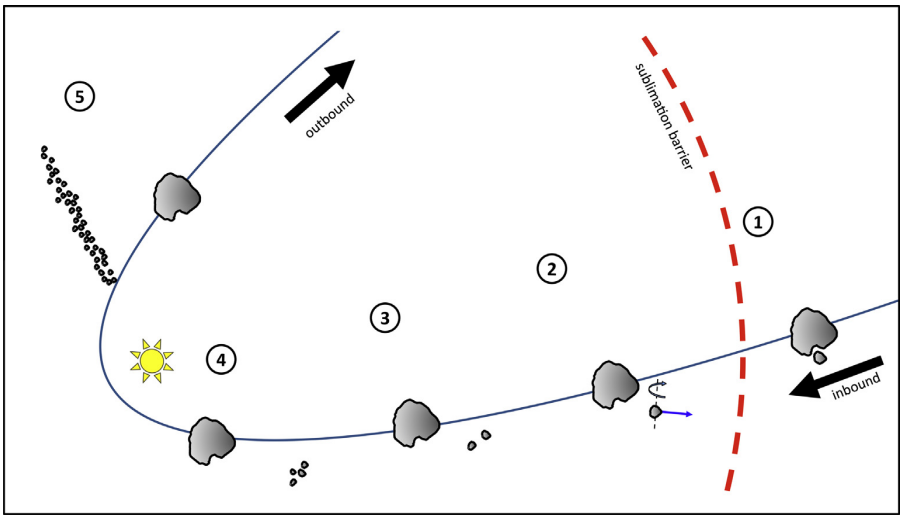

Fig. 2. *A Cartoon of SYORP-induced Stria Formation.* The five steps of stria formation are illustrated above including (1) parent chunk release, (2) sublimation-driven anti-sunward drift and rotational acceleration, (3) rotational fission, (4) fragmentation cascade, and (5) transition from sublimation to radiation pressure domination of anti-sunward drift. After step 5, the stream of small micron-sized chunks appears observationally as a stria.

orders of magnitude larger in radius than those transported by radiation pressure alone for a given acceleration of the material relative to the nucleus.

We model parent chunks as balls of pure H_2O ice with such low albedos, that they effectively absorb all incident solar radiation, similar to Steckloff et al. (2015a). We note that these assumptions certainly do no accurately describe the real composition and structure of the parent chunks, which are likely complicated agglomerates of ices and refractory materials with albedos of only a few percent. However, these assumptions illustrate the conditions under which sublimation pressure is maximized, and therefore, define the upper bound of the sublimation pressure acting upon parent chunks. Assuming that the subliming gas is in thermal equilibrium with its source ice and that all incident solar radiation is either re-radiated to space or applied toward overcoming the ice's latent heat of sublimation (Whipple, 1950), Steckloff et al. (2015a) show that the sublimation pressure acting on a surface element of cometary material is determined by the following two equations

$$(1-A)\frac{L_{solar}}{4\pi r_h^2 \lambda}\cos\phi = \alpha_{(T)}\sqrt{\frac{m_{mol}}{2\pi RT}}P_{ref}e^{\frac{\lambda}{R}\left(\frac{1}{T_{ref}}-\frac{1}{T}\right)} \quad (1)$$

$$P_{sub(r_h,\phi)} = \frac{2}{3}(1-A)\frac{L_{solar}}{4\pi r_h^2 \lambda}\sqrt{\frac{8RT}{\pi m_{mol}}}\cos\phi \quad (2)$$

where A is the bond albedo of the material, $\alpha_{(T)}$ is the temperature-dependent sublimation coefficient of the volatile species, L_{solar} is the Sun's luminosity, r_{helio} is the heliocentric distance of the object, λ is the ice's latent heat of sublimation, ϕ is the solar phase of the element of surface relative to the subsolar point, m_{mol} is the molar mass of the ice species, R is the ideal gas constant, T is the temperature of the sublimating gas (assumed to be in thermal equilibrium with its source ice), and P_{ref} is an experimentally determined vapor pressure at temperature T_{ref}. Since Eq. (1) is transcendental, we solve for temperature (T) numerically, then insert it into Eq. (2) to determine the sublimation pressure of a given surface area element. This formulation assumes that the coma around the volatile-rich body is optically thin (Steckloff et al., 2015a, 2015b), which is valid for heliocentric distances greater than ~0.05 AU for cometary bodies up to ~1 km (Drahus, 2014). This method of computing sublimation pressures provides similar results to previous methods of computing sublimative forces on comet nuclei (e.g. Whipple, 1950; Marsden et al., 1973; Sekanina, 2003), but is instead based on the theoretical (rather than empirical) relationship between vapor pressure and temperature, and is therefore useful for volatile species for which limited empirical data exists (Steckloff et al., 2015a). We plot this dynamic sublimation pressure at the subsolar point in Fig. 3. To compute the net force acting upon a volatile-rich object, we integrate Eq. (2) over the surface of the object.

Once a parent chunk is broken up into small grains and devolatilized, following the remaining steps detailed below, radiation pressure dominates the non-gravitational behavior of the grains. At this point, radiation pressure streams the chunks into a long lineament as in Sekanina and Farrell (1980), creating the observed striae. However, sublimation pressure is responsible for moving the bulk mass of stria material to the location of stria formation.

3.3. Step 2 continued: Rotational acceleration due to a sublimation-driven YORP-like effect (SYORP)

The back-reaction from anisotropic volatile emission rotationally accelerates striae parent chunks. As a gas molecule escapes from the surface of a parent chunk, it transports angular momentum relative to the center of mass of the parent chunk. The sum of the individual torques from each gas molecule sublimating off of the parent chunk creates a net rotational acceleration of the nucleus (unless that comet possesses perfect symmetry). Thus, in addition to changing the linear motion of a chunk's center of mass, diurnal sublimation can also change a chunk's rotation about its center of mass. We assess the strength of this angular acceleration by analogizing this effect to the well-studied YORP effect (Rubincam, 2000; Bottke et al., 2002; Vokrouhlicky and Capek, 2002; Capek and Vokrouhlicky, 2004; Scheeres, 2007; Rozitis and Green, 2013).

Gas molecules sublimate near the surface of a parent chunk and diffuse through its porous structure, where the gas mean free path is significantly larger than the pores of the cometary material. Eventually these molecules reach the surface, where the last scattering of each gas molecule can be treated independently and the gas emission profile is Lambertian (the probability of being ejected

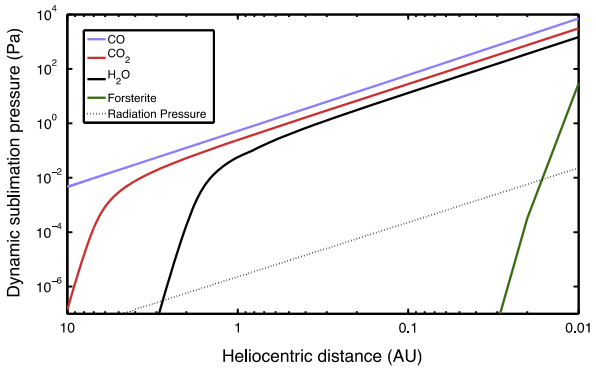

Fig. 3. *Peak Sublimation Pressure as a Function of Heliocentric Distance.* We adopted Fig. 4 from Steckloff et al. (2015a) to show the variation in peak sublimation pressure for an assumed albedo of 0 as a function of heliocentric distance for common cometary volatile species (H_2O, CO_2, and CO) and the mineral Forsterite, which was found in the coma of Comet Wild 2 (Zolensky et al., 2006). For the formation of striae, we focus on the H_2O sublimation curve, as we are positing that H_2O sublimation is responsible for stria formation. Clearly visible is the point (~1 AU) beyond which the sublimation pressure drops off much more quickly. Strength of radiation pressure is added for reference.

in any given direction is proportional to the cosine of the angle made between that direction and a vector normal to the local surface of the parent chunk [pp. 227–230 in Gombosi, 1994]). Since gas molecules and photons are emitted in a nearly identical fashion, we are able to utilize the theory developed for the photon-driven YORP effect to quantify these sublimation-driven torques.

3.3.1. The YORP effect

Since the numerous instantaneous torques acting on a body are infinitesimal in duration and may be oriented in opposing directions, the YORP effect is a time-averaged phenomenon. The secular rotational acceleration rate due to the YORP effect for an object of radius R and density ρ is (Scheeres, 2007):

$$\frac{d\omega}{dt} = \left(\frac{G_1}{a_\odot^2\sqrt{1-e_\odot^2}}\right)\frac{3C_Y}{4\pi\rho R^2} \tag{3}$$

where $a_\odot$ and $e_\odot$ are the object's heliocentric semi-major axis and eccentricity, C_Y is a shape-dependent coefficient with typical values between 10^{-3} and 10^{-2} (Scheeres, 2007; Rozitis and Green, 2013), and $G_1 \approx 10^{14}$ kg km s^{-2} is related to the speed of light c and the solar constant $W_\odot$ = 1.361 kW m^{-2}, which is defined at 1 AU:

$$\frac{G_1}{(1\text{ AU})^2} = \frac{W_\odot}{c} \tag{4}$$

Note that the magnitude of the rotational acceleration scales inversely with surface area and density, and scales linearly with the absolute strength of the solar radiation pressure at the object's location and with its shape-dependent coefficient C_Y, which is defined independent of size (Scheeres, 2007). The coefficient C_Y is determined by the thermally emitted photons, since the absorbed solar radiation contributes no net torque (Rubincam and Paddack, 2010).

3.3.2. The SYORP effect

Since gas molecules carry significantly more momentum than photons, the instantaneous torques acting upon the body are much greater than for the YORP effect. We parameterize this sublimation-driven YORP (SYORP) effect by modifying the YORP effect rotational acceleration equations (Eqs. (3) and (4)). Since sublimating gas molecules behave like photons at the surface of the parent chunk, sublimation-driven angular acceleration should depend on the shape of the object in the same manner as emitted photon-driven angular acceleration. Therefore, the shape dependent coefficient for sublimation C_S should be the same as that for photons C_Y. Physically, the coefficient C_S represents the fraction of the spin and orbit averaged sublimative momentum flux that contributes a torque due to shape asymmetry. Thus we assume that $C_Y \approx C_S$ for the purposes of our order of magnitude considerations, and should have a value that lies in the range 10^{-3}–10^{-2} based on asteroid shapes (Scheeres, 2007; Rozitis and Green, 2013), which should be representative of the shapes of cometary nuclei to first order. This is consistent with recent work that implies the values of C_S for cometary nuclei may lie within a small range of values (Samarasinha and Mueller, 2013).

The absolute strength of the gas sublimation pressure P_S is very different than thermal emission pressure

$$P_Y = G_1/a_\odot^2\sqrt{1-e_\odot^2}. \tag{5}$$

We parameterize this difference with a quantity γ, which is the ratio of the sublimation pressure to the radiation pressure:

$$\gamma = P_S/P_Y \tag{6}$$

The angular acceleration associated with SYORP is directly analogous to the angular acceleration associated with YORP:

$$\frac{d\omega}{dt} = \frac{3P_SC_S}{4\pi\rho R^2} = \frac{3\gamma P_YC_Y}{4\pi\rho R^2} \tag{7}$$

where we have taken advantage of both the new parameter γ and the equivalence between the two shape factors C_S and C_Y.

Since a subliming gas molecule carries significantly more momentum than an emitted thermal photon, we might naively expect γ to be greater than one. However, if gas emission is significantly reduced relative to thermal emission, γ may be less than one. We use Eqs. (5) and (2) for the radiation P_Y and sublimation P_S pressures respectively to compute the ratio γ as a function of heliocentric distance. Near the Sun, the chunk is cooled predominantly through sublimative cooling and energy is lost primarily through overcoming a species latent heat of sublimation. Since the incident solar energy flux scales as the inverse square of heliocentric distance, the sublimative mass-loss rate and resulting sublimation pressures (and therefore gamma) scale approximately (but not exactly) as an inverse square law with heliocentric distance. Further from the Sun, however, the chunk is predominantly cooled by blackbody radiation, and the sublimative mass-loss rates fall far short of the inverse square law, resulting in a steep drop off in gamma with increasing heliocentric distance. This leads to a shape of the gamma curves in which they rise steeply with decreasing heliocentric distance until reaching an approximately constant value (see Fig. 4).

3.4. Step 3: Critical failure of the body

We define a critical rotation rate ω_{crit}, above which the centripetal acceleration required to hold the body together overcomes the tensile strength of the body, leading to fragmentation. Since these chunks survived ejection from the cometary nucleus intact, they are necessarily stronger than their parent nucleus, which typically have strengths on the order of a few Pascals (Sekanina and Yeomans, 1985; Asphaug and Benz, 1996; Melosh, 2011; Bowling et al., 2014; Steckloff et al., 2015a; Thomas et al., 2015). For these icy chunks, self-gravitational forces are dominated by even this weak strength limit (Scheeres et al., 2010). Thus gravity has a negligible effect in holding these icy parent chunks together. To estimate ω_{crit}, we approximate the icy parent chunks as rectangular prisms, where the long axis ($a = 2R$) is twice the length of the other two sides, which we assume to be equal in length ($b = c = R$). The maximum tensile force exerted along the long axis of the body due to strength is then

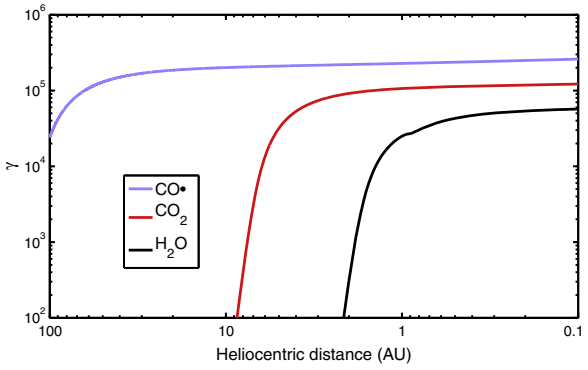

Fig. 4. *A plot of the gamma factor for various species.* Above is a plot of γ (ratio of sublimation pressure to radiation pressure) versus heliocentric distance for various volatiles. We computed these values based on a planar surface element composed purely of the respective volatile, with the Sun located at the zenith. Sublimation pressure data for all volatiles obtained from Steckloff et al. (2015a). We observe that the volatiles activate at larger heliocentric distances, building up the sublimation pressure as the sublimating object moves inward. Closer to the Sun the volatile becomes fully activated, and nearly scale with $\propto 1/r_{helio}^2$, causing the γ–gamma curves to flatten out to a nearly a constant value.

$$F_{tensile} = A\sigma_t = R^2\sigma_t \tag{8}$$

where A is the cross-sectional area perpendicular to the long axis, and σ_t is the material tensile strength. The centripetal force at which the body fails (fragments) under principal axis rotation is

$$F_{cent} = ma_{cent} = \frac{1}{2}\rho\omega^2 R^4 \tag{9}$$

At the critical rotation rate, $F_{tensile} = F_{cent}$, thus the critical rotation rate (above which the object fragments) is

$$\omega_{crit} = \sqrt{\frac{2\sigma_t}{\rho R^2}} \tag{10}$$

We estimate the SYORP timescale by assuming that the parent chunk starts at rest and compute the amount of time required to spin the chunk up to ω_{crit}. We integrate the expression for angular acceleration (Eq. (7)) with respect to time (τ), set the constant of integration to zero (for chunks starting at rest), and set this resulting expression for angular velocity (ω) equal to ω_{crit}

$$\tau_S = \frac{R\sqrt{32\rho\sigma_t}}{\gamma P_Y C_Y} \tag{11}$$

This timescale defines the duration of an SYORP cycle.

3.5. Step 4: Runaway fragmentation cascade

We now consider the fragmentation of the parent chunk. Since the chunk slowly spins up to the point of fragmentation, the parent clump likely fragments along a single plane of weakness[1], resulting in two roughly equal-sized daughter chunks. If we assume that the two daughter chunks are equal in mass, and that the total volume of material is preserved, then the daughter chunks will have a radius $\sqrt[3]{1/2}$ of the parent chunk. Such a size decrease is associated with a corresponding increase in the tensile strength of the daughter chunk. According to Griffith Crack Theory (Brace, 1961) and assuming a Weibull distribution of flaws within the material, the strength scales approximately as $\sim\sqrt{1/s}$, where s is the size of the object. Thus, the daughter clumps will have a tensile strength that is approximately $\sqrt[6]{2} \approx 1.12$ times the tensile strength of the parent chunk.

After fragmentation, the daughter chunks will be rotating approximately at a rate $\omega_{crit,p}$ (the critical rotation rate of its parent chunk), with the exact value depending on geometry. Thus, instead of starting at rest (as is assumed for the initial parent chunk), the daughter chunks already are rotating at a significant fraction of their own ω_{crit}

$$\omega_0 = \omega_{crit,p} \tag{12}$$

$$= \sqrt{\frac{1}{\sqrt[3]{2^2}\sqrt[6]{2}}}\omega_{crit} \tag{13}$$

$$C = \frac{\omega_0}{\omega_{crit}} \approx 0.75 \tag{14}$$

which reduces the time needed for the daughter chunks to spin up to fragmentation proportionally. Therefore, the timescales to fragmentation for all chunks (except for the initial parent chunk) are $(1 - C) \approx 25\%$ of the time to rotational fission from rest. Therefore, while the initial parent chunk will require the full τ_S to spin up to fragmentation, all ensuing daughter chunks will only require $(1 - C)\tau_S$ to spin up to ω_{crit}.

If we compute the ratio of the SYORP timescales (Eq. (11)) for the daughter clump versus the parent clump, we find that

$$\frac{\tau_{daughter}}{\tau_{parent}} = \frac{(1-C)R_{daughter}\sqrt{\sigma_{daughter}}}{(1-C)R_{parent}\sqrt{\sigma_{parent}}} \tag{15}$$

$$= \sqrt[3]{1/2}\,\sqrt[12]{2} \tag{16}$$

$$= \sqrt[12]{\frac{1}{8}} \approx 0.84 \tag{17}$$

assuming that ρ and C_s are the same for parent and daughter chunks. Since this ratio of SYORP timescales is less than 1, each successive generation of chunks will have a shorter lifetime than the previous generation, leading to a runaway cascade of fragmentation. Such a cascade is consistent with the modeling of Nishioka (1998) and Jones and Battams (2014) for the creation of dust necessary to explain striae.

We next estimate the duration of the entire cascade of fragmentation events, which is equivalent to the elapsed time between parent chunk ejection from the nucleus and the onset of stria formation. We first compute the number of fragmentation steps needed to fragment a parent chunk into micron-sized dust, which is the suspected size of stria grains (Sekanina and Farrell, 1980). Since daughter chunks have a radius $1/\sqrt[3]{2}$ times the size of their parent chunks, the radius of a chunk in the nth generation is

$$R_n = R_0 2^{-\frac{n}{3}} \tag{18}$$

where R_0 is the size of the initial parent chunk ejected from the nucleus. Thus, the number of generations needed to reach size R_n is

$$n = -3\frac{\log_{10}(R_n) - \log_{10}(R_0)}{\log_{10}(2)} \tag{19}$$

Therefore, a parent chunk of ~10–100 m in radius requires ~70–80 generations to produce micron sized dust.

Since the SYORP timescale decreases with each subsequent generation, we can analytically solve for the total amount of time needed for a parent chunk to fragment into the nth generation

$$T_n = \tau_0 + \tau_0(1-C)\sum_{i=1}^{n}\left(\frac{\tau_n}{\tau_{n-1}}\right)^i \approx \tau_0 + 0.25\tau_0\sum_{i=1}^{n}(0.84)^i \tag{20}$$

where τ_0 is the SYORP timescale of the initial parent chunk and $C = \omega_0/\omega_{crit}$, which accounts for the nonzero initial rotation of the daughter chunks. The first ~10 generations, which together reduce parent chunk radii by an order of magnitude, dominate this total

[1] As opposed to a sudden shock of the material, which may result in many forked fractures and numerous fragments if the shock is traveling faster than the velocity of Raleigh surface waves within the material (order of ~100 m/s).

timescale, occupying over 90% of the time needed to reach sufficiently small fragments. Thus, the time required for an ejected parent chunk to fragment into micron-sized stria grains (and therefore the duration of the stria-forming fragmentation cascade) is effectively independent of the size of the final grain

$$T_{fragmentation} \approx T_n \approx 2.31\tau_0 \approx 2.31\frac{R_0\sqrt{32\rho\sigma_{t,0}}}{\gamma P_Y C_Y} \quad (21)$$

where $\sigma_{t,0}$ is the tensile strength of the parent chunk.

After each fragmentation event, classical YORP theory predicts that, on average, half of the daughter chunks will continue to spin up to ω_{crit}, while the other half will spin down towards a stationary state. For those chunks that spin down to a low velocity rotation state, the literature is currently inconclusive as to whether or not they will be captured into a low velocity tumbling state (Vokrouhlicky and Capek, 2002; Cicalo and Scheeres, 2010; Breiter et al., 2011). If the chunk is not captured in a tumbling state, then it will pass through a low velocity rotation state and emerge accelerating with the opposite sense of rotation. This has been a standard and successful assumption in the literature matching both near-Earth and main asteroid belt spin period distributions (Rossi et al., 2009; Marzari et al., 2011). After making this assumption, then nominally half the chunks take 175% of the SYORP timescale τ_S to fragment while the other half take 25% of τ_S. This factor of a few difference of the fragmentation timescale is smaller than the expected order of magnitude variations of the SYORP shape coefficient C_S.

When the chunks are large and the SYORP fragmentation timescales are relatively long, the chunks that fragment much faster or much slower than the average chunk could drift away from the pack contributing to background dust production and possibly form separate mini-striae. As the SYORP fragmentation cascade progresses and the fragmentation timescales decrease, even chunks with very different fragmentation timescales will be unable to drift appreciably apart from one another. If only half the initial parent chunk's mass ends up in the stria, then the initial parent chunks must be approximately ¼ larger in radius to account for the mass that fails to form striae. While a sublimative analog to the Tangential YORP Effect will increase the fraction of chunks that accelerate in the direction of their rotation (Golubov and Krugly, 2012; Golubov et al., 2014) and therefore contribute to stria formation, we conservatively neglect this contribution.

3.6. Step 5: Onset of stria formation

As the fragmentation cascade continues, the resulting fragments become not only smaller, but also increasingly devolatilized. At some point, the resulting grains within the fragment swarm are so small and devolatilized, that solar radiation pressure dominates their behavior, and they stream anti-sunward as in previous models. While we assume that all daughter chunks are of an equal size and have an idealized distribution of flaws, rotational fragmentation will create chunks that are only approximately equal. While these different sizes will not produce large separations between chunks during earlier generations, variations in size during the final generations will cause the grains to separate from one another via solar radiation pressure according to their differing β values, forming a stria (Sekanina and Farrell, 1980). We therefore consider the point at which a parent chunk completes its fragmentation cascade to be the onset of stria formation.

3.7. Modeling and constraints on stria formation

We now estimate the constraints of SYORP-driven stria formation on Comet West. We approximate Comet West's orbit as a parabola with a perihelion of 0.197 AU, and numerically investigate the heliocentric and cometocentric distances of stria formed from our scheme as a function of the heliocentric distance of parent chunk ejection. We numerically integrate the motion of hypothetical parent chunks ejected from the nucleus between 180 days pre-perihelion to 90 days post-perihelion, and record their heliocentric and cometocentric distances at which they complete their fragmentation cascades. We assume that parent chunks that have not completed their fragmentation cascades by the time they reached a post-perihelion heliocentric distance of 10 AU will not form stria because this distance is much greater than the heliocentric distance beyond which water ice sublimation shuts down. We assume the separation between the comet and the parent chunk is small compared to their heliocentric distances, which allows us to approximate the change in the cometocentric distance (d_{comet}) of the parent chunk by assuming that its cometocentric drift is due entirely to the effects of dynamic sublimation pressure

$$\Delta d_{comet} = \frac{1}{2}a_{(r_{helio})}\Delta t^2 + vt = \frac{3P_{sub(r_{helio})}}{8\rho R}\Delta t^2 + v\Delta t \quad (22)$$

where $a_{(r_{helio})}$ is the acceleration of the parent chunk due to sublimation pressure, $P_{sub(r_{helio})}$ is the heliocentric distance dependent sublimation pressure, ρ is the density of the parent chunk, and v is the parent chunk's cometocentric velocity. We assume that this distance montonically increases. This is an admittedly simplified model, which accounts only for a one-dimensional change in the cometocentric distance. However, the largest sources of error are likely the uncertainties in the physical properties of the parent grains. This one-dimensional model is therefore sufficient for our purpose of understanding the order of magnitude behavior of parent chunks, and we reserve two or three-dimensional modeling of stria formation with a deeper study of parent chunk properties for another paper.

Our assumed initial velocity of the parent chunk (~1 m/s) relative to the nucleus is negligible compared to the average velocity needed to move a parent chunk from the nucleus to the cometocentric location of stria formation (~100–1000 m/s) in the weeks between passing the sublimation barrier (the heliocentric distance within which H_2O sublimation becomes the dominant cooling mechanism of the nucleus) and forming a stria. Therefore, we can treat the parent chunks as though they were initially at rest. Additionally, because the parent chunks have an initial velocity comparable to the comet's escape velocity, the parent chunk will quickly move several nucleus radii away from the nucleus, to a point where the cometary gravity is negligible compared to solar gravity or sublimation pressure (while still being relatively close to the nucleus when compared to the cometocentric distance of stria formation). We therefore ignore the negligible effects of cometary gravity on this calculation. We assume that that parent chunk has a tensile strength of 10 Pa, which is the expected order of magnitude when the ~1 Pa strength of ~1 km comet nuclei (Sekanina and Yeomans, 1985; Asphaug and Benz, 1996; Bowling et al., 2014; Thomas et al., 2015; Steckloff et al., 2015a) is scaled to a ~10 m chunk using a $\sqrt{1/s}$ strength scaling law (Brace, 1961). We use a time step of 6 h in the numerical modeling.

In Fig. 5, we plot the heliocentric distance of the onset of stria formation (the point at which the fragmentation cascade is complete) as a function of the heliocentric distance of ejection of a 10 m parent chunk for a comet with the orbit of Comet West. We plot two different cases of the SYORP coefficient C_S, which illustrate two different behaviors in Fig. 5: one in which the parent chunk parameters restrict all striae formation to post-perihelion ($C_S = 0.0035$), and another in which the parent chunk parameters allow for the formation of some pre-perihelion striae ($C_S = 0.01$), which puts a bulge in the curve near perihelion.

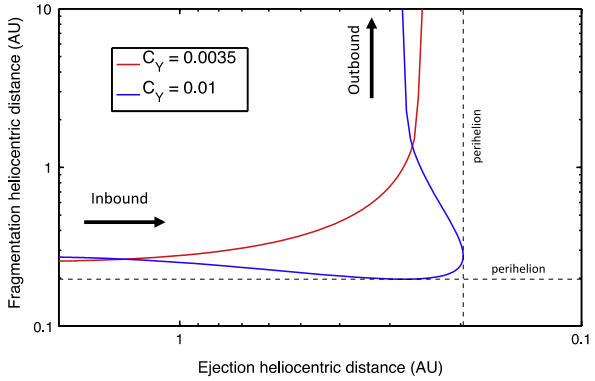

Fig. 5. *Comet West stria formation heliocentric distance versus parent chunk ejection heliocentric distance.* We plot the heliocentric distance of fragmentation for each simulated 10 m parent chunk ejected from Comet West at 6 h intervals as a function of the heliocentric distance of parent chunk ejection for two values of the SYORP coefficient C_Y = 0.01 and 0.0035. This plot reveals that the overwhelming majority of ejected parent chunks would produce stria between 0.2 and 0.3 AU (near perihelion), consistent with observations (Sekanina and Farrell, 1980). Additionally, parent chunks ejected beyond the sublimation barrier (~1 AU) form striae at near the same heliocentric distance (the stria barrier), leading to the asymptotic behavior of the inbound part of the curves. Meanwhile, few chunks ejected after the sublimation barrier have time to fragment before passing back beyond the sublimation barrier, leading to the asymptotic behavior of the outbound part of the curves.

For the case where C_S = 0.01 (which is the upper bound of the expected range of SYORP coefficients, and therefore represents the strongest expected response to SYORP), we find that the heliocentric distance of stria formation has little dependence on the heliocentric distance of parent chunk ejection, with the vast majority of parent chunks forming striae within a narrow window of heliocentric distances (for a given parent chunk size and SYORP coefficient). Because of the sublimation barrier, any parent chunk ejected beyond ~1 AU will experience neither a significant SYORP effect nor sublimation pressure until it reaches the sublimation barrier. After crossing the sublimation barrier, the rapid increase in SYORP torques that peak at perihelion will induce a peak in the number of parent chunks completing their fragmentation cascades, and would therefore cause a burst of stria formation near- and post-perihelion. Meanwhile, Fig. 5 reveals that very few parent chunks ejected post-perihelion have sufficient time to undergo the SYORP fragmentation cascade (Section 3.6) to form striae before passing back across the sublimation barrier, and is only possible for parent chunks that have a very strong response to SYORP torques (i.e. smaller radii and larger SYORP coefficients).

Thus, our model predicts that large, Comet West-like stria should preferentially form after the comet reaches near-perihelion and ~1 AU (water sublimation barrier), with a large burst of striae forming near perihelion, consistent with observations of striae (Sekanina and Farrell, 1980; Pittichová et al., 1997). This is not to suggest that no striae can form prior to perihelion. Striated comet nuclei likely eject a population of parent chunks with a distribution of sizes and SYORP coefficients. Because the SYORP response is size-dependent, our model predicts that smaller parent chunks will be able to respond quickly enough to the weaker pre-perihelion SYORP torques to form striae (assuming that SYORP coefficients are independent of size.) However, these early striae would contain significantly less material than the larger striae that form later, and may therefore be unobservable. Thus, while our SYORP model of stria suggests that any comet capable of ejecting icy chunks could form striae, they may not stand out above background dust emission. Therefore, a careful pre-perihelion study of striated comets could confirm this aspect of SYORP theory.

4. Striae of Comet West

We lastly apply our model to the striae of Comet West as a proof of concept of the SYORP model. We use this rudimentary one-dimensional model to estimate the sizes and SYORP coefficients of the initial parent chunks needed to match the estimated heliocentric and cometocentric distances of its striae (Sekanina and Farrell, 1980). Sekanina and Farrell (1980) obtain these distances by modeling the motion of devolatilized dust under the effects of solar gravity and radiation pressure. Although the Sekanina and Farrell (1980) model of stria formation differs from the model presented in this paper, both models of dust behavior post-formation are identical. Therefore, the heliocentric and cometocentric distances of stria formation that were obtained by post-formation stria dust modeling are applicable to our model.

We list the heliocentric and cometocentric distances of stria formation for the observed stria of Comet West from Sekanina and Farrell (1980), along with our parent chunk radii and SYORP coefficients (C_S) that best fit those distances in Table 1. Each heliocentric and cometocentric distance pair have two unique solutions for parent chunk radius and SYORP coefficient: one solution for the pre-perihelion portion of the comet's orbit, and a second solution for the post-perihelion portion of the orbit. Because the striae in Sekanina and Farrell (1980) were observed post-perihelion, we restrict ourselves to this set of solutions.

The best-fit parent chunks' SYORP coefficients (C_S) lie between 0.00029 and 0.00126, and their best-fit radii lie between 15 and 110 m. These SYORP coefficients are on the low size of their expected range of ~0.001–0.01 (Scheeres, 2007; Rozitis and Green, 2013), which is based on repurposing YORP coefficients to SYORP. While this may be a result of model assumptions, we acknowledge that it may be indicative of a fundamental difference between the YORP and SYORP effects. The YORP and SYORP coefficients are shape-dependent parameters that describe the second order torques that arise from asymmetries in the shape of the object. Unlike the YORP effect, SYORP depends on the loss of material from the surface of the object that can eliminate asymmetries in its shape over time, particularly at smaller size scales. If the object becomes more symmetrical, its SYORP coefficient will drop over time. Therefore, time-averaged SYORP coefficients may be, as a whole, smaller than their YORP counterparts. While our model

Table 1
Heliocentric and cometocentric locations of stria formation for Comet West and their best-fit parent chunks. This table lists the modeled heliocentric and cometocentric distances of formation for 16 striae of Comet West (Sekanina and Farrell, 1980). These distances were obtained by modeling the post-formation dynamics of the dust that composed each stria. This table also lists our best fit radius and SYORP coefficient for each striae.

Heliocentric distance (AU)[a]	Cometocentric distance (Gm)[a]	Best fit parent radius (m) (error $R^{+10\%}_{-27\%}$)	Best fit parent C_S (error $C_S^{+6\%}_{-2\%}$)
0.2284	2.56	32.5	0.00056
0.2924	7.58	16.4	0.00029
0.2696	5.34	20.5	0.000355
0.2581	4.2	24	0.000406
0.2606	4.1	24.75	0.000415
0.2535	3.27	30.5	0.000493
0.2683	4.06	26.5	0.000433
0.2506	2.8	35	0.000555
0.2592	2.92	34	0.000530
0.2517	2.14	47	0.000688
0.2543	1.97	50	0.000715
0.2785	2.94	37	0.000544
0.2769	2.29	49	0.00067
0.2624	1.1	95	0.00114
0.2685	0.96	110	0.00126
0.2841	1.12	105	0.00118

[a] Sekanina and Farrell (1980).

assumes a static SYORP coefficient, these best-fit SYORP coefficients are more representative of an average value. Therefore, while the initial SYORP coefficient of a parent chunk may be comparable to its YORP coefficient, the loss of mass required by SYORP may result in a lower average SYORP coefficient than the average YORP coefficient (were the chunk not sublimating).

The best-fit radii of the parent chunks fall within the expected ~10–100 m range. The estimated error in the size of the radii of the parent chunks is a result of uncertainly in the magnitude of the average dynamic sublimation pressure. Steckloff et al. (2015a) estimate the uncertainly in the sublimation pressure to be up to ~10% for pure H_2O ice sublimation. Additionally, we use a dynamically new Comet C/2012 S1 (ISON), which is a reasonable analog to the predicted pristine parent chunks, to estimate uncertainties associated with sublimation contributions from less common but more volatile species and the active fraction of the parent chunks' surfaces. We estimate that the small contributions from less common sublimating volatile species (CO_2, CO, etc.) to be up to ~10%, based on their relative abundances (McKay et al., 2014; Weaver et al., 2012) and relative volatilities (Steckloff et al., 2015a). Unlike JFC nuclei which have only small fractions of their nuclei that are active, the entire surface of Comet ISON appeared to be active (Steckloff et al., 2015b), which is consistent with the thermally primitive nature of long-period comets. While this would suggest that fragments of such a nucleus (i.e. stria parent chunks) would similarly be active all over, we do not understand what mechanism may be responsible for their ejection. We consider the case in which the ejection mechanism lofts a partially exposed chunk of material, and conservatively estimate that the exposed region of that chunk (perhaps 20% of its surface) is devolatilized and inactive (or equivalently, that a larger portion of its surface is partially devolatilized). Because we do not currently have a well-studied ejection mechanism that we could use to better constrain these uncertainties, we adopt the conservative estimate of 20% as the uncertainly in the active area.

These errors are not symmetrical about our best fit solution. Our model assumes the maximum possible sublimation pressure and active area, and uncertainties in their values can only revise them downward. We therefore end up with an asymmetrical error in the average sublimation pressure of $P_{sub}^{+10\%}{}_{-25\%}$ from propagation of errors. We run these uncertainties through our model to estimate the uncertainties in the radii of the parent chunks of the striae from Sekanina and Farrell (1980) to be $\varepsilon R = R_{-27\%}^{+10\%}$, and the uncertainty in the corresponding SYORP coefficients to be $\varepsilon C_S = C_{S_{-2\%}}^{+6\%}$.

With 16 parent chunks, we can generate a Size–Frequency Distribution (SFD), which plots the number of chunks larger than a particular size (see Fig. 6). We neglect to include parent clumps smaller than 20 m in this power law fit, as the power law shows a break in the trend, which likely indicates observational bias near the limit of detection. The cumulative-SFD represents the number of chunks greater than a given size, and appears to follow a clear power law ($N(>R) \propto R^q$) with a best-fit power law index (q) of −1.4. However, a power law index between −2.0 and −1.1 is consistent with the estimated errors in our model, and power law indexes between −1.1 and −4.0 are consistent with the estimated errors of the chunks up to 50 m in radius. This cumulative-SFD power-law index is consistent with the index of $q = -1.92 \pm 0.20$ for Jupiter Family Comets (JFCs) with radii larger than 1.25 km (Snodgrass et al., 2011), but is only marginally consistent with the index of ~−1 that describes the impactor population (<~2 km) in the young terrains of Europa (Bierhaus et al., 2012).

The differential Size–Frequency Distribution (differential-SFD) is generated by taking a derivative of the cumulative-SFD with respect to object radius generates the differential Size–Frequency Distribution (differential-SFD). The differential-SFD for all parent

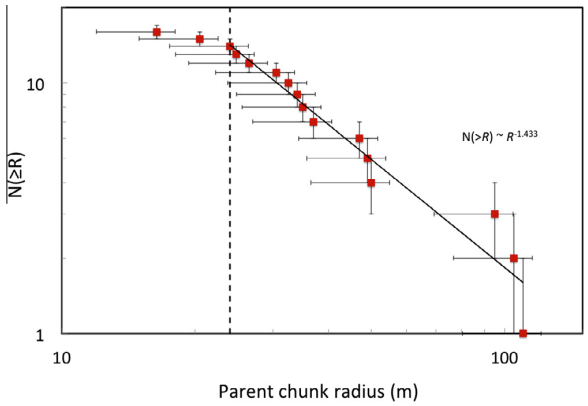

Fig. 6. *Cumulative Size–frequency distribution of the best-fit parent chunks of Comet West's striae.* Here we plot the number of chunks larger than a given parent chunk size. Vertical error bars are $\sqrt{N}$, while horizontal error bars are the estimated $\sim_{-27\%}^{+10\%}$ uncertainly in parent chunk radius. Vertical dashed line represents a break in the size–frequency distribution, which we believe is due to observational bias.

chunks has a power-law slope of −2.4 (−3.0 to −2.1), but values between −2.1 and −5 are consistent with the estimated errors of the chunks up to 50 m in radius. This is consistent with the differential-SFD index of the fragments of Comet 73P/Schwassmann-Wachmann 3 Nucleus B of −2.11 (Fuse et al., 2007) or −2.56 (large fragments $F > 10$ mJy) (Reach et al., 2009), but inconsistent with its small fragments ($F < 10$ mJy) index of -1.84 (Reach et al., 2009). This range of differential-SFD power-law indexes for all parent chunks of Comet West is inconsistent with the differential-SFD indexes of −4.7 to −6.6 (Kelley et al., 2013) and −3 to −4 (Rotundi et al., 2015) that describe the chunks and grains in the inner comae of Comets 103P/Hartley 2 and 67P Churyumov-Gerasimenko respectively. However, the two latter populations are for small chunks (up to ~1 m in radius), and the differential-SFD power-law slope for parent chunks of Comet West up to 50 m in radius is consistent with both of these populations. It is presently unclear whether these similar power law indexes indicate a similar origin, composition, or evolution of these different populations, and further study is warranted to place these cometary populations into a common context and explore how evolutionary and ejection processes may alter these SFDs.

5. Discussion

Thus far our analysis has assumed that the sublimation fronts for the volatile ices are located at the surface of the chunks, rather than below. Comet ISON's dust activity, which is a proxy for gas sublimation, was located predominantly on the sunward side of the nucleus (Li et al., 2013b). This is common for comet nuclei (Whipple, 1950; Keller et al., 1986; Feaga et al., 2007; Belton, 2013; Gulkis et al., 2015), and suggests that the volatile sublimation front is close enough to the surface of the nucleus to respond to the diurnal thermal wave (Steckloff et al., 2015a), such that the time required for a pulse of heat at the surface to propagate to the sublimating volatiles is short compared to the rotation period. This behavior is consistent with the low thermal inertias of cometary material (Lisse et al., 2005; Lamy et al., 2008; Davidsson et al., 2013; Groussin et al., 2013; Gulkis et al., 2015). However, if the rotation period of a parent chunk were to become comparable to this thermal lag time during SYORP spin up, then the chunk's gas emissions would begin to lose their sunward directionality, and

sublimation pressure would begin to cease driving the chunk anti-sunward.

Shutting down the anti-sunward sublimation-driven acceleration would not affect the SYORP torques, which, like the YORP effect, only depends on the shape of the chunk. Therefore a chunk in this situation would cease to accelerate heliocentrically, but would drift cometocentrically at a constant rate and continue to spin up to the point of fragmentation, at which point this cycle would repeat with the daughter chunks. Because the antisunward acceleration would episodically shut down, the resulting cometocentric distance of stria formation would be reduced. However, since neither the thermal lag time between the nuclear surface and the volatile ices nor the depth of the volatile ices of Oort Cloud comets is known, these considerations are currently merely unconstrained speculation.

The SYORP mechanism, while explaining why most observed striae form near- or post-perihelion, predicts that striae may also form pre-perihelion within ~1 AU of the Sun. However, the parent chunks that would form these earlier striae would have to undergo their fragmentation cascades in a shorter period of time, and would therefore be significantly smaller than the parent chunks that form post-perihelion striae. Because these smaller parent chunks would form striae that contain less material than the post-perihelion striae, these earlier striae are expected to be faint and likely to remain undetected. A careful pre-perihelion study of comets that produce post-perihelion striae may be able to confirm this aspect of the SYORP theory.

Additionally, we assume that H_2O sublimation is driving the stria formation process. However, if more volatile species such as CO_2 or CO are driving striae formation, then striae may form further from the Sun, form faster, and contain more material. Additionally, if parent chunks are ejected via sublimation of supervolatile species from a discrete location of the nucleus, then parent chunks may be diurnally ejected. If this process occurs within the sublimation barrier of the driving species, then it may lead to the formation of striae that are regularly spaced within the cometary tail, and that form at an interval approximating the rotation period of the nucleus.

Our model relies on the ability of comet nuclei to eject ~10–100 m sized chunks at escape velocity (~1 m/s). Long-period Comet C/1992 B2 (Hyakutake) experienced an outburst that ejected chunks consistent with the parent chunks in our model (Desvoivres et al., 2000; Schleicher and Woodney, 2003). However, it is unclear whether or not the comet formed striae due to limited observations of the comet post-perihelion. Similarly, Jupiter Family Comet 17P/Holmes produced fragments consistent with parent chunks (Stevenson et al., 2010), however its distant perihelion of 2 AU would likely prevent the vigorous sublimation that is necessary in our model to form striae. Spacecraft flybys of comet nuclei (such as Giotto, Deep Space 1, Deep Impact, Stardust, DIXI, and Stardust-NExT) would be very unlikely to resolve the ejection of parent-sized chunks of material due to their limited time of encounter, and would almost certainly require a Rosetta-style mission to observe the nucleus of a striated comet for an extended period of time.

The Rosetta spacecraft itself has observed decimeter to meter-sized chunks of material moving at near escape velocity at Comet 67P/Churyumov-Gerasimenko (Rotundi et al., 2015) and would certainly be able to detect the ejection of objects as large as parent chunks. However, because striae are a rare phenomenon and Jupiter Family Comets are so thermally processed, we would not necessarily expect that 67P/Churyumov-Gerasimenko would be able to eject parent chunks at escape velocity, which is required to form striae. Indeed, Rosetta has discovered ~10–100 m chunks of material that may have been ejected from the nucleus of 67P/Churyumov-Gerasimenko, but lacked sufficient velocity to escape the nucleus' gravity (Thomas et al., 2015). Direct observation of the ejection of ~10–100 m chunks of material would be much more likely by a spacecraft at a long period comet or active centaur. However, failure to detect the ejection of ~10–100 m chunks of material at these bodies would not necessarily invalidate this theory, since it predicts that only some bodies are capable of ejecting these chunks.

It is plausible that a particularly active comet could eject parent chunks at velocities an order or two of magnitude greater than the comet's escape velocity. Such parent chunks could drift significantly farther from the nucleus than other parent chunks, and would form striae far from the cometary tail. However, if these parent chunks are ejected sufficiently far from the Sun in the centaur region, they may drift so far from the nucleus that they would form dust features too far from the nucleus to be easily associated with the comet. The Rosetta spacecraft currently in orbit around the nucleus of Comet 67P/Churyumov-Gerasimenko may be able to directly observe the ejection of large chunks of material from the nucleus during perihelion, and perhaps even obtain a velocity profile of the ejected population.

Additionally, our model may predict observable intermediate stages of stria formation. Because we begin with a single parent chunk, the initial stages of stria formation would be unobservable. We have already shown that daughter chunks with radii that are comparable to the initial parent chunk predominantly occupy the duration of the SYORP fragmentation cascade. Thus, as the daughter chunks drift away from the nucleus, they remain unobservable. However, as the runaway fragmentation cascade nears completion, a very large number of small chunks are produced very rapidly. Thus, immediately prior to the onset of stria formation, an observable cloud of material may appear in the tail of the comet that then streams outward into a stria.

While we assume that each step of the SYORP fragmentation cascade produces two identical daughter chunks (size and shape), it is likely that these two chunks vary from one another. If this variation is small, then the fragmentation cascade would be insignificantly affected and the daughter chunks will still complete their fragmentation cascades at approximately the same time. However, if this variation is large, then one daughter chunk may undergo a significantly faster fragmentation cascade, and complete its fragmentation before drifting a significant distance from the nucleus. This would manifest itself as a source of fine-grained debris in the tail of the comet located between the nucleus and the striae. Additionally, if the fragmentation of the larger daughter chunks (early stages of the fragmentation cascade) is messy and produces fine-grained debris, then it would also manifest itself as an additional source of fine-grained material between the nucleus and striae. In either of these cases, one may see a diffuse or wispy tail of material distinct from the striae or the rest of the dust tail. However, if the fragmentation cascade is more ideal, or if the dust tail is bright, then this feature may not be visible or even existent.

Lastly, while we have only applied SYORP to parent chunks on the order of ~10–100 m in radius, there is no reason why SYORP would not affect much larger icy objects within the Solar System. Indeed, the SYORP mechanism should be able to change the spin state of icy objects of all sizes. The limiting factor for SYORP is heliocentric distance, as the effect shuts down beyond the sublimation barrier of the driving volatile species. While we have here only considered the sublimation of water ice (which shuts down beyond ~1 AU), CO_2-driven SYORP would be active out to ~10 AU, while CO-driven SYORP would remain active out to ~100 AU! Therefore, as long as the appropriate volatile species is present and abundant, SYORP can provide torques to objects throughout the observable Solar System.

6. Summary and conclusions

We have proposed a new sublimation-driven model for the formation of striae within the tails of comets that provides a natural explanation for why comets with perihelia within 0.6 AU only form striae within ~1 AU of the Sun after reaching the near-perihelion portion of their orbits. Our model easily allows a large amount of material to be transported as a single unit to the location of stria formation, a major weakness of existing stria formation schemes. As part of our driving mechanism, we describe a new, sublimation-driven analog to the YORP effect (SYORP), which allows large (~10–100 m) parent chunks to fragment quickly enough to form stria within the inner Solar System. If large numbers of parent chunks with similar sizes and shapes are ejected prior to the comet passing within the sublimation barrier, then these parent chunks should produce a sudden burst of striae. However, the ejection of parent chunks with a range of sizes and shapes is more likely.

We apply our model to the striae of Comet West, and find that parent chunks with radii between 15 m and 110 m ($^{+10\%}_{-27\%}$), which are consistent with expected sizes. The sizes of these parent chunks follow a power-law cumulative size–frequency distribution (cumulative-SFD) with a power-law index of $-1.4^{+0.3}_{-0.6}$ ($-1.5^{+0.4}_{-2.5}$ for parent chunks less than 50 m radius), which is consistent with the index of -1.92 ± 0.20 for Jupiter Family Comets with radii larger than 1.25 km (Snodgrass et al., 2011) and marginally consistent with the index of ~−1 for the impactor population into the young terrains of Europa (Bierhaus et al., 2012). The differential Size–Frequency Distribution (differential-SFD) of $-2.4^{+0.3}_{-0.6}$ is consistent with 73P/Schwassmann-Wachmann 3 Nucleus B's large fragments (Reach et al., 2009) or all fragments (Fuse et al., 2007). The differential-SFD for parent chunks less than 50 m in radius of $-2.5^{+0.4}_{-2.5}$ is consistent with the differential-SFD indexes of the particles in the inner comae of Comets 103P/Hartley 2 (Kelley et al., 2013) and 67P/Churyumov-Gerasimenko (Rotundi et al., 2015). The mechanism responsible for lofting these parent chunks off of the surface of the nucleus is unknown, but we speculate that it may be the resulting gas drag from a cometary outburst, consistent with the observed parent-sized chunks of Comet 17P/Holmes (Stevenson et al., 2010) and Comet C/1996 B2 (Hyakutake) (Desvoivres et al., 2000; Schleicher and Woodney, 2003). The SYORP coefficients (C_S) of Comet West's parent chunks are 0.00029–0.00126 ($^{+6\%}_{-2\%}$), which is on the low side of the expected range of ~0.001–0.01 (Scheeres, 2007; Rozitis and Green, 2013). This may be due to the loss of surface material that is inherent in the SYORP mechanism, and which may remove the asymmetries in the shape of the body that generate the sublimative torques that create the SYORP effect.

We also predict that fainter, potentially observable striae may form earlier than the larger easily observable striae. However, these early striae would tend to form from smaller parent chunks, and would therefore be harder to detect. Additionally, our mechanism suggests that any comet capable of ejecting icy chunks can produce striae, which may or may not be large enough to be observable. Lastly, we speculate on possible intermediate stages of stria formation in our mechanism that may be observable. One would appear as a cloud of material present immediately prior to stria formation, which may or may not be visible above the background of the dust tail. The other depends on imperfections during the SYORP fragmentation cascade, and may appear as a faint wispy tail-like feature located in the dust tail between the nucleus and the striae if the fragmentation is sufficiently imperfect and the dust tail is sufficiently dim.

Acknowledgments

We wish to thank and acknowledge H. Jay Melosh (Purdue University), Michael Combi (University of Michigan) and Nalin Samarasinha (Planetary Science Institute) for useful conversations and comments that improved this project. Jordan K. Steckloff wishes to thank H. Jay Melosh (Purdue University) for funding this research and providing helpful comments and context. Seth A. Jacobson wishes to acknowledge support from the European Research Council (ERC) Advanced Grant "ACCRETE" (contract number 290568).

References

Asphaug, E., Benz, W., 1996. Size, density, and structure of Comet Shoemaker-Levy 9 inferred from the physics of tidal breakup. Icarus 121, 225–248.
Belton, M.J.S., 2010. Cometary activity, active areas, and a mechanism for collimated outflows on 1P, 9P, 19P, and 81P. Icarus 210, 881–897.
Belton, M.J.S., 2013. The sources of the unusual dust jets seen in Comet 103P/Hartley 2. Icarus 222, 653–661.
Belton, M.J.S. et al., 2011. Stardust-NExT, Deep Impact, and the accelerating spin of 9P/Tempel 1. Icarus 213, 345–368.
Bierhaus, E.B. et al., 2012. The role of ejecta in the small crater populations on the mid-sized saturnian satellites. Icarus 218, 602–621.
Bottke Jr., W.F. et al., 2002. The effect of Yarkovsky thermal forces on the dynamical evolution of asteroids and meteoroids. Asteroids III 395–408.
Bowling, T.B. et al., 2014. The strength of Comet 67P/Churyumov-Gerasimenko. American Astronomical Society – Division of Planetary Science Meeting #46, Abstract #100.03.
Brace, W.F., 1961. Dependence of fracture strength of rocks on grain size. Penn State Univ. Mineral Expt. State Bullet. 76, 99–103.
Breiter, S., Rozek, A., Vokrouhlicky, D., 2011. Yarkovsky–O'Keefe–Radzievskii–Paddack effect on tumbling objects. Mon. Not. R. Astron. Soc. 417, 2478–2499.
Brownlee, D.E. et al., 2004. Surface of young Jupiter Family Comet 81P/Wild 2: View from the Stardust Spacecraft. Science 304 (5), 1764–1769.
Bruck Syal, M. et al., 2013. Geologic control of jet formation on Comet 103P/Hartley 2. Icarus 222, 610–624.
Capek, D., Vokrouhlicky, D., 2004. The YORP effect with finite thermal conductivity. Icarus 172, 526–536.
Chesley, S.R. et al., 2013. An updated rotational model for Comet 9P/Tempel 1. Icarus 222, 516–525.
Cicalo, S., Scheeres, D.J., 2010. Averaged rotational dynamics of an asteroid in tumbling rotation under the YORP torque. Celest. Mech. Dynam. Astron. 106, 301–337.
Davidsson, B.J.R. et al., 2013. Thermal inertia and surface roughness of Comet 9P/Tempel 1. Icarus 224, 154–171.
Desvoivres, E. et al., 2000. Modeling the dynamics of cometary fragments: Application to Comet C/1996 B2 Hyakutake. Icarus 144, 172–181.
Drahus, M., 2014. Rotational disruption of comets with parabolic orbits. In: AAS/Division for Planetary Sciences Meeting Abstracts 46, #200.04.
Feaga, L.M. et al., 2007. Asymmetries in the distribution of H_2O and CO_2 in the inner coma of Comet 9P/Tempel 1 as observed by Deep Impact. Icarus 190, 345–356.
Fernández, Y.R., 2009. That's the way the comet crumbles: Splitting Jupiter-family comets. Planet. Space Sci. 57, 1218–1227.
Froehlich, H.-E., Notni, P., 1988. Radiation pressure – A stabilizing agent of dust clouds in comets? Astron. Nach. 309, 147–155.
Fuse, T. et al., 2007. Observations of fragments split from nucleus B of Comet 73P/Schwassmann-Wachmann 3 with Subaru telescope. Pub. Astron. Soc. Jpn. 59, 381–386.
Golubov, O., Krugly, Y.N., 2012. Tangential component of the YORP effect. Astrophys. J. 752, L11–L15. http://dx.doi.org/10.1088/2041-8205/752/1/L11.
Golubov, O., Scheeres, D.J., Krugly, Y.N., 2014. A three-dimensional model of tangential YORP. Astrophys. J. 794, 22–30. http://dx.doi.org/10.1088/0004-637X/794/1/22.
Gombosi, T.I., 1994. Free molecular aerodynamics. In: Gaskinetic Theory, first ed. Cambridge University Press, Cambridge, UK.
Green, S.F. et al., 2004. The dust mass distribution of Comet 81P/Wild 2. J. Geophys. Res. 109, E12S0. http://dx.doi.org/10.1029/2004JE002318.
Groussin, O. et al., 2013. The temperature, thermal inertia, roughness and color of the nuclei of Comets 103P/Hartley 2 and 9P/Tempel 1. Icarus 222, 580–594.
Gulkis, S. et al., 2015. Subsurface properties and early activity of Comet 67P/Churyumov-Gerasimenko. Science 347. http://dx.doi.org/10.1126/science.aaa0709.
Gutiárrez, P.J., Davidsson, B.J.R., 2007. Non-gravitational force modeling of Comet 81P/Wild 2. II. Rotational evolution. Icarus 191, 651–664.
Gutiárrez, P.J. et al., 2003. Long-term simulations of the rotational state of small irregular cometary nuclei. Astron. Astrophys. 406, 1123–1133.
Hammel, H.B. et al., 1987. Albedo maps of Comets P/Halley and P/Giacobini-Zinner. Astron. Astrophys. 187, 665–668.
Hermalyn, B. et al., 2013. The detection, localization, and dynamics of large icy particles surrounding Comet 103P/Hartley 2. Icarus 222, 625–633.

Jones, G., Battams, K., 2014. Dust tail striae: Lessons from recent comets. Asteroids, Comets, Meteors, 249.
Julian, W.H., 1990. The Comet Halley nucleus – Random jets. Icarus 88, 355–371.
Keller, H.U. et al., 1986. First Halley multicolour camera imaging results from Giotto. Nature 321, 320–326.
Kelley, M.S. et al., 2013. A distribution of large particles in the coma of Comet 103P/Hartley 2. Icarus 222, 634–652.
Kharchuk, S.V., Korsun, P.P., 2010. Striated features in the dust tail of Comet C/2006 P1 (McNaught). Kinem. Phys. Celest. Bodies 26 (6), 322–325.
Lamy, P.L. et al., 2004. The sizes, shapes, albedos, and colors of cometary nuclei. In: Festou, M., Keller, H.U., Weaver, H.A. (Eds.), Comets II. University of Arizona Press-Tucson, AZ.
Lamy, P.L. et al., 2008. Spitzer Space telescope observations of the nucleus of Comet 67P/Churyumov-Gerasimenko. Astron. Astrophys. 489, 777–785.
Li, J.-Y. et al., 2007. Deep Impact photometry of Comet 9P/Tempel 1. Icarus 191, 161–175.
Li, J.-Y. et al., 2013a. Photometric properties of the nucleus of Comet 103P/Hartley 2. Icarus 222, 559–570.
Li, J.-Y. et al., 2013b. Characterizing the dust coma of Comet C/2012 S1 (ISON) at 4.15 AU from the Sun. Astrophys. J. Lett. 779, L3 (5 pp).
Lisse, C.M. et al., 2005. Rotationally resolved 8–35 μm Spitzer Space telescope observations of the nucleus of Comet 9P/Tempel 1. Astrophys. J. 625, L139–L142.
Marsden, B.G., Sekanina, Z., Yeomans, D.K., 1973. Comets and nongravitational forces. V. Astron. J. 78 (2), 211–225.
Marzari, F., Rossi, A., Scheeres, D.J., 2011. Combined effect of YORP and collisions on the rotation rate of small Main Belt asteroids. Icarus 214, 622–631.
McBride, N. et al., 1997. The inner dust coma of Comet 26P/Grigg-Skjellerup: Multiple jets and nucleus fragments? Mon. Not. R. Astron. Soc. 289, 535–553.
McDonnell, J.A.M. et al., 1987. The dust distribution within the inner coma of Comet P/Halley 1982i – Encounter by Giotto's impact detectors. Astron. Astrophys. 187, 719–741.
McKay, A. et al., 2014. Evolution of fragment-species production in Comet C/2012 S1 (ISON) from 1.6 AU to 0.4 AU. Asteroids, Comets, Meteors 2014, 365.
Meech, K.J. et al., 2011. Deep Impact, Stardust-NExT and the behavior of Comet 9P/Tempel 1 from 1997 to 2010. Icarus 213, 323–344.
Melosh, H.J., 2011. Slopes and mass movement. In: Planetary Surface Processes, first ed. Cambridge University Press, Cambridge, UK.
Mysen, E., 2004. Rotational dynamics of subsolar sublimating triaxial comets. Planet. Space Sci. 52, 897–907.
Mysen, E., 2007. The dynamics of globally active triaxial comets, with applications to asteroid rotation. Mon. Not. R. Astron. Soc. 381, 301–307.
Neishtadt, A.I. et al., 2002. Evolution of comet nucleus rotation. Icarus 157, 205–218.
Neishtadt, A.I. et al., 2003. The Influence of reactive torques on comet nucleus rotation. Celest. Mech. Dynam. Astron. 86, 249–275.
Nishioka, K., 1998. Finite lifetime fragment model 2 for synchronic band formation in dust tails of comets. Icarus 134, 24–34.
Oberst, J. et al., 2004. The nucleus of Comet Borrelly: A study of morphology and surface brightness. Icarus 167, 70–79.
Peale, S.J., Lissauer, J.J., 1989. Rotation of Halley's comet. Icarus 79, 396–430.
Pittichová, J. et al., 1997. An early investigation of the striated tail of Comet Hale-Bopp (C/1995 O1). Earth, Moon Planets 78, 329–338.
Reach, W.T. et al., 2009. Distribution and properties of fragments and debris from the split Comet 73P/Schwassmann-Wachmann 3 as revealed by Spitzer Space telescope. Icarus 203, 571–588.
Richardson, J.E. et al., 2007. A ballistics analysis of the Deep Impact ejecta plume: Determining Comet Tempel 1's gravity, mass, and density. Icarus 190, 357–390.
Rodionov, A.V. et al., 2002. An advanced physical model of cometary activity. Planet. Space Sci. 50, 983–1024.
Rossi, A., Marzari, F., Scheeres, D.J., 2009. Computing the effects of YORP on the spin rate distribution of the NEO population. Icarus 202, 95–103.
Rotundi, A. et al., 2015. Dust measurements in the coma of Comet 67P/Churyumov-Gerasimenko inbound to the Sun. Science 347 (6 pp) 3905.
Rousselot, P., 2008. 174P/Echeclus: A strange case of outburst. Astron. Astrophys. 480 (2), 543–550.
Rozitis, B., Green, S.F., 2013. The influence of global self-heating on the Yarkovsky and YORP Effects. Mon. Not. R. Astron. Soc. 433 (1), 603–621.
Rubincam, D.P., 2000. Radiative spin-up and spin-down of small asteroids. Icarus 148, 2–11.
Rubincam, D.P., Paddack, S.J., 2010. Zero secular torque on asteroids from impinging solar photons in the YORP effect: A simple proof. Icarus 209 (2), 863–865.
Samarasinha, N.H., Belton, M.J.S., 1995. Long-term evolution of rotational stress and nongravitational effects for Halley-like cometary nuclei. Icarus 116, 340–358.
Samarasinha, N.H., Mueller, B.E.A., 2013. Relating changes in cometary rotation to activity: Current status and applications to Comet C/2012 S1 (ISON). Astrophys. J. Lett. 775, L10 (6 pp).
Scheeres, D.J., 2007. The dynamical evolution of uniformly rotating asteroids subject to YORP. Icarus 188, 430–450.
Scheeres, D.J. et al., 2010. Scaling forces to asteroid surfaces: The role of cohesion. Icarus 210, 968–984.
Schleicher, D.G., Woodney, L.M., 2003. Analyses of dust coma morphology of Comet Hyakutake (1996 B2) near perigee: Outburst behavior, jet motion, source region locations, and nucleus pole orientation. Icarus 162, 190–213.
Sekanina, Z., 2003. Erosion model for the sungrazing comets observed with the Solar and Heliospheric Observatory. Astrophys. J. 597, 1237–1265.
Sekanina, Z., Farrell, J.A., 1978. Comet West 1976. VI – Discrete bursts of dust, split nucleus, flare-ups, and particle evaporation. Astron. J. 83, 1675–1680.
Sekanina, Z., Farrell, J.A., 1980. The striated dust tail of Comet West 1976 VI as a particle fragmentation phenomenon. Astron. J. 85, 1538–1554.
Sekanina, Z., Yeomans, D.K., 1985. Orbital motion, nucleus precession, and splitting of periodic Comet Brooks 2. Astron. J. 90, 2335–2352.
Sidorenko, V.V., Scheeres, D.J., Byram, S.M., 2008. On the rotation of Comet Borrelly's nucleus. Celest. Mech. Dynam. Astron. 102, 133–147.
Sierks, H. et al., 2015. On the nucleus structure and activity of Comet 67P/Churyumov-Gerasimenko. Science 347. http://dx.doi.org/10.1126/science.aaa1044.
Snodgrass, C. et al., 2011. The size distribution of Jupiter Family comet nuclei. Mon. Not. R. Astron. Soc. 414, 458–469.
Steckloff, J.K. et al., 2015a. Dynamic sublimation pressure and the catastrophic breakup of Comet ISON. Icarus 258, 430–437. http://dx.doi.org/10.1016/j.icarus.2015.06.032.
Steckloff, J.K. et al., 2015b. The size and fragmentation of the nucleus of Comet C/2012 S1 (ISON). In: LPSC XLVI, Abstract #2723.
Stevenson, R., Kleyna, J., Jewitt, D., 2010. Transient fragments in outbursting Comet 17P/Holmes. Astron. J. 139, 2230–2240.
Szegö, K. et al., 2001. Dynamical effects of Comet P/Halley gas production. Astron. Astrophys. 370, L35–L38.
Thomas, P.C. et al., 2013. Shape, density, and geology of the nucleus of Comet 103P/Hartley 2. Icarus 222, 550–558.
Thomas, N. et al., 2015. The morphological diversity of Comet 67P/Churyumov-Gerasimenko. Science 347. http://dx.doi.org/10.1126/science.aaa0440.
Vokrouhlicky, D., Capek, D., 2002. YORP-induced long-term evolution of the spin state of small asteroids and meteoroids: Rubincam's approximation. Icarus 159, 449–467.
Weaver, H.A. et al., 2001. HST and VLT investigations of the fragments of Comet C/1999 S4 (LINEAR). Science 292, 1329–1333.
Weaver, H. et al., 2014. Ultraviolet spectroscopy of Comet ISON (2012 S1). In: Asteroids, Comets, Meteors 2014, p. 604.
Whipple, F.L., 1950. A comet model. I. The acceleration of Comet Encke. Astrophys. J. 111, 375–394.
Wilhelm, K., 1987. Rotation and precession of Comet Halley. Nature 327, 27–30.
Zolensky, M.E. et al., 2006. Mineralogy and petrology of Comet 81P/Wild 2 nucleus samples. Science 314, 1735–1739.